Master's thesis

NTNU
Norwegian University of Science and Technology
Faculty of Engineering
Department of Energy and Process Engineering

Øistein Farmen

Ammonia as an alternative to LNG

Master's thesis in Energy and Environmental Engineering
Supervisor: Jacob Joseph Lamb
Co-supervisor: Schalk Cloete, and Carlos Arnaiz del Pozo
June 2023

NTNU
Norwegian University of
Science and Technology

Øistein Farmen

Ammonia as an alternative to LNG

Master's thesis in Energy and Environmental Engineering
Supervisor: Jacob Joseph Lamb
Co-supervisor: Schalk Cloete, and Carlos Arnaiz del Pozo
June 2023

Norwegian University of Science and Technology
Faculty of Engineering
Department of Energy and Process Engineering

NTNU
Norwegian University of
Science and Technology

Abstract

Cost-effective decarbonization of the global fuel supply is becoming increasingly important to mitigate the rising socioeconomic costs of climate change. Hence, this thesis investigates the potential of displacing liquefied natural gas (LNG) with blue ammonia produced from natural gas. With the recent Russia-Ukraine crisis aggravating global concerns over energy security, the diversification of fuel supply (e.g., LNG imports from multiple suppliers instead of pipelines from Russia) has gained substantial interest, necessitating a comprehensive analysis of the economic competitiveness, technological feasibility, and environmental implications of these energy carriers. Blue ammonia is promising because it releases no CO_2 upon combustion and is easily liquefied for international trade via ship.

This research presents an in-depth techno-economic analysis of the LNG and ammonia value chain from production facilities in the United States to importing terminals in Germany. This is achieved by modeling four scenarios in Aspen Plus: medium (1x) and large-scale (10x) production facilities for LNG and ammonia each. Natural gas input to the 1x and 10x trains are set to approximately 1.5 GW and 15 GW, respectively. The LNG plant is modeled using the propane precooling mixed refrigerant process (C3MR), and the ammonia plant is modeled using the advanced membrane-assisted auto-thermal reforming (MA-ATR) process. For both fuels, the 1x train is assumed to import electricity from the grid, whereas the 10x train generates electricity on-site. A consistent methodology is then employed to conduct independent economic assessments for the production plants, terminals, and shipping using the Standardized Economic Assessment (SEA) Tool. Utilizing this evaluation approach encourages a consistent and reliable comparison of the key performance indicators across the energy carriers.

The findings indicate that while the final thermal efficiency of the ammonia value chain is $\sim$30% lower than that of the LNG value chain, ammonia gains economic competitiveness against LNG when reasonable CO_2 taxes are applied. Specifically, ammonia reaches cost-parity with LNG at a CO_2 tax rate of \$104.08/tonne for the 1x train and \$78.81/tonne for the 10x train assuming natural gas prices at \$2.5/GJ, and electricity at \$60/MWh. The levelized cost of the product (LCOP) for the 1x train scenarios resulted in \$12.78/GJ for LNG and \$13.03/GJ for ammonia, making ammonia 2% more expensive at CO_2 prices of \$100/tonne. In larger-scale operations, the 10x train scenarios show an LCOP of \$11.35/GJ for LNG and \$10.04/GJ for ammonia. Ammonia production, being more capital- and electricity-intensive, benefits from the economies of scale and on-site power production of the 10x trains, thereby lowering costs by 13%.

Of numerous parameters investigated in the sensitivity analysis, natural gas and CO_2 handling costs emerged as the most influential on the prospects of ammonia fuel. The lower efficiency of the ammonia value chain makes low-cost natural gas feedstock essential, whereas the potential of using the captured CO_2 for enhanced oil and gas recovery (EOGR) can strongly improve competitiveness. Thus, future ammonia fuel plants should be sited close to low-cost oil and gas operations that can productively utilize the CO_2 stream.

Despite these promising prospects of ammonia as a substitute for LNG, this transition demands substantial infrastructural, technological, and policy-level enhancements. Most importantly, a policy is needed to create a market for initially more expensive ammonia fuels, thereby stimulating the supply-side, distribution, and demand-side activity required to drive down costs via technological progress and scale. Despite the challenges, the shift towards blue ammonia could have far-reaching implications for the future global energy system, providing a cost-effective and secure fuel supply to mitigate climate change without jeopardizing the economic development prospects of billions of global citizens still living in poverty.

Sammendrag

Kostnadseffektiv dekarbonisering av den globale energiforsyningen blir stadig viktigere for å redusere de økende sosioøkonomiske kostnadene knyttet til klimaendringer. Denne masteroppgaven undersøker potensialet for å erstatte flytende naturgass (LNG) med blått ammoniakk produsert fra naturgass. Krigen i Ukraina har forverret globale bekymringer med tanke på energisikkerhet. Dette har ført til at diversifisering av energiforsyningen (for eksempel LNG-import fra flere leverandører i stedet for rørledninger fra Russland) har fått en betydelig interesse, noe som krever en omfattende analyse av økonomisk konkurranseevne, teknologisk gjennomførbarhet, og miljøimplikasjoner av disse energibærerne. Blått ammoniakk er lovende fordi den ikke slipper ut CO_2 ved forbrenning og er lett å flytendegjøre som muliggjør internasjonal handel ved skipsfart.

Denne oppgaven presenterer en teknisk-økonomisk analyse av LNG- og ammoniakkverdikjeden fra produksjonsanlegg i USA til importterminaler i Tyskland. Dette oppnås ved å modellere fire scenarier i Aspen Plus: et enkelt mellomstort anlegg (1x) og et storskala anlegg skalert opp med ti parallelle enkle anlegg (10x), for LNG og ammoniakk hver. Strømningsraten til naturgass som går inn til 1x- og 10x-anleggene er satt til omtrent 1,5 GW og 15 GW, henholdsvis. LNG-anlegget er modellert ved prosessen med forkjøling ved bruk av propan og blandet kjølemiddel (C3MR), og ammoniakkanlegget er modellert ved bruk av prosessen med membranassistert auto-termisk reformering (MA-ATR). For begge energibærerne antas det at 1x-anlegget importerer elektrisitet fra nettet, mens 10x-anlegget har et internt kraftverk. En konsekvent metodikk er deretter brukt til å utføre uavhengige økonomiske vurderinger for produksjonsanleggene, eksport- og importterminalene, og skipsfarten ved hjelp av Standardized Economic Assessment (SEA) Tool. Denne evalueringsmetoden oppfordrer til en konsekvent og pålitelig sammenligning av nøkkelindikatorene for hver energibærer.

Resultatene indikerer at selv om den endelige termiske effektiviteten for verdikjeden til ammoniakk er ∼30% lavere enn den for verdikjeden til LNG, oppnår ammoniakk økonomisk konkurranseevne mot LNG når fornuftige CO_2-skatter blir implementert. Ammoniakk treffer kostnadsparitet mot LNG ved en CO_2-skatt på \$104,08/tonn for 1x-anlegget og \$78,81/tonn for 10x-anlegget, når naturgass koster \$2,5/GJ, og strømprisen er \$60/MWh. Nivåjustert produksjonskostnad (LCOP) for 1x-anleggene resulterte i \$12,78/GJ for LNG og \$13,03/GJ for ammoniakk, noe som gjør ammoniakk 2% dyrere når CO_2-prisen er på \$100/tonn. I større operasjoner viser 10x-anlegg scenariene en LCOP på \$11.35/GJ for LNG og \$10.04/GJ for ammoniakk. Ammoniakkproduksjon krever mer strøm og kapital enn LNG-produksjon, og derfor tar ammoniakk-anlegget større nytte av skalafordeler og strømproduksjonen på stedet for 10x-anleggene enn LNG, og senker dermed kostnadene med 13%.

Av flere parametere som ble undersøkt i sensivitetsanalysen fremsto naturgass-prisen og kostnader knyttet til CO_2-håndtering de viktigste for utsiktene til ammoniakk. Ammoniakk har en mye lavere termisk effektivitet ved produksjon enn LNG, og dette indikerer at billig naturgass er viktig. I tillegg kan potensialet for å bruke trykksatt CO_2 til å forbedre olje- og gassutvinning (EOGR) sterkt påvirke og forbedre konkurranseevnen til ammoniakk. Derfor bør fremtidige ammoniakkproduksjonsanlegg være plassert i nærheten av lønnsomme olje- og gassoperasjoner slik at anlegget kan produktivt utnytte CO_2-en.

Til tross for lovende utsikter ved å erstatte LNG med ammoniakk, krever dette skiftet betydelige forbedringer i infrastruktur, teknologi, og politiske initiativer. Det viktigste vil være å fokusere på å skape et marked for den ammoniakken som allerede blir produsert for dermed å stimulere aktivitetet i forsyningskjeder, distribusjonsnettverk, og danne en etterspørsel som kreves for å drive ned kostnadene via teknologisk innovasjon og storskala utbygginger. Tatt utfordringene i betraktning, vil en overgang til blått ammoniakk kunne ha utbredte implikasjoner for det fremtidige globale energisystemet, og dermed gi en kostnadseffektiv og sikker energiforsyning uten å redusere økonomiske utviklingsmuligheter for milliarder av mennesker globalt.

Preface

This master's thesis concludes the 5-year M. Sc program in Energy and Environmental Engineering at the Norwegian University of Science and Technology (NTNU). This work was performed in the spring of 2023 within the Department of Energy and Process Engineering under the guidance of Jacob J Lamb and co-supervisors at SINTEF Industry, Schalk Cloete, and Carlos Arnaiz del Pozo.

The study dives into the potential for blue ammonia as an alternative to LNG. The study's groundwork is modeling a complete LNG liquefaction plant and a blue ammonia production plant in Aspen Plus and using these technical parameters for an economic assessment in the Standard Economical Assessment (SEA) Tool. It has been a privilege to delve into the realms of these energy carriers that have proven challenging and rewarding.

I am sincerely grateful to Jacob J Lamb and Schalk Cloete for their unmatched assistance this spring. Schalk Cloete's vast understanding and expertise in chemical processes and techno-economic assessments have been invaluable for this dissertation. I am grateful for their effort and time in helping me navigate this work; their contribution has been truly valued. Additionally, I want to thank Jacob J Lamb for allowing me to engage in such an exciting project and for his assistance in finalizing the thesis. Lastly, I would like to acknowledge my family for their constant support and friends for all the fun I had during my studies at NTNU.

Norwegian University of Science and Technology
Trondheim, June 2023

Øistein Farmen

Table of Contents

List of Figures

List of Tables

Nomenclature

Acronyms

ACF	Annualized cash flow
AGRU	Acid gas removal unit
APS	Announced Pledges Scenario
ASU	Air separation unit
ATR	Auto-thermal reforming
BEC	Bare erected cost
BM	Boston-Mathias
BOG	Boil-off gas
C3MR	Propane precooling mixed refrigerant process
CAPEX	Capital expenditure
CBAM	Carbon Border Adjustment Mechanism
CCS	Carbon capture and storage
CEPCI	Chemical Engineering Plant Cost Index
CH_3OH	Methanol
CHRE	Cryogenic heat recovery exchanger
CIS	Commonwealth of Independent States
CO_2e	Carbon dioxide equivalents
COCA	CO_2 avoidance cost
CS	Carbon steel
Cu	Copper
CWHE	Coil-wound heat exchangers
DMR	Dual mixed refrigerant
EOGR	Enhanced oil and gas recovery
EOS	Equation of state
EPC	Engineering, procurement, and construction
FOM	Fixed operational and maintenance costs
GSR	Gas switching reforming
GWP	Global warming potential
HFO	Heavy fuel oil
HP	High pressure
IEA	International Energy Agency
IPCC	Intergovernmental Panel on Climate Change
KBR	Kellogg, Braun and Root
LAC	Linde ammonia concept
LCOP	Levelized cost of product
LH_2	Liquefied hydrogen
LNG	Liquefied natural gas
LOHC	Liquid organic hydrogen carriers
LP	Low pressure
LPG	Liquefied petroleum gas
MA-ATR	Membrane assisted auto-thermal reforming
MCHE	Main cryogenic heat exchanger
MITA	Minimum temperature approach
MP	Medium pressure
MR	Mixed refrigerant
NG	Natural gas
Ni	Nickel

NPV	Net present value
NZE	Net Zero Emissions Scenario
OC	Owners costs
OECD	Organisation for Economic Co-operation and Development
OPEX	Operational expenditure
PC	Process contingency
PEM	Proton exchange membrane
POX	Partial oxidation
PT	Project contingency
R&D	Research and development
RKS	Redlich-Kwong Soawe
SCC	Specific capital cost
SMR	Steam methane reforming
SOC	Specific operating cost
SOEC	Solid oxide electrolyzers
SS	Stainless steel
STEPS	Stated Policies Scenario
STU	Storage, transport and utilization
TCR	Total capital requirement
Ti	Titanium
TOC	Total overnight cost
TPC	Total plant cost
VLGC	Very large gas carrier
VOM	Variable operational and maintenance costs

Symbols

ϕ	Capacity factor
C	Cost
E	Power demand
η	Efficiency
F_{BM}	Bare module factor
H	Enthalpy
J	Objective function
μ_{J-T}	Joule-Thomson coefficient
M	Million
Mt	Million tonnes
MTPA	Million tonnes per annum
LHV	Lower heating value
n	number of units
P	Pressure
Q	Heat
S	Entropy
SC	Specific consumption
SF	Split fraction
SPC	Specific power consumption
T	Temperature
TED	Thermal energy demand
TPA	Tonnes per annum
U	Internal energy

UA	Thermal transmittance
$	US dollar
V	Volume
VF	Vapor fraction
W	Work
Y	Capacity

Subscripts

CV	Control volume
r	Discount rate
el	Electricity
eq	Equivalent
e	Exit
i	Inlet
JT	Joule-Thomson
p	Permeate
P	Product
ST	Steam turbine
t	Time
a	Vaporous ammonia

Superscripts

e	train exponent
f	unit exponent

1 Introduction

1.1 Motivation

Global energy consumption has increased with an average growth per annum of 1.3% since 2011, with 2021 contributing to the most significant increase in history [1]. This increase was driven by emerging economies, with China as the largest source of growth. Following the trajectory in which the energy system is progressing, the energy demand is expected to increase by 19% to 2050 [2]. Half of the global population (∼4 billion people) still lives on less than $7/day [3]. These countries rather care about getting cheap and practical energy than mitigating climate change, which is a vital fact for rich-world citizens concerned about climate change to understand. However, the requirement to decrease emissions to align with 1.5-2.0°C temperature increase has left policymakers with projected scenarios to accomplish this by the end of the 21st century [2]. Accommodating this goal requires deep decarbonization of all sectors of the economy, where efforts are implemented for low-carbon electricity, heat, transportation, and industrial applications.

1.1.1 Decarbonizing the Natural Gas Sector

One of the significant contributors to world energy growth in the past decade is the increased use of natural gas, with a relative change of 25% [1]. However, the combustion of natural gas has a significant environmental impact, contributing to 22% of total CO_2 emissions in 2021. Large natural gas reserves remotely located have introduced LNG as an energy vector instead of a traditional pipeline infrastructure for natural gas trade. LNG has proven an economically viable option for the inter-regional trade of natural gas [4]. The LNG trade has introduced competition and diversification of the energy system in different parts of the world. China, India, and emerging countries are the primary growth markets for natural gas consumption [1]. Here, emerging markets have embraced natural gas-fired power plants for electricity generation, providing a cleaner alternative to coal.

The LNG value chain has evolved dramatically since it was introduced in the late 1960s and gained enormous interest in the past years due to large natural gas reservoirs located in inconvenient locations, facilitating a natural gas trade between countries [4]. Further, it is expected that this fuel source will likely dominate as the primary energy carrier during the first half of the 21st century due to its high energy density, high conversion efficiency, and lower carbon intensity compared to other fossil fuels [5]. The infrastructure supporting the LNG value chain is robust, including diverse production methods, sizeable LNG carriers, and extensive upstream and downstream pipeline networks across various regions [6].

Deep decarbonization of electricity production at a reasonable cost seems plausible, but the problem is that electricity currently only accounts for 20% of final energy consumption [2]. Fuels, on the other hand, account for 76% of final energy consumption, and their decarbonization is much more challenging. Hence, this is an area that needs urgent energy research, development, and demonstration attention.

As the natural gas value chain has a significant environmental impact, low-carbon options emerge to facilitate widespread decarbonization of the economy [7]. Securing climate neutrality not only in the power sector but across the entire economy presents a great techno-economic and societal hurdle. The hydrogen economy is a concept gaining renewed interest as a potential solution for extensive decarbonization. Hydrogen offers the possibility of replacing the use of fossil fuels in various sectors, including power, fuel, transport, industry, and residential buildings. While hydrogen is gaining recognition as a critical player in decarbonizing the global economy, it presents considerable logistical and economic challenges due to its low energy density, especially in transportation,

storage, and distribution [8]. As a result, ammonia is being explored as an alternative because of its advantageous properties, including its boiling point and storage capabilities [9]. Though primarily used in nitrogen-based fertilizer production, ammonia shows potential as a fuel source for thermal power generation and transportation and can be converted back to hydrogen when required.

Blue ammonia, produced from natural gas with integrated CO_2 capture, could prove as a viable energy carrier instead of LNG, heading towards a low-carbon economy. Ammonia has several advantages compared to LNG, including higher liquefaction temperature, easier storage, and handling, and does not emit any CO_2 upon combustion. Further, existing infrastructure, such as pipeline networks, LNG carriers, and exporting and importing terminals for the natural gas value chain, may be repurposed for facilitating the use of ammonia [10].

Interest in producing ammonia from fossil fuels with carbon capture is increasing, with new synthesis methods being introduced to minimize CO_2 emissions and improve the performance of blue ammonia plants [11]. Studies by Arnaiz del Pozo et al. 2022 consider a techno-economic analysis of a future ammonia production plant based on the gas-switching reforming (GSR) principle, compared to already existing plants utilizing the Linde Ammonia Concept (LAC) and Kellogg Braun & Root (KBR) production methods. Previous works by Cloete et al. 2020 emphasize a new ammonia production technology where MA-ATR is used for integrating CO_2 capture, providing a cost-effective alternative to reference plants [7].

1.1.2 Russia's Invasion on Ukraine

The global energy crisis, triggered by Russia's invasion of Ukraine, has severely disrupted Europe's energy supply, demonstrating the vulnerability of relying on a single, geopolitically complex source [2]. Russia, the world's largest exporter of fossil fuels, restricted its natural gas supply to Europe, transforming a post-pandemic recovery into a full-blown energy crisis. This sudden shift has led to unprecedentedly high prices for spot purchases of natural gas and significant increases in electricity costs worldwide. Europe, heavily reliant on Russian gas, has felt these effects severely, pushing governments to act swiftly to safeguard their citizens from the immediate impacts of the crisis, emphasizing the urgent need for energy security.

In response to the Russian gas shortage, Europe has significantly increased its import of LNG to help mitigate the shortfall [2]. This step highlights the crucial role of LNG in providing energy security in the current crisis. Europe's increased LNG demand has altered the global energy trade dynamics, diverting supplies from Asia, thus hampering developing world growth. This crisis underscores the importance of diversifying energy sources and strengthening resilience in energy value chains. The current situation has also restated the strategic value of accelerating renewable energy projects, improving energy efficiency, and adopting a balanced energy mix to reduce the risk of future disruptions and ensure long-term energy security.

1.2 Knowledge Gaps

Levelized costs for low-carbon fuels and corresponding CO_2 price intervals provide indispensable insights for global policymakers to facilitate the transition towards a greener economy. No existing literature has performed a comprehensive, bottom-up techno-economic evaluation of ammonia as a potential alternative to LNG as an energy vector. A study by Raj et al. 2016, investigated a techno-economic assessment of Canadian LNG production for Asian delivery [12]. Meanwhile, previous works by Arnaiz del Pozo et al. 2020 [11], and Cloete et al. 2020 [7], assess the competitiveness of newer, more efficient blue ammonia production techniques by determining levelized costs compared to reference plants. However, these studies do not address costs associated with exporting and importing terminals or shipping. In addition, the large uncertainties involved in any techno-

economic assessment mean that comparisons of LNG and ammonia costs calculated by different studies may be misleading. This highlights the need for a reliable comparison between these two energy vectors in a unified study.

1.3 Research Objective

This work strives to address this knowledge gap, conducting a techno-economic evaluation of ammonia as a potential alternative energy carrier to LNG. The study uses a consistent, bottom-up techno-economic method to determine the levelized cost of LNG and ammonia production. Additionally, the CO_2 avoidance cost (COCA) for ammonia production is computed, revealing the CO_2 price points at which ammonia proves economically competitive with LNG in international energy trade. A sensitivity analysis is included to evaluate the impact of various parameters on LCOP and COCA.

A C3MR LNG plant and an MA-ATR ammonia plant are modeled in Aspen Plus under similar assumptions, facilitating a direct comparison. These models provide technical performance parameters, which are then employed in an economic assessment to estimate capital and operational costs. The scope of the thesis, illustrated in Figure 1, contains the production plants, export terminal, shipping, import terminal, and downstream emissions in the LNG value chain. To reduce European reliance on Russian gas, the trade route selected for this study is from Sabine Pass, US, to Wilhelmshaven, Germany.

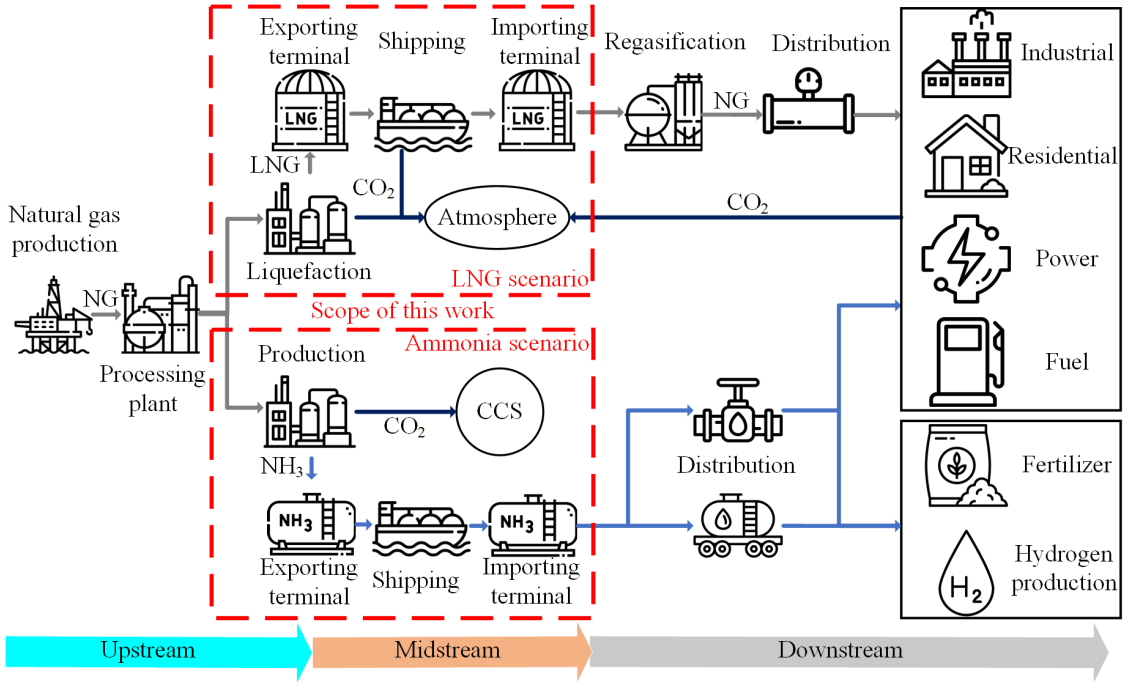

Figure 1: Graphical representation of the LNG and blue ammonia value chains, including the techno-economic components analyzed for the scope of this thesis. CO_2 is released into the atmosphere in the LNG value chain while its captured, transported and stored in the ammonia value chain.

Historically, large gas reservoirs are required for the realization of LNG projects [13]. Commercialized natural gas-based ammonia plants typically possess lower capacities than base-load LNG facilities [4]. However, the increasing demand for natural gas has led to profitable extraction from smaller reserves for international LNG trade. This study addresses this by considering two plant sizes for LNG and ammonia facilities. The first involves a single-train approach where electricity

from the grid is used for plant auxiliary components. The other approach scales the plants by introducing ten trains, capitalizing on economies of scale via a modular scaling factor, reflecting the cost advantages of increasing production. High power consumption in the 10x train plants necessitates an internal power plant consuming natural gas and hydrogen as fuel in the LNG and ammonia plants.

1.4 Outline of the Thesis

Section 2 includes the necessary background information, thermodynamic principles, economic fundamentals, a literature review of LNG and ammonia, and summarizing the goals for the thesis. It also includes a comprehensive review of the existing literature. Subsequently, Section 3 explains the technical assessment conducted via modeling the C3MR LNG and MA-ATR ammonia plants using both single and ten-fold train approaches in Aspen Plus. In addition, Section 4 provides a detailed breakdown of the economic assessment for all four scenarios, encapsulating capital and operational costs. The essential performance parameters, derived from the Aspen Plus sheets, are expressed in Section 5, along with an economic assessment executed to estimate the final levelized costs and CO_2 avoidance cost for each scenario. In conclusion, the most significant aspects of this study are summarized in Section 6.

Since this is a continuation of the project thesis, parts of the theory and methodology are reused for this master thesis. For the theory, this includes the introduction in Section 2.1, Sections 2.1.2, 2.1.3, 2.2, and parts of Section 2.4. Additionally, as the C3MR LNG plant was modeled in the project thesis, however, with different input parameters and flow rates, parts of methodology in Section 3 are reused from previous work.

2 Theory

2.1 Background

The need for energy transportation is crucial to ensure reliable energy access worldwide. An energy vector or carrier is a substance or a physical phenomenon that can be converted into mechanical work or heat. This energy carrier acts as an energy transmitter, moving energy from primary sources in the value chain to the user. Various forms of energy carriers exist, such as electricity, heat, and fuels in solid, liquid, and gaseous states [14]. The type of technology used for energy transportation depends on the physical composition of the energy carrier. For example, liquid energy carriers are moved through pipelines or tanks, solid energy carriers are shipped or transported by trucks or rail wagons, and electricity is sent through power grids. One major downside with energy carriers is that each conversion step leads to energy loss and carbon emissions. Additionally, more advanced and complex conversion processes require more expensive equipment and higher capital investments [15]. The cost-benefit from using primary energy sources determines an energy carrier's market reach.

Various strategies and methods transport energy from the primary source to the end user. The choice of energy carrier depends on availability, transportation distance, cost, and demand [4]. New energy carriers are being introduced as the world moves towards more sustainable and flexible energy systems. The net or lower heating value (LHV) is the energy content of the fuel, not including the heat recovery from the water vapor. For gaseous and liquid energy carriers, the amount of energy packed into a given volume, or volumetric energy density, is more critical than specific energy. With lower volumetric energy density, larger tanks and pipelines are needed to provide the same energy. Figure 2 shows different energy carriers and their volumetric energy density.

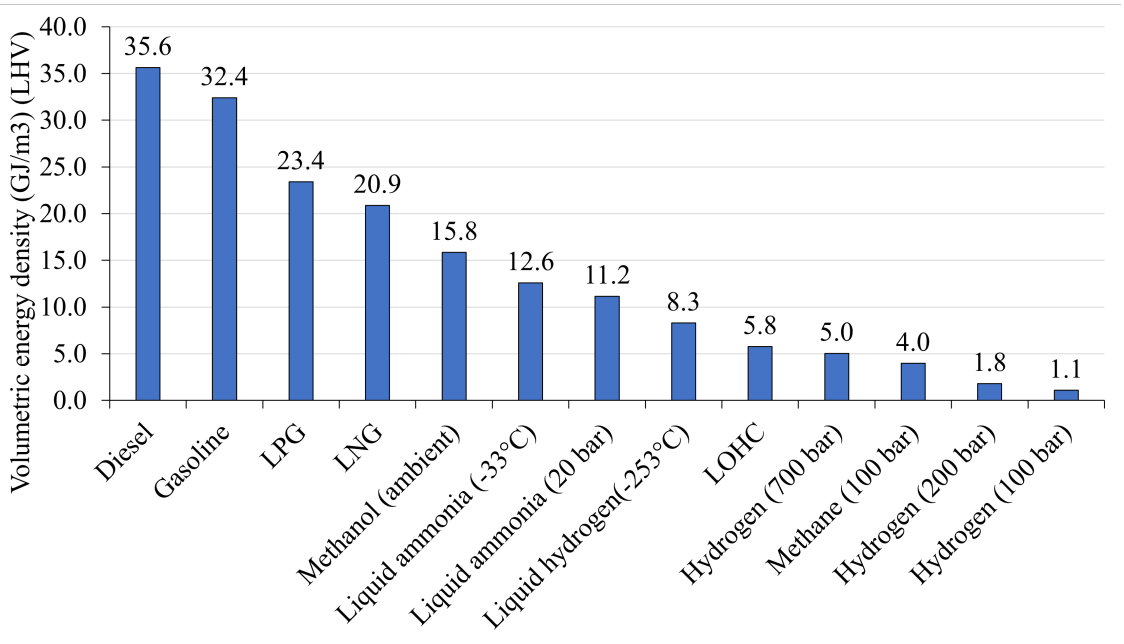

Figure 2: Volumetric energy density of various energy carriers under normal operating conditions [16].

2.1.1 IEA's Scenarios for the Next Three Decades

The International Energy Agency (IEA) has formulated four unique scenarios to simulate and forecast upcoming energy patterns and their possible effects on the worldwide environment and economy. These scenarios include the Stated Policies Scenario (STEPS), Accelerated Energy Transition Scenario (APS), and Net Zero Emissions (NZE) [2]. According to the scenarios, these policies will be used when evaluating LNG and ammonia's role as energy carriers in 2030 and 2050. Future projections for production rates, demand, and CO_2 prices in various regions will be discussed.

The Stated Policies Scenario (STEPS) mainly represents current policies and actions declared by governments across the globe, functioning as a foundation for grasping the global energy system's course. The Accelerated Energy Transition Scenario (APS) proceeds a step further, exploring the potential consequences of an even quicker and more extensive adoption of eco-friendly energy technologies, focusing on renewable sources and energy conservation. Finally, the Net Zero Emissions (NZE) scenario describes a world that has zero greenhouse gas emissions by 2050, accomplished through bold policy initiatives, technological advancements, and shifts in human behavior.

2.1.2 Electricity, Coal and Oil

Electricity, an energy carrier, originates from primary energy sources. It travels from producers to consumers via an electrical grid. Over the next two decades, reliance on electricity as an energy carrier is projected to increase [17]. Low-carbon electricity from renewable sources is set to triple, while high-carbon electricity could be reduced by half. However, one major drawback of electrical power grids is transmission losses. When electricity is sent over longer distances, the power line's temperature rises, resulting in thermal energy losses [18]. For instance, a high-voltage direct current line loses 3% of its power per 1000 km, and a subsea setup loses 10%, respectively. Despite these challenges, electricity is the primary energy carrier for short and medium distances.

Coal, a solid substance of carbon and hydrocarbons, forms over millions of years when plant matter is subjected to heat and pressure. Since the 1880s, coal has played a significant role in electricity generation. Power plants use coal to produce high-pressure steam, which drives turbines. As per BP's Energy Outlook, coal contributes 36.7% of global electricity production [1]. Various methods transport coal from mines to markets, including railroads, trucks, barges, conveyors, pipelines, and dry bulk ships. Despite being abundant and cost-effective, coal is the largest emitter of CO_2, responsible for 40% of total CO_2 emissions by fuel type. Therefore, shifting away from coal-fired power plants and implementing alternatives to lower emissions is crucial.

Crude oil, a thick black liquid composed of hydrocarbon mixtures, develops over millions of years when organic material is buried under specific rock formations and exposed to heat and pressure. Since the mid-19th century, oil wells have been a vital energy source. Products derived from crude oil are used for heating, electricity generation, and transportation. Crude oil's varying hydrocarbon chain lengths account for its diverse applications. Refineries process petroleum, separating and sorting hydrocarbons based on end-user requirements. The most common petroleum products include gasoline, diesel, and jet fuels. In 2021, oil comprised 29% of global primary energy consumption [1]. Crude oil is transported from wells to refineries, including tankers, pipelines, trucks, and railroads. The chosen transportation method depends on factors like volume and destination. Trucks offer flexibility for short-distance transport, while railroads are cost-effective for long-distance transport when pipelines are not an option. Oil tankers are ideal for global transportation due to their large capacity, offering a lower cost per barrel than railroads. Pipelines, however, are the most economical, safe, and energy-efficient oil transportation method, making them the preferred choice for all distances.

2.1.3 Natural Gas

Natural gas is produced from oil wells, natural gas fields, or coal beds and primarily consists of methane. This compound is used for electricity generation, heating, transportation, and raw material production. In 2021, natural gas comprised 22.9% of global electricity generation [1]. Figure 3 illustrates the world's total natural gas reserves by region, with the Middle East and Commonwealth of Independent States (CIS) countries holding the most significant shares at 40.2% and 30.1%, respectively [19]. Natural gas use is rising and is projected to be the fastest-growing fossil fuel. Its combustion results in significantly lower greenhouse gas emissions than other fossil fuels [20]. Natural gas-fired power plants are considered vital in phasing out coal-fired power plants and reducing emissions in the medium term [21]. According to Intergovernmental Panel on Climate Change (IPCC), natural gas is the cleanest burning fossil fuel [22]. Gas-fired power plants have the highest power generation efficiency compared to conventional power plants, reaching up to 63% in a combined cycle approach [23]. However, as a fossil fuel, its long-term strategy remains uncertain in the context of emerging renewable energy sources.

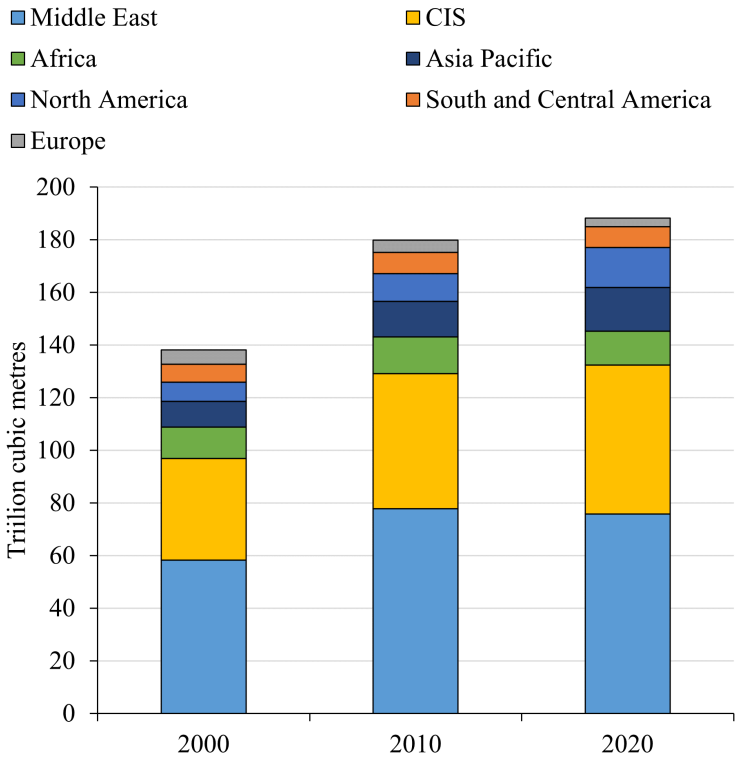

Figure 3: Total proved reserves of natural gas by region in 2000, 2010 and 2020 [19]. Commonly understood as the volumes, which according to geological and engineering data, can be reliably extracted from identified reservoirs in the future, given the present economic and operational conditions.

Abundant and versatile natural gas reserves are located worldwide. With current reserves and consumption rates, about 48 years of natural gas are left [19]. Natural gas is also crucial for energy security, the uninterrupted energy availability at an affordable price. With the increased reliance on renewable energy sources, maintaining a high level of energy security becomes essential. Unlike solar and wind power technologies, natural gas-fired power plants offer flexibility with fast start-up and shutdown times. Given its high energy content, high thermal efficiency, and low greenhouse gas emissions, natural gas is a sensible choice to replace coal-fired power plants.

The global warming potential (GWP) measures the heat absorbed by a greenhouse gas in the atmosphere, expressed in carbon dioxide equivalents (CO_2-eq), with CO_2 having a GWP of 1. The climate change impact of greenhouse gases is determined by their duration in the atmosphere and heat absorption capacity. Methane, a potent greenhouse gas, has a GWP 80 and 25 times higher than CO_2 over 20 and 100 years, respectively [24]. Methane has contributed to 30% of the rise in global temperature since the industrial revolution [25], highlighting the importance of preventing natural gas leaks.

Gas flaring, burning natural gas during oil and gas extraction, is often employed for safety and economic reasons. Although it wastes resources that could be used otherwise, gas flaring helps manage the high and variable pressures associated with extraction. Supply often exceeds demand in remote and inaccessible areas due to logistical and economic challenges in transporting the gas for processing. Without regulations, gas flaring becomes the most economically viable option for operators. According to the IEA, gas flaring in 2021 released 270 Mt of CO_2 and 8 Mt of methane (200 Mt CO_2-eq), accounting for 1.15% of the total CO_2 emissions that year.

The Natural Gas value chain

The natural gas value chain comprises several integral components and processes for delivering gas to end users. Figure 4 provides an overview of this value chain, which includes natural gas production, transmission, and distribution. Natural gas is gathered from wells both onshore and offshore, with a gathering system of small pipelines connecting the well to a significant pipeline or processing plant.

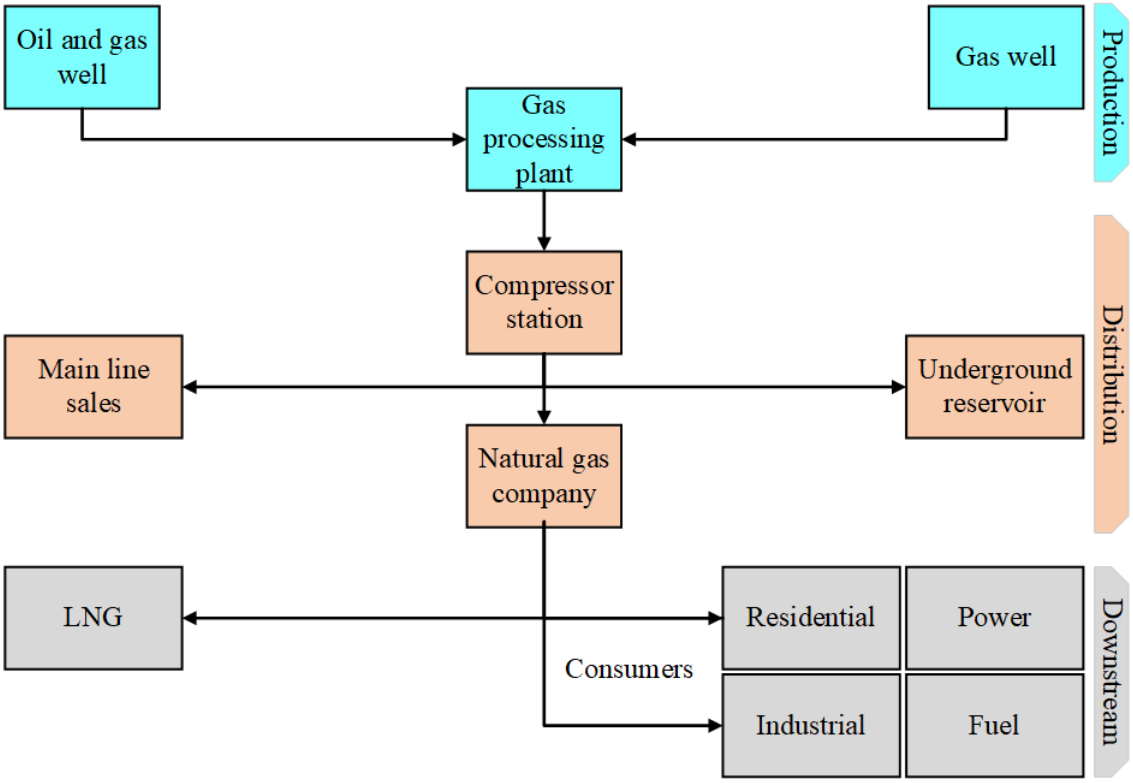

Figure 4: The natural gas value chain, including production, distribution and downstream uses [26].

Extraction and Processing
The composition of natural gas extracted from the well varies based on the production field and reservoir characteristics, requiring treatment at a processing plant to ensure safe and efficient operation within the distribution network. There are two types of natural gas, wet and dry. The gas is classified as dry if the methane content exceeds 85%. Wet natural gas, apart from methane, typically contains water vapor and heavier hydrocarbons such as ethane, propane, butane, and pentane. It also commonly includes nonhydrocarbons such as alkanes, carbon dioxide, nitrogen, and hydrogen sulfide. Natural gas liquids like propane, butane, and pentanes are sold separately from the natural gas stream. Dry natural gas, the end product, must meet quality and safety standards to be sold as consumer-grade pipeline natural gas.

Transportation and Storage
The reservoir and processing plant are often located far from demand centers, facilitating the global trade of natural gas. High-pressure pipeline networks are the traditional method for transporting natural gas, designed for fast and efficient movement from the processing facility to high-demand areas. These pipelines are commonly used for domestic transport and across state borders. In reducing the volume of gas and further meeting transportation requirements, natural gas pipelines operate under high pressure, maintained by compressor stations placed periodically along the pipe, usually at intervals of 75 to 150 kilometers [27].

Natural gas sees seasonal demand, with higher usage in the winter for heating [4]. Thus, natural gas is injected into storage fields during lower-demand summer months for withdrawal in the high-demand winter period. Maintaining high pressure in the pipeline for efficient fuel transport is also crucial, hence using storage facilities to ensure constant pressure. These facilities can be aquifers, depleted gas reservoirs, or salt caverns, with depleted fields being the most common storage method, accounting for 80% in the United States [28]. Gas is injected into these facilities, creating pressure to create a storage tank. Natural gas can also be stored as LNG, reducing its volume and allowing storage in tanks, further discussed in Section 2.4.

2.1.4 Hydrogen

Hydrogen and its derivatives could play a critical role in decarbonizing sectors where it is challenging to abate emissions and implement alternative solutions [29]. Hydrogen, a chemical energy carrier, is versatile, capable of generating heat and power through an electrochemical process in a fuel cell. Unlike a battery, fuel cells do not require recharging and continuously provide heat and power as long as fuel is supplied. In this process, the only by-product is water vapor. Fuel cells can operate at efficiencies exceeding 60%, surpassing what is achievable by internal combustion engines [30]. Hydrogen is predominantly used in petroleum refining, fertilizer production, metal treatment, and food processing [31].

As of 2021, the demand for hydrogen is almost entirely met by fossil fuels, with natural gas and coal accounting for 62% and 19%, respectively [10]. The share of hydrogen production as a by-product from oil stood at 18%. Low-emission hydrogen production, whether from fossil fuels with carbon capture or through electrolysis, accounted for just 0.74% of total production in 2021. Global hydrogen production reached 94 Mt, with associated CO_2 emissions of 900 Mt. China is the largest consumer of hydrogen, with a 30% share, followed by the United States and the Middle East, each with a 12% share [32]. Given current policy settings, hydrogen demand is projected to increase to 115 Mt by 2030 [10], with most of this growth coming from traditional industrial applications.

The traditional method of hydrogen production from fossil fuels results in significant greenhouse gas emissions [10]. Alternative hydrogen production methods are necessary to meet various emission targets set by policymakers. Carbon capture utilization and storage (CCS) could be implemented in

existing hydrogen production plants that use fossil fuels as a raw material input. CCS technologies are expected to become increasingly important for decarbonizing the hydrogen value chain [29]. Moreover, as renewable energy capacity grows, viable storage options become necessary. Hydrogen production could offer a direct storage solution for renewable electricity through the electrolysis process in fuel cells when power demand is low.

Hydrogen value chain

The hydrogen value chain is presented in Figure 5 and includes activities from the production to the downstream uses. The process begins with production, achieved through various methods. The produced hydrogen is then stored and transported, which can present significant challenges due to its low density and reactivity [33]. These stages may involve technologies such as high-pressure tanks, cryogenic storage, pipelines, or carriers like liquid organic hydrogen carriers (LOHCs) and ammonia. The value chain also includes distribution infrastructure to get hydrogen to the end user, such as industrial consumers, hydrogen fueling stations for vehicles, or power plants for electricity generation. Finally, the value chain includes the end use of hydrogen, such as fuel cells, industrial processes, or power generation.

Production

Hydrogen can be produced through various methods, including steam methane reforming (SMR), auto-thermal reforming (ATR), gasification, and electrolysis. The most common method, SMR, involves reacting natural gas with steam under high temperatures and pressures in the presence of a catalyst, producing a hydrogen-rich mixture composed of carbon monoxide, carbon dioxide, and hydrogen [32]. While SMR does lead to carbon dioxide emission, its environmental impact can be mitigated by implementing carbon capture and storage technologies.

Gasification is another fossil fuel-based hydrogen production method. This method for producing hydrogen is a process that transforms materials rich in carbon, such as coal, biomass, or waste, into synthesis gas, also known as syngas. This mixture contains hydrogen, carbon monoxide, and carbon dioxide. The process involves preparing and gasifying the feedstock under either partial oxidation or steam reforming conditions. Further, the syngas is cleaned before generating hydrogen through the water-gas shift reaction. Finally, the hydrogen is purified using pressure swing adsorption or membrane separation. This versatile technique for hydrogen production can make use of a variety of feedstocks and be combined with carbon capture and storage solutions. However, the overall efficiency and environmental effects are influenced by factors such as the type of feedstock, the gasification technology employed, and the methods used for processing syngas.

Electrolysis is a different approach to hydrogen production, using electrical energy to split water molecules into hydrogen and oxygen. This process involves an electrolyzer, which houses an anode and a cathode separated by an electrolyte. When an external voltage is applied, water molecules disintegrate into protons and oxygen gas at the anode. The free protons move to the cathode, reacting with electrons to form hydrogen gas. The characteristics of electrolyzers vary depending on the electrolyte material used, with the three main types being proton exchange membrane (PEM), alkaline, and solid oxide (SOEC) electrolyzers. Factors like electrode materials, electrolyte type, and applied voltage can influence the efficiency of the electrolysis process [30]. The potential to couple hydrogen production with renewable energy sources has brought electricity-based feedstocks to the forefront of interest in hydrogen production.

Hydrogen Based Fuels

Hydrogen can be combined with other elements, such as carbon or nitrogen, to make hydrogen-based products. Hydrogen-based energy carriers include compounds that store and transport

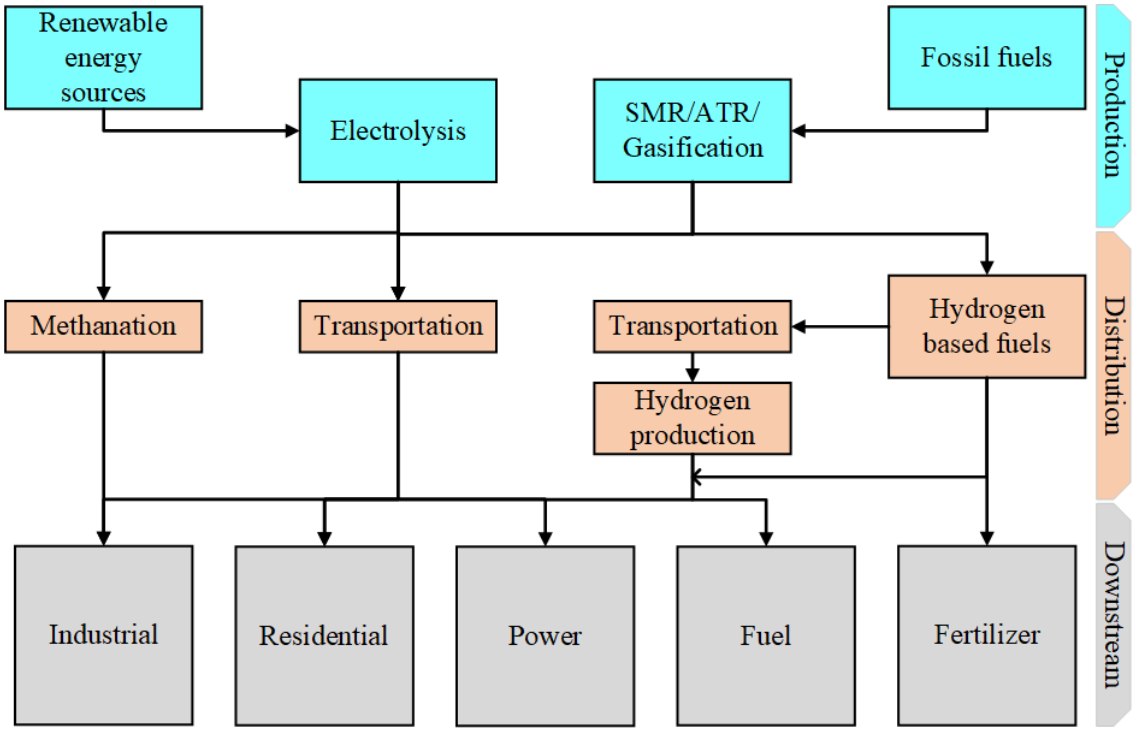

Figure 5: The hydrogen value chain, including production, distribution and downstream uses [34].

hydrogen for subsequent energy conversion. Hydrogen at its molecular level is the most direct and standard form, but its gaseous state at ambient conditions can pose challenges in storage and transportation [29]. To overcome these issues, alternative hydrogen carriers have been developed. Ammonia (NH_3) is a prominent example, containing 17.6% hydrogen and offering high volumetric energy density [35]. Other hydrogen carriers are LOHC and synthetic hydrocarbons. Methanol (CH_3OH) is an example of a LOHC derived from hydrogen and carbon dioxide, with a hydrogen content of 12.6%. Nevertheless, implementing liquefied hydrogen and LOHCs encounters obstacles mainly due to significant conversion losses and low technology readiness levels at specific stages [33].

Transportation and Storage

Similar to coal, oil, and natural gas, chemical energy carriers can be stored and transported over longer distances. Transportation and storage of hydrogen, a vital aspect of the emerging hydrogen economy, entails the vital parts of the value chain of hydrogen from production facilities to end-users. Gaseous hydrogen can be distributed through high-strength steel or advanced polymeric pipelines [36]. Despite its considerable initial capital investment, it can offer a cost-effective solution for long-term hydrogen distribution [37]. Alternatively, liquefied hydrogen (LH_2) can be transported in cryogenic tankers, requiring energy-intensive cooling systems to maintain the hydrogen at -253°C.

Transporting hydrogen as a gas presents several challenges due to its inherent properties, which can impact the efficiency and safety of the process [33]. At ambient conditions, hydrogen has a low mass density of 0.09 kg/m^3 [35]. Facilitating proper transportation and storage conditions includes either compression up to pressure levels of around 700 bar or cryogenic cooling to -253°C to achieve liquefaction [38]. The high pressures and low temperatures involved require specialized materials and containers to minimize leakage, embrittlement, and pressure fluctuations. Secondly, hydrogen's low volumetric energy density, even when compressed or liquefied, implies that large volumes must be transported to meet energy demands, potentially increasing costs and logistical

complexities. Furthermore, hydrogen's flammability and wide range of flammable concentrations in the air pose safety risks during transportation and necessitate strict precautions [39].

Ammonia could be a feasible alternative to gaseous hydrogen due to several advantageous properties. It exhibits a high hydrogen content, and volumetric energy density, thus enabling more efficient transport and storage [35]. Ammonia can be stored as a liquid at relatively moderate pressures at around 10 bar or low temperatures at -33°C, requiring less energy-intensive containment systems than gaseous hydrogen [40]. Additionally, ammonia benefits from an established production and distribution infrastructure in the fertilizer industry, facilitating its integration into the hydrogen economy. However, it is essential to consider ammonia's toxicity and pungent odor, which necessitate careful handling and safety measures during transportation and storage. Despite these challenges, ammonia offers a promising solution for hydrogen transportation due to its good energy density and existing infrastructure, as long as safety concerns are adequately addressed.

2.2 Thermodynamic Fundamentals

Thermodynamic relations presented in Sections 2.2.1-2.2.4 are derived from "*Fundamentals of Engineering Thermodynamics, 9th Edition*" by Moran et al. 2018 [41].

2.2.1 First and Second Law of Thermodynamics

The fundamental thermodynamic relations are the first and second laws of thermodynamics. The first law of thermodynamics describes the conservation of energy, and it states that energy can neither be created nor destroyed. For a change in internal energy (U), in terms of heat flow into the system (δQ), and work done by the system (δW) for a closed system may be written

$$\delta U = \delta Q - \delta W \tag{1}$$

The second law of thermodynamics states that the entropy of an isolated system (dS) never decreases

$$dS \geq 0 \tag{2}$$

Then according to the second law of thermodynamics from Equation 2, we have a reversible process with $\delta Q = TdS$. By letting the work done by the system on its surroundings be reversible $\delta W = PdV$, and substituting from Equation 1, the internal energy in terms of temperature (T), entropy (S), pressure (P), and volume (V) may be written

$$dU = TdS - PdV \tag{3}$$

By using thermodynamic potentials, the internal energy expressed in terms of enthalpy (H) is

$$dH = TdS - VdP \tag{4}$$

For a control volume (CV) involving a steady-state process. Mass enters and leaves the system as shown in Figure 6, where heat and work interact with the surroundings.

For a steady-state process, the total energy contained in the control volume is constant. Therefore the energy change of the system is zero. Then the first law of thermodynamics from Equation 1, can be expressed as

$$\dot{Q}_{CV} - \dot{W}_{CV} = \sum_i \dot{m}_i h_i - \sum_e \dot{m}_e h_e = 0 \tag{5}$$

where i is the inlet stream and e is the outlet stream, $\dot{Q}_{CV}$ and $\dot{W}_{CV}$ is the rate of energy transfer as heat and work done by the control volume derived from Equations 3 and 4, $\dot{m}$ and h is the fluid mass flow rate and the specific enthalpy of the fluid, respectively.

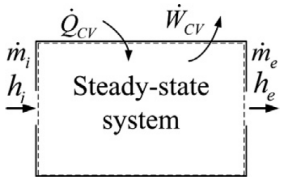

Figure 6: A control volume of mass, enthalpy, heat, and work interactions.

2.2.2 Refrigeration Cycle

Refrigeration is a cyclic principle used to transfer heat from a substance with a low temperature to a substance with a higher temperature. The most common method of transferring heat is using a vapor-compression cycle. This cycle consists of four components, compressor, condenser, expansion valve, and evaporator. Figure 7 presents an overview of a refrigeration cycle.

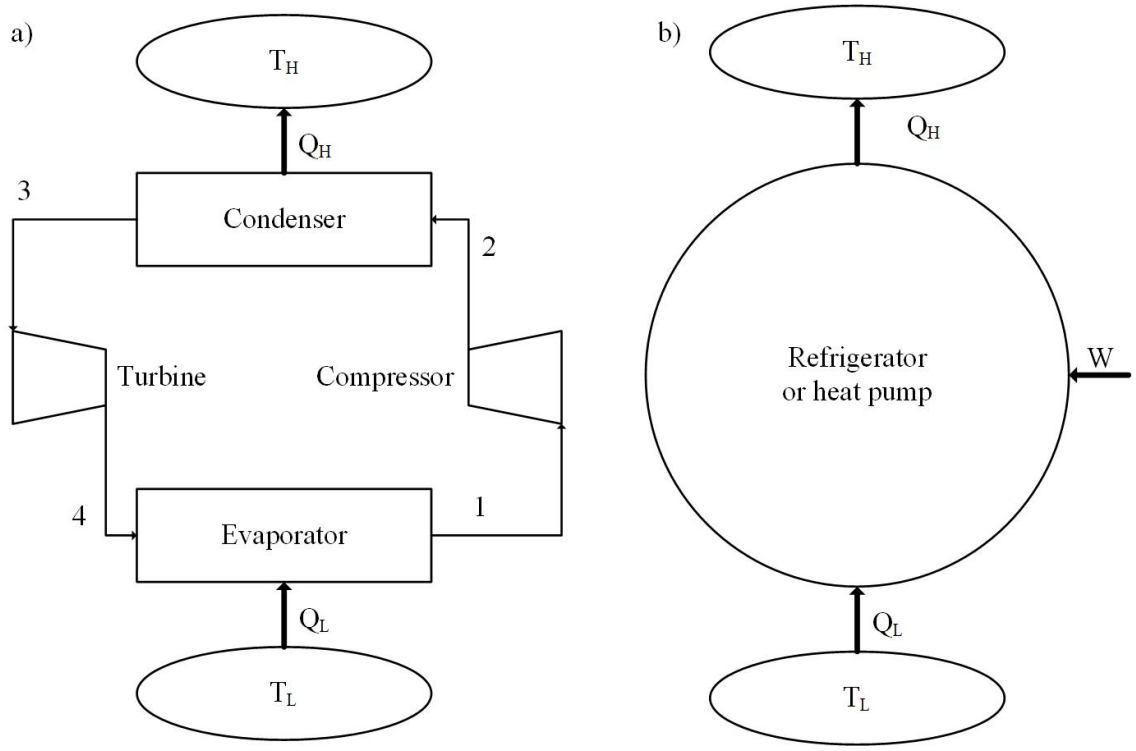

Figure 7: a) The vapor compression refrigeration cycle, and b) schematic of a refrigeration cycle.

From the evaporator, the refrigerant absorbs heat (Q_L) from a low-temperature substance. For the refrigerant to reach condensing pressure, a compressor with power input (W) is used to increase the pressure of the working fluid. In the condenser, the high-temperature working fluid rejects heat by cooling into the liquid state to a lower-temperature substance. Before the evaporator inlet, the working fluid passes through an expansion valve to decrease pressure and give a low temperature to ensure a two-phase mixture. Figure 7b) shows a simplified schematic of the refrigeration cycle.

A Carnot cycle is a useful theoretical model for further understanding the refrigeration principle. This cycle is a model of a heat engine where the addition of heat energy produces energy in the form of work. Here, work is added to the system to provide heat rejection for the high-temperature sink. The process can be describes using the following approach:

(1→2) Work is added to the system for an ideal compression at constant entropy; this increases the refrigerant temperature.

(2→3) Heat rejection of the refrigerant due to the surrounding temperature T_h.
(3→4) Ideal expansion at constant entropy, decrease in pressure and temperature of the refrigerant.
(4→1) Heat absorption from the heat source at constant evaporation temperature T_L.
The reversed Carnot cycle is shown as pressure-enthalpy and temperature-entropy diagrams in Figure 8.

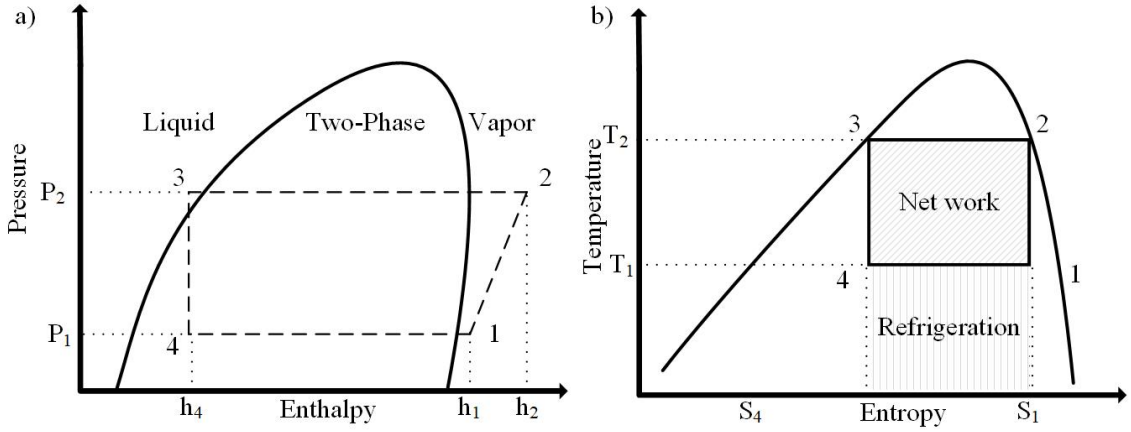

Figure 8: a) Diagram for the reversed Carnot refrigeration cycle for pressure-enthalpy, and b) temperature-entropy [42].

In all reversible types of refrigerant systems, the heat source and sink are assumed to occur at zero temperature difference. Therefore, the condensing temperature (T_H) during the heat rejection process and evaporating temperature (T_L) during the heat absorption process are equal to the ambient temperature.

The refrigeration effect Q_L is shown in Figure 8a and is expressed as

$$Q_L = T_L \cdot (S_1 - S_4) \tag{6}$$

where S_4 and S_1 is the entropy before and after the evaporator, respectively. With the first law of thermodynamics from Equation 1, the compressor work for the reverse Carnot cycle (W_{rev}) can be the expressed as

$$W_{rev} = (T_H - T_L) \cdot (S_1 - S_4) \tag{7}$$

2.2.3 Liquefaction of Gases

The liquefaction of gases is done by refrigerating the gas to temperatures below the critical temperature. Here, the liquid is formed at a suitable pressure below the critical pressure. First, the gas is compressed to a higher pressure. The high-pressure gas passes through a countercurrent heat exchanger. After the heat exchanger, some liquid is produced. Then, the gas is sent through an expansion process. The low-pressure and temperature gas is again sent into the compressor.

The countercurrent heat exchanger heats the low-pressure gas before the compression and cools the gas before expansion. The principle behind refrigeration is that the process gas absorbs heat from environments with lower temperatures. Therefore, some components in the liquefaction process are placed in ambient temperatures where heat is rejected to a coolant. In this compression and cooling process, the enthalpy and entropy of the gas stream are reduced. Temperature reduction is accomplished due to the heat exchange between the cool and hot gas and further cooling in the expansion process. There are two expansion processes used for cooling. First, a throttling device can cool the process gas by an isenthalpic expansion. This process is known as the Joule-Thomson

effect, and it is expressed as

$$\mu_{JT} = \left(\frac{\partial T}{\partial P}\right)_H \tag{8}$$

where μ_{JT} is the Joule-Thomson coefficient, H is the enthalpy, and S is the entropy. The coefficient is a property of each specific gas and can be negative, zero, or positive. The second method of reducing temperature through an expansion process is adiabatic expansion through a device that produces work. For an ideal case, this process is reversible and, therefore, isentropic. Further, the isentropic expansion coefficient is defined as

$$\mu_S = \left(\frac{\partial T}{\partial P}\right)_S \tag{9}$$

Expansion by a throttling valve in Equation 8 is known as the internal work method. Using an expansion engine in Equation 9 produces work by removing energy from the gas and is also known as the external work method.

2.2.4 Pinch Analysis

Heat exchangers in liquefaction processes often demand a high amount of energy, making it essential to optimize them for reduced energy consumption. One approach to achieve this optimization involves pinch analysis, a methodology aimed at minimizing the energy consumption of a process plant. This method involves analyzing heat flows, establishing energy targets, defining process improvements, and identifying inefficiencies. Within the context of pinch analysis, heating and cooling streams couple according to heat load against temperature. A typical representation of hot and cold composite curves is presented in Figure 9. The point on these curves where the closest approach occurs is the pinch point, representing the area of greatest constraints within the process. Achieving the energy target involves using heat exchangers to recover the hot and cold streams within two separate systems.

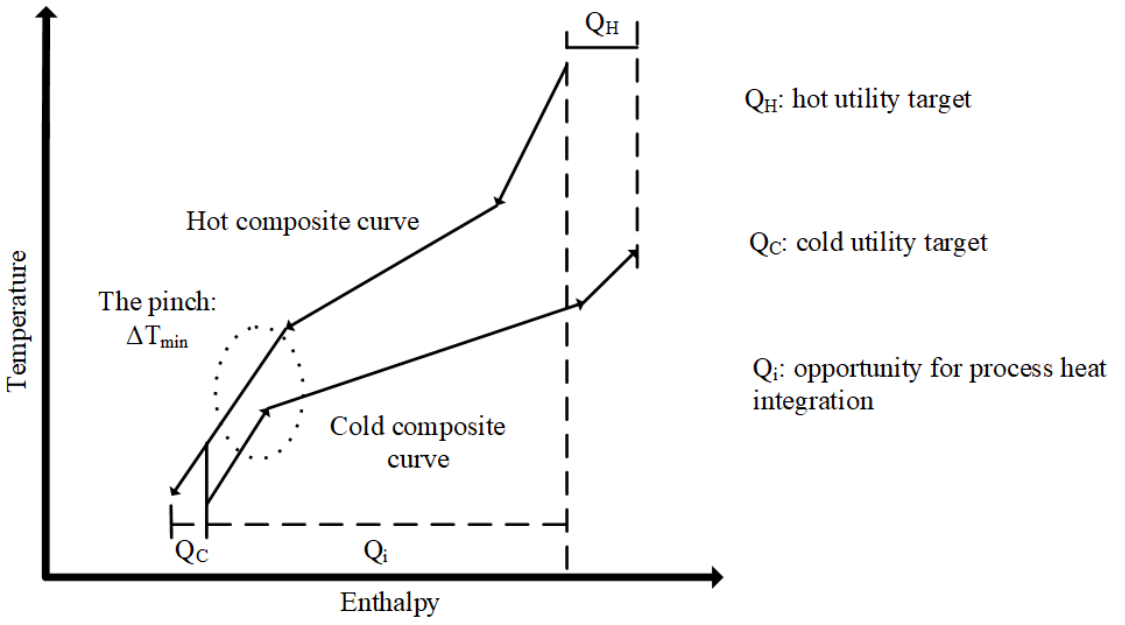

Figure 9: Typical hot and cold composite curves in a pinch point analysis [43].

The implementation of pinch analysis methodology allows for calculating the minimum heat requirement necessary for heat exchangers to meet their energy targets. However, this method presents limitations due to the temperature being the sole parameter of the streams. In cryogenic

liquefaction systems, compression and expansion processes alter the condensation and boiling temperatures required for heat transfer. As a result, a close relationship exists between compressor power and pressure levels and the temperature approach. Therefore, the hot and cold composite curves determine the required refrigeration duty.

2.2.5 Key Performance Indicators

A set of standard metrics are outlined to assess energy and environmental performance, particularly CO_2 emissions. The essential product efficiency (η_P) is determined using Equation 10, which considers the LHV of both natural gas input and the output from the plant. To calculate the net efficiency (η_{net}), the electricity consumption ($\dot{W}_{net}$) is taken into account, assuming that the energy value of the product is similar to that of electricity, presented in Equation 11.

$$\eta_P = \frac{\dot{m}_P \cdot LHV_P}{\dot{m}_{NG} \cdot LHV_{NG}} \tag{10}$$

Here, $\dot{m}_P$ and $\dot{m}_{NG}$ are the product and natural gas mass flow rates, respectively. Further, LHV is the lower heating value where P, and NG denote the product and natural gas value. To accommodate for electricity usage, equivalent natural gas consumption is determined by adjusting for the electricity. This is achieved by dividing the electricity consumption by a heat-electricity equivalent (η_{el}) of 63%, which is characteristic of a combined cycle power plant [44]. The equivalent natural gas consumption is then employed to calculate an equivalent product efficiency $\eta_{P,eq}$ in Equation 12.

$$\dot{m}_{NG,eq} \cdot LHV_{NG} = \dot{m}_{NG} \cdot LHV_{NG} + \frac{\dot{W}_{net}}{\eta_{el}} \tag{11}$$

$$\eta_{P,eq} = \frac{\dot{m}_P \cdot LHV_P}{\dot{m}_{NG,eq} \cdot LHV_{NG}} \tag{12}$$

Here, $\dot{m}_{NG,eq}$ is the equivalent natural gas mass flow rate. The specific power consumption (SPC) is the amount of electricity used per product delivered. It is an important metric to assess the thermodynamic performance of any liquefaction and production scheme [45]. The metric provides the amount of product that can be reached given a certain available power. It is measured in kWh/tonne and defined as

$$SPC = \frac{E_{el}}{\dot{m}_P \cdot \phi \cdot 3.6} \tag{13}$$

Here, E_{el} is the power demand, and ϕ is the capacity factor. In addition to these efficiencies, specific consumption SC and equivalent specific consumption SC_{eq} are widely-used performance indicators, defined in Equation 14 and Equation 15, respectively.

$$SC = \frac{\dot{m}_{NG} \cdot LHV_{NG}}{\dot{m}_P} \tag{14}$$

$$SC_{eq} = \frac{\dot{m}_{NG,eq} \cdot LHV_{NG}}{\dot{m}_P} \tag{15}$$

Finally, to account for the CO_2 emitted E_{CO_2} for the LNG route or captured for the ammonia route C_{CO_2}, the specific CO_2 output per product is presented in Equations 16, and 17, respectively.

$$E_{CO_2} = \frac{\dot{m}_{CO_2}}{\dot{m}_{LNG}} \tag{16}$$

$$C_{CO_2} = \frac{\dot{m}_{CO_2}}{\dot{m}_{NH_3}} \tag{17}$$

2.3 Economic Fundamentals

2.3.1 Capital Expenditure

Capital Expenditure (CAPEX) includes expenses for the development, expansion, or modernization of the facility and equipment. Various cost components are considered when evaluating CAPEX, shown in Figure 10. Bare erected cost (BEC) for direct construction costs. Total plant cost for adjusting for the process contingency (PC) for potential cost overruns and project contingency (PT) for unforeseen expenses during project execution. Total overnight costs (TOC) contain the aggregate of all CAPEX costs, providing a comprehensive view of the financial commitment required for the project. Finally, the total capital requirement (TCR) is the TOC but with the addition of interest and escalation.

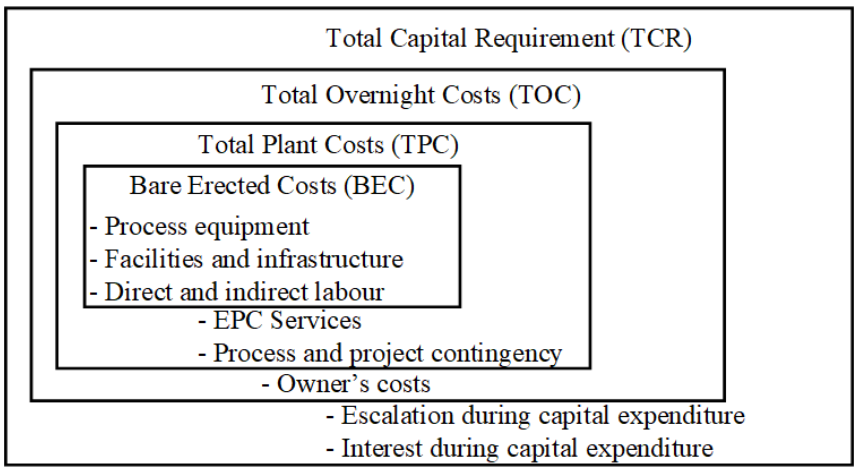

Figure 10: Capital cost breakdown [46].

2.3.2 Operational Expenditure

Operating expenditure (OPEX) includes ongoing expenses for efficient facility functioning. Typical costs include salaries for plant personnel, raw material input, feedstock procurement, utility costs, routine maintenance, safety measures, quality control, environmental compliance, and insurance. Effective management of OPEX is essential for sustaining profitability, minimizing production downtime, and ensuring environmentally responsible operations.

2.3.3 Econonomies of Scale

Economies of scale is a fundamental economic concept that describes a situation in which a firm or an industry's average costs per unit decrease as the scale of output increases [47]. This phenomenon arises due to several factors, such as the ability to purchase inputs in bulk, the spread of fixed costs over a higher number of units, increased specialization of employees and machinery, and the potential for greater technological efficiency. Essentially, the more a firm produces, the cheaper each product unit can become, assuming all else remains constant.

Large process plants can substantially benefit from economies of scale in several ways [48]. Capital costs can be spread over a larger production volume, reducing per-unit costs and potentially increasing profit margins. Additionally, purchasing inputs in bulk allows these plants to negotiate lower prices, further reducing production costs. Technological efficiencies, another benefit, are achieved through investment in advanced, automated machinery, which enhances production

efficiency and precision. Operational efficiencies are realized through labor specialization and integrated processes, which streamline production and reduce waste. By strategically leveraging these benefits, large process plants can lower per-unit costs, increase productivity, and gain a competitive advantage.

2.3.4 Key Performance Indicators

Using the breakdown of costs from Figure 10, a performance metric regarding capital investment can be derived. As the TOC contains the aggregate of all CAPEX costs, it provides a comprehensive view of the financial commitment required for the project. A specific capital cost (SCC) metric is defined in Equation 18.

$$SCC = \frac{TOC}{\dot{m}_P \cdot LHV_P} \tag{18}$$

The levelized cost of the product (LCOP) is defined as the selling price of the product that yields a net present value (NPV) of zero upon the conclusion of the plant's operational lifespan. The NPV is calculated by aggregating the annualized cash flows, as presented in Equations 19 and 20.

$$NPV = \sum_{t=0}^{n} \frac{ACF_t}{(1+r)^t} \tag{19}$$

Here, ACF_t is the annualized cash flow, r is the discount rate, and t is time.

$$ACF_t = \phi \cdot (LCOP \cdot P_{Product} - C_{VOM}) - C_{Capital} - C_{FOM} \tag{20}$$

Here, ϕ symbolizes the capacity factor, $P_{product}$ denotes the annual production, C_{VOM}, $C_{Capital}$, and C_{FOM} denotes the cost for variable operating and maintenance, capital, and fixed operations and maintenance, respectively.

From the calculations for LCOP, other economic metrics can be derived as useful for evaluating ammonia as an alternative to LNG. A common metric for assessing carbon capture and storage technologies is the cost of CO_2 avoidance (COCA). As the ammonia value chain has zero emission of CO_2 due to assuming a 100% capture rate and the 1x train importing carbon-free electricity, further discussed in Section 3.2.2, the COCA directly reflects the price of CO_2 where the plant achieves competitiveness towards the LNG plant. The expression for COCA is defined in Equation 21.

$$COCA = \frac{LCOP_{NH_3} - LCOP_{LNG}}{E_{CO_2,LNG} - E_{CO_2,NH_3}} \tag{21}$$

Here, E_{CO_2} is the specific emission in tonnes per unit product.

2.4 LNG

In regions where large and accessible natural gas reserves are close to demand centers, pipelines have been a reliable, safe, and economical method for natural gas transportation for over a century [4]. They adapt effectively to supply and market conditions. However, when natural gas reserves are located in inconvenient locations, alternative transportation methods become necessary. Natural gas can be liquefied and stored in tanks for overseas shipment, enabling remote gas fields to connect with high-demand markets unreachable by pipeline. Figure 11 presents the cost comparison of pipeline transportation versus LNG per distance, showing that LNG is an economically viable option for long-distance transport. LNG shipping overseas diversifies markets previously dominated by pipelines, introduce competition, and provides increased energy supply and security for high-consuming nations. Furthermore, the LNG industry reduces global energy trade constraints, increases supply and demand flexibility, and contributes to a more efficient energy system [4].

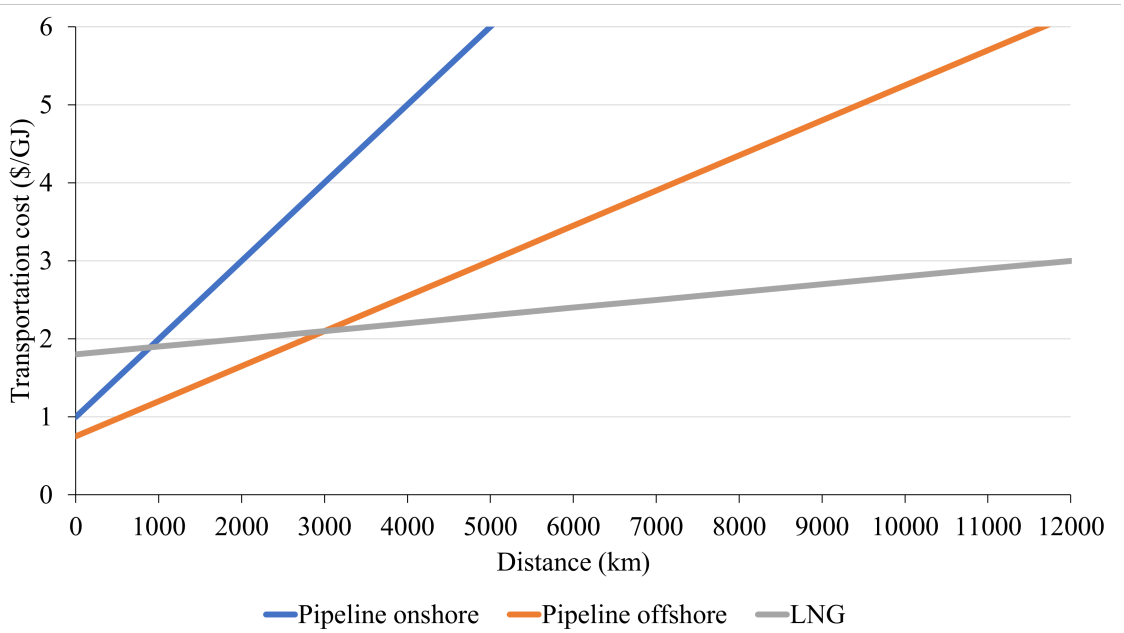

Figure 11: Transportation costs of pipeline versus LNG [49].

Over the last decade, inter-regional pipeline trade has increased by 8.4% [1]. Surpassing pipeline trade for the first time in 2020, the LNG trade has seen an increase of 57% over the same period. By the end of 2021, global liquefaction capacity reached 459.9 MTPA [50]. The LNG value chain has made notable advancements in the liquefaction process, including higher thermodynamic efficiency, reduced capital costs, and expanded plant capacity [4]. Other significant developments include improved technologies, more efficient value chains, lowered investment thresholds, and expanded market boundaries.

Future forecasts for the LNG trade are challenging to project due to volatile market conditions, competition from pipeline trade, emerging new technologies, and project start-up delays [51]. Global gas demand is also influenced by economic growth [52]. The COVID-19 economic downturn caused a 5% drop in natural gas demand [1]. These downturns can affect the utilization of installed value chain capacities. However, LNG's global commodity status means that growth in natural gas demand can be met in many countries. Figure 12 presents current demand by sector and future natural gas demand in the STEPS, APS, and NZE scenarios. Factors such as higher natural gas prices, lower LNG production costs, rising supply and demand centers, and the need to phase out coal and oil to reduce emissions, all contribute to an expected increase in LNG trade in the coming years based on stated policies.

From 2020 to 2021, the global LNG trade increased by 5.3% [1]. A strong post-COVID recovery led to a surge in LNG imports. Asia Pacific countries are the largest importers, holding a 72% share. While Japan and South Korea have historically been the largest consumers, China surpassed Japan in LNG imports for the first time in 2021. Over ten years, Chinese LNG imports have risen dramatically from 16.9 to 109.5 bcm. Figure 13 shows that LNG trade is projected to grow strongly over the next decades in the STEPS scenario, driven by increasing gas demand in emerging Asian countries. As China, India, and other Asian countries phase out coal and oil, LNG imports are expected to be the incremental source of increased gas use.

The United States (18.4%), Qatar (20.7%), and Australia (20.9%) are currently the leading exporters of LNG. Traditionally, Qatar has been the world's top LNG supplier, boasting over 100 bcm of annual LNG exports. Over the past decade, the United States and Australia have significantly increased their exports, with annual growth rates of 49.1% and 15.3%, respectively. In 2021,

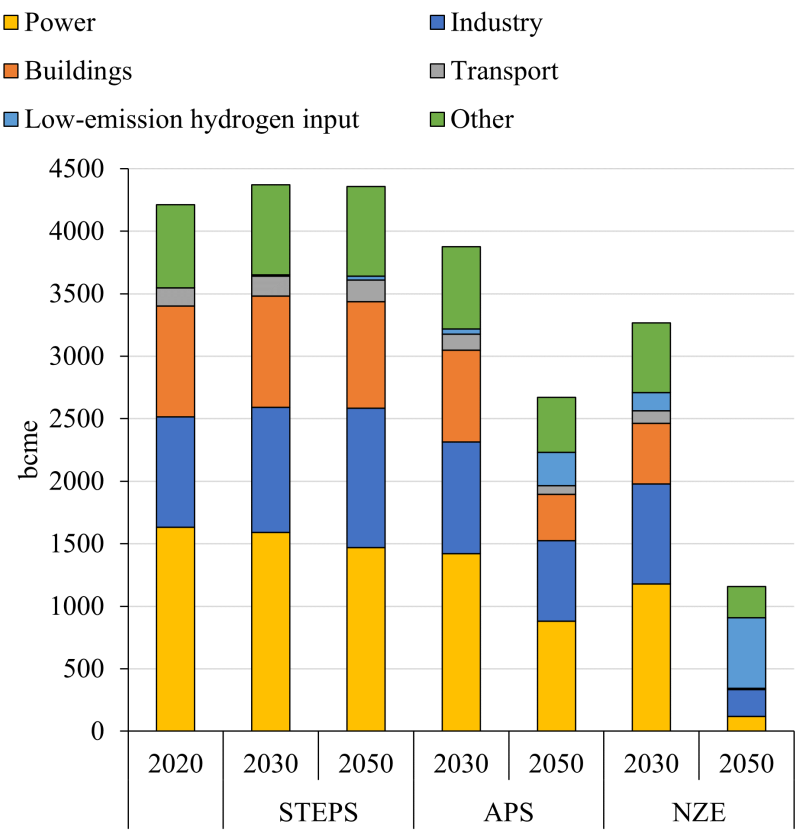

Figure 12: Natural gas demand by scenario [2]. bcme = Billion cubic metres of natural gas equivalent; STEPS = Stated Policies Scenario; APS = Announced Pledges Scenario; NZE = Net Zero Emissions Scenario.

Australia outpaced Qatar, becoming the largest exporter with 108.1 bcm. Rising LNG demand necessitates an increase in export capacity. The United States is projected to account for over 40% of the increase in LNG exports until 2030 [17]. Additionally, substantial supply increases from the Middle East, Russia, and Africa contribute to the growth in LNG exports.

2.4.1 Value Chain

Several facilities are needed and dependent upon one another to develop and commercialize LNG projects. The upper part of Figure 1 provides an overview of the LNG value chain, including upstream, midstream, and downstream activities. Upstream stages in the LNG value chain include well exploration, natural gas production, gas treatment, processing, and the liquefaction process. Midstream activities involve the exporting terminal, transportation, and the importing terminal. The downstream value chain includes regasification of the LNG, distribution networks, and markets comprising end-of-use consumers, including fuel, residential, power generation, and industrial uses.

Liquefaction

Natural gas undergoes liquefaction when cooled to approximately -162°C at atmospheric pressure, resulting in a volume reduction of about 1/600th [51]. This volume reduction means that one tonne of LNG contains the same energy amount as 1,400 cubic meters of natural gas. The liquefaction process is based on the refrigeration principle, as discussed in Section 2.2.2. The refrigerant can be part of the natural gas feed in an open-cycle process or circulate through a liquefier in a closed-cycle

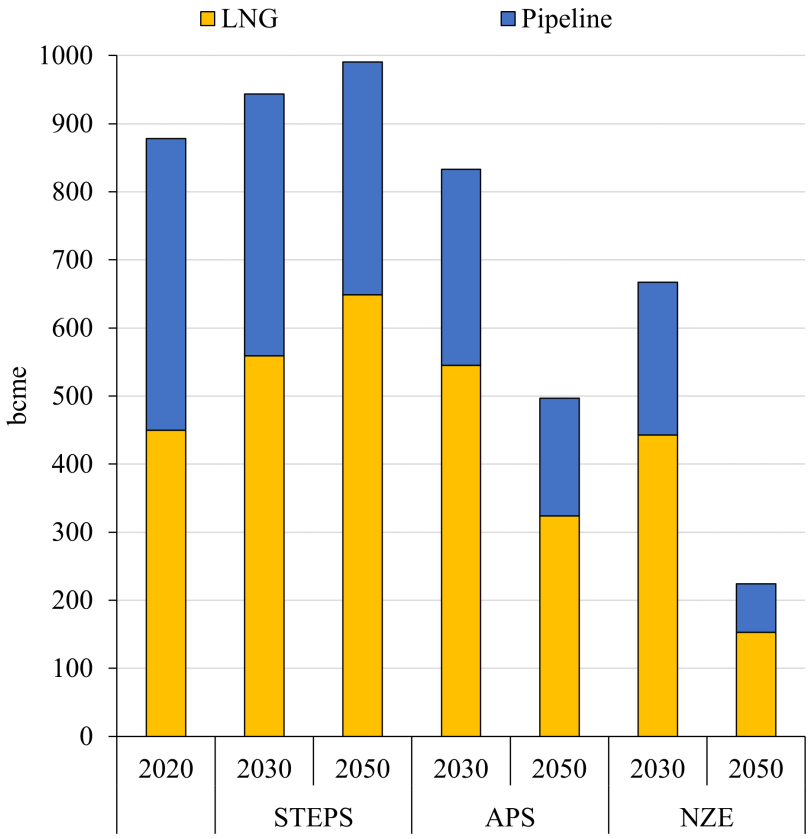

Figure 13: LNG demand by scenario [2]. bcme = Billion cubic metres of natural gas equivalent; STEPS = Stated Policies Scenario; APS = Announced Pledges Scenario; NZE = Net Zero Emissions Scenario.

process. Various technologies and processes exist for natural gas liquefaction, with the common goal of cooling the natural gas to roughly -163°C at atmospheric pressure. LNG production pathways are discussed in Section 2.4.4.

LNG plants are classified into peak shaving, small, medium, and large-scale baseload plants, with plant capacity measured in MTPA. Large-scale baseload plants, having capacities greater than 3 MTPA, are typically located near large natural gas reservoirs across various regions [51]. An LNG plant may comprise several parallel units, termed trains. Over the past 50 years, the capacity of a single train has steadily increased, with train sizes up to 7.8 MTPA now operational in Qatar [53]. Peak-shaving plants, small-scale facilities with capacities up to 0.3 MTPA, help to balance demand fluctuations during the summer and winter months [4]. Mid-scale LNG plants, having capacities of up to 3 MTPA, have become feasible due to smaller gas reservoirs in remote locations.

The concept of parallel trains allows for uninterrupted production when one train undergoes maintenance. Adjusting the number of trains in a facility enables the producer to meet market demands and provide flexibility in shipping logistics [51]. Another consideration for implementing parallel trains is equipment limitations within the liquefaction plant. Higher train capacities tend to reduce the unit cost of production, thus offering a competitive advantage [54]. In the liquefaction plant, the compressor driver is a significant cost component, and efficiency improvements for gas turbine drivers can offset the increased capital costs of expanding single trains. However, maintaining high plant reliability and availability is crucial to fully realizing the cost benefits of implementing larger trains.

Transportation
Once liquefied and stored, LNG is loaded onto specially designed LNG carriers. These vessels transport large amounts of LNG between export and import terminals at a pressure slightly above atmospheric [55]. LNG vessels' sizes range from less than 30,000 m^3 to 266,000 m^3, with most modern carriers ranging from 150,000 m^3 to 160,000 m^3 [4]. The tank design insulates the cryogenic LNG and ensures the integrity of the hull system. A small fraction of the LNG boils during shipping due to the imperfect insulation and refrigeration properties, known as the boil-off gas (BOG) rate, typically varying between 0.05% and 0.15% of the total LNG volume per day [55]. Boil-off gas can be reliquefied, used as fuel, or burned to produce steam. The simplicity of steam production using boil-off gas has led to the dominance of steam turbine propulsion systems over the past few decades. However, due to lower efficiency, fuel flexibility, reliability, availability, and safety reasons, the steam propulsion system's market share has declined [56]. Emerging propulsion systems include two-stroke slow-speed diesel engines and gas turbine propulsion systems, further discussed in Section 4.2.3.

Importing Terminals
Marine vessels deliver LNG to receiving terminals with a regasification unit, storage facilities, and a downstream pipeline system [55]. The transfer of LNG is performed by a set of unloading arms, moving the liquid to a storage tank. The design of these tanks should at least accommodate the incoming LNG from the vessel. Larger capacity terminals are being constructed to match the growing capacity of LNG carriers [4]. From the storage tank, the LNG proceeds to the regasification system, where it returns to its gaseous state. The gas delivery from the terminals must meet specific requirements set by pipeline companies and distributors, who regulate feed gas composition and quality to ensure a stable, safe, and reliable operation of the pipeline network. Typical specifications for natural gas delivery hinge on the heating value and gas composition ranges.

2.4.2 Environmental Aspects

The LNG value chain involves several environmental factors that require diligent attention and management to reduce its ecological impact. During the extraction and production phase, controlling methane emissions, a highly potent greenhouse gas, is essential to minimize the damaging effects of natural gas operations [24]. Increasing energy efficiency in the liquefaction plant and utilizing alternative compressor drivers could help reduce the environmental impact of the LNG plant [51]. Additionally, utilizing marine vessels that combust natural gas for propulsion instead of heavy fuel oil can provide emissions reductions due to specific emissions of 56 and 72 kg CO_2 per GJ combusted, respectively [20].

The downstream emissions are the most significant contributor, with around 75% of the total emissions [57]. These emissions originate from the combustion process of natural gas at the end user. The upstream production, liquefaction, and shipping emissions contribute to around 13%, 8%, and 4% of the total emissions, respectively. However, natural gas is a cleaner substitute for other fossil fuels like coal and oil, emitting fewer pollutants for power generation, heating, and industrial processes [20]. Nevertheless, employing efficient combustion technologies and emission control methods in these end-use applications is critical to reducing the release of pollutants and greenhouse gases. Embracing environmentally responsible practices throughout the LNG value chain is crucial for the sector's long-term viability and societal acceptance and competitiveness within the energy market.

2.4.3 Costs and Economic Implications

Production

Several critical CAPEX costs contribute to the overall investment required for its construction and setup within the liquefaction plant. Among these expenses is the acquisition and installation of cryogenic heat exchangers and compressors. Furthermore, the costs for installing gas purification systems, essential for eliminating impurities and contaminants such as CO_2, hydrogen sulfide (H_2S), and water from the natural gas feed, demand consideration [51]. Additionally, developing power generation and utility systems, and providing the required electricity, heating, and cooling to the plant, brings significant costs. While CAPEX constitutes a major portion of the project investment, it is crucial to also account for operational costs (OPEX). Important operational costs within the liquefaction plant include continuous labor and maintenance expenses, equipment replacement for uninterrupted and efficient operations, utility costs for electricity, water, and fuel, and the consumption of chemicals and coolants for gas treatment and liquefaction processes.

LNG projects are highly capital-intensive, with the liquefaction plant representing approximately 50% of the total capital expenditure within the LNG value chain [58]. Table 1 outlines the average costs for liquefaction plants derived from a comprehensive sample of projects [59]. LNG plants established in the United States or the Middle East are significantly more cost-effective than those erected in other high-cost locations. A significant challenge related to large LNG plants is the substantial time and investment capital needed to construct the liquefaction facility. Baseload LNG projects demand considerable proven natural gas reserves; for example, an annual LNG production of one million tonnes requires 1.5 trillion cubic feet of gas reserves for 20 years [13]. Reductions in CAPEX for LNG plants have been realized through improved designs, expansion of train sizes, and increased competition among manufacturers [51]. While historically, long-term contracts requiring significant investments were necessary for the development of baseload LNG projects, the opening of new value chains enables more LNG plants to enter the market efficiently.

Table 1: Liquefaction plant costs in 2018 by region, values derived from Steuer et al. 2019 [59]

Project Location	**Capacity cost**	
	($/tpa)	**($/GJ)**
All locations	946	3.31
Remote / high cost locations	1,226	4.29
Qatar	482	2.31
USA	660	2.31
West Africa	1,084	3.79
Russia	1,292	4.52
Australia	1,789	6.26

Storage

In the context of LNG receiving terminals, the LNG storage tanks represent the most costly equipment [58]. Large LNG storage tank expenditures can fluctuate based on tank size, construction materials, location, and current market conditions. Typically, the construction costs for these large-scale LNG storage tanks can span from $1.7 to $2.1 per tonne, as demonstrated in Table 2, with larger tanks reaping the benefits of economies of scale.

Shipping

The demand for LNG carriers is witnessing a consistent upward trend, with shipping rates being a highly volatile parameter [62]. In one year from April 2022, these rates have oscillated between

Table 2: Storage terminal cost intervals for LNG storage based on reference literature

Reference literature	**Terminal Capacity m^3**	**Terminal Costs ($M)**	**Specific cost $/tonne**
Riviera 2013 [60]	230,000	200	1.9
CNOOC 2021 [61]	220,000	166	1.7
Raj et al. 2016 [12]	160,000	150	2.1

$38,000 and $375,000 per day [63]. The costs associated with LNG shipping are variable and depend on factors such as vessel operation, tank capacity, availability, and distance covered. Furthermore, market conditions and supply-demand dynamics are crucial in determining shipping costs. It is anticipated that OPEX reductions for LNG carriers could be achieved by introducing larger carrier sizes and vessels equipped with BOG reliquefication capabilities [4]. The volatility in LNG carrier rates can be attributed to several factors influencing the supply and demand dynamics within the LNG shipping industry [64]. These factors include seasonal variations in demand, geopolitical issues, weather conditions, vessel availability, shipping routes, contract structures, technological advancements, and market speculation. While these elements interact and fluctuate, shipping rates are highly sensitive to changes in market conditions that contribute to increased volatility

2.4.4 Production Methods

Liquefaction Background

The principle of natural gas liquefaction revolves around refrigeration, whereby a process gas stream condenses into liquid within a cryogenic environment [45]. In an open-cycle process, the refrigerant constitutes a part of the pretreated gas stream. Conversely, in a closed-cycle process, the refrigerant circulates within a liquefier or a heat exchanger. Cryogenic temperatures range from -150°C to absolute zero at -273°C. Work is added to the refrigerant compressors, and heat is dissipated in air or water coolers to achieve the cryogenic temperatures requisite for natural gas liquefaction.

There are several established methods for natural gas liquefaction processes [51]. Figure 14 illustrates a typical cooling curve for natural gas. This cooling curve can be divided into precooling, liquefaction, and subcooling, each characterized by different specific heats represented as curve slopes along the process. For any liquefaction process, the most thermodynamic efficient one is that which closely replicates the shape of the natural gas cooling curve. The primary objective of the liquefaction process is to optimize the refrigeration process, thereby maximizing the LNG production per unit of power consumed. The LNG process design can be optimized to align closely with the natural gas cooling curve. Components in the design, refrigerant selection and composition, and power consumption relative to available compressor drivers are tools for optimization. A closer temperature approach between the refrigerant and gas stream necessitates a lower required heat exchanger area. The type of liquefaction process corresponds with the refrigeration method cycle deployed, classified into cascade cycles, mixed refrigerant (MR), and expansion-based processes. Figure 14 presents the duty curve for the different cycles concerning the cooling curve for natural gas.

The motivation for extracting stranded natural gas reserves has led to improvements in liquefaction technology [4]. This progression is evident in the evolution from small and medium-scale LNG plants producing less than 3 MTPA to larger base-load production facilities capable of generating more than 3 MTPA. The liquefaction process in the LNG sector is characterized by its significant capital and energy demands [51]. The advent of larger LNG plants has yielded enhancements in energy efficiency and reductions in capital costs per tonne of LNG produced. Moreover, mixed refrigerant cycles are on the rise due to their ability to evaporate over a broad temperature

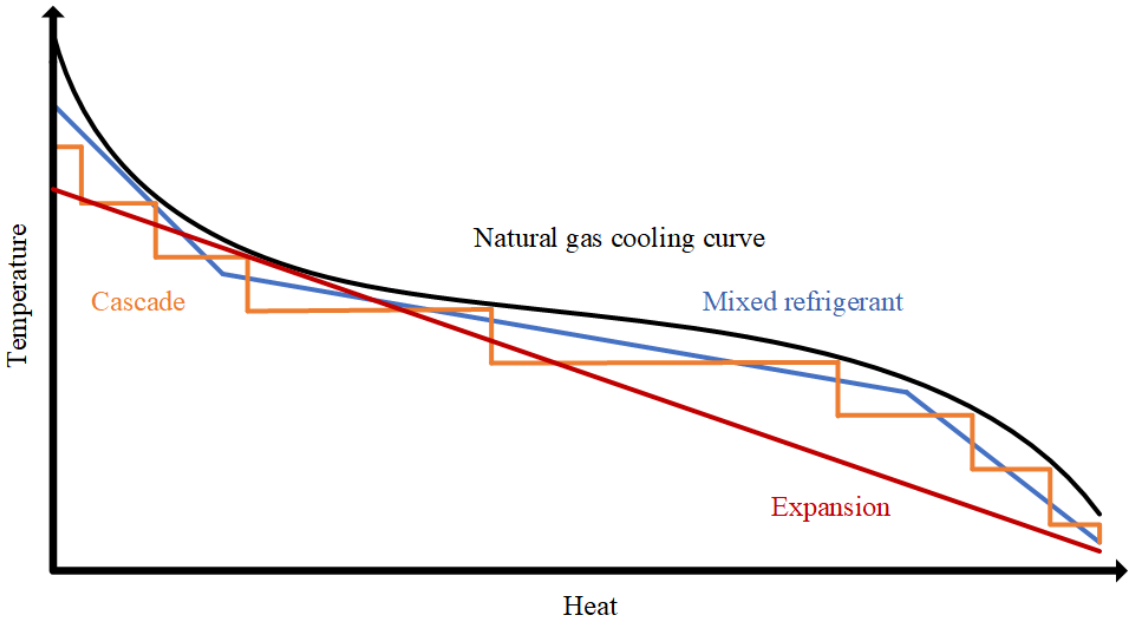

Figure 14: Cooling curves for cascade and mixed refrigerant processes.

spectrum.

Cascade Cycles

In the cascade process, the refrigerants vaporize at different but constant temperatures. The cascaded refrigerants use pure refrigerants in each cycle. This process provides a high level of flexibility due to the ability to control each refrigerant circuit [51]. The cascade cycle is suited for large train capacities with low requirements for the heat exchanger area and a low power requirement offset. The process also has low technical risks and utilizes standard equipment making the construction time short. A disadvantage of the cascade cycle is the high capital cost of investments and low flexibility in natural gas feed composition variations.

Figure 15a presents a design schematic for a cascade process. Propane, ethylene, and a multistage methane refrigeration circuit are used to balance refrigeration loads. The three refrigerant cycles are operated at different temperature levels with individual compression levels. Air or water cooling condenses the propane stream, while the propane stream condenses the ethylene stream. The heat exchangers are less advanced than the coil-wound heat exchangers (CWHE) in the C3MR process. The largest train to date is 5.2 MTPA, but larger trains are possible with multiple turbine and driver configurations [65].

Mixed Refrigerant Cycles

The motivation for introducing mixed refrigerant cycles is to match the cooling curve for natural gas closely. Various components in the mixed refrigerant vaporize at different temperatures. Mixed refrigerant composition is therefore a tool of optimization to minimize heat exchanger duty and energy usage. One of the advantages of MR cycles is the ability to adjust the refrigerant composition to accommodate changes in feed gas composition, flow, and operating conditions [51]. However, MR cycles face limitations in optimally matching the broad spectrum of cooling temperatures encountered in the liquefaction process, leading to a lower thermal efficiency compared to pure refrigerants. Furthermore, the necessity for precise blending fractions among the different components extends the start-up time for MR processes compared to cascade processes.

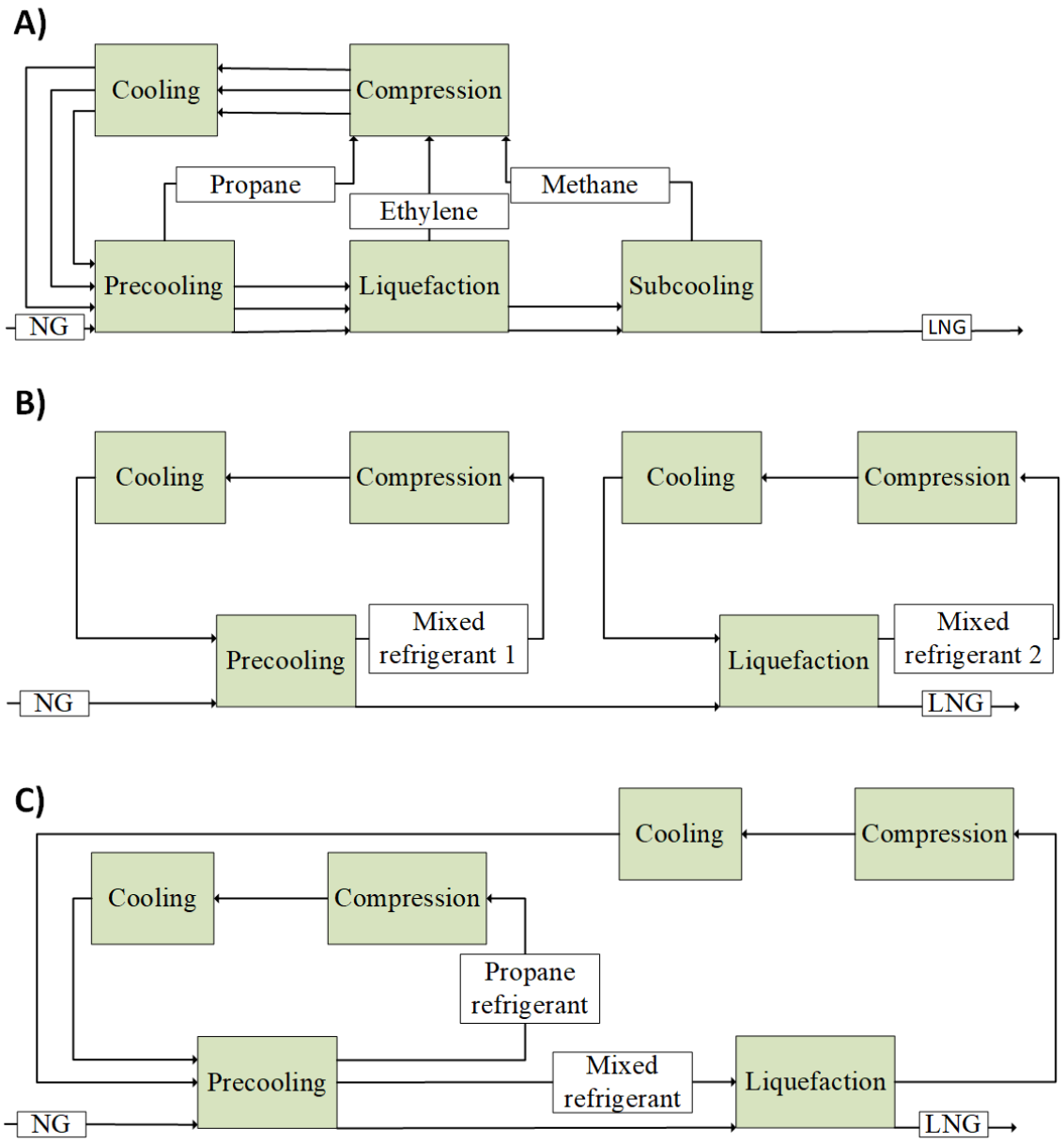

Figure 15: Simplified flow sheets of different LNG production methods. a): Cascade process; b) DMR Process; c) C3MR cycle.

DMR Cycles

The dual mixed refrigerant (DMR) cycle utilizes two distinct MR cooling cycles [51]. Initially, a heavier MR is used in the first cycle to precool the gas. Subsequently, the natural gas is condensed in the second cycle through a lighter MR. Due to the split in heat exchanger duty, the size of heat exchangers in the DMR cycle is approximately half of that in the single mixed refrigerant process. The DMR process has several variations, differentiated by the number of refrigerants used in the cooling cycles. A standard DMR process depicted in Figure 15b involves the first MR cycle precooling the natural gas stream to roughly -50°C. The DMR cycle configuration bears similarities to the C3MR in the precooling process, but it uses MR instead of propane. Introducing two MR cycles offers greater flexibility in managing the load for each cycle. In the DMR process, the MR composition can be adjusted to navigate temperature and handling constraints. Unlike the C3MR process, which utilizes a pure refrigerant, propane, for precooling, the DMR process is better suited for cold-climate LNG plants.

C3MR Cycle
The C3MR process, pioneered by Air Products & Chemicals, stands as the most prevalent liquefaction process, claiming a significant 75% market share in LNG plants [66]. This technology accommodates large train capacities, reaching up to 7 MTPA. As depicted in Figure 15c, the C3MR process comprises two refrigeration cycles. The initial cycle utilizes propane as a pure refrigerant for precooling the natural gas to approximately -40°C within a kettle-type heat exchanger, typically across three or four distinct pressure levels. The propane is compressed to high pressure, facilitating its condensation via ambient air or cooling water. In the subsequent cycle, a mixed refrigerant is used for the liquefaction and subcooling of natural gas. The MR composition integrates methane, ethane, propane, butane, and nitrogen. As per Figure 14, the MR composition is optimized to align with the cooling curve for natural gas closely. After the precooling cycle, the MR is partially condensed before entering the Main Cryogenic Heat Exchanger (MCHE).

Within the MCHE, the natural gas stream is subcooled and liquefied from -40°C to around -162°C. The MR is segregated into a gaseous and liquid stream, each passing through separate circuits within the MCHE. The initial liquid stream provides cooling for the natural gas within the hot (lower) bundle of the MCHE. Subsequently, the liquid stream is evaporated through a JT valve to cool the cold (upper) bundle. The gaseous stream flows through a JT valve to further cool the natural gas within the cold bundle. Then, the liquid and gaseous stream outputs are combined to deliver additional cooling for the lower bundle and ensure complete stream vaporization. Finally, the vaporized MR is compressed and cooled via ambient air or water and redirected to the propane precooling cycle.

In a C3MR process, the propane precooling cycle cools the feed gas to around -40°C. Subsequently, the heavier components' saturation temperature characteristics facilitate refrigeration until methane and nitrogen subcool the natural gas to -162°C. A tight correlation between the heat exchanger duty curve and the natural gas cooling curve translates to reduced requirements for heat exchanger area and compressor power. MCHEs are deployed to integrate numerous streams into a single unit and are prevalent in many energy-intensive and industrial cryogenic processes. Given their high energy intensity in LNG plants [51], a comprehensive analysis of the heat exchanger's design, optimization, development, and selection is vital for the facility's overall efficiency.

2.5 Ammonia

One of the most pressing challenges today is the concurrent increase in human population and the global commitment to phase out fossil fuels in pursuit of net-zero emission targets[2]. As the population grows, the demand for chemicals essential for food production increases [3]. Demand for ammonia as the primary component of all mineral nitrogen fertilizers is responsible for approximately 70% of total utilization [67]. Given its higher volumetric energy density and superior storage and handling properties compared to hydrogen, as elaborated in Section 2.1.4, ammonia presents a more favorable alternative. Moreover, it benefits from an established and reliable infrastructure [33]. Ammonia production routes vary based on the raw materials employed and the technology implemented. The European Union defines low-carbon ammonia production as the route wherein direct greenhouse gas emissions are reduced by approximately 70% [68]. Low-carbon solutions include green and blue ammonia, primarily distinguished by the hydrogen production method.

Ammonia production relies heavily on fossil fuels, with natural gas accounting for over 70% of total production and the remainder derived from coal gasification [67]. China is the largest producer at 30%, followed by Russia, the Middle East, the United States, the European Union, and India, each contributing around 10%. Other applications include industrial, explosives, specialty materials, and synthetic fibers. In 2021, the ammonia demand reached approximately 190 million tons, representing two-thirds of the industrial sector's total hydrogen demand [10]. In 2020, the European Union imported 4 Mt, equivalent to 20% of global trade [67]. Furthermore, ammonia production

constituted 1.3% of global energy demand and 1.0% of energy-related CO_2 emissions. Notable advancements in ammonia production processes have been achieved, such as enhanced energy efficiency, emission reductions, novel modeling approaches, and implementing CO_2 taxation to promote low-carbon mitigation strategies [69].

Based on the different scenarios introduced in Section 2.1.1, future ammonia production, demand, and trade are expected to increase significantly, as shown in Figure 16 [67]. With current policy settings, production is expected to increase by 40% towards 2050, driven mainly by the demand for fertilizer. For the APS in 2050, 190 Mt of ammonia is needed as an energy carrier in addition to fertilizer and other uses, adding up to twice the amount produced in 2020 [70]. In the NZE scenario towards 2050, demand for ammonia is tripled to around 600 Mt compared to 2020 production levels.

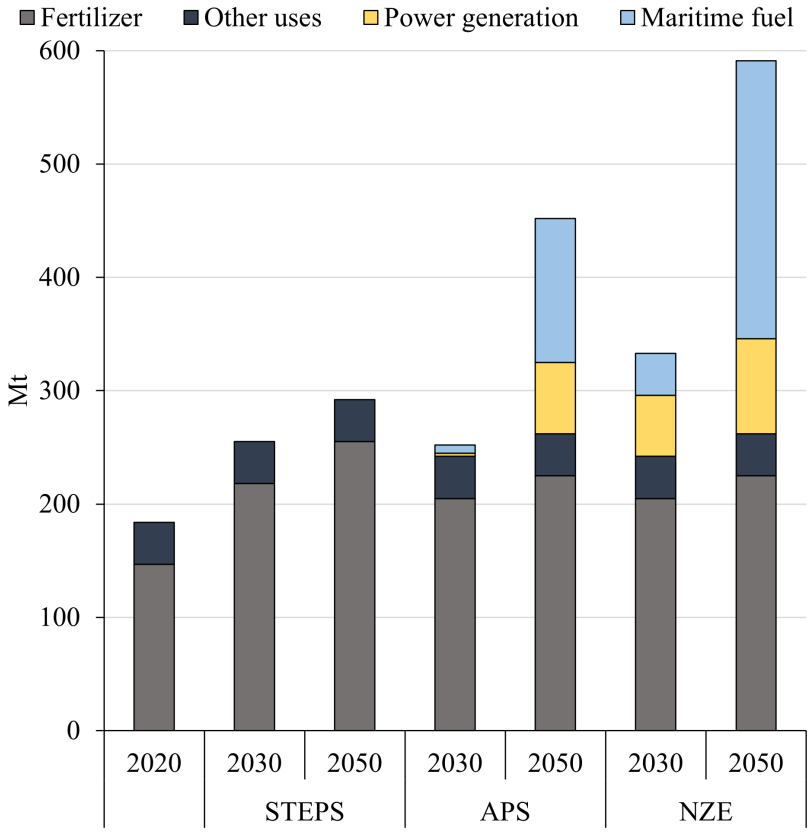

Figure 16: Ammonia demand in different sectors based on IEA's scenarios [67]. STEPS = Stated Policies Scenario; APS = Announced Pledges Scenario; NZE = Net Zero Emissions Scenario.

2.5.1 Value Chain

The ammonia value chain from natural gas with CCS is an intricate process that involves upstream, midstream, and downstream components, as presented in the bottom part of Figure 1. Here, the figure also expresses what parts of the value chain are the scope of this thesis. Upstream operations begin with extracting natural gas, which is then processed through SMR, ATR, or gasification, as discussed in Section 2.1.4. This hydrogen is further processed with nitrogen in the Haber-Bosch process to produce ammonia. The CO_2 generated during hydrogen production is captured and stored. The midstream stage involves the transportation of ammonia over long distances. Given the nature of ammonia, it is typically transported in fully refrigerated gas carriers to maintain its stability and safety. These carriers are designed to maintain low temperatures that keep the ammonia in a liquid state, which optimizes storage capacity and facilitates safe handling [40]. The

downstream stage involves distributing and using ammonia in various sectors.

Production

There are several routes for producing ammonia. Color codes in ammonia production represent different production methods and their associated carbon dioxide emissions. Grey ammonia is produced using the conventional Haber-Bosch process, where hydrogen is derived from natural gas or other fossil fuel-based feedstocks, resulting in significant CO_2 emissions [16]. Blue ammonia is produced similarly to grey ammonia but with CCS technologies to significantly reduce the carbon footprint. Green ammonia is produced using hydrogen derived from water electrolysis powered by renewable energy sources, generating no direct CO_2 emissions. These color codes help to distinguish the environmental impact and sustainability of each ammonia production method.

Ammonia plant sizes vary in ranges from small-scale to large-scale plants of 0.1-4.0 Mt production rate annually [71]. The largest single-train capacities are up to 1.3 MTPA, while novel large-scale technologies allow for single-train production rates up to 2.0 MTPA. Larger plants could benefit from economies of scale, but several considerations must be considered. These include feedstock availability and infrastructure, capital investment requirements, market demand, transportation and logistics infrastructure, environmental and regulatory compliance, and technological advancements. Each factor is crucial in deciding the optimal plant size that aligns with available resources, market conditions, and long-term sustainability while balancing financial and environmental considerations.

Transportation

When ammonia is transported over longer distances, it is liquefied and stored in fully refrigerated tanks on gas carriers [40]. These fully refrigerated gas carriers are specialized vessels designed for transporting liquefied gases at controlled temperatures and ambient pressure over long distances. These ships feature large, insulated cargo tanks made of materials resistant to the specific gas being transported, ensuring that the cargo remains in its liquid state throughout the journey. Equipped with advanced refrigeration systems, either direct expansion or indirect systems, these carriers maintain the cargo at temperatures below their respective boiling points and at near atmospheric pressure, playing a crucial role in the safe and efficient transportation of liquefied gases between production facilities and end-user markets. These vessels vary in size from 15,000 to 84,000 m^3, where sizes of 25,000 - 50,000 m^3, 25,000 - 50,000 m^3, and >70,000 m^3 are classified as medium, large, and very large gas carriers (VLGC), respectively [72].

Exporting and Importing Terminals

Ammonia can be stored in fully refrigerated large-scale storage tanks, maintained as a liquid at atmospheric pressure and around -33°C [33]. These tanks are insulated and equipped with cooling systems to ensure that the ammonia remains stable and in its liquid state. However, some challenges are associated with refrigerated ammonia storage [16]. Maintaining such low temperatures requires energy, leading to higher operational costs. Second, the insulation and cooling systems demand regular maintenance to ensure their efficiency and prevent potential leaks or temperature fluctuations. Third, safe storage and handling of ammonia is crucial due to its toxic and corrosive nature, necessitating robust containment measures, safety equipment, and personnel training. Finally, constructing and commissioning large-scale refrigerated storage facilities include considerable capital costs, which must justify sufficient demand and market conditions for ammonia.

Downstream Uses

Ammonia is primarily used for agricultural fertilizer, contributing to around 1.3% of the entire energy sector respective CO_2 emissions [67]. The fertilizer industry could lower its emissions by

introducing low-emission production pathways such as green and blue ammonia. Further, ammonia proves promising for applications as an energy carrier and fuel for various combustion processes [73]. Compared to hydrogen, ammonia can store and transport energy more efficiently and safely, making it an attractive option for the growing hydrogen economy. Further, low-carbon ammonia can be an alternative to LNG for energy transportation and storage, especially in regions with large natural gas reservoirs and where prices are low.

Regarding combustion applications, ammonia can be used as a fuel for power generation, either directly or by blending with other fuels. Ammonia can be co-fired with coal, natural gas, or biomass to reduce greenhouse gas emissions from power plants or used as fuel in industrial processes. Extensive research is currently being developed for ammonia-fueled engines in the maritime and transportation sectors [71]. Adopting low-carbon ammonia in various applications can substantially decrease CO_2 emissions across various sectors and accelerate the global transition towards cleaner and more efficient energy systems.

2.5.2 Environmental Aspects

Greenhouse gas emissions from ammonia production vary based on feedstock, conversion technology, and whether CCS technologies are utilized [67]. About two-thirds of the CO_2 emissions in the SMR process, further discussed in Section 2.1.4 largely rely on hydrogen production before the ammonia synthesis loop, where the reforming process occurs [74]. The rest are diluted in the form of natural gas combustion for heating purposes. If the dilute CO_2 is also captured, the combined CO_2 capture rate could reach 95%. In the ATR process, hydrogen production and heating are combined in a single reactor, resulting in a concentrated CO_2 output stream with a possible capture rate of 98% [75]. Even though ammonia is carbon-free upon utilization, the emissions linked to its production can sometimes surpass those of coal or natural gas they replace in co-firing applications [73]. As a result, it is crucial to thoroughly evaluate the entire range of emissions when determining the potential climate advantages of employing these energy carriers.

Transport emissions should also be evaluated when considering the overall environmental impact of the ammonia value chain. Where ships are utilized for overseas transport, heavy fuel oil (HFO) is currently used for propulsion [55]. This fuel has a significant environmental impact and would add 3-10 gCO_2/MJ to the emissions, depending on shipping route and vessel size [73]. MAN Energy Solutions are currently developing a fuel-flexible ammonia engine that would allow co-firing ammonia boil-off gas from refrigerated tanks [76]. Other innovations include Mitsubishi's 40MW class gas turbine that can combust 100% ammonia, expected to be commercialized in 2025 [77]. Ammonia demand for maritime applications is expected to increase dramatically, reaching between 100 and 1000 Mt by 2050 in a 1.5 °C [73].

2.5.3 Costs and Economic Implications

Production

CAPEX refers to the upfront costs of constructing and commissioning the production plant. Typically, the higher the plant capacity, the lower the specific CAPEX per ton of ammonia produced due to economies of scale [78]. OPEX includes the ongoing costs of operating and maintaining the ammonia production facility. This comprises labor costs, maintenance, insurance, catalysts, membranes, oxygen carriers, and process water. Natural gas is the primary feedstock for blue ammonia production. The cost of natural gas can significantly impact the overall production cost of ammonia, as it accounts for a substantial portion of the operating expenses [7]. Electricity is required to power various equipment in the ammonia production process and the CCS system. Electricity costs will vary depending on the facility's region's local utility rates, regulatory framework, and energy mix [79]. Some ammonia production plants may include on-site electricity generation using

combined heat and power systems or renewable energy sources to manage electricity costs.

Integrating CCS in ammonia production adds additional CO_2 capture, compression, transport, and storage costs [67]. The cost of CCS depends on the specific capture technology used, the amount of CO_2 captured, and the distance to the storage site. It also influences CCS's regulatory frameworks and financial incentives, such as carbon pricing or tax credits. It is essential to recognize that these cost components may vary depending on plant size, location, technology choices, and market conditions. Optimizing these cost components through technological advancements, process integration, and economies of scale is crucial to improving ammonia production's economic viability from natural gas, including CCS.

The main cost components in ammonia production are the CAPEX, natural gas, and electricity costs. CAPEX costs constitute around 30-40% of the total production costs [29]. Production costs of ammonia from natural gas are $110-430 per tonne today [74]. CCS could add $100-150 per tonne to this cost, bringing up to $170-465 per tonne of low-emission ammonia production from fossil fuels. Table 3 provides production costs based on reference literature. The reference production costs from IEA and IRENA are average industry costs based on different production methods and locations. The KBR, LAC, and GSR process plants are discussed in Section 2.5.4, derived from previous works by Arnaiz del Pozo et al. 2020 [7].

Table 3: Production cost intervals for ammonia production from natural gas with CCS based on reference literature. IEA's and IRENA's estimations are average industry costs, while the KBR, LAC, and GSR process plants are specific production methods.

Reference literature	**Natural gas price**	**Production costs**	
	$/GJ	**$/GJ**	**$/tonne**
IEA 2021 [73]	1.1-6.3	13-25	240-450
IRENA 2022 [71]	1.9-9.5	13-25	170-465
KBR Process: Arnaiz del Pozo et al. 2020 [7]	3.8-7.1	15-21	275-375
LAC Process: Arnaiz del Pozo et al. 2020 [7]	3.8-7.1	15-21	273-373
GSR Process: Arnaiz del Pozo et al. 2020 [7]	3.8-7.1	13-17	233-313

Storage

Fully refrigerated large-scale ammonia storage tanks range in capacities between 4,550 and 60,000 tonnes [80]. A typical tank is made of carbon steel comprising less material than pressurized tanks, which explains why they are favorable for large-scale storage [72]. Various estimates for the CAPEX of installed storage are reported, with values ranging greatly as presented in Table 4. Operational costs for large-scale refrigerated ammonia storage tanks involve several ongoing expenses, such as equipment, maintenance, repairs, labor costs, safety and security measures, environmental compliance, and insurance.

Table 4: Storage terminal cost intervals for ammonia storage based on reference literature

Reference literature	**Terminal Capacity (tonne)**	**Terminal Costs ($M)**	**Specific cost $/kg**
IEA 2021 [73]	43,351-55,790	209-291	4.8-5.2
IEA 2019 [81]	34,100-56,700	68-97	1.71-2.0
Bartels et al. 2016 [9]	25,000	20	0.8

Shipping

VLGC shipping rates are highly volatile, and one-year prices from April 2022 have ranged between

$27,000 and $127,000 [63]. Similar to LNG carrier rates, VLGC carrier rates are highly volatile for many of the same reasons. These factors shape the balance between the demand for transportation and the available shipping capacity, affecting market conditions and the volatility of shipping rates. Fluctuations in production levels, economic shifts, political developments, seasonal demand changes, and vessel design innovations all play crucial roles in determining the supply and demand balance in the VLGC market.

Enhanced Oil and Gas Recovery

Where future ammonia plants incorporating CCS are located nearby oil and gas operations, the compressed CO_2 can extract additional oil and gas. This is discussed by Roussanaly et al. 2014, where the financial benefits of utilizing CO_2 in enhanced oil and gas recovery (EOGR) processes are discovered [82]. This pressurized CO_2 can be worth about $30 per tonne of CO_2 avoided or cost $30 per tonne at the high-cost end. Other findings include an additional recovery of 5 to 15%, which could raise the economic margins. The analysis from Roussanaly et al. 2014 demonstrates that integrating CO_2 capture, transportation, and storage into EOR operations can yield significant economic and environmental advantages, making it a promising approach for both the energy and climate sectors.

2.5.4 Production Methods

The Haber Bosch Process

The Haber-Bosch process functions through a series of sequential steps, beginning with the production of hydrogen [83]. Hydrogen is typically generated by SMR, ATR, or water electrolysis. The following purification stage ensures that the nitrogen and hydrogen gases are free of contaminants and impurities, which could otherwise hinder the catalytic reaction or reduce the quality of the ammonia produced.

The actual synthesis of ammonia occurs in the presence of an iron-based catalyst under high pressure and temperature conditions [83]. Nitrogen and hydrogen gases are introduced into a reactor, where they react over the catalyst surface to form ammonia. This reaction is exothermic and characterized by a dynamic equilibrium, which means that the forward reaction (formation of ammonia) and the reverse reaction (decomposition of ammonia) occur simultaneously. The reaction is typically carried out at pressures between 150 and 350 bar in temperatures of 400-500 °C. These conditions favor the forward reaction and promote the formation of ammonia. The catalyst plays a crucial role in breaking the strong nitrogen triple bond, reducing the activation energy required for the reaction, and increasing the overall reaction rate. Once the reaction is complete, the ammonia produced is cooled and separated from the unreacted nitrogen and hydrogen gases, which are then recycled back into the process for improved efficiency.

Reference Plants

KBR Purifier NH_3 process

The KBR Purifier ammonia process is presented in Figure 17a and enhances the conventional Haber-Bosch process through its innovative synthesis loop design, which comprises several vital components that contribute to the efficient utilization of reactants and the effective separation of ammonia from unreacted nitrogen and hydrogen gases [84]. In the KBR Purifier process, the proprietary purifier column is critical, efficiently separating ammonia from unreacted gases. The column operates on selective absorption, with the lean solution of ammonium carbamate capturing the ammonia present in the mixed-gas stream. The unreacted hydrogen and nitrogen gases are then purged and recycled back into the synthesis loop, improving the overall process efficiency

and reducing feedstock requirements. The rich ammonium carbamate solution is decomposed to recover ammonia and carbon dioxide, which is recycled back into urea production.

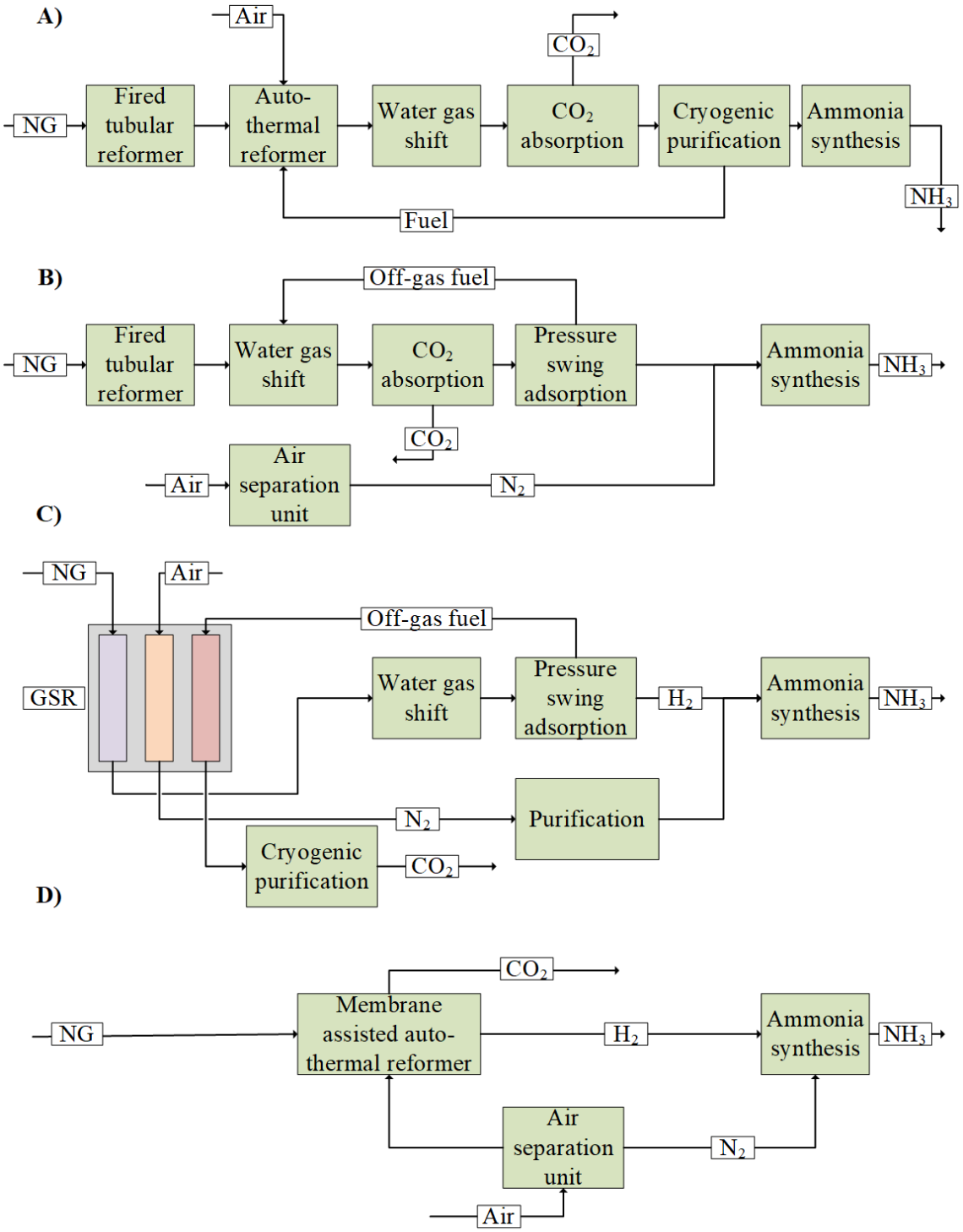

Figure 17: Different ammonia production technologies: a) KBR; b) LAC; c) GSR; d)MA-ATR. The figure is partly derived from Arnaiz del Pozo et al. 2020 [7].

LAC Linde NH_3 concept

The LAC Linde Ammonia Concept integrates several process steps and components to create a streamlined and energy-efficient ammonia production method, presented in Figure 17b [7]. The

integration of air separation and hydrogen production stages is achieved by combining an air separation unit (ASU) and an SMR. The ASU produces a nitrogen-rich stream by separating nitrogen from the atmospheric air, while the SMR generates hydrogen by reacting methane with steam. These two streams are combined to form the syngas mixture with the appropriate hydrogen-to-nitrogen ratio for ammonia synthesis. Another critical component of the LAC process is the radial-flow converter, which optimizes heat transfer efficiency and catalyst utilization during ammonia synthesis. This converter design ensures uniform distribution of the syngas mixture across the catalyst bed, resulting in a higher ammonia conversion rate. Moreover, the radial-flow converter facilitates heat recovery generated during the exothermic reaction, which can be used elsewhere to minimize energy consumption. After the synthesis, ammonia is separated from the unreacted gases and purified using suitable separation and purification techniques. In contrast, the unreacted hydrogen and nitrogen gases are recycled back to the synthesis loop, further enhancing the overall efficiency of the LAC Linde Ammonia Concept.

Future Plants

GSR-NH_3 plant

The gas switching reforming (GSR) process builds upon the conventional SMR method, widely used for hydrogen production, by employing a unique cyclic operation that allows for better heat integration and reduced energy consumption, presented in Figure 17c) [7]. In the GSR ammonia process, two reactors are used. In the first reactor, natural gas undergoes the endothermic SMR step, where methane reacts with steam at high temperatures in the presence of a nickel-based catalyst, producing hydrogen, carbon monoxide, and carbon dioxide. Simultaneously, the second reactor is heated by combusting fuel gas and air, generating heat stored in the reactor's thermal energy storage system. Once the SMR reaction in the first reactor is completed, the reactors switch roles. The previously heated second reactor now carries out the SMR step, while the first reactor is heated using fuel gas combustion. This alternating operation enables efficient heat transfer from the combustion step to the endothermic SMR step. The GSR ammonia process offers improved energy efficiency and reduced greenhouse gas emissions compared to conventional SMR-based ammonia production methods by optimizing the heat integration within the system. The hydrogen produced through the GSR process can then be combined with nitrogen obtained from air separation to form the syngas mixture required for ammonia synthesis. The GSR ammonia process presents a promising and sustainable alternative to traditional ammonia synthesis technologies through its unique reactor-switching approach and enhanced heat integration.

MA-ATR ammonia plant

Membrane-Assisted Autothermal Reforming (MA-ATR) is an innovative ammonia production technology that aims to enhance the efficiency and sustainability of hydrogen production, shown in Figure 17d) [7]. This process combines the benefits of ATR, which integrates SMR and partial oxidation (POX) into a single process, with the advantages of membrane separation technology. By integrating these technologies, the MA-ATR process could offer a more straightforward and cost-effective pathway for ammonia synthesis. For the modeling part of this thesis, an MA-ATR ammonia process plant is developed in Aspen Plus, further discussed in Section 3.2.

In the MA-ATR process, natural gas is first mixed with steam and oxygen to experience an endothermic steam methane reforming reaction and an exothermic partial oxidation reaction simultaneously within a single reactor. The resulting syngas mixture, which contains hydrogen, carbon monoxide, and carbon dioxide, is then passed through a hydrogen-selective membrane, allowing for the continuous separation and extraction of high-purity hydrogen. The remaining syngas, primarily a pure stream of carbon dioxide, can be further processed or utilized in other chemical processes or captured and stored. Integrating ATR and membrane separation technology enables the MA-ATR process to optimize the hydrogen production rate, composition, and purity while minimizing the

energy consumption and carbon footprint associated with conventional hydrogen production methods. The hydrogen produced through the MA-ATR process can then be combined with nitrogen from air separation to form the syngas mixture required for ammonia synthesis. The MA-ATR process presents a promising and sustainable alternative to traditional ammonia synthesis methods through its unique integration of ATR and membrane separation technologies [7].

2.6 Goals of the Thesis

By using the C3MR LNG and MA-ATR ammonia plants, including exporting and importing terminals and shipping, investigating the viability and implications of ammonia as a potential substitute for LNG in the global energy landscape is the primary focus of this thesis. Motivated by the growth in global energy consumption, coupled with the need for widespread decarbonization of the economy and the urgency of energy security, it investigates the role of ammonia and LNG in the global energy system. This investigation is even more pressing in light of the significant environmental impacts of the natural gas value and the evolving geopolitical dynamics that emphasize the importance of diversifying energy sources. Considering the need for energy sources that can be used in multiple sectors while offering logistical advantages, blue ammonia produced from natural gas with integrated CO_2 capture emerges as a viable energy carrier. However, no comprehensive, bottom-up techno-economic evaluation of ammonia compared to LNG exists, creating a significant gap in the existing literature and motivating this study's focus.

The main objectives of this thesis are as follows: First, to model a medium (1x train) and large-scale (10x train) C3MR LNG plant and an MA-ATR ammonia plant in Aspen Plus under similar assumptions, thus facilitating a direct comparison. These models provide technical performance parameters, which will be employed in an economic assessment to estimate capital and operational costs. Second, to conduct a techno-economic evaluation of ammonia as a potential alternative energy carrier to LNG. This evaluation will involve a consistent, bottom-up techno-economic method to determine the levelized cost (LCOP) of LNG and ammonia production. Furthermore, the CO_2 avoidance cost (COCA) for ammonia production will be computed, revealing the CO_2 price points at which ammonia proves economically competitive with LNG in international energy trade. A sensitivity analysis is conducted to evaluate the impact of various parameters on LCOP and COCA. Lastly, the thesis seeks to consider different plant sizes for LNG and ammonia facilities and address economies of scale's impact on the techno-economic evaluation. By fulfilling these objectives, the thesis aims to provide a reliable comparison between LNG and ammonia in a unified study and to contribute valuable insights to policymakers aiming to facilitate a transition towards a greener economy.

3 Technical Assessment Methodology

A techno-economic analysis using the same approach for both energy carriers was conducted to facilitate a consistent methodology for directly comparing LNG and ammonia. A graphical representation of the methodology implemented in this work is presented in Figure 18. Two scenarios for each energy carrier were analyzed. These were a mid-scale single-train approach and a large-scale ten-train approach.

The technical assessment for the LNG was done by modeling the liquefaction of natural gas in a C3MR process plant. The production of ammonia from natural gas with CCS was modeled using the MA-ATR ammonia process plant discussed by Cloete et al. 2020 [7]. Aspen Plus was used for the modeling and simulation of both processes. The software allows users to build a process model and simulate complex calculations. Both steady-state and dynamic processes can be simulated, and the software can also analyze the energy performance of process designs.

The same natural gas feed rate was utilized to encourage an equal comparison between the two energy carriers. From previous work in the project thesis, the flow rate was determined using the maximum amount of produced LNG using two LMS100 gas turbines with a combined power output of 226 MW. Resulting in a natural gas input of 306.30 kg/s for a single large train C3MR process plant. The MA-ATR ammonia plant modeled in Aspen Plus is based on previous works from Cloete et al. 2020 [7], with modifications discussed in Section 3.2 for equal comparison to the LNG plant. In the study by Cloete et al. 2020, the ammonia plant's initial natural gas flow rate was around 40 times lower than the initial LNG plant of 306.30 kg/s. To resolve this issue, the ammonia plant was scaled four times up, while the LNG plant was scaled ten times down by introducing two scenarios for each plant. The first scenario is a 1x train approach consuming power from the grid with a natural gas feed rate of 30.63 kg/s. The second scenario is a 10x train approach consuming 306.3 kg/s of natural gas, where a fraction of the product is combusted in a power plant. This approach created the four scenarios presented under the "technical assessment" ribbon in Figure 18. Another reason for introducing two different sizes for each plant was to analyze the techno-economic impact economies of scale have.

It is assumed that the natural gas feed is partly purified of contaminants and that heavier hydrocarbons are removed. A desulphurization unit is used in both processes to remove excess sulfur in the stream. For the LNG plant, an acid gas removal unit (AGRU) removes the fraction of CO_2 in the natural gas composition presented in Table 5. The ammonia plant can handle this CO_2 fraction, and therefore an AGRU is not required. Table 5 represents the natural gas specification used for simulations.

Table 5: Natural gas specifications

Item	**Value**	**Units**
Feed flow rate	30.63	kg/s
Feed pressure	70	bar
Feed temperature	15	°C
Methane content (CH_4)	89.0	%
Ethane content (C_2H_4)	7.0	%
Propane content (C_3H_6)	1.0	%
n-Butane content (C_4H_8)	0.11	%
Nitrogen content (N_2)	0.89	%
Carbon dioxide content (CO_2)	2.0	%

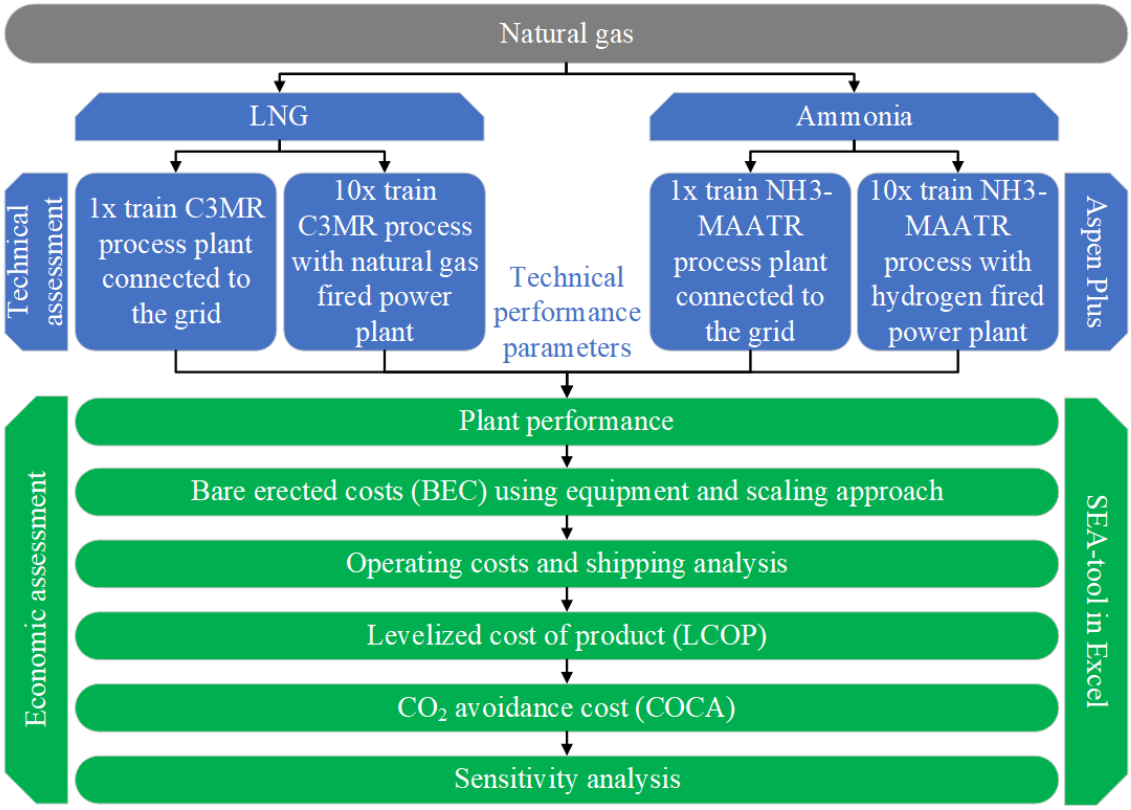

Figure 18: Graphical representation of the methodology employed in this work. Aspen Plus was used for the modeling of the plants. Further, the SEA Tool developed by Arnaiz del Pozo et al. 2022 was used for the economic assessment [85].

3.1 LNG Plant Modeling

The thermodynamic fluid package Peng-Robinson equation of state (EOS) was used for simulations. This EOS has been used extensively in previous research on natural gas liquefaction processes [86] due to its wide range of operational applicability for light hydrocarbons [87].

Scenario Configurations

The modeling part of the technical assessment was to build, optimize, and simulate a baseload liquefaction plant based on the C3MR process. The size of these plants is constrained by available equipment, such as heat exchanger sizes and compressor drivers [51]. As one of the objectives discussed in Section 1.1, utilizing natural gas resources of any size may be essential to provide energy security in the future. Therefore, a 1x train is introduced as a scenario where the LNG plant is connected to the power grid. Additionally, as discussed in Section 2.5.1, large-scale ammonia plants with natural gas feed rates of the 10x LNG train do not exist. Therefore, a 1x train size for an LNG plant provides an equal comparison to the case for a small to mid-scale 1x train ammonia production plant.

Two gas turbines were chosen as compressor drivers to determine the size of the liquefaction model for the 10x LNG train simulated in Aspen Plus. Using on-site power generation, the 10x train LNG plant can be located in remote locations disconnected from the power grid. General Electric LMS100 is an aeroderivate gas turbine with a net power output of 113 MW with 43% efficiency [88]. It is a relatively new gas turbine with market-leading efficiency, start-up time, and flexibility options. With two LMS100 gas turbines, 226 MW of power for the refrigerant compressors is available. The process modeling and simulations were performed with this constraint in available

power.

The Modeling Process
A brief description of the C3MR process was given in Section 2.4.4. The following Section will explain the C3MR process in more detail. First, a process description of the propane precooling cycle and the cryogenic cooling of natural gas down to -163°C is given. Second, modeling assumptions done to perform the simulations are examined. Further, which design specs implemented in the process are then discussed. Lastly, the whole liquefaction process is optimized using Aspen Plus' built-in optimization tool. Simulation results and technical performance parameters are discussed in Section 3.1.

The flowsheet was split into two parts to model the propane precooling cycle and the MCHE separately. The two cycles depend on one another, but assumptions were made that allowed the optimization of each cycle in different flowsheets. This approach allowed the software to handle less workload and therefore run quicker. The propane precooling cycle is presented with orange propane streams in the left part of Figure 19. The MCHE cycle is in the right part with blue mixed refrigerant streams. When both processes worked optimally, they were combined into a complete liquefaction process, shown in Figure A.1 from Appendix A.1. Complete material flows for both 1x and 10x trains are presented in Figure A.6, and A.7, respectively in Appendix A.3. A schematic of the LNG plant is shown in Figure 19, with stream data from key plant locations in Table 6.

Table 6: Stream conditions at different key locations in the C3MR LNG process plant, (slightly higher temperature)*, and (1.5% lower flow rate)** for 10x train scenario.

Stream	**Temp**	**Pressure**	**Flow**	**Species mol fractions**				
	(°C)	(bar)	(kg/s)	N_2	CH_4	C_2H_6	C_3H_8	C_4H_{10}
1	15.00	70.00	30.63	0.01	0.91	0.07	0.01	0.00
2	-40.31	68.50	30.63	0.01	0.91	0.07	0.01	0.00
3	20.00	40.00	58.24	0.07	0.41	0.38	0.11	0.03
4	20.00	8.37	81.73	0.00	0.00	0.00	1.00	0.00
5	-160.75*	63.50	30.63	0.01	0.91	0.07	0.01	0.00
6	-162.39*	1.01	30.63	0.01	0.91	0.07	0.01	0.00
7	-40.09	38.50	42.63	0.02	0.28	0.49	0.16	0.04
8	-40.09	38.50	15.24	0.16	0.65	0.17	0.01	0.00
9	-40.09	38.50	0.37	0.16	0.65	0.17	0.01	0.00
10	-160.75	33.50	15.24	0.16	0.65	0.17	0.01	0.00
11	-160.75	36.00	0.37	0.16	0.65	0.17	0.01	0.00
12	-160.75	33.50	15.61	0.16	0.65	0.17	0.01	0.00
13	-40.78	3.25	58.24	0.07	0.41	0.38	0.11	0.03
14	-162.39*	1.01	0.93	0.13	0.86	0.00	0.00	0.00
15	-162.39*	1.01	29.70**	0.01	0.91	0.07	0.01	0.00

3.1.1 Process Description

Propane Precooling Process
The natural gas feed enters at 70 bar and 15°C (stream 1). This stream contains 2% CO_2, which needs removal before entering the liquefaction cycle because of the risk of dry ice buildup. The modeling of CO_2 removal is based on the findings by Pellegrini et al. 2019 [89], resulting in a CO_2 fraction of 50 ppm in the natural gas stream entering the propane precooling process. The stream is precooled through three kettle-type heat exchangers until reaching -40.3°C at the precooling exit (stream 2). The incoming compressed mixed refrigerant (stream 3) at 40 bar and 20°C is

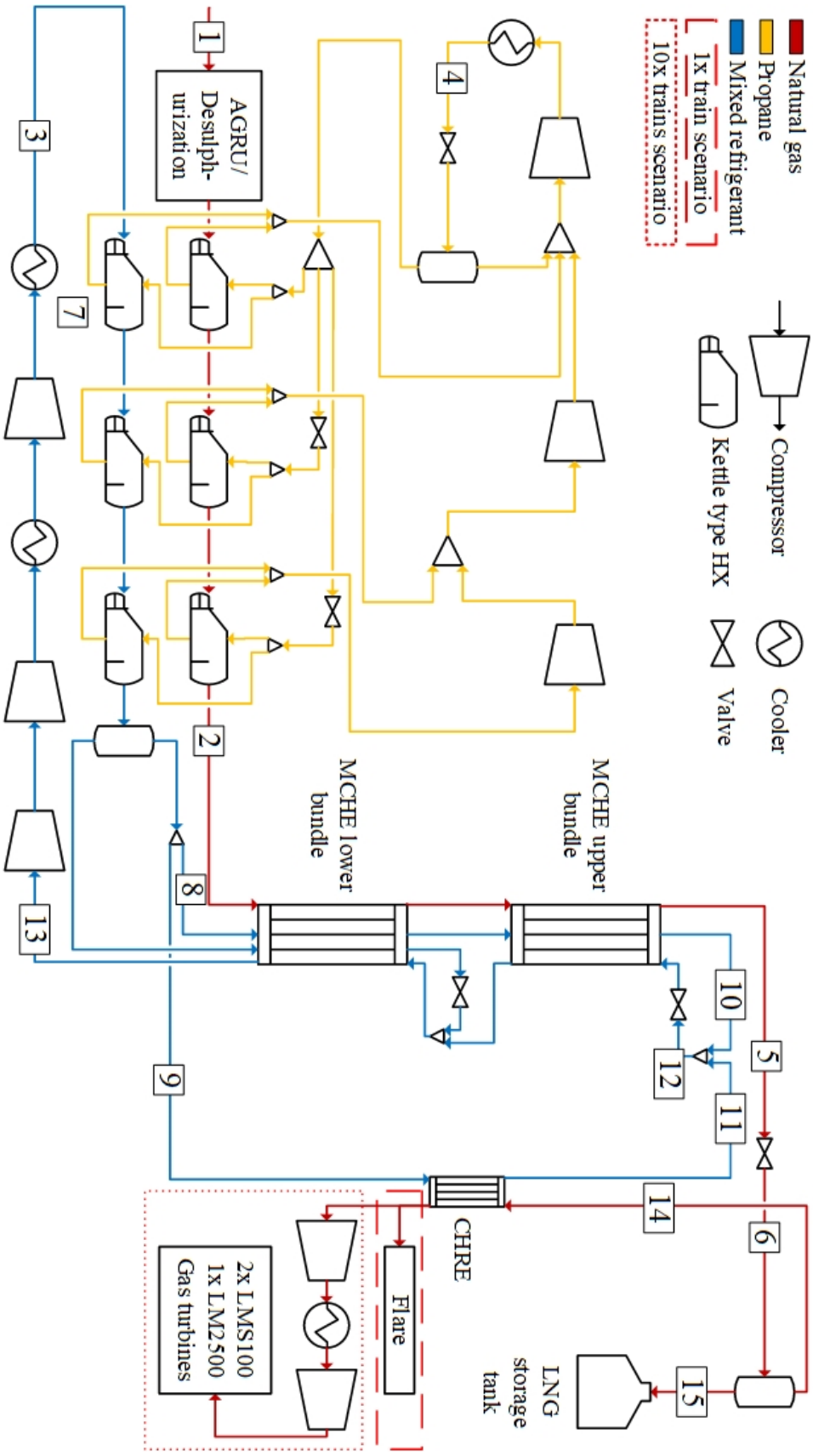

Figure 19: Schematic of the C3MR LNG process plant with modifications for the 1x and 10x trains in the red lines.

cooled to the same temperature in the other three kettle heat exchangers. Cooling is provided by a high-pressure propane stream that is condensed to 20°C using seawater as a cooling medium (stream 4). The propane stream is expanded through a JT valve before the liquid fraction enters a splitter.

The pressure letdown and heat exchange is performed in three stages. The splitter separates the incoming stream into three separate streams for a parallel pressure layout. The propane pressure levels decrease through JT valves, and further cooling of the streams is provided. The natural gas and mixed refrigerant heat exchangers are designed separately for design purposes and economic assessment reasons, discussed in Section 4.2. Consequently, the flow is separated to provide the correct propane stream fraction to each heat exchanger. Separate propane streams enter the cold side of the heat exchanger and vaporize, cooling down the natural gas and mixed refrigerant. After the heat exchangers, the propane streams are sent back for compression. The heat exchangers must fully superheat the propane to avoid liquid being fed to the compressors. The hot propane streams are mixed and sent to the compressors for a pressure increase. Finally, the propane is liquefied through the condenser and enters the precooling cycle again (stream 4).

MCHE Process

When the natural gas exits the propane precooling process, it enters the MCHE. This coil-wound heat exchanger has a very high area to provide cryogenic cooling for the natural gas stream. The natural gas is cooled in the MCHE to around -160°C by the mixed refrigerant in the upper bundle (stream 5). Due to LNG storage implications, the natural gas pressure is decreased through an isenthalpic JT valve to atmospheric pressure. Here, further cooling is provided, and a temperature of around -163°C at the valve outlet is obtained (stream 6). The stream is flashed where the liquid fraction is stored in LNG tanks at the exporting terminal, and the LNG vapor stream is either flared or used as fuel for the gas turbines, depending on the scenario. The electricity grid supplies power for the compressors in the 1x train. Consequently, the LNG vapor is flared into the atmosphere. To minimize the vapor fraction and the amount flared to the atmosphere, the outlet temperature of the upper bundle of the MCHE is set as low as possible. For the 10x train scenario, the outlet temperature of the MCHE upper bundle was selected to provide enough LNG vapor to power the two LMS100 gas turbines. The 1x and 10x train configurations for the flaring and gas turbines modeled in Aspen Plus are presented in Figures A.2 and A.3 in Appendix A.1.

After the precooling, the mixed refrigerant stream is separated in a flash vessel. The liquid MR stream and a fraction of the vapor enter the first cycle of the MCHE (stream 7 and 8). The other part of the vapor flows to the cryogenic heat recovery exchanger (CHRE) (stream 9). The vapor and liquid streams in the MCHE pass through separate circuits and are cooled, liquefied, and subcooled by internal heat exchange. Liquid MR is taken out after the lower bundle and flows through a JT valve to reduce its temperature and provide sufficient cooling for the respective area of the MCHE. After the upper bundle, the MR vapor stream (stream 10) is mixed with the outlet stream from the CHRE (stream 11). The mixed MR stream (stream 12) flowing into the upper bundle decreases pressure and temperature through the valve to provide further cooling in the MCHE. As the low-pressure refrigerant streams flow down to the upper and lower bundle of the MCHE, the streams are vaporized and superheated by cooling natural gas and the other MR streams.

The cold outlet MR stream of around -40°C is sent to the refrigerant compressors for recompression before entering the propane precooling cycle (stream 13). Compression of the mixed refrigerant is performed over three stages with intercooling between, typical for existing designs [90]. Using three refrigerant compressors restricts the outlet temperature of the MR from being too high. The outlet pressure of the mixed refrigerant entering the propane precooling cycle is 40 bar at 20°C after the condenser (stream 3).

After separating the vapor and liquid fraction of the natural gas in the final separation vessel, the

vapor fraction flows to the CHRE to provide cooling for the MR stream (stream 14). Further, the vapor stream is either flared for the 1x train or sent for compression in the 10x train scenario. The LMS100 gas turbines used in the 10x train do not operate at cryogenic temperatures, and the fuel gas is heated through the CHRE and compressed to 48 bar. The compression is performed in two stages, with cooling in between to reach a desired fuel gas temperature of around 200°C.

3.1.2 Modelling

The modeling assumptions are presented in Table 7. For CO_2 removal, an acid gas removal unit (AGRU) was modeled as a black box using assumptions discussed by Pellegrini et al. 2019 [89]. A small boiler or the excess gas turbine heat supplied the heating duty required for the AGRU within the plant for the 1x train and 10x train, respectively. The refrigerant compressor efficiencies were modeled as a polytropic using the GPSA method with an 80% efficiency [45]. The cooling medium used in the condenser depends on site conditions, modeled as seawater with a temperature of 15°C. The heat exchangers in the precooling cycle were modeled as kettle-type heat exchangers. The propane precooling heat exchangers' degree of superheat was modeled as 10°C, with a pinch point temperature of 2°C and a pressure drop of 0.5 bar. These are commonly used values for kettle-type heat exchangers, derived from Pozo et al. 2021 [45].

Table 7: Propane precooling process and MCHE modelling assumptions

Item	**Value**	**Units**
Mixed refrigerant feed pressure	40	bar
Polytropic compressor efficiency	80	%
Sea water temperature	15	°C
Propane precooling heat exchangers degree of superheating	10	°C
Propane precooling heat exchangers pinch point temperature	2	°C
Propane precooling heat pressure drop	0.5	bar
MCHE MITA	2	°C
CHRE MITA	2	°C
MCHE pressure drop per bundle	2.5	bar

With temperatures from the propane streams and assumptions in Table 7, the heat exchangers were modeled using outlet pressure and temperature as input parameters. Pressure levels are design variables discussed in a later paragraph. The three propane compressors were modeled with constant pressure ratios due to industrial and design purposes. As the pressure letdown and heat exchange is performed in three stages, the propane is sent back to compression after each stage. The compressor duty was determined by the required pressure for the propane stream to be liquid when cooled to 20°C in the condenser. Consequently, the pressure ratio was optimized to minimize compressor duty. The best pressure ratio over the three compressors was around 2.0 bar, leaving an outlet pressure of 8.0 bar.

The MCHE was modeled by combining two cold boxes to allow the streams to be let down in pressure at separate stages. The minimum temperature approach (MITA) for the two cold boxes was 2°C to provide a safety margin for the heat exchanger to perform and give a reasonable exchanger area. The pressure drop for each cold box was assumed to be 2.5 bar. The lower bundle was modeled by implementing design specifications for the temperature approach, the pressure drop, and the MITA of 2°C. The upper bundle was modeled using the pressure drop and keeping the outlet temperature of the natural gas and MR equal. The hot stream outlet temperature out of the upper bundle was different in the 1x and 10x trains. For the 1x train, the outlet temperature was set to minimize the flaring rate. For the 10x train, the outlet temperature was set to specify the vapor fraction required to fuel the two gas turbines. The outlet temperature of the hot stream

in the CHRE was set the same as the hot outlet temperatures in the upper bundle of the MCHE due to the efficient mixing of the streams. The valves were modeled as JT valves to ensure an isenthalpic expansion process.

Design Specifications

Design specifications were implemented to reach the target of 10°C superheat for the kettle-type heat exchangers. Propane mass flow and split fractions are design specifications variables to deliver the cooling duty specified in the heat exchangers. Each propane pressure level has its corresponding temperature and specific enthalpy. A new specific enthalpy was found using a 10°C superheat approach from the propane stream. This value was used as a target for the cold-outlet stream of heat exchangers to reach. Design specifications for the three natural gas heat exchangers varied the propane mass flow rate. Design specifications for the other heat exchangers varied the split fractions in the three propane splitters.

The natural gas inlet flow was varied in a design specification to obtain a power consumption of the compressors of 226 MW in the 10x train. Three design specifications regarding the cooling duty of the lower bundle of the MCHE were implemented. The first one ensured the same temperature before mixing the MR outlet streams from the lower bundle. Here the difference between the inlet and outlet temperature over the lower bundle was varied using the inlet natural gas flow temperature as a reference. Two design specifications were used to ensure the outlet temperature of the liquid and vapor fraction of MR was matched to the outlet temperature of natural gas in the lower bundle. Here, the inlet-outlet temperature approach was varied to achieve the same outlet temperature for the hot streams.

Optimization

An optimal design represents the design with the most desired objectives. The objective could be to minimize costs or emissions. Other objectives could be to maximize plant efficiency or production output. The optimization of a design is done by utilizing mathematical techniques to optimize a specific value in an objective function. Variables being changed during optimization are called design variables. In this objective function, different constraints apply, and a limited number of design variables are available. Variables that are fixed during optimization is called are called design parameters.

The optimization of the precooling cycle was performed manually due to limitations in the built-in optimization tool in Aspen Plus. The optimization tool could not access the specific enthalpies for the propane streams after the kettle-type heat exchangers. The optimization objective function for the propane precooling cycle was to minimize compressor work done by the three propane compressors. The optimization was done by an iterative approach using compressor pressure ratio and valve outlet pressures as design variables, given the heat exchangers' degree of superheat.

The optimization objective function J was to minimize the compressor work done by the precooling and MCHE cycle to maximize the possible LNG production. In a complete C3MR process, most of the power consumed is from the mixed refrigerant compressors. Optimization for the MCHE cycle was performed using Aspen's tool for optimization calculations. The objective function was to minimize the power consumption of the MR compressors and can be expressed as

$$min\ J = f(x) = \sum W = C_{LP} + C_{MP} + C_{HP} \tag{22}$$

were C_{LP}, C_{MP}, and C_{HP} is the power consumption of the compressor in the low-pressure (LP), medium-pressure (MP), and high-pressure (HP) stages, respectively. Here, compressor consumption is calculated from Equation 7 in Section 2.2.2.

A series of constraints were implemented in the optimization to give the process a feasible operation. Both the lower and upper bundles of the MCHE and the CHRE were modeled with a MITA of 2°C.

The valve outlet pressures were design variables to ensure efficient mixing of the MR streams after the upper and lower bundle but with the constraint of equal outlet pressure levels. A constraint was used on the cold outlet MR stream in the lower bundle to keep the stream entirely vaporized to avoid a partly liquid stream being fed to the compressors (stream 13).

From the objective function in Equation 22, design variables include the MR valve pressures, the LP and MP compressors outlet pressures, the MR composition, and the split fraction used to separate the stream to the CHRE. The MR composition is a vital factor in reducing the overall power consumption of the process, as discussed using the pinch analysis method in Section 2.2.4. For Aspen to allow optimization of the MR composition, the flow rates were split into five components and mixed into one MR stream. This was done to access each component in the optimization tool. Since there is no intercooling between the low- and medium-pressure compressor stages, only one of the compressors was chosen as an optimization variable, while the other was kept constant. This was done to ease the optimization tool and cut the simulation running time.

As discussed in the theory part in Section 2.4.4, the most thermodynamic efficient natural gas liquefaction process is where the refrigerant duplicates the cooling curve. The mixed refrigerant composition was optimized to provide a close approach to the composite curves. The temperature profile for the lower bundle of the MCHE is presented in Figures A.4, and A.5 in Appendix A.2. Here, cooling duty for the natural gas is calculated in Aspen Plus from Equation 6 in Section 2.2.2.

10x train Driver Configuration

The hot stream outlet temperature out of the upper bundle was determined using the vapor fraction after the isenthalpic expansion to atmospheric pressure in the last expansion valve (stream 6). The LMS100 gas turbine has an efficiency of 43% [88]. Using two LMS100 gas turbines as compressor drivers require a theoretical thermal energy demand of $2 \cdot 113$ MW$/0.43 = 526$ MW. Usually, fuel gas compressors are powered by a small power plant within the liquefaction plant. This auxiliary power plant consists of one or more small gas turbines to provide additional electricity to different plant sections. An LM2500 gas turbine was modeled as the fuel gas compressor driver with an efficiency of 38.4% [91]. To fuel the LM2500, a small portion of the LNG vapor is combusted. Combining the required thermal energy demand for the two LMS100 and the LM2500, an energy balance was conducted between the heat duty in the LNG vapor and the thermal energy demand. The energy balance is expressed as

$$VF(T) \cdot \dot{m}_{NG} \cdot LHV_{NG}(T) = TED_{LMS100} + TED_{LM2500} \tag{23}$$

were VF is the natural gas vapor fraction, $\dot{m}_{NG}$ is the total natural gas flow rate, LHV_{NG} is the lower heating value of the vaporized natural gas at 15°C, THD_{LMS100}, and TED_{LM2500} is the thermal energy demand for the two LMS100, and the LM2500, respectively.

A limitation of the Aspen Plus software is that the LHV of a stream cannot be accessed in a design specification or the optimization tool. An iteration was conducted to achieve an actual thermal demand of 526 MW to utilize the gas turbines' power output completely. The vapor fraction and the LHV are both related to gas temperature. Consequently, an iterative approach was performed to vary the hot outlet stream temperature in the upper bundle of the MCHE in addition to varying the natural gas inlet flow rate. Through this iteration, the LHV had to be updated manually in a calculator block due to the limitations mentioned. After several iterations, the calculator block converged when the actual thermal demand reached its theoretical optimized value of 526 MW. Here, the design specification for the natural gas flow rate reached 306.3 kg/s, used as the natural gas flow rate for the 10x train scenarios. Therefore, as discussed at the start of the technical assessment in Section 3, the 30.63 kg/s flow rate was introduced for the 1x train scenario.

3.2 Ammonia Plant Modeling

Modeling the MA-ATR ammonia process plant is based on studies conducted by Cloete et al. 2020 [7]. In this work, modifications have been made to the MA-ATR process and the ammonia synthesis loop to facilitate a direct comparison to the LNG process. Redlich-Kwong-Soawe (RKS) equation of state with Boston-Mathias alpha function (RKS-BM) is the property package used to simulate the entire process. To assess a more complex membrane-assisted gas switching reforming concept than the one available in Aspen Plus, the MA-ATR reactor was modeled in ANSYS FLUENT by Wassie et al. 2018 [92]. The technical performance parameters in the study on the MA-ATR reactor were used as input parameters to the rest of the MA-ATR process and ammonia synthesis loop. Consequently, as seen in Figure 20, the MA-ATR reactor and the ASU were modeled as black boxes. For a direct comparison to the LNG process, several parameters in the MA-ATR results were scaled up, including the permeate and retentate stream, to account for the natural gas flow rate increase.

The Modeling Process
A brief description of the MA-ATR ammonia process is given in Section 2.5.4. The following sections will explain the process and provide the methodology for modeling the different sections of the plant. First, a process description for the MA-ATR process and the ammonia synthesis loop is provided. Second, modeling assumptions for the respective sections of the plant are presented and kept the same as in the LNG process where possible. Lastly, the design specifications used in Aspen Plus are discussed to keep specific operating conditions satisfied. Figure 20 presents a schematic from the flow sheet modeled in Aspen Plus. A complete process flowsheet from Aspen Plus is displayed in Figures B.1-B.5 with 10x train configurations in Figure B.6, all from Appendix B.1. Complete material flows for both 1x and 10x trains are presented in Figure B.7, and B.8, respectively in Appendix B.2.

3.2.1 Process Description

The schematic overview of the MA-ATR ammonia process plant is shown in Figure 20, with stream conditions at key plant locations in Table 8. From Cloete et al. 2019, a conventional double-column cryogenic distillation process is utilized for the ASU [93]. Nitrogen and oxygen are produced at purities of 99.5% and 95.0%, respectively. The ASU inlet's airflow rate is adjusted to produce the necessary amount of H_2 for the desired NH_3 production, resulting in excess nitrogen released into the atmosphere.

In the ASU, the oxygen is compressed to 50 bar and used in the reactor to convert any excess fuel from the membranes. The products containing retentate (CO_2 and H_2O) (stream 5) are used for preheating the natural gas in three stages. The natural gas feed enters at 15°C and 70 bar (stream 1) with the composition presented in Table 5. This stream is preheated by the incoming retentate from the MA-ATR reactor. First, the natural gas is heated to 300°C before being desulphurized. Further, the stream is heated to 385°C before entering the pre-reforming process occurring at 414°C. In the pre-reformer, the higher hydrocarbons are converted before being heated in the feed preheater to 550°C (stream 4). Subsequently, this stream undergoes reforming into syngas within the MA-ATR reactor. Modeled as a block box, the hydrogen permeates through the membranes, thereby inducing a favorable shift in the reaction equilibrium towards enhanced hydrogen production.

Nitrogen (stream 9) is compressed to around 5 bar and serves as the purge stream within the membranes, intending to reduce H_2 partial pressure. This facilitates hydrogen extraction at elevated absolute pressure, decreasing compression work before the ammonia loop. The resulting permeate stream consists of a H_2:N_2 mixture of 3:1 at 5 bar and 700°C. This high-temperature permeate

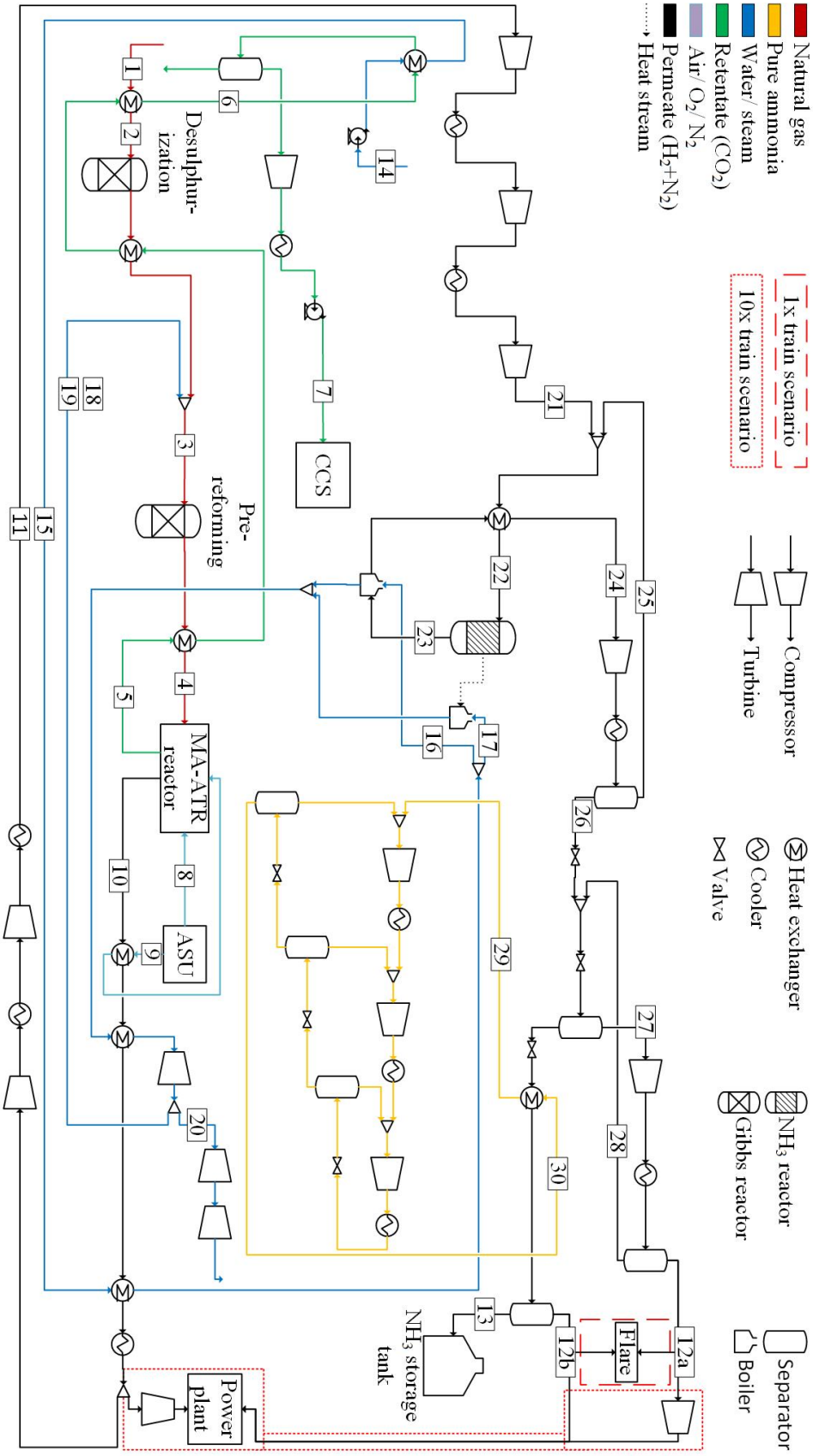

Figure 20: Schematic of the MA-ATR ammonia process plant with modifications in the red dotted line for the 10x train scenario.

Table 8: Stream conditions at different key locations in the MA-ATR ammonia process, (13%)*, and (5%)** lower for 10x train scenario.

Stream	**Temperature**	**Pressure**	**Flow**	**Species mol fractions**							
	(°C)	(bar)	(kg/s)	N_2	O_2	CO_2	H_2O	H_2	CH_4	C_{2+}	NH_3
1	15.00	70.00	30.63	0.01	0.00	0.02	0.00	0.00	0.89	0.08	0.00
2	300.00	68.60	30.63	0.01	0.00	0.02	0.00	0.00	0.89	0.08	0.00
3	413.76	52.60	88.12	0.00	0.00	0.01	0.65	0.00	0.32	0.02	0.00
4	550.00	51.06	88.12	0.00	0.00	0.02	0.60	0.03	0.34	0.00	0.00
5	700.00	49.50	102.58	0.01	0.00	0.62	0.36	0.00	0.00	0.00	0.00
6	206.12	46.59	102.58	0.01	0.00	0.62	0.36	0.00	0.00	0.00	0.00
7	24.57	110.00	83.12	0.01	0.00	0.97	0.00	0.00	0.00	0.00	0.00
8	368.00	50.00	25.69	0.01	0.95	0.00	0.00	0.00	0.00	0.00	0.00
9	680.00	5.00	52.12	1.00	0.00	0.00	0.00	0.00	0.00	0.00	0.00
10	700.00	5.00	63.35	0.25	0.00	0.00	0.00	0.75	0.00	0.00	0.00
11	25.00	21.56	63.35*	0.25	0.00	0.00	0.00	0.75	0.00	0.00	0.00
12a	20.00	56.14	0.61*	0.20	0.00	0.00	0.00	0.61	0.00	0.00	0.19
12b	-34.10	1.08	0.50*	0.03	0.00	0.00	0.00	0.08	0.00	0.00	0.87
13	-34.10	1.08	61.70*	0.00	0.00	0.00	0.00	0.00	0.00	0.00	1.00
14	15.00	1.01	88.61**	0.00	0.00	0.00	1.00	0.00	0.00	0.00	0.00
15	185.00	84.60	88.61**	0.00	0.00	0.00	1.00	0.00	0.00	0.00	0.00
16	282.00	114.50	33.85**	0.00	0.00	0.00	1.00	0.00	0.00	0.00	0.00
17	282.00	112.20	54.93**	0.00	0.00	0.00	1.00	0.00	0.00	0.00	0.00
18	430.00	112.20	88.78**	0.00	0.00	0.00	1.00	0.00	0.00	0.00	0.00
19	442.56	52.60	57.49	0.00	0.00	0.00	1.00	0.00	0.00	0.00	0.00
20	442.56	52.60	31.29*	0.00	0.00	0.00	1.00	0.00	0.00	0.00	0.00
21	140.10	205.00	63.35*	0.25	0.00	0.00	0.00	0.75	0.00	0.00	0.00
22	321.31	200.94	214.35*	0.24	0.00	0.00	0.00	0.71	0.00	0.00	0.05
23	450.00	198.95	214.35*	0.19	0.00	0.00	0.00	0.57	0.00	0.00	0.24
24	80.00	191.01	213.80*	0.19	0.00	0.00	0.00	0.57	0.00	0.00	0.24
25	20.00	206.25	150.99*	0.23	0.00	0.00	0.00	0.69	0.00	0.00	0.07
26	20.00	206.25	62.81*	0.00	0.00	0.00	0.00	0.01	0.00	0.00	0.99
27	21.52	20.00	1.19*	0.13	0.00	0.00	0.00	0.39	0.00	0.00	0.48
28	20.00	56.14	0.58*	0.00	0.00	0.00	0.00	0.00	0.00	0.00	1.00
29	-34.01	0.88	11.51*	0.00	0.00	0.00	0.00	0.00	0.00	0.00	1.00
30	-35.01	0.90	11.51*	0.00	0.00	0.00	0.00	0.00	0.00	0.00	1.00

stream (stream 10) preheats the nitrogen stream coming from the ASU (stream 9). The high-pressure steam from the NH_3 synthesis reactor is preheated from 190°C after the main economizer (stream 15) to 274°C in the second economizer. This high-pressure steam is split and sent to the NH_3 reactor for producing superheated steam at 110 bar and 350°C. Here, heating is provided for stream 16 and 17 by cooling the outlet stream of the NH_3 reactor and from heat extraction within the reactor, respectively. Further, the streams are combined (stream 18) and superheated to 550°C through heat exchange with the permeate stream from the MA-ATR reactor, and flows to a high-pressure steam turbine for expansion to 52.6 bar. Then, around one-third of the steam is sent for further expansion in the medium and low-pressure steam turbines (stream 20), while the other fraction is added as process steam before the pre-reforming stage (stream 19).

The resulting cooled permeate stream is compressed in five stages with intercooling using seawater at 15°C until reaching 205 bar. Here, the high-pressure permeate stream temperature is increased to around 320°C in a recuperator before entering the NH_3 synthesis reactor. The NH_3 synthesis reactor operates at 450°C resulting in an equilibrium conversion of around 24% ammonia in the product gas (stream 23). The product stream is cooled down in two stages through heat exchange with the high-pressure steam and the incoming high-pressure permeate, leaving a temperature of 80°C (stream 24). Further, the stream is compressed to 210 bar and cooled to 20°C before entering

a vapor-liquid separator. The vapor fraction is recycled into the permeate stream entering the recuperator, and the liquid stream is expanded in two stages until reaching 20 bar at 22°C, with an ammonia purity of 99%. Next, the stream is sent to another vapor-liquid separator, where the vapor fraction is compressed, cooled, and recycled (stream 28), while the liquid fraction is sent for further cooling. Finally, the liquid fraction is cooled down in an ammonia heat pump system to around -34°C at atmospheric pressure.

Scenario Configurations

Based on the scenario, stream 12a and stream 12b are either flared or used as fuel for a power plant. The excess vapor fraction is flared as the 1x train scenario consumes power from the grid, similar to the LNG plant. For the 10x train approach, a hydrogen power plant is used for powering all the compressors and pumps. Figure 20 shows the scenario differences in red. For the ten trains scenario, around 13% of the hydrogen power plant's permeate produced is used as fuel. This fraction is based on an energy balance between the thermal demand of the power plant and the total consumption of the MA-ATR ammonia plant, further discussed in Section 3.2.2.

3.2.2 Modeling

Modeling assumptions for the MA-ATR ammonia process plant are presented in Table 9. The polytropic efficiency for the compressor and the seawater temperature was the same as in the LNG plant at 80% and 15°C, respectively. Heat exchanger pressure drop was modeled as 2%, derived from Spallina et al. 2016 [94]. The pre-heating MITA for natural gas is 20°C, due to high-temperature increases. Sea water is pumped from the source and increased in pressure to 2 bar. Intercooling hot stream outlet temperature is based on the correspondent pressure level of the stream. For the low-pressure permeate (stream 10→11), the hot stream outlet temperature from the two intercoolers between the compressor stages was modeled as 25°C, with a MITA of 10°C. For the medium-to-high pressure permeate streams (11→21), the hot stream outlet temperature was set at 45°C, with a MITA of 10°C. Due to a close temperature approach in the permeate-economizer, the MITA of the economizers was modeled at 2°C. Lastly, the condensers used for the final liquefaction of ammonia and in the heat pump system have a hot stream outlet temperature of 22°C and a MITA of 5°C.

Table 9: MA-ATR ammonia process modeling assumptions

Item	Value	Units
Polytropic compressor efficiency	80	%
Sea water temperature	15	°C
Heat exchanger/ reactor pressure drop	2	%
Pre-heating MITA	20	°C
LP Intercooling hot stream outlet temperature	25	°C
MP/HP Intercooling hot stream outlet temperature	45	°C
Intercooling MITA	10	°C
Condenser hot stream outlet temperature	22	°C
Condenser MITA	5	°C
Economizer MITA	2	°C

The desulphurization and pre-reformer were modeled as adiabatic Gibbs reactors, which utilize the concept of minimizing the Gibbs free energy. For the ammonia synthesis reactor, a Gibbs reactor was also used but with a restriction in chemical equilibrium. In contrast to an adiabatic approach, the reaction temperature was specified at 450°C. As the inlet pressure to the ammonia liquefaction loop (stream 26) is high, several expansion stages were required before reaching proper storage

properties. The liquefaction process is based on the reverse Carnot refrigeration cycle discussed in Section 2.2.2. Here, the liquefaction of ammonia was modeled using expansion, vapor-liquid vessels, compression, and condensers sequentially before entering a heat pump system to reach -34°C. Expansion valves are modeled as JT valves through an isenthalpic expansion process. The flash vessels separate the vapor and liquid streams at a constant temperature.

Design Specifications

Several design specifications were implemented to get a feasible operation of the process plant. The two boilers raise steam to power the steam turbines and provide steam to the pre-reformer. To get the correct steam temperature, the cold stream outlet temperature was controlled by a design specification varying the water inlet mass flow rate. Here, stream 16 and 17 were varied to reach a temperature of 350°C before being superheated by the permeate stream. Other design specifications include the inlet water flow rate of all the intercoolers and condensers. As in the LNG plant, a pinch point temperature of 2°C is desirable to reduce overall compressor work, discussed in Section 2.2.4. The inlet water flow rate is varied to reach a cold outlet stream of 22°C, 27°C, and 47°C for the condensers, LP/MP intercoolers, and the HP intercoolers, respectively. Finally, a design specification for the ammonia heat pump system was introduced. For optimal longer-term storage reasons, ammonia was liquefied at atmospheric pressure. This was done by varying the cold stream mass flow rate to reach a hot inlet-outlet temperature approach of -3°C, resulting in a final ammonia temperature of -34°C (stream 13).

10x train Driver Configuration

Due to significant power demand, the 10x train scenario for the LNG and ammonia is equipped with a power plant. In the 10x train ammonia plant scenario, a fraction of the permeate stream containing around 75% hydrogen is used as fuel in a hydrogen-fired power plant. Additionally, the fraction of vaporous ammonia flared in the 1x train scenario is recycled into the power plant, providing an additional fuel supply. Like the LNG plant, an energy balance determines the fuel supply necessary to power the entire plant. This energy balance is achieved by adding up all the power consumption from the ASU, compressors, and pumps and subtracting the power produced by the steam turbines. The resulting power demand is then produced by the hydrogen-fired power plant. Typical power plant efficiencies for combined cycles are around 63% [44]. The energy balance is expressed as

$$TED = \frac{W_{ASU} + W_{comps} + W_{pumps} - W_{ST}}{0.63} \tag{24}$$

Here, TED is the thermal energy demand for the power plant to generate the required power . W_{ASU}, W_{comps}, and W_{pumps} are the total power consumption of the ASU, compressors, and pumps, respectively. W_{ST} is the power produced by the steam turbines. The thermal energy demand can be expressed as

$$TED = SF_p \cdot LHV_p \cdot \dot{m}_p + LHV_a \cdot \dot{m}_a \tag{25}$$

Here, SF_p, LHV_p, and $\dot{m}_p$ are the split fraction, lower heating value, and the mass flow rate of the permeate stream flowing out of the first intercooler, respectively. LHV_a, and $\dot{m}_a$ is the lower heating value and the mass flow rate of the combined vaporous ammonia stream from the ammonia liquefaction loop (stream 12a and 12b). By combining equation 24 and 25, the required split fraction of the permeate stream to fuel the power plant was around 13%.

4 Economic Assessment Methodology

After modeling the 1x train and 10x train approach for both LNG and ammonia in Aspen Plus, the technical performance parameters were used as input parameters in the economic assessment. The four scenarios provide different technical results based on the plant performance simulations in Aspen Plus. Parameters include mass and energy balances, environmental performances, raw material use, and choice of equipment for delivering the end product. In the following section, a methodology for an economic assessment of the technical performance of each scenario is conducted.

As discussed in Section 2.4.3 and 2.5.3, production and storage are the energy carriers' most significant costs in the value chains. Therefore, the value chain boundaries include production, exporting terminal, shipping, and importing terminal with storage. Upstream conditions such as natural gas extraction, processing plants, and pipeline networks were not considered before entering the production plant. Further, the scope does not include the economic costs of end-of-use downstream markets after the fuels are stored at the import terminal. However, the end-of-use combustion of natural gas that releases CO_2 was accounted for.

Table 10: Target cost basis details for the economic assessment

Location	US Gulf Coast
Year	2023
Currency	USD ($)

Exporting terminal, shipping, and importing terminal assumptions for all four scenarios are provided in Table 11. As discussed in the motivation in Section 1.1.2, the choice of shipping route is from Sabine Pass, Texas, to Wilhelmshaven, Germany. This route is 11,637 km, resulting in a roundtrip journey of 32 days at 30 km/h [95]. Importing storage capacity is set at 14 days to compare the four scenarios equally. Exporting storage capacity is based on the production rate of the plant and the shipping storage capacity. A value of $2 \cdot t_{ship}$ was chosen for days of storage, where t_{ship} is the time between ships entering the exporting terminal.

Table 11: Terminal assumptions and shipping route parameters for the round trip from Sabine Pass to Wilhelmshaven

Item	**Value**	**Unit**
Export terminal storage capacity	$2 \cdot t_{ship}$	days
Import terminal storage capacity	14	days
Shipping distance	11,637	km
Speed	30	km/h
Journey	32	days

4.1 SEA Tool

One of the main objectives of the thesis is to develop an equal techno-economic comparison between the LNG and ammonia value chains. Therefore, a consistent approach was taken to evaluate the different value chain costs. The Standardized Economic Assessment Tool (SEA Tool) developed jointly by the Flow Technology Group from SINTEF Industry and the Department of Energy Engineering from Universidad Politécnica de Madrid in Microsoft Excel was used for the economic assessment [85]. This tool aims to offer an easy-to-use, versatile, and transparent approach to evaluating the financial aspects of chemical and energy plants, specifically emphasizing their environmental impact and long-term sustainability.

The equipment correlations from Turton [96] and capacity cost correlations for various units are employed, adapting the source to correspond with the target cost basis for evaluation, as presented in Table 10. Location factors account for variances in material and labor expenses in distinct regions globally [97]. The principal economic assumptions concerning capital cost estimation, fixed (FOM) and variable (VOM) operating costs, and cash flow analysis variables are presented in Table 12.

A sensitivity analysis can also be conducted in the SEA Tool to examine the impact of critical economic assumptions. These parameters include natural gas and electricity prices, equipment material choices, CO_2 tax, CO_2 transport and storage costs, modular and MCHE scaling exponents, and costs for membranes. The impact on LCOP and COCA was evaluated by varying the parameters mentioned within realistic assumptions.

Table 12: Economic assessment assumptions, including capital estimation methodology, operating and maintenance costs, and cash flow analysis assumptions

Item	**Value**	**Unit**
Capital Estimation Methodology		
Bare Erected Cost (BEC)	SEA Tool Estimate	$M
Engineering Procurement and Construction (EPC)	10% BEC	$M
Process Contingency (PC)	0% BEC	$M
Project Contingency (PT)	20% (BEC + EPC + PC)	$M
Owners Costs (OC)	15% (BEC + EPC + PT)	$M
Total Overnight Costs (TOC)	BEC + EPC + PT + OC	$M
Total Capital Requirement (TCR)	111% TOC	$M
Operating and Maintenance Costs		
Maintenance	2.5	%TOC
Insurance	1.0	%TOC
Labour	60.000	$/y-p
Operators	40	p/train [98]
Natural Gas	2.5	$/GJ
Electricity	60	$/MWh
CO_2 tax	100	$/tonne
Cash Flow Analysis Assumptions		
Capacity factor first four years	65	%
Capacity factors remaining years	90	%
Discount rate	8.0	%
Construction period	4	years
Plant lifetime	25	years

The first input parameters to the SEA Tool were the energy and mass balances from the four scenarios. Here, the values of power consumption and producing units were specified. Further, the thermal balances, total auxiliary consumptions, and gross and net efficiencies were calculated. The second Section of the plant overview is the environmental performance. For the LNG value chain, natural gas is used in the power plant, shipping, and the downstream combustion of the fuel, additionally, some heavy fuel oil is combusted as supplementary fuel in the LNG carriers. Combustion of natural gas emits CO_2, and the overall greenhouse gas emissions from the liquefaction plant to the end-of-use were calculated. Finally, fuels and raw material inputs were specified to calculate the final thermal efficiency and costs for these inputs.

4.1.1 Capital Cost Breakdown

The capital cost breakdown is based on several high-level reports, further discussed in the "SEA Tool - User Guide" [46]. One of the main targets for using the SEA Tool is to provide a reasonable estimate for the BEC for each unit in a process plant. The plant location determines the currency, cost year, and location of the cost correlation references. As different units may use data from various sources, the cost of each unit is adjusted to the target cost basis using an exchange rate, Chemical Engineering Plant Cost Index (CEPCI), and location factors (to account for differences in material and labor costs across world regions). Equation 26 demonstrates how cost estimation in the source basis (A) is adjusted to the target basis (B)

$$C_B = C_A \cdot \frac{F_{L_B}}{F_{L_A}} \cdot \frac{CEPCI_B}{CEPCI_A} \cdot E_{AB} \tag{26}$$

In this equation, E_{AB} represents the currency exchange rate from basis A to B and F_L accounts for labor and material adjustments between regions. The factors are derived from weighted material and labor relative values, further discussed in the user guide [46].

From Table 12, the different costs in a complete capital estimation methodology are presented. Here, the BEC accounts for process equipment, facilities, infrastructure, and the direct and indirect costs of installation and labor. The EPC accounts for the costs related to engineering, procurement, and construction. Process contingencies relate to extra capital costs to specific components or units that present a lower level of readiness or maturity. Project contingency is associated with the additional capital costs of site-related risks. Owners' costs, such as land, financing, permits, and fees, are added to determine the TOC. Finally, the TCR is calculated by adding the capital expenditure during cost escalation and interest.

Calculating the BEC using the SEA Tool was done using two approaches. An equipment approach was taken for the different components in the Aspen Plus flowsheets, such as compressors, heat exchangers, vessels, pumps, and reactors. This approach uses individual equipment cost correlations from parameters such as material, pressure levels, and bare module factors to evaluate the BEC. The other method for calculating the BEC is the scaling approach. When assessing costs for process units, equipment, or other parts in the value chain where specific equipment parameters are hard to access, the scaling approach was used to gather information based on references in the literature.

Due to economies of scale, further discussed in Section 2.3.3, a modular scaling exponent was applied when using the equipment approach in the 10x train scenarios. After the configurations in the 1x train Aspen Flowsheet to account for the power plant configuration in both scenarios, the train was scaled ten times up. Here, a modular scaling exponent of 0.9 was utilized. Therefore, this parameter is highly uncertain and included in the sensitivity analysis in Section 5.2.3.

Equipment Approach

BEC estimation is based on the correlations from Turton et al. 2008 [96]. Purchased equipment costs are normalized to 2001 in US dollars, while the bare module factors for field installation cost are from Guthrie et al. 1969 [99]. For a unit operating at ambient pressure using carbon steel as material, Equation 27 determines the cost (C_p^0) using a logarithmic expression.

$$log_{10}C_p^0 = K_1 + K_2 log_{10}(A) + K_3[log_{10}(A)]^2 \tag{27}$$

Here, A is the capacity or size parameter of the equipment within limits. K_1, K_2, and K_3 are specific constants to each type and subtype of equipment.

Where operating pressures differ from atmospheric, a pressure correction factor F_P is applied,

expressed in Equation 28.

$$log_{10}F_P = C_1 + C_2 log_{10}(P) + C_3[log_{10}(P)]^2 \tag{28}$$

For vessels used to determine vapor-liquid separators or reactor costs, the pressure correction factor is determined in Equation 29.

$$F_{P,vessel} = \frac{\frac{P \cdot D}{2[850 - 0.6 \cdot P]} + 0.00315}{0.0063} \tag{29}$$

Here, P represents the absolute pressure (bar), D is the diameter (m), and $F_{P,vessel}$ is always greater than 1.

Finally, factors for different construction materials are provided for each subtype, and the bare module factors are calculated in equation 30. The bare module factor F_{BM} may be provided directly for certain equipment. The final cost of the bare module is calculated by multiplying the purchased equipment cost with the bare module factor:

$$C_{BM} = C_P^0 F_{BM} = C_B^0 (B_1 + B_2 F_M F_P) \tag{30}$$

This factor is determined within equipment capacity limits, and therefore when the upper limit is exceeded, a scaling cost law is applied with an exponent of 0.67. As Arnaiz del Pozo et al. 2022 discussed, an exponent of 0.67 gives reasonable results for common equipment such as compressors, heat exchangers, and turbines [46].

In the SEA-Tool, a set of correlations from Turton et al. 2008 are already provided depending on equipment and subtype [96]. Therefore, when utilizing the equipment approach, each subtype contains its corresponding required input parameters and the resulting output. An overview of different equipment used in the LNG and ammonia plant concerning input and output parameters is provided in Table 13. When using the equipment approach for calculating the BEC, each component's technical parameters are extracted from the different Aspen flowsheets and used as input parameters into the specific equipment and subtype presented in Table 13. The result is a set of rows in the SEA Tool that adds up all the respective BECs for each component and calculates the final cost for that part of the process.

Table 13: Correlation input and output parameters for equipment, (*) indicates both regular and clad coated options. Values are derived from Turton et al. 2008 [96]

	Correlation Input				***Correlation Output***				
Equipment	**Capacity**	**Pressure**	**Material**	**Other Spec.**	C_B^0	F_P	F_M	F_{BM}	C_{BM}
Compressors	kW	-	CS/SS/Ni	-	195	-	-	2.7	533
Turbines	kW	-	CS/SS/Ni	-	177	-	-	3.5	619
Drives	kW	-	N/A	-	289	-	-	1.5	433
Pumps	kW	bar	Cl/CS/SS/Ni	-	2,450	1.0	1.6	4.0	9,758
Heat exchangers	m^2	bar	CS/CU/SS/Ni/Ti	Subtype	21,120	1.0	1.0	3.3	69,486
Vessels	m^3	bar	CS*/SS*/Ni*/Ti*	Diameter (m^2)	3,143	1.0	1.0	4.0	12,794

The choice of material for compressors, heat exchangers, flash vessels, and condensers depends on factors such as the operating temperature, corrosive environments, and budget constraints. Carbon steel is typically used for low-cost applications where the temperature ranges between -75°C and 430°C [100]. Stainless steel is generally corrosion-resistant, with a more comprehensive temperature operating range than carbon steel, and is often used in compressors [101]. Stronger alloys include titanium (Ti) and Ni (Ni). Titanium has exceptional corrosion resistance in seawater environments [102]. Ni is typically used for excellent corrosion resistance and reduces the risk of hydrogen embrittlement over a wide range of temperatures [103]. The main disadvantage of titanium and Ni is the high material costs compared to carbon and stainless steel.

A separate calculation was performed in the SEA Tool to extract the surface area and volume for the heat exchangers and vessels, respectively. The thermal transmittance (UA value) was extracted from Aspen's heat exchanger results to calculate the surface area further. Whether there is a phase change over the heat exchanger determines the thermal transmittance of the process. Additionally, a pressure exponent is implemented to account for the pressure level in the heat exchanger. Table 14 presents the heat exchanger values used for calculations. Inlet flow rates and densities of the liquid and vapor fractions were used for the flash vessels to calculate the internal volume.

Table 14: Heat exchange reference parameters

Item	**Value**	**Unit**
Pressure exponent	0.7	-
Gas at 1 atm	40	W/m^2K
Liquid	1500	W/m^2K
Phase change	4000	W/m^2K

Scaling Approach

When feasible, the equipment approach is always taken because of the method's more accurate in and depth analysis for calculating the BEC. However, this approach is not always possible for specific equipment or other parts of the value chain. Consequently, an alternative method for calculating the BEC is the scaling approach. This technique relies on academic literature with cost assessment using the same unit scope. Utilizing this methodology incorporates the economies of scale principle; whereas the equipment size increase, the specific cost per unit capacity decreases. The generalized formula for economies of scale introduces cost reductions when adding several trains operating at the same capacity. Some synergies introduce cost reductions when building additional trains at the facility. The scaling cost law for economies of scale is presented in Equation 31.

$$C = C_0 \left(\frac{n}{n_0}\right)^e \left(\frac{Y/n}{Y_0/Y_n}\right)^f \tag{31}$$

Here, C_0 and Y_0 are the reference cost and capacity, respectively. Further, Y is the desired scaled-up capacity, f is the unit exponent, and e is the train exponent. Typical values for f and e are 0.67 and 0.9, as Arnaiz del Pozo et al. 2022 discussed, respectively [46].

The economic assessment of the different units in the LNG and ammonia value chain was modeled using both the equipment and scaling approach. As the LNG and ammonia plant was modeled in Aspen Plus, discussed in Section 3, the equipment approach was taken for most of the units. An overview of the scaling parameters from reference literature for calculating the BEC for each component is outlined in Table 15. Using reference literature, the CO_2 removal unit in the LNG plant, the ASU, and the pre-reforming in the ammonia plant were modeled as black boxes. For both processes, a desulphurization unit was also introduced as a black box to remove excess sulfur content in the feed stream. Consequently, the scaling approach was taken for the economic assessment in the SEA Tool. Further, calculating the BEC for the power plant, exporting, and importing terminal for both scenarios were analyzed from academic literature; hence the scaling approach was utilized.

4.1.2 Operational Cost Breakdown

Costs for FOM, VOM, and fuel and raw material that are general for all four scenarios are displayed in Table 12. Fixed maintenance, insurance, and labor costs are derived from Spallina et al. 2016 [94]. Using reference literature, around 40 persons are employed per MTPA LNG. The 1x train

Table 15: Reference costs, capacities and basis cost year for calculating the BEC by the scaling approach for various process components in the C3MR LNG plant and MA-ATR ammonia plant

Process Component	Scaling parameter	Ref. capacity	Ref. cost ($M)	Scaling factor	Cost year	Reference literature
LNG plant						
CO_2 removal unit	Inlet flowrate (kg/s)	68.2	128	0.80	2019	Pellegrini et al. 2019 [89]
Exp. & imp. terminal	Volume (m^3)	160,000	150	0.67	2016	Raj et al. 2016 [12]
Ammonia plant						
Air separation unit	Inlet flow rate (kg/s)	1	7.8	0.76	2022	Arnaiz del Pozo et al. 2022 [104]
Pre-reforming	Thermal input (MW)	1800	17.5	0.75	2005	Cloete et al. 2020 [7]
Desulphurization	Thermal input (MW)	413.8	0.66	0.67	2011	Gazzani et al. 2011 [105]
Power plant	Power (kW)	1	1000	1	2021	IEA 2022 [106]
Exp. & imp. terminal	Mass (tonne)	25,000	20.2	0.67	2006	Bartels et al. 2008 [9]

LNG plant is close to one MTPA of production. Consequently, the 1x train scenario employs 40 people, while the 10x train scenario has a labor force of 400 persons.

The costs that have the most significant effect on the LCOP are those related to fuel, raw materials, and CO_2 tax in the LNG scenario. The prices of natural gas and electricity are highly unpredictable, as discussed in Sections 2.4.3 and 2.1, respectively. The cost of natural gas was $2.5/GJ, and the electricity cost was $60/MWh. Further, the CO_2 price used in the base case scenario was $100/tonne. These parameters are crucial for the final cost assessment. Therefore, Section 5.2.3 presents a sensitivity analysis of the impact of natural gas, electricity, and CO_2 prices on the LCOP.

4.2 LNG

The LNG value chain capital costs were divided into three units for the 1x train scenario and four for the 10x train scenario, where a power plant is included. The LNG plant consists of precooling, liquefaction, and the power plant. Another cost-intensive component is the exporting and importing terminals, expressed as a single unit. The equipment approach was taken for the propane precooling and liquefaction process, excluding the CO_2 removal and desulphurization units. Economic correlations for the scaling approach for the CO_2 removal unit and the exporting and importing terminal were found using existing literature by Pellegrini et al. 2019 [89] and Raj et al. 2016, respectively [12]. The power plant used for the 10x train scenario uses a direct cost relation derived from the "2020 Gas Turbine World Handbook"; therefore, no scaling approach is required [107]. Shipping, fixed and variable operation, and maintenance costs are part of the operational costs.

4.2.1 Production Plant

Precooling and Liquefaction Process

The bare module costs were calculated using Equation 30 with the cost functions presented in Table 13. Each equipment bare module cost is calculated by the appropriate cost correlation. When calculating the BEC using the equipment approach, each component purchase cost is first calculated based on the size. Further, more expensive materials and higher operating pressures are accounted for using material and pressure factors. Table 16 presents process components with the respective material and operating pressure.

Stainless steel was used as a material for propane compressors. The propane flash vessel separating the liquid and vapor part operates at around -4°C and carbon steel was used due to the viable operating range. From Section 3.1.2, the cooling medium is seawater at 15°C; consequently, a

Table 16: LNG process plant components material choices, (*) refers to the 10x train

Process	Material	Process	Material
Propane Precooling		**Liquefaction**	
Propane compressors	SS	MR compressors	SS
Flash vessel	CS	MCHE	Ni/Ni
Condenser	CS/Ti	Condensers	CS/Ti
NG kettle reboilers	CS/CS	MR flash vessel	Ni
MR kettle reboilers	CS/CS	NG flash vessel	Ni
Water pump	Ni		
MR compressors	SS	**Power Plant**	
		NG Compressors*	SS

titanium alloy was used for corrosion resistance in the condenser. Both the NG and MR kettle reboilers operate at temperatures between -40°C to 20°C, and thus carbon steel heat exchangers were used for cost reasons. The seawater pump supplying the whole LNG plant with cooling water must be highly corrosive resistant. The SEA-Tool did not allow a titanium alloy for the centrifugal pump; therefore, nickel (Ni) was used.

Due to the wide operating temperature and general corrosion resistance, the NG and MR compressors in the liquefaction process were modeled as stainless steel compressors. In the MCHE, several MR streams of different pressures and temperatures enter and reenter while natural gas is cooled down to around -163°C. Consequently, a strong alloy that can handle vast temperature variations and corrosion load is required. Material use of the MCHE is somewhat uncertain due to a limited amount of suppliers with various technologies [108]. The material of choice for the MCHE was Ni, which increased the cost of the LNG plant dramatically. A sensitivity analysis on the material for MCHE is conducted in Section 5.2.3. Both the MR condensers use seawater for cooling, and a titanium alloy is required for corrosion resistance. Lastly, the NG and MR flash vessels operate at low temperatures, so a Ni-based vessel similar to the MCHE was utilized.

Further discussed in Section 2.4.3, the MCHE is the highest single-cost component in an LNG plant. For the equipment approach across the four scenarios, the unit exponent was set at 0.67, further discussed in Section 4.1.1. However, this exponent was changed to 0.80 due to a lower value being too optimistic for such a high-cost component. This variable affects the overall cost of the 1x and 10x LNG plants and is included in the sensitivity analysis in Section 5.2.3.

Because the AGRU and desulphurization units were modeled as black boxes, the scaling approach was taken for calculating the BEC. As discussed in Section 3.1.2, the AGRU reduces the CO_2 mole fraction from 2% down to 50 ppm in the natural gas feed stream. A desulphurization unit removes fractions of sulfur in the feed stream. Reference literature parameters for utilizing the scaling approach for the units are presented in Table 15. Results for purchase costs of these units, before the bare erected costs are presented in Table 17.

Table 17: AGRU and desulphurization parameters in the 1x and 10x train LNG plants. AGRU and desulphurization cost basis year are 2019 and 2011, respectively

	AGRU		***Desulphurization***	
Plant scenario	**Capacity (kg/s)**	**Cost ($M)**	**Capacity (MW)**	**Cost ($M)**
1x train	1.50	6.0	1,497	1.4
10x train	15.0	38	14,974	6.5

Power Plant
The last unit in the LNG plant is the power plant configuration for the 10x train scenario. Using 2020 values from the "Gas Turbine World Handbook 2020", purchase costs of $40M and $12.5M for the LMS100 and LM2500 were found, respectively [107]. An installation cost factor of 1.67 was used for both turbines, accounting for site preparation, civil works, electrical interconnection, control systems, and other necessary components.

4.2.2 Exporting and Importing Terminal

As discussed in Section 2.4.3, storage tanks in the exporting and importing terminal are one of the major cost components in the LNG value chain. A scaling approach was taken for both the exporting and importing terminals from the paper by Raj et al. 2016 with reference parameters in Table 15 [12]. Table 18 presents the required number of tanks, the scaled capacity, and the corresponding purchase cost of the tanks using 0.90 as the train exponent. As later discussed in Section 4.2.3, the assumed days of storage for the export terminal are two times the days between ships arrive at the port. For the importing terminal, a constant value of 14 days is assumed.

Table 18: LNG export and import storage terminal parameters for the 1x and 10x train LNG scenarios

	Export terminal			***Import terminal***		
Terminal scenario	**Number (# tanks)**	**Capacity (m^3)**	**Cost ($M)**	**Number (# tanks)**	**Capacity (m^3)**	**Cost ($M)**
1x train	1	96,282	107	1	75,572	105
10x train	3	160,000	403	5	160,000	741

4.2.3 Shipping

Briefly discussed in Section 2.4.1, the LNG shipping industry is a critical part of the value chain, responsible for transporting natural gas from production facilities to consumer markets. LNG carriers of around 140,000 to 160,000 m^3 are the most common, as discussed in Raj et al. 2016 [55]. From this reference, an LNG vessel with a capacity of 160,000 m_3 was used in the 10x train scenario with laden and ballast BOG rates of 0.075% and 0.0375%, respectively. Reference parameters for the 1x train and 10x train approach are presented in Table 19. The laden voyage is the loaded route from the US to Germany, while the ballast voyage is the returning trip. From the findings in the paper, 60% and 30% of the BOG are used fuel for the LNG vessel in the laden and ballast voyage, respectively. The propulsion configuration system in the LNG vessel is a dual fuel system, where HFO meets the remaining fuel requirement, which parameters are shown in Figure 20. Based on the volatility of LNG carrier rates discussed in Section 2.4.3, an average hire rate of $60,308/day for a 160,000 m_3 LNG carrier was used in the years between 2015 and 2021 [109].

Table 19: LNG shipping parameters for the 1x and 10x train LNG scenarios, with 2016 as cost basis year

Ship scenario	**Capacity (m^3)**	**BOG-rate laden (%)**	**BOG-rate ballast (%)**	**Hire rate ($/day)**
1x train	40,000	0.100	0.05	23,823
10x train	160,000	0.075	0.038	60,308

A smaller LNG vessel is required because the LNG production rate from the 1x train is much lower than for the 10x train. If the same LNG carrier is used for the 1x train scenario, 57 days of

storage is required for the exporting terminal to account for the ships only arriving every 28th day. Consequently, a smaller vessel with a storage capacity of 40,000 m^3 [110] is introduced. This vessel has slightly higher BOG rates of 0.10% and 0.05%, respectively. Due to the lack of references regarding LNG carrier vessel rates for small-to mid-scale LNG carriers, the scaling approach is taken for calculating the daily hire rate for the 40,000 m^3 vessel. Using the scaling cost law from reference parameters in Table 19 for the 10x train, the corresponding daily hire rate for the 40,000 m_3 vessels is $23,823.

Table 20: Heavy fuel oil parameters, [20]*, [111]**

Item	Value	Unit
LHV	41,760*	kJ/kg
Spec. CO_2 emissions	3.0*	kg CO_2/kg fuel
Fuel price	317**	$/tonne

4.3 Ammonia

The economic evaluation of the ammonia value chain within the SEA Tool was partitioned into four distinct components for the single train configuration and five components for the tenfold train configuration, incorporating the power plant. The methodology for determining the BEC included both equipment and scaling-based approaches. The ammonia production facility, designated as NH_3 MA-ATR, comprises the MA-ATR process and the ammonia synthesis loop, wherein equipment-based and scaling approaches are implemented. The BEC was calculated using the scaling approach for the power plant and both terminals, drawing upon data from relevant literature sources. Costs for shipping, fixed and variable operation, and maintenance costs are included in the operational costs.

4.3.1 Production Plant

MA-ATR Process
The MA-ATR process consists of the MA-ATR reactor, desulphurization, pre-reforming, ASU, and the CCS loop. Using Equation 30 with cost functions in Table 13, bare erected costs for the MA-ATR reactor and the CCS loop were calculated using the equipment approach with relations from Turton et al. 2008 [96]. With material choices expressed in Table 21, and pressure factor correlations from Table 13, more expensive materials and higher operating pressures were accounted for.

The CO_2 flash vessels and pump were made of carbon steel, whereas the compressor was made of stainless steel. Due to heat exchange with seawater, the retentate economizer was made of carbon steel on the hot side and titanium on the cold side. The natural gas preheaters were made of carbon and stainless steel because of large temperature fluctuations. The MA-ATR reactor modeling was based on the study by Cloete et al. 2019 [93]. Assumptions from the study are presented in Table 22. The required surface area for the reactor was found using the assumptions provided. Further, an iteration was done regarding the number of reactors versus total costs, where the reactors ranged from one to ten. Consequently, five reactors were used per train for the MA-ATR process. Using the same analogy for the choice of material for process equipment as in the LNG case, the reactor shell and liner were modeled as carbon steel and Ni shells, respectively. The inner Ni-alloy material carries the temperature and embrittlement loads, while the outer carbon steel shell carries the pressure load.

The desulphurization and pre-reforming of natural gas before entering the MA-ATR reactor were modeled as black boxes using the scaling approach for the economic assessment. Additionally,

Table 21: Ammonia process components material choices, (*) refers to the 10x train

Process	Material	Process	Material
MA-ATR process		**Ammonia synthesis loop**	
CO_2 compressor	SS	Permeate compressors	Ni
Economizer	CS/Ti	Retentate compressors	SS
Preheaters	CS/SS	Other compressors	CS
Flash vessel	CS	Steam turbines	SS
CO_2 pump	CS	Intercoolers & condensers	CS/Ti
MA-ATR reactor shell	CS	Recuperator	Ni/Ni
MA-ATR reactor liner	Ni	Superheater	Ni/Ni
		Heat pump heat exchangers	CS/CS
Power Plant		Water pumps	Ni
Fuel gas compressor*	Ni	MA-ATR reactor shell/liner	CS/Ni
		MA-ATR reactor heat exchanger	Ni/Ni

Table 22: MA-ATR reactor modeling assumptions

Item	Value	Unit
Diameter	3.6	m
Height	8.4	m
Insulation	0.2	m
Shell pressure	50	bar
Insulation density	200	kg/m^3
Insulation cost	0.1	$/kg
Oxygen carrier density	3400	kg/m^3
Oxygen carrier volume fraction	0.5	-
Membrane volume fraction	0.5	-
Membrane diameter	0.05	m

BEC calculations for the ASU used for nitrogen and oxygen in the reactor were calculated from reference literature. Each process component regarding reference capacity, cost, scaling factor, cost year, and reference literature is presented in Table 15. Results for purchase cost, before erected costs, are presented in Table 23. Instead of having ten of each unit when scaled up to the 10x train scenario, the ASU, desulphurizer, and the pre-reformer are instead modeled as one larger unit for enabling economies of scale.

Table 23: ASU, desulphurization, and pre-reforming parameters in the 1x and 10x train LNG plants. ASU, desulphurization, and pre-reforming cost basis year was 2022, 2011, and 2005, respectively

	ASU		***Desulphurization***		***Pre-reforming***	
Plant scenario	**Capacity (kg/s)**	**Cost ($M)**	**Capacity (MW)**	**Cost ($M)**	**Capacity (MW)**	**Cost ($M)**
1x train	25.7	91.6	1497	15.24	1497	1.56
10x train	257.0	528	14,974	85.72	14,974	7.31

Ammonia Synthesis Loop

The process of producing and liquefying ammonia starts at the permeate outlet from the MA-ATR reactor, known as the ammonia synthesis loop. It involves various equipment and components, as shown in Figure 20, except for the MA-ATR process and the power plant for the 10x train

scenario. The equipment approach was used to determine the BEC of the process components in the ammonia synthesis loop. Table 21 provides information on the material choices for these components.

After leaving the MA-ATR reactor, the permeate stream is at high temperatures and has a 3:1 H_2:N_2 mole ratio. To handle this, Ni-alloy heat exchangers are used in the nitrogen heat exchanger and superheater. The permeate stream is then cooled using seawater, which requires a titanium alloy to prevent corrosion in the economizer and intercooling stages. To handle the high flow rates of hydrogen, Ni-alloy compressors are used for the five-stage compression of the permeate stream. However, Ni-based compressors are expensive and a major cost component of ammonia plants. Therefore, a sensitivity analysis of the compressor material is performed in Section 5.2.3. Finally, the high-pressure permeate stream is heated in a Ni-alloy recuperator before entering the MA-ATR reactor.

Modeling assumptions of the MA-ATR reactor were derived from previous works by Cloete et al. 2019 [93]. A consistent iterative approach was applied to determine the optimal number of reactors providing the lowest cost, resulting in five reactors per train. Table 24 summarizes the assumptions made for the ammonia synthesis reactor. As in the MA-ATR reactor, a Ni alloy was used for the internal heat exchange in the MA-ATR reactor and the liner to resist pressure and risk for hydrogen embrittlement. The outer shell was a carbon steel alloy to handle high operating pressure.

Table 24: Ammonia synthesis reactor modeling assumptions

Item	**Value**	**Unit**
Diameter	2.4	m
Height	7.0	m
Insulation	0.2	m
Shell pressure	200	bar
Insulation density	200	kg/m^3
Insulation cost	0.1	\$/kg
Catalyst density	3400	kg/m^3
Catalyst volume fraction	0.3	-
Catalyst cost	0.3	\$/kg

Process equipment after the MA-ATR reactor, including the recycling loop and heat pump system, comprises a set of compression and cooling steps before being liquefied. The cold side of the seawater coolers is made of titanium for corrosion resistance. The ammonia compressors are made of stainless steel, while the vapor-liquid vessels are made of carbon steel to handle the pressure loads. In the heat pump system, the three compressors and vessels are made of carbon steel due to a narrow temperature range and use a pure compound as a cold stream.

Power Plant

For the 10x train scenario, a power plant is included due to the large power demand and to make the plant independent from the electricity grid. As discussed in Section 3.2.1, 13% of the permeate stream produced in the MA-ATR reactor is used for fuel in the power plant, with additional supply from the vapor fraction in the ammonia synthesis loop. For the permeate stream to be used as fuel it is compressed to 35 bar by a Ni-alloy compressor. A direct cost reference was used for calculating the power plant cost based on the yearly average of IEA's power plant costs per capacity installed [106]. This is based on a combined cycle gas turbine plant that costs \$1000/kW from the year 2021. From Section 3.2.2, the total power demand in the 10x train process is 1,277 MW, resulting in a purchase cost of \$1,277M.

4.3.2 Exporting and Importing Terminal

Similar to the LNG scenario, a scaling approach was taken by reference literature from Bartels et al. 2008 to calculate the BEC for the importing and exporting terminal in the ammonia value chain [9]. Large-scale ammonia storage tanks range between 15,000 and 60,000 tonnes [80]. Consequently, a storage capacity per tank of 60,000 tonnes was used at the exporting and importing terminal, equivalent to 111,848 m^3. Reference parameters from the study are displayed in Table 15 with 0.67 as the scaling factor from the cost basis year of 2006. Exporting terminal capacity in the number of days two times the shipping frequency, expressed in the assumptions from Table 11. Table 25 presents the number of tanks, tank capacity, and calculated purchase costs.

Table 25: Ammonia export and import storage terminal parameters in the 1x and 10x train LNG scenarios, with 2006 as the cost basis year

	Export terminal			***Import terminal***		
Terminal scenario	**Number (# tanks)**	**Capacity (tonne)**	**Cost ($M)**	**Number (# tanks)**	**Capacity (tonne)**	**Cost ($M)**
1x train	2	60,000	89	2	60,000	89
10x train	7	60,000	210	10	60,000	289

4.3.3 Shipping

As further discussed in Section 2.5.1, fully refrigerated gas carriers are used for ammonia shipping over long distances. The largest liquefied petroleum gas (LPG) carrier ever built, the BW Gemini, was used for the 1x train scenario, with a capacity of 84,000 m^3 [112]. The BW Gemini is a dual-fuel propulsion vessel that can use LPG gas in the engines. Ammonia as fuel for shipping is discussed in Section 2.5.1, and for this assessment, it is assumed that both the vessels are utilizing 100% ammonia-fed engines for propulsion. The BW Gemini's fuel consumption using LPG is 35.6 tonne/day and 32.4 tonne/day for the laden and ballast voyage, respectively [113]. As the energy content in liquefied ammonia is lower than for LPG, more ammonia is required for the engines. For the laden and ballast voyage, the fuel consumption calculations for the 1x and 10x train vessels are presented in Table 26.

The carrier hire rate for the vessels used in the 1x train and 10x train scenarios are presented in Table 26. Further discussed in Section 2.5.1, ammonia carriers are expected to increase in size as demand for low-carbon fuels emerges. If the BW Gemini were used for the 10x train scenario, it would require one ship every day to account for the large production of the ammonia plant. Consequently, it was assumed that ammonia carriers would eventually reach the size of the largest LNG carriers of 266,000 m^3 [114].

Table 26: Ammonia shipping parameters in the 1x and 10x train LNG scenarios

Ship scenario	**Capacity (m^3)**	**Fuel use laden (tonne)**	**Fuel use ballast (tonne)**	**Hire rate ($/day)**
1x train	84,000	1,495	1,363	40,000
10x train	266,000	3,889	3,544	86,589

Using this carrier, nine days of storage are required for the exporting terminal. This carrier's fuel consumption was calculated by extrapolating the fuel consumption values for the increase in LNG carrier sizes, discussed in Section 4.2.3, with respective values for carrier size and fuel consumption for the BW Gemini. From the shipping costs discussion in Section 2.5.3 regarding the volatility

of carrier rates, an average value for the VLGC daily rate was found in the years from 2017-2020 [115]. The scaling approach was utilized to calculate the carrier hire rate for the non-existing 266,000 m^3 gas carrier using the VLGC carrier rate as a reference.

4.3.4 Variable Operation and Maintenance Costs

In addition to the general economic evaluation assumptions presented in Table 12, variable operating costs specific to the ammonia value chain are presented in Table 27. Oxygen carrier and catalyst parameters were derived from Spallina et al. 2016 and have an assumed lifetime of five years [94]. Membrane costs were derived from Acquaviva et al. 2009 and have a lifetime of two years with an 80% cost recovery factor upon replacement [116]. The process water cost used to raise steam for the MA-ATR reactor was also derived from Spallina et al. 2016 [94]. CO_2 transportation and storage costs were in the base case assumed to be zero due to the pressurized CO_2 being utilized to extract more natural gas in the reservoir, further discussed in Section 2.5.3. This parameter is highly uncertain and is therefore included in the sensitivity analysis in Section 5.2.3.

Table 27: Ammonia value chain variable operating and maintenance costs

Item	**Value**	**Unit**
Oxygen carrier	15	\$/kg
Membrane	500	\$/ft^2
Catalyst	5	\$/kg
CO_2 transport	0	\$/tonne
Process water	2	\$/m^3

5 Results and Discussion

Results will be presented and further discussed in three main sections. First, the technical performance of the four different scenarios, including heat balances, energy efficiencies, environmental performance, and a power breakdown of the plants, will be discussed. Here, technical parameters for the shipping analysis will also be included. Secondly, the economic performance of the four scenarios is presented, including capital costs breakdown, operational costs, and the calculation of levelized costs of product (LCOP) and CO_2 avoidance cost (COCA). Finally, two sensitivity analyses are conducted to evaluate how LCOP and COCA are affected by changing parameters such as natural gas and electricity price, CO_2 tax and capture cost, MCHE scaling exponent and material, modular scaling exponent, membrane cost, and permeate compressor material.

5.1 Technical Results

The energy and environmental breakdown of the four different production plants simulated in Aspen Plus are presented in Table 28. Values for heat balances, energy efficiencies, environmental aspects, and power breakdown of different unit components are presented for each scenario.

Table 28: Production plant technical performance results

Scenario		***1x train***		***10x train***	
		LNG	**NH_3**	**LNG**	**NH_3**
Item	**Unit**	**Value**			
Plant size	MTPA	0.84	1.75	8.31	15.29
Heat Balance					
NG input	MW_{th}	1,497.4	1,497.4	14,947.0	14,974.0
Product output	MW_{th}	1,462.8	1,143.3	14,410.1	9,975.3
Energy					
η_P	%	97.7	76.4	96.2	66.6
$\eta_{P,eq}$	%	95.3	67.1	96.2	66.6
SC	GJ/tonne	50.4	24.3	51.2	27.8
SC_{eq}	GJ/tonne	51.7	27.6	51.2	27.8
SPC	kWh/tonne	247.7	652.9	254.6	731.8
Environmental					
$\dot{m}_{CO_2}$	kg/s	3.5	83.1	45.9	831.3
E_{CO_2}	tonne/tonne	0.12	-	0.16	-
C_{CO_2}	tonne/tonne	-	1.35	-	1.54
Power Breakdown					
Consumers					
Propane compressors	MW_{el}	6.7	-	66.2	-
MR compressors	MW_{el}	16.8	-	160.4	-
Pumps	MW_{el}	0.3	2.2	3.5	24.2
H_2/N_2 compressors	MW_{el}	-	110.2	-	961.9
ASU compressors	MW_{el}	-	31.5	-	315
Fuel gas compressors	MW_{el}	-	-	11.2	92.8
Other compressors	MW_{el}	-	28.9	-	273.5
Producers					
Power plant	MW_{el}	-	-	241.3	1,276.4
Steam turbines	MW_{el}	-	42.3	-	391.0
Total Auxiliaries	MW_{el}	23.8	172.9	241.3	1,667.4
Net Power	MW_{el}	-23.5	-130.5	0	0

As discussed in Section 3, the natural gas inputs to the processes are set the same with the 10x train scenario scaled ten times up. The natural gas LHV from Aspen Plus with composition and parameters from Table 5 was 48,887 kJ/kg. Using a 30.63 and 306.30 kg/s feed rate, 1,497.4 and 14,947.0 MW of natural gas thermal input are used for the 1x and 10x trains, respectively.

Table 29 presents the technical shipping parameters regarding the fuel consumption used for the different vessels. Choice of vessels, respective fuel consumption, and BOG-rate for laden and ballast voyage for LNG and ammonia are discussed in Sections 4.2.3 and 4.3.3 respectively. It was assumed that the LNG carrier consumes the BOG as fuel for propulsion, while the rest is supplied by HFO. As discussed in Section 2.5.2, marine vessels powered by ammonia or other low-carbon fuels are expected to be commercialized in 2025. Consequently, the ammonia carriers utilize 100% ammonia-fired engines.

Table 29: Shipping analysis technical performance results, including exporting terminal, fuel consumption and total fraction of cargo consumed for the 1x and 10x LNG and ammonia carriers

Scenario		***1x train***		***10x train***	
		LNG	**NH_3**	**LNG**	**NH_3**
Carrier size (m^3)		**40,000**	**84,000**	**160,000**	**266,000**
Item	**Unit**	**Value**			
Carrier size	TJ	893	1,068	3,571	3383
Exporting terminal					
Ship frequency	days	7.1	10.7	2.9	4.1
Ship frequency	ships/year	52	34	128	90
Storage capacity	days	15	22	6	9
Fuel use					
Natural gas	TJ	21	-	64	-
Heavy fuel oil	TJ	26	-	77	-
Ammonia	TJ	-	53	-	138
Total fuel consumption	TJ/roundtrip	47	53	141	138
Fraction of cargo consumed	%	2.4	5.0	1.8	4.1

CO_2 emissions from the 1x and 10x LNG train are presented in Table 30. As discussed in Section 3.1, the LNG vapor fraction was flared for the 1x train and used for fuel in the 10x train approach. Other emission sources in the LNG plant include the AGRU, where CO_2 was removed before entering the liquefaction process. Emissions related to shipping include the BOG and HFO used as fuel in the engines, with combined emissions of 5.0 kg/s and 37.1 kg/s in the 1x and 10x train scenarios, respectively. HFO has higher CO_2 emissions than natural gas and contributes to around 61% of the total shipping emissions in the LNG route.

Table 30: CO_2 emissions for the LNG value chain, where the emissions from the 1x plant is due to flaring and the 10x train is because of the gas turbines

Scenario	***1x train***	***10x train***
Emission source	**Value (kg/s)**	
Flaring	2.0	-
Turbines	-	30.9
AGRU	1.5	15.0
Shipping	5.0	37.1
Consumption	798	792.9
Total CO_2 emissions	88.3	875.9

The CO_2 emission distribution across the LNG value chain from liquefaction to downstream uses

is shown in Figure 21. The largest fraction of CO_2 emissions in the LNG value chain was the downstream combustion of the gas with a 90.4% and 90.5% share for the 1x and 10x train, respectively. A larger portion of HFO was consumed for propulsion in the small-scale LNG carrier, which is the main reason why shipping emissions in the 1x train are 1.5% higher than in the 10x train.

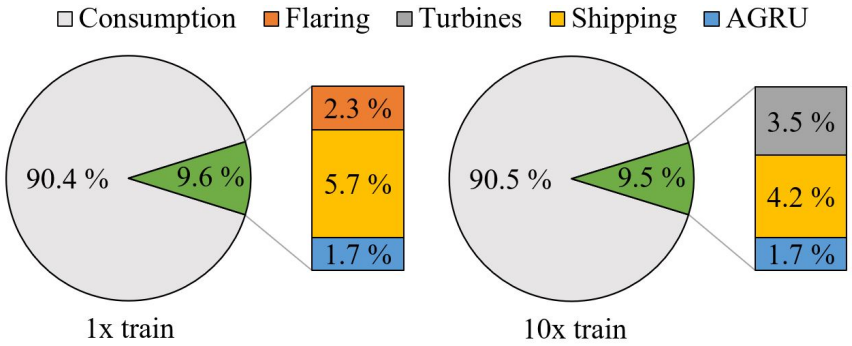

Figure 21: CO_2 emission distribution from the LNG value chain, where the emissions from the 1x plant is due to flaring and the 10x train is because of the gas turbines.

The final thermal efficiency for the different scenarios is presented in Figure 22. Here, power supplied by the grid, the fuel used for engines in the shipping, and the supplementary HFO use is subtracted from the thermal efficiency of the production plants. The resulting efficiency provides a fuel efficiency analysis throughout the LNG and ammonia value chain until reaching downstream purposes.

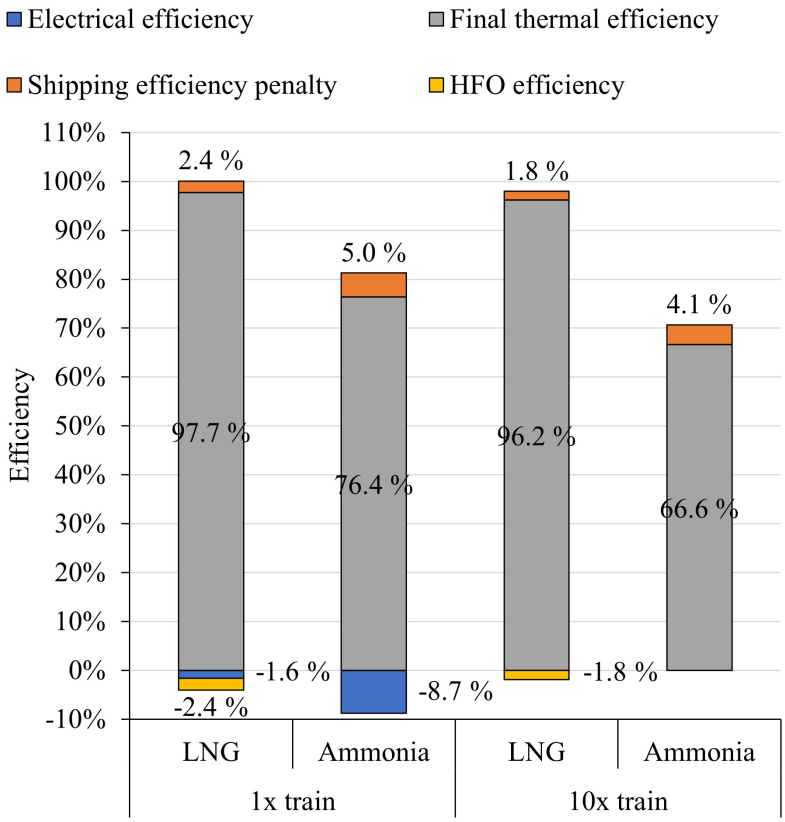

Figure 22: Final thermal efficiencies for the four different scenarios, where the electrical and heavy fuel oil efficiency are negative due to being supplied to the process rather than withdrawn as the fraction of the cargo used for shipping.

These results will now be discussed in greater detail, comparing LNG and ammonia in the 1x and 10x configurations.

5.1.1 1x Train

Production

Table 28 shows that the ammonia plant is much less efficient than the LNG plant. The LNG process loses only 2.3% of the incoming heating value due to flaring. Imported electricity to drive the refrigeration process subtracts another 2.4% in terms of equivalent efficiency. For ammonia production, on the other hand, irreversibilities in the two chemical transformation steps (NG to H_2 and H_2 to NH_3) cause much larger losses. In addition, substantial electricity imports are required, mainly to compress the H_2 & N_2 stream from 5 bar to 200 bar and to power the ASU. Overall, these factors drive the equivalent efficiency of the ammonia process 28.2 %-points below that of the LNG process.The specific energy consumptions are affected by the conversion efficiencies, but the main difference between the LNG and ammonia plants is the much lower LHV of ammonia.

Another important technical performance metric is the SPC. Previous works by Arnaiz del Pozo et al. 2021 found an SPC of between 324 kWh/tonne and 358 kWh/tonne for a closed and open cycle cascade configuration for the LNG process [45]. Other studies by Khan et al. 2016 found that SPC could range between 205 kWh/tonne and 240 kWh/tonne in a C3MR process based on various operating conditions [117]. SPC in the 1x LNG train was 247 kWh/tonne, slightly above the suggested range by Khan et al. 2016 and below the values found by Arnaiz del Pozo et al. 2021. SPC for the KBR, LAC, and GSR ammonia plants discussed in Section 2.5.4 was 201 kWh/tonne, 224 kWh/tonne, and 640 kWh/tonne, respectively. The 1x MA-ATR plant is similar to the GSR plant in power consumption, seen in Table 28 with an increase of 2%.

Power from the grid is used to power the different auxiliaries in the systems. Power consumption in the C3MR process was mainly due to the propane and mixed refrigerant compressors consuming 6.7 MW and 16.8 MW, respectively. The MA-ATR ammonia process has significantly higher power requirements to pressurize the hydrogen stream out of the reactor to around 200 bar. The hydrogen compressors and the ASU consume the majority of power in the process, with 110.2 MW and 31.5 MW, respectively. Compared to the C3MR process, the ammonia production plant consumes almost six times the power.

In exchange for its relatively low efficiency shown in Table 28, the chemical conversion completed by the ammonia plant avoids all emissions involved in the LNG plant. From Table 30, flaring of natural gas in the 1x LNG plant accounts for 2.3% of the final LNG value chain emissions. It was assumed that the imported electricity from the grid is completely carbon neutral. However, to account for the impact on levelized costs and costs for CO_2 avoidance, a sensitivity analysis for the grid emissions is performed in Section 5.2.4 where a typical natural gas combined cycle power plant with respective emissions of 330 kg/MWh are analyzed [118].

Shipping

As the volumetric energy density for LNG is around 1.8 times higher than liquefied ammonia, larger carrier sizes are required for ammonia carriers to deliver the same amount of energy. From Table 29, the ammonia carrier size is double the size, while the energy delivered is only 20% higher. With a higher energy density in the LNG carrier tanks, a smaller fraction of the final cargo is used as fuel compared to the ammonia carrier. For the shipping route from Sabine Pass to Wilhelmshaven, 97.6% and 95.0% of the production output is delivered at the receiving terminals in Germany for the LNG and ammonia scenario, respectively.

Even though the LNG carrier was half the size in terms of volumetric capacity compared to the ammonia carrier, the fuel consumption is nearly the same per roundtrip. As discussed in Section

4.2.3, the BOG rate of the small-scale LNG carrier was assumed to be 0.10% and 0.05% for the laden and ballast, respectively. This BOG provides 60% and 30% of the fuel to the engines in the laden and ballast voyage, respectively, while the rest is provided by HFO. Studies by Raj. et al. 2016 discussed different BOG rates versus carrier sizes [55]. Here, smaller capacity carriers have a tendency to have higher BOG, with intervals ranging between 0.10% to 0.15%. Other fleet operators prove BOG rates as low as 0.035% for LNG carriers [119]. As the BOG rate is directly used to calculate the fuel consumption of both natural gas and HFO in the LNG carrier, it reflects why a high BOG rate gives a high fuel consumption.

Final Thermal Efficiency

Figure 22 shows that 95.3% of the natural gas heating value entering the system eventually reaches the final destination as LNG after losses from flaring during production and BOG consumption during shipping. In addition, the LNG value chain requires imports of electricity and HFO equivalent to 4% of the natural gas feed. The amount of ammonia reaching the final destination is much lower at 71.4%, mainly due to conversion losses during production but also due to consumption in the VLGC. Additionally, the ammonia plant requires electricity equivalent to 8.7% of the natural gas feed.

5.1.2 10x Train

Production

The natural gas flow rate was scaled ten times up to account for a 10x train configuration. The major difference between the 1x and 10x trains from a technical standpoint is that the 10x trains produce their own power by consuming some fuel locally. Thus, the thermal efficiency is lower, but the equivalent efficiency is similar. This is also the reason why the LNG and ammonia output is less than 10x higher. Plant and net plant efficiencies are equal due to internal power production from the power plants in both scenarios. The plant efficiency for the ammonia plant was 29.6%-points lower compared to the LNG plant. Compared to the 1x train scenario, the net plant efficiencies were slightly higher for the LNG plant due to the utilization of the LNG vapor as fuel for the gas turbines instead of flaring to the atmosphere.

Power input from the grid in the 1x train and power plant efficiency in the 10x train used both 63% efficiencies for power production in the ammonia plants. Further, the excess ammonia vapor is flared in the 1x train but at a negligible fraction. However, the equivalent efficiency of the 10x plant declines by 0.5 %-points relative to the 1x plant because the power plant consumes hydrogen produced at approximately 85% efficiency in the MA-ATR reactor.

The SPC is a measurement for evaluating the power consumption per tonne of product, not including the natural gas duty. It represents power imports in the 1x trains and internally generated power in the 10x trains. The outlet LNG vapor fraction of the LNG scenario was set to provide the right fuel injection rate to the gas turbines. However, in the 1x train, the LNG vapor fraction was minimized to reduce the flaring rate. This allows the 1x LNG train to produce around 3% more LNG per power consumed. As discussed, parts of the permeate stream are used for hydrogen gas turbines, so ammonia production was directly affected by the power plant. Consequently, the SPC for the ammonia trains was around 12% higher compared to the 1x train due to the lower ammonia production flow rate.

LNG and ammonia production are highly energy-intensive processes. Extracting up to 1,276.4 MW in the 10x ammonia train, equivalent to around one million US households from the electrical grid, would require a large power plant and a well-established electrical infrastructure [120]. Thus, a large combined cycle power plant is constructed on-site for the 10x ammonia plant. The power breakdown for each component in the LNG scenario was very similar to the 1x train, with only

minor differences. It can also be mentioned that, when dividing by the number of trains, the large-scale ammonia plant has a 4% lower power demand for all auxiliaries than the 1x train, mainly driven by the lower required duty for permeate compression to 200 bar, and that part of the permeate is consumed in the power plant.

From the CO_2 emissions presented in Table 30 and emission distribution in Figure 21, the 10x LNG value chain achieves lower specific CO_2 emissions than the 1x train mainly due to economies of scale for shipping. A larger portion of the HFO was consumed in the small-scale LNG carrier, which has a higher emission intensity that increases shipping emissions by 36%. For the ammonia value chain, the 10x plant can legitimately claim zero CO_2 emissions because it does not import any electricity that might be associated with CO_2 emissions.

Shipping

The capacity choice of the LNG carrier used in the 10x train approach reflects the current market's largest share of available LNG vessels. Larger vessels tend to decrease the BOG rate due to higher volume per surface area [55]. A lower BOG rate was assumed for the 10x train at 0.075% and 0.0375% for the laden and ballast voyage, respectively. Additionally, with a larger storage capacity, less fraction of the total fuel is consumed for propulsion. From Table 29, the large-scale LNG carrier consumes 1.5% less of the total storage capacity for the engines than the 1x train vessel. The same approach for calculating fuel consumption was used here as in the 1x train but with a lower BOG rate.

As discussed in Section 4.3.3, accounting for the large ammonia output of the 10x train production plant requires one VLGC of 84,000 m^3 to enter the exporting terminal almost every day. Therefore, by assuming a carrier size of 266,000 m^3 and extrapolating fuel consumption values for the LNG scenario with respective values for the increase in ammonia carrier size, the fuel consumption for the large-scale ammonia carrier resulted in 138 TJ/roundtrip. Due to economies of scale and higher tank capacity, the large-scale ammonia carrier consumed 4.1% of the total liquefied ammonia on board. Similar to the discussion in Section 5.1.1, the total fuel consumption for the large-scale ammonia carrier is lower even though the capacity is higher than the LNG carrier. The assumed BOG rate in the large-scale LNG carrier is lower than the small-scale, and the values are derived from the already existing LNG vessels with BOG rates ranging from 0.035% - 0.085% [119]. Further, calculations for fuel consumption on the ammonia carriers are derived from the average fuel use of LPG per day at a speed of around 30 km/h. This variable is based on LPG-fueled vessels, and when switching to an ammonia-fired engine, efficiencies could increase compared to conventional engines because ammonia has a high octane number, meaning that internal combustion engines can achieve higher compression ratios (which leads to greater efficiency) without encountering knock.

Final Thermal Efficiency

Figure 22 shows that 96.2% of the natural gas heating value entering the LNG value chain eventually ends up as LNG, which is around 1.5%-points higher than the 1x LNG train due to several factors. First, the net plant efficiency was 0.9%-points higher because of the natural gas utilized as fuel instead of flaring. Further, the increased vessel size decreases the BOG rate and specific fuel consumption, giving lower shipping and HFO efficiency penalty at 1.8% and 1.8%, respectively. Finally, since the power is produced internally, no electrical input from the grid lowers the final thermal efficiency.

In the 10x ammonia train, shown in Figure 22, 66.6% of the natural gas heating value entering the ammonia value chain ends up at the receiving terminals in Germany. The final thermal efficiency was 9.8%-points lower than for the 1x train approach, mainly because of the hydrogen fraction used for internal power production. Further, similar to the 10x LNG scenario, increased vessel size decreases specific fuel consumption and the fraction of ammonia used for propulsion. Here, the shipping efficiency penalty decreased by 0.9%-points using the extrapolating approach discussed

in Section 4.3.3.

5.2 Economic Results

The economic performance of the four scenarios is presented in three sections. First, the base case results for the 1x LNG and ammonia scenarios are discussed, including capital costs, operational costs, levelized cost of the product, and CO_2 avoidance cost. Secondly, the same approach is conducted with the 10x train approach. Finally, a sensitivity analysis analyzing key performance parameters that affect the levelized cost of product and the CO_2 avoidance cost is performed to evaluate at what intervals and assumptions ammonia provides competitiveness relative to LNG. Table 31 presents a breakdown of the economic results, including capital costs, operational costs, and key performance indicators.

Table 31: Economic assessment results, including capital costs, operational costs, and key performance indicators

Scenario		***1x train***		***10x train***	
		LNG	**NH_3**	**LNG**	**NH_3**
Item	**Unit**	**Value**			
Capital costs					
BEC distribution					
Precooling	$M	36.7	-	297.8	-
Liquefaction	$M	213.3	-	1,536.1	-
MA-ATR	$M	-	213.2	-	1,378.6
NH_3 synthesis loop	$M	-	419.4	-	3,078.4
Power plant	$M	-	-	154.5	1311.5
Exporting terminal	$M	113.9	89.1	467.8	275.2
Importing terminal	$M	103.6	89.1	740.9	379.3
Total BEC	$M	467.5	810.9	3,197.0	6,422.9
EPC	$M	46.8	81.1	319.7	446.7
Total contingency	$M	102.9	178.4	703.3	1,111.6
TPC	$M	617.1	1,070.3	4,220.1	7,981.3
OC	$M	92.6	160.6	633.0	1,000.5
TOC	$M	709.7	1,230.9	4,853.1	8,981.7
TCR	$M	787.7	1,366.3	5,386.9	9,969.7
SCC	$/kW	502.93	1149.48	346.63	995.30
Operational costs					
Operating labour	$M/year	2.2	2.2	21.8	21.5
Maintenance	$M/year	17.8	34.2	121.3	249.2
Insurance	$M/year	7.1	13.7	48.5	99.7
Natural gas	$M/year	118.1	118.1	1,181.4	1,181.4
Electricity	$M/year	12.5	68.6	-	-
Shipping	$M/year	50.2	44.0	324.9	251.9
CO_2	$M/year	278.6	-	2,760.9	-
Oxygen carrier	$M/year	-	2.2	-	17.2
Membranes	$M/year	-	5.5	-	43.5
Process water	$M/year	-	3.6	-	36.3
Total OPEX	$M/year	486.5	292.1	4,456.1	1900.7
SOC	$/GJ	10.88	8.72	10.04	6.46
Key Performance Indicators					
LCOP	$/GJ	12.78	13.03	11.35	10.04
COCA	$/tonne	-	104.08	-	78.81

Overall, as presented in Table 31, the ammonia scenarios are more capital-intensive than LNG. The total overnight costs in $M for the ammonia scenarios are 73% and 85% higher compared to LNG for the 1x and 10x trains, respectively. Further, operational costs are 40% and 57% lower for the 1x and 10x ammonia scenarios compared to LNG, respectively. Finally, the levelized cost of the product presents ammonia as a cheaper alternative in the 10x scenario and more expensive in the 1x train scenario. Ammonia becomes competitive against LNG at CO_2 prices of $104.08/tonne and $78.81/tonne for the 1x and 10x train scenarios, respectively.

Specific capital cost (SCC) distribution in the LNG and ammonia value chains are presented in Figure 23, derived from Equation 18 in Section 2.3.4. The value chain components were split into precooling, liquefaction, power plant, and the exporting and importing terminal for the LNG scenarios. In the ammonia approach, the different CAPEX components include the MA-ATR process, ammonia synthesis loop, power plant, and the exporting and importing terminal.

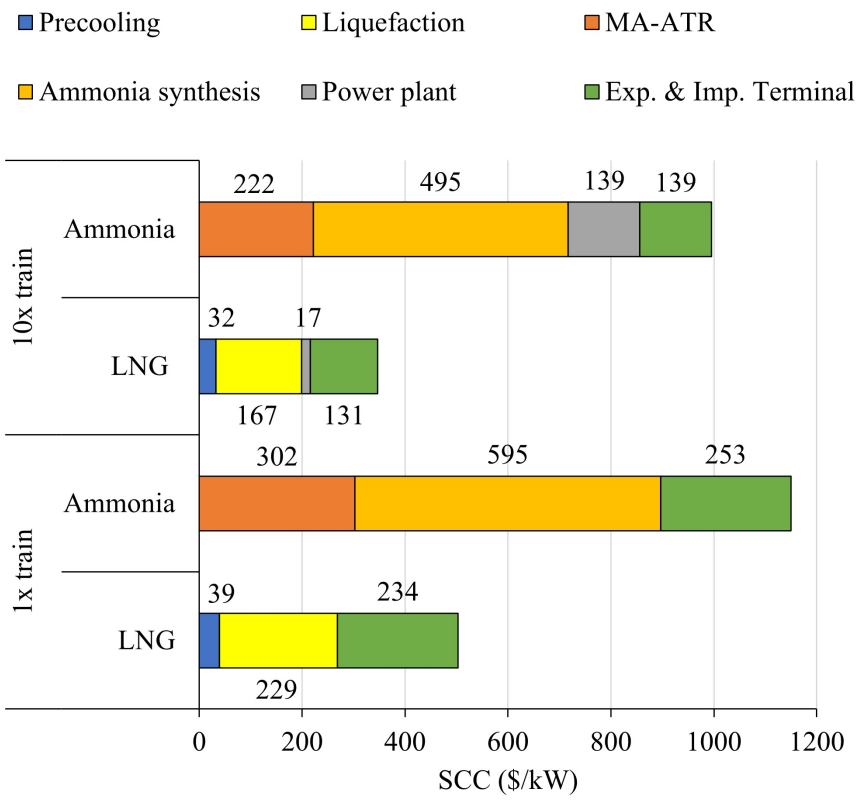

Figure 23: Specific capital costs, i.e., the ratio between total overnight costs and plant capacity, in $/kW for the four different scenarios.

Specific operating costs (SOC) across the LNG and ammonia value chain are presented in Figure 24 in terms of $/GJ. Calculations are performed in the SEA-Tool using Equations 19 and 20 in Section 2.3.4. SOC includes shipping, fixed and variable operating and maintenance costs, natural gas and electricity costs, and cost for CO_2 emissions.

Finally, when accounting for both capital and operating costs, the levelized cost of product is presented in Figure 25. Utilizing a consistent methodology for both the technical and economic assessment conducted in Sections 3 and 4, the LCOP expresses a price comparison of LNG and ammonia value chains from a production plant in the United States to demand centers in Germany. With base case parameters for CAPEX and OPEX components from Table 12 and shipping route specifications in Table 11, ammonia is competitive towards LNG with the increased plant size from

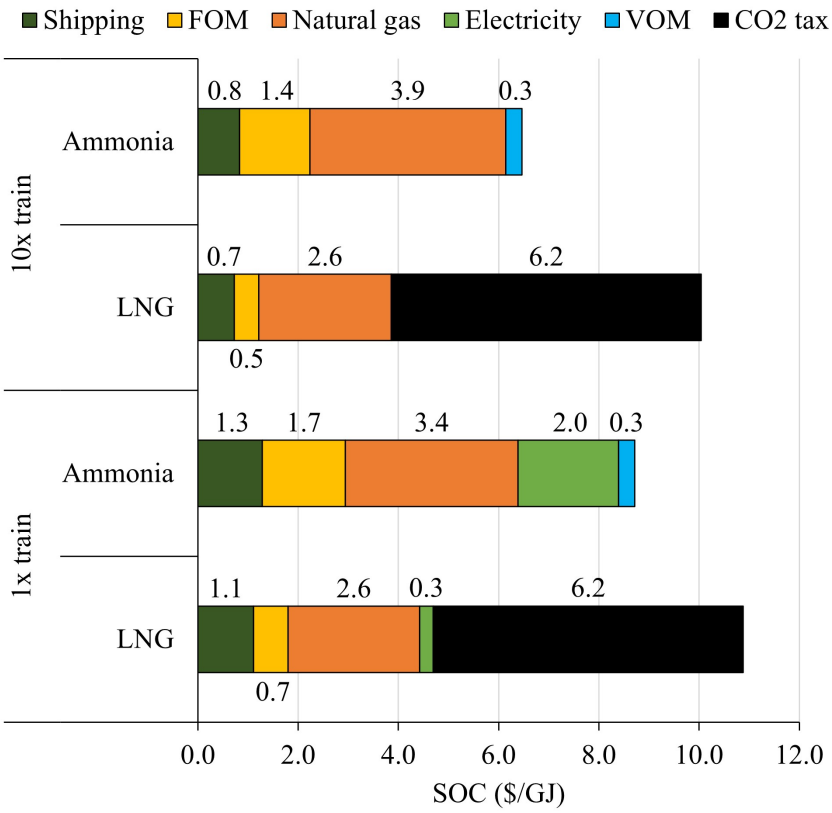

Figure 24: Specific operating costs (SOC), i.e., the ratio between total levelized operational costs over a lifetime of generating asset in $/GJ for the four different scenarios.

one to ten trains.

These results will now be discussed in greater detail, comparing economic performance in the LNG and ammonia for the 1x and 10x configurations.

5.2.1 1x Train

Capital Costs

The ammonia plant has a 73% higher TOC and 129% higher SCC than the LNG scenario due to expensive Ni-alloy permeate compressors constructed in a Ni-alloy to account for the low-temperature loads in the 3:1 H_2:N_2 permeate stream. The difference in SCC is larger than in TOC because of the lower efficiency of the ammonia plant. The most expensive part of the LNG plant is the liquefaction process, where the material cost factor is high for the Ni-alloy-based MCHE due to temperature and corrosion loads when natural gas is liquefied. However, the MA-ATR process in the ammonia plant cancels out the major cost for the MCHE in the LNG plant. Further, the cost of exporting and importing terminals in the LNG plant is around 18% higher due to higher quality materials required for keeping the LNG at -163°C, further discussed in Section 2.4.3.

Operational Costs

Ammonia operational costs are 40% lower than for LNG primarily because of the CO_2 tax of $100/tonne involving the LNG scenario emitting 88.3 kg/s of CO_2, presented in Table 30. Further, the SOC is 20% lower for the ammonia train when accounting for the lower energy content of the product delivered compared to the LNG scenario. Maintenance and insurance costs were assumed

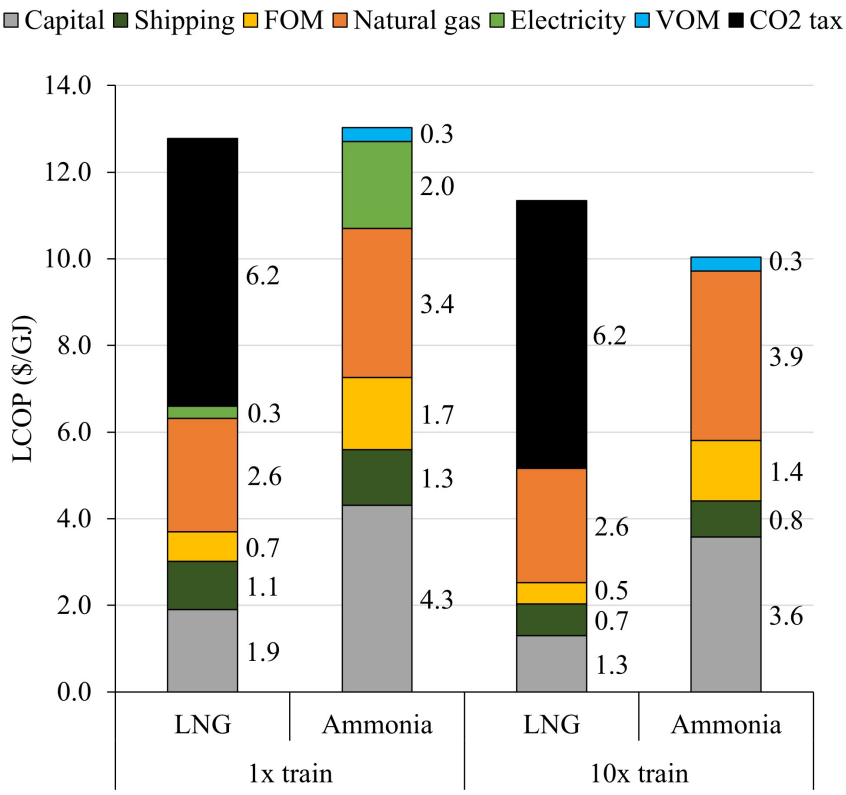

Figure 25: Levelized costs of product (LCOP), i.e., the ratio between total levelized costs over a lifetime of generating asset in $/GJ for the four different scenarios.

as 2.5% and 1.0% of the TOC, respectively. Consequently, as the TOC for ammonia is significantly higher, costs for maintenance and insurance increase. Electricity consumption accounts for 3% and 24% of all operational costs in the LNG and ammonia scenarios, respectively.

As the ammonia exporting terminal can handle longer periods of storage than the LNG terminals due to easier handling and storage, fewer ammonia carriers are required for shipping than LNG vessels. Due to the economies of scale involved in a smaller number of larger vessels, this results in slightly lower shipping costs for the ammonia value chain. Finally, VOM costs, such as oxygen carriers and membrane replacements and process water utilized in the ammonia train, correspond to around 4% of the operational costs.

Economic Performance

From Table 31, the 1x train LNG and ammonia scenarios result in an LCOP of $12.78/GJ and $13.03/GJ, respectively. As seen in Figure 25, the capital-intensive ammonia value chain contributes to 33% of the final LCOP. On the other hand, CO_2 taxation of the emissions from the LNG value chain has the largest share of 48%. Further, natural gas increases the LCOP for ammonia more than for LNG because of the differences in plant efficiency discussed in Section 5.1.1. At a CO_2 price of $100/ tonne, the 1x train ammonia value chain is not competitive with LNG due to the LCOP being 2% higher.

Derived in Equation 21 in Section 2.3.4, the COCA directly reflects the price of CO_2 where the ammonia value chain achieves cost parity with LNG. For the 1x train ammonia plant, where CO_2 tax rates of $104.08/tonne or higher emerge, the plant reaches cost parity with the LNG value chain.

As discussed in Section 2.5.4, Arnaiz del Pozo et al. 2022 performed a techno-economic assessment on three blue ammonia production methods using the SEA-Tool for calculations [11]. The base case in the reference study used higher natural gas prices due to being located in Europe. However, the reference study also performed an assessment of the LAC process in Saudi Arabia, where prices for natural gas and electricity were \$2.2/GJ and \$43/MWh, respectively. If restricting the LCOP for the MA-ATR ammonia value chain in this work to only the production plant and scaling down the natural gas input to the plant, a comparison can be performed to the reference study. The 1x train MA-ATR ammonia process employed in this work resulted in a levelized cost of \$190/tonne, giving a 27.5% cost saving to the LAC process with Saudi-Arabian raw material prices used in the reference study. Compared to the GSR process, which is another future plant, the costs for MA-ATR for ammonia production are reduced by 21%.

5.2.2 10x Train

Capital Costs

To account for economies of scale when increasing the number of trains in parallel to ten, a modular scaling factor of 0.9 was utilized, further discussed in Section 4.1.1. Both the modular scaling factor used for the equipment approach and the scaling factor implemented in the scaling cost law significantly affects both scenarios' capital costs. The LNG plant output is 9.85 times higher, while the TOC is only increased by a factor of 6.84. Since the ammonia plant requires a large power plant to account for the high power demand, the output is 8.73 times higher, while the TOC is 7.30 times higher. The large combined cycle hydrogen power plant in the ammonia scenario accounts for 13% of the TOC, compared to only 3% for the smaller gas turbines in the LNG plant.

In the 10x train scenarios, the ammonia plant has an 85% higher TOC and 188% higher SCC compared to LNG. The ammonia plant requires more capital investment than the LNG plant. Therefore, the ammonia scenario benefits from economies of scale to a higher degree than the LNG plant. Compared to the 1x train scenarios, the cost advantage of adding ten trains is now reduced for the LNG plant. Economies of scale impact the 10x ammonia train by lowering specific capital costs by 15% despite the addition of the large power plant. This is one of the main reasons why ammonia becomes more competitive in the 10x train scenario against LNG.

From Table 31, the exporting and importing terminals for both the value chains thrive from economies of scale. Specific capital costs from terminals in the LNG and ammonia scenario are reduced by 44% and 45%, respectively. From Table 18 and 25 in Section 4, a higher plant output from the plants facilitates the construction of larger storage tanks, which lowers the number of tanks in total.

Operational Costs

Total operational costs and specific operational costs presented in Figure 24 are 57% and 36% lower for the ammonia plant compared to the LNG plant, respectively. Similar to the discussion for the 1x train, CO_2 tax rate of \$100 is the primary driver of high operational costs in the LNG value chain. With both plants profiting from economies of scale, lower specific FOM costs are achieved compared to the 1x train scenarios. Further, specific VOM costs in the 10x ammonia scenario are decreased by 14% primarily due to the impact of economies of scale on membrane replacement costs.

By utilizing larger carriers for shipping, fewer roundtrips are required, and the specific annual costs for shipping are reduced by 35% and 43% for the LNG and ammonia scenarios, respectively. The reduction in SOC for ammonia shipping is highly uncertain due to a number of factors. First, the carrier size and propulsion technology are not yet commercialized. Secondly, the fuel

consumption estimation is based on extrapolation from LPG-fired VLGC BW Gemini parameters, further discussed in Section 4.3.3. Lastly, daily hire rates are highly volatile and difficult to project for the 266,000 m^3 fully refrigerated gas carrier used in the 10x ammonia train value chain scenario.

Economic Performance
Through a consistent methodology in both the technical and economic approach, the 10x LNG and ammonia value chains resulted in an LCOP of \$11.35/GJ and \$10.04/GJ, respectively. Consequently, scaling up the plants to a 10x train approach, the ammonia scenario provides savings of 12% compared to LNG in terms of LCOP over a 25-year plant lifetime using the base case parameters. Economies of scale lower the fraction of capital costs in the assessment of LCOP for the LNG by 3% compared to the 1x train. Further, the main driver of lowering LCOP in the ammonia scenario is the transition from electricity consumption from the grid at \$60/MWh to an on-site power generation where electricity is produced at a lower cost from hydrogen produced from cheap local natural gas.

Economies of scale lower the equipment cost for process components in the 10x ammonia plant, but the power plant cancels out the reduction in capital cost fraction of the LCOP compared to the 1x train. Further, a CO_2 taxation rate of \$78.81/tonne applied for emissions in the LNG value chain indicates the point where ammonia is the better alternative.

5.2.3 Sensitivity Analysis

A sensitivity study of the economic assessment results to nine key parameters was performed to evaluate the impact on LCOP and COCA. Figure 26 presents the LCOP sensitivity analysis on the 1x and 10x LNG and ammonia plants. Further, a sensitivity study with COCA as the target parameter is presented in Figure 27 to enhance the analysis of where ammonia reaches cost parity with LNG for the 1x and 10x train sizes. For easier interpretation of the impact of various parameters on the LCOP and COCA, the y-axis intervals in each respective Figure are constant throughout subfigures a)-i).

Natural Gas Price
The natural gas price is one of the most important parameters in assessing the final LCOP and COCA. The ammonia plants are more affected by the natural gas price, seen as a steeper curve in Figure 26a. Both plants consume the same amount of natural gas, but since the ammonia plant has lower final thermal efficiency, it is more affected by fluctuations in natural gas prices. At a natural gas price of \$1.8/GJ, the 1x ammonia train reaches cost parity with the 1x LNG train. The ammonia scenario benefits of lower natural gas prices, and the 10x train starts to lose its advantage of natural gas prices exceeding \$4.9/GJ.

For the COCA in Figure 27a, the 10x train is more sensitive to fluctuations in natural gas prices, seen as a steeper curve because of the lower thermal efficiency caused by additional fuel consumption for on-site power production. This reflects in areas where natural gas prices are higher; the COCA rises faster than for the 1x train approach. As a consequence, multiple train ammonia plants built in the US or Middle East, where natural gas prices are low, are advantageous towards small plants where a high CO_2 tax is required for its competitiveness. These are the typical locations where LNG facilities are constructed and where large-scale ammonia facilities may be built in the future.

Electricity Price
Since the 10x train scenarios have an internal power generation, they are independent of electricity price fluctuations seen in Figure 26b. Since the 1x ammonia plant consumes a substantial amount

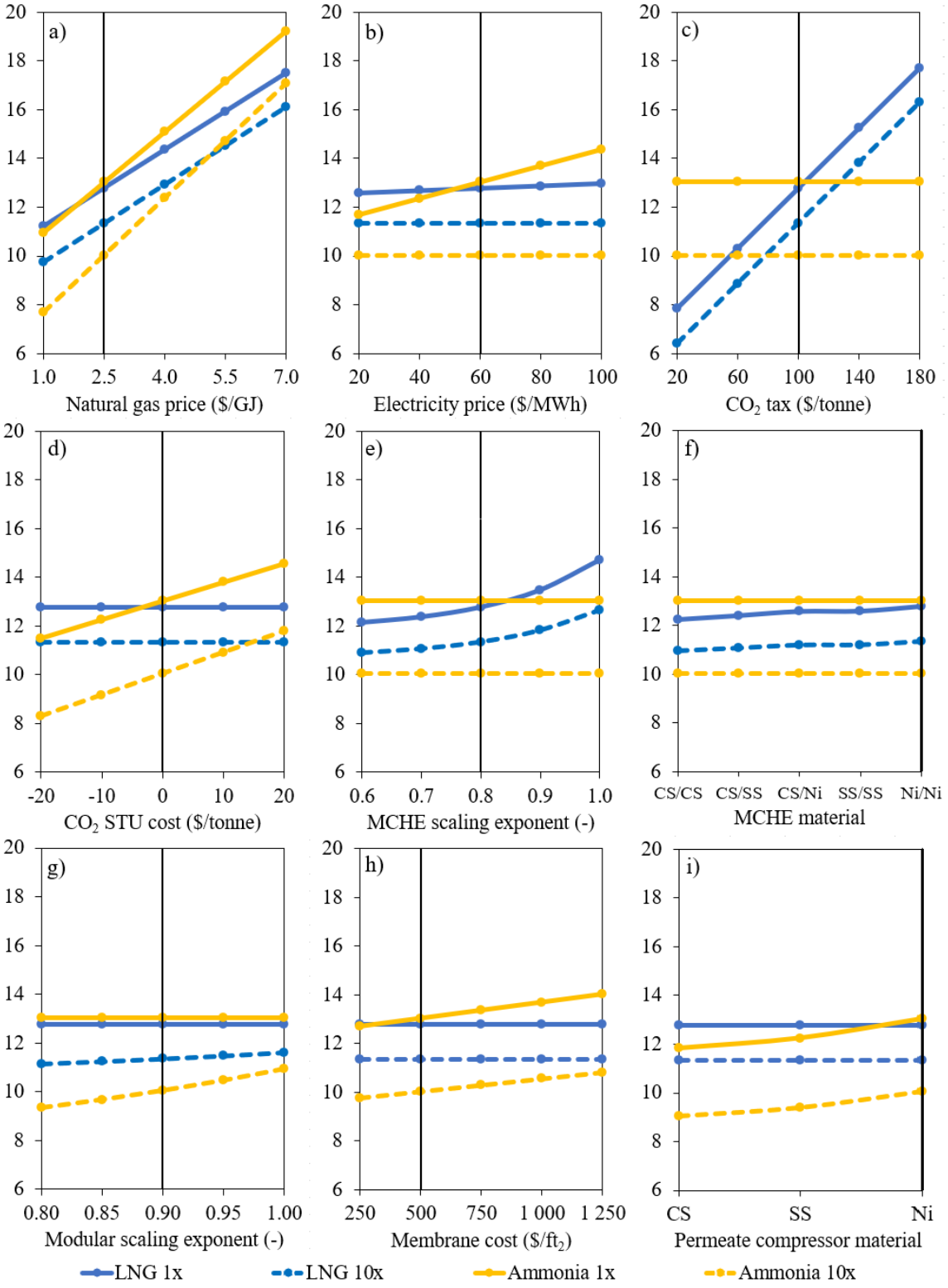

Figure 26: Sensitivity analysis of important parameters in the four scenarios with LCOP as the target impact value. LCOP ($/GJ) is the y-axis, and the black line is the base case parameters.

of electricity, it is significantly more sensitive to changes in electricity cost compared to the LNG plant. At an electricity price of around $52/MWh, the LCOP for the 1x ammonia plant becomes lower than the 1x LNG plant while the other parameters remain constant.

Cost for CO_2 avoidance varies greatly in the 1x train and is constant for the 10x train seen in

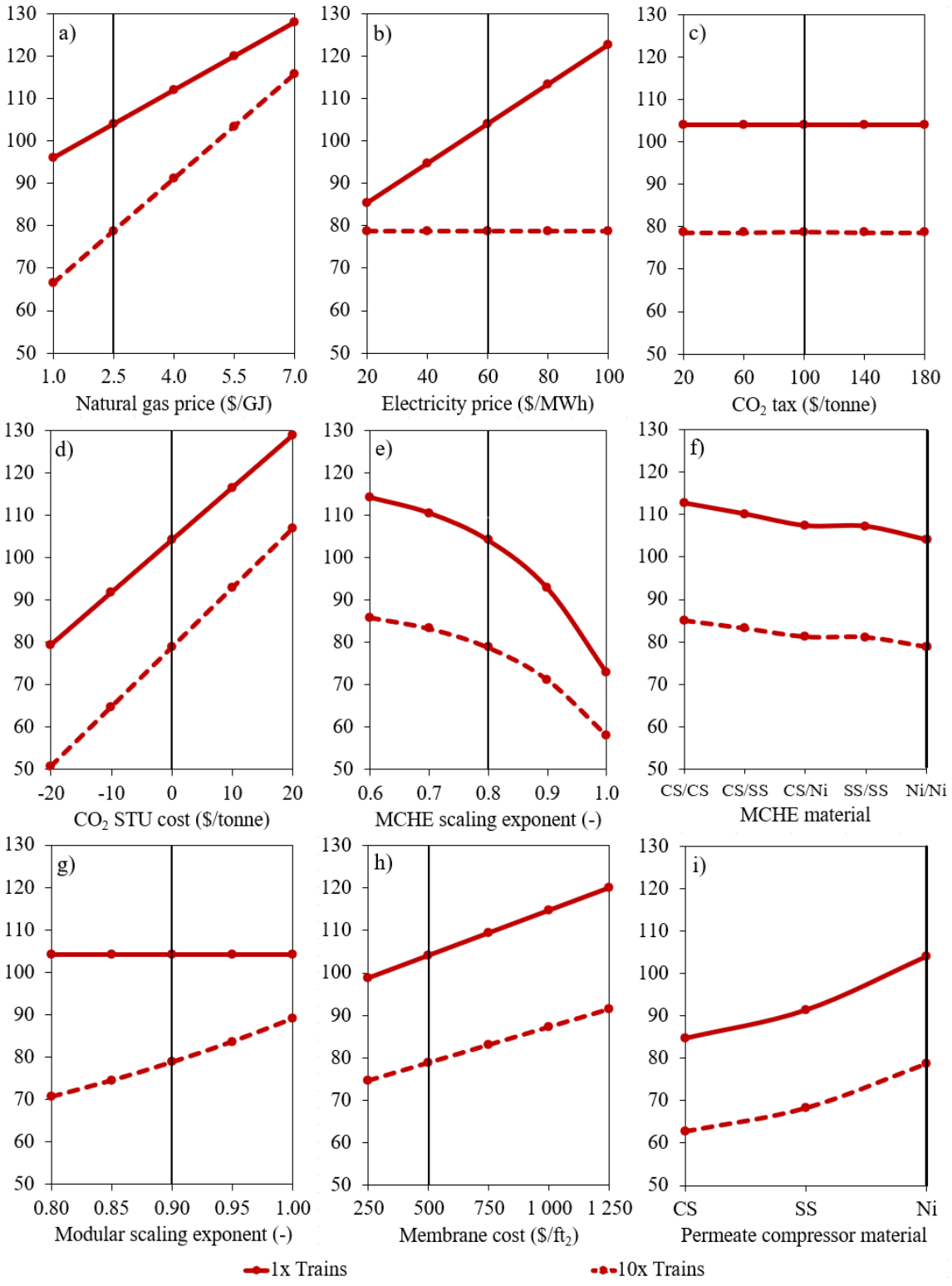

Figure 27: Sensitivity analysis of important parameters in the four scenarios with COCA as the target impact value. COCA ($/tonne) is the y-axis, and the black line is the base case parameters.

Figure 27b. Higher electricity prices require a higher CO_2 tax rate for the 1x train while the 10x train is unaffected. Higher electricity prices will justify electrically self-sufficient plants, and on-site power production can be more efficient at larger scales when more efficient gas turbines can be used. Both the analysis on LCOP and COCA of the 1x ammonia train reflects the justification of building smaller scale plants in areas where power is accessible and cheap.

CO_2 Price

In addition to natural gas prices, the price for emitting CO_2 in dollars per tonne for the LNG plants is a very influential parameter in assessing the LCOP presented in Figure 26c. As previously discussed, the ammonia plants become more economical at CO_2 prices of \$78.81/tonne and \$104.08/tonne for the 10x and 1x trains, respectively. At low CO_2 prices, both LNG plant sizes have lower levelized costs until reaching around \$55/tonne when the 10x ammonia plant reaches cost parity with the 1x LNG plant. Further, at around \$115/tonne, the small-small scale ammonia plant is more economical than the 10x LNG train.

CO_2 Storage and Utilization Costs

Cost implications of storage, transport, and utilization (STU) of CO_2 significantly impact the economics of the two ammonia plants featuring CO_2 capture, as illustrated in Figure 26d. The portability of ammonia could lead to future developments where ammonia manufacturing facilities are strategically located near oil and gas sites, thereby conveniently capitalizing on lucrative enhanced oil and gas recovery opportunities, which could potentially be valued at roughly \$30/tonne of avoided CO_2 [82]. The 10x plant is more economical at STU costs lower than \$15/tonne. For the 1x train to provide competitiveness, a profit is required of around \$3/tonne. At CO_2 STU profits reaching \$20/tonne, the 1x ammonia train proves advantageous over the 10x LNG plant.

CO_2 STU costs are one of the most important parameters in assessing the COCA, presented in Figure 27d. In the cost-intensive spectrum at \$20/tonne, COCA for the 1x and 10x train approaches reach \$130/tonne and \$115/tonne, respectively. However, where the ammonia plant is situated close to oil and gas operations and enhanced recovery is feasible, the plants quickly ramp up competitiveness towards LNG production. In this case, the ammonia scenario is more economical at CO_2 prices of \$80/tonne and \$50/tonne for the 1x and 10x plant sizes, respectively. In the 10x train, each 1 \$/tonne reduction in STU costs reduces the COCA by about 1.6 \$/tonne because of the relatively low efficiency of the ammonia train (significantly more CO_2 is captured per GJ of ammonia output than emitted per GJ of LNG output).

MCHE Scaling Exponent

The main cost component for the LNG plant is the coil-wound heat exchanger used for the cryogenic cooling of natural gas, discussed in Section 2.4.3. According to Martin et al. 2004, suppliers for these large heat exchangers are limited, making them less cost-competitive [108]. Illustrated in Figure 26e, MCHE scaling exponent significantly impacts the cost assessment for LNG. If no economic advantages are gained when scaling up the MCHE, the levelized costs for LNG increase exponentially in both scenarios. Further, if the scaling exponent increases to around 0.84, the 1x train ammonia plant becomes more economical than the 1x train LNG plant. Because of the limited amount of suppliers and the high costs for cryogenic heat exchangers, their costs may fluctuate greatly depending on market conditions.

Illustrated in Figure 25, capital costs account for 15% and 11% of the final levelized costs in the 1x and 10x LNG plant scenarios, respectively. Therefore, COCA in the 1x scenario is more sensitive to the MCHE scaling exponent than the 10x train, expressed in Figure 27e. When LNG plant costs increase due to lower cost benefits for the MCHE, lower CO_2 prices are required for the ammonia plants to become a feasible alternative to LNG.

MCHE Material

In addition to the MCHE scaling exponent, material choices in the coil-wound heat exchanger affect the LCOP, seen in Figure 26f. A Ni-based alloy was utilized for both sides of the heat exchanger due to high-temperature loads. If technologies for lower quality materials such as carbon steel can handle the loads for cryogenic cooling, the LCOP can decrease by around 4%. Similar to the discussion for the MCHE scaling exponent, the 1x LNG train is more affected by the material choice

compared to the 10x LNG train. Other materials for these capital-intensive units are currently being developed where materials such as stainless steel, special steel alloys, carbon steel, copper, and aluminum are being utilized [121].

When utilizing cheaper materials in the coil-wound heat exchanger, the COCA increases due to the fact that the LNG plant becomes more economical. Where a carbon steel compound is utilized for both the heat exchanger's hot- and cold sides. Figure 27f shows that the COCA increases by around 8% and 7% for the 1x and 10x train, respectively.

Modular Scaling Exponent

To utilize the benefits of economies of scale discussed in Section 2.3.3, a modular scaling factor was applied to the 10x trains elaborated in Section 4.1.1. The effect of the modular scaling exponent on the levelized costs is presented in Figure 26g. Capital costs in the 10x train account for 12% and 36% for the LNG and ammonia plants, respectively. Therefore, the modular scaling exponent has a larger influence on the ammonia plant, seen as a steeper slope than the LNG plant. From the discussion in Section 5.2.2, it is clearly visualized that by scaling up the ammonia plant using a representative modular scaling factor, the ammonia scenario is more sensitive to economies of scale than the LNG scenario.

Further, Figure 27g illustrates the modular scaling exponent range impact on COCA. Since the ammonia plant thrives by scaling up the trains and lowering the modular scaling exponent, decreasing the exponent to 0.8 results in reductions of CO_2 prices to \$70/tonne. However, if no modular scaling exponent is applied, the CO_2 price required for competitiveness in the 10x train is at \$89/tonne.

Membrane Costs

As membranes are the most expensive part of the MA-ATR process, accounting for around 32% of the total BEC, membrane costs impact on the LCOP is presented in Figure 26h. Increased membrane costs will affect the competitiveness of ammonia towards LNG. If extrapolating prices to around \$1,500/ft^2, the 10x ammonia plant will erode its cost advantage over the LNG plant. However, research by Acquaviva et al. 2009 sets a goal for membrane costs to be less than \$500/ft^2, suggesting that with ongoing progress and scale benefits tied to membrane production, the cost benefits of the ammonia plant could potentially grow in comparison to the LNG scenario in this economic assessment [116].

Figure 27h illustrates a linear relationship between the membrane costs and their impact on COCA. More cost-effective membranes result in lower CO_2 prices required for the ammonia plants to provide competitiveness towards LNG. Further, the COCA increases linearly by around \$5/tonne per \$250/ft^2 increase in membrane costs.

Permeate Compressor Material

Elaborated in Section 4.3.1, the five-stage compression of the permeate stream requires protection against hydrogen embrittlement and pressure loads using a Ni-alloy as material. The presence of inert nitrogen will reduce the risk of embrittlement, but nitrogen constitutes only a quarter of the stream. However, as discussed in Section 5.2.1, the Ni-alloy compressors are highly capital intensive and responsible for around 25% of the total capital costs in the ammonia value chain. Consequently, as illustrated in Figure 26i, utilizing cheaper materials such as carbon or stainless steel can lower levelized costs by around 9% and 6%, respectively. From the figure, the 1x train becomes more economical than LNG if this modification is made to the compressors. A similar reduction is observed for the 10x train.

Figure 27i shows that a downgrade in material quality for the permeate compressor directly im-

proves the competitiveness of the ammonia scenario. Replacing the Ni-alloy with carbon or stainless steel lowers the COCA by around 19% and 13%, respectively. Here, the 1x train is reduced to $85/tonne, and the 10x train is reduced to $63/tonne. However, it is important to note that if cheaper materials are used, the risk of hydrogen embrittlement has to be addressed, most likely by applying protective coatings to all the surfaces in contact with the hydrogen-rich gas.

5.2.4 Further Work and Outlook for Making Ammonia an Alternative to LNG

Projection for LNG and Ammonia Demand

Where natural gas is produced in areas where prices are low and production rates are high, LNG proves competitive as an energy transportation method across boundaries compared to conventional pipelines. Additionally, with the increased focus on energy security in all regions of the world due to Russia's invasion of Ukraine and its consequences for the European gas supply, demand for natural gas and LNG is expected to increase in the STEPS scenario outlined in Section 2.4. Demand for natural gas is reduced because of the transition to low-carbon options in the APS and NZE scenarios. However, demand for LNG slightly increases towards 2030 in the APS and NZE, but as alternatives for energy trade emerge, LNG as an energy vector is set to decrease until 2050.

Following the trajectory of emission targets aligned with the APS and NZE, alternatives for energy transportation methods across regions are required. Here, in addition to the downstream uses discussed in Section 2.5, ammonia could be a candidate for a low-carbon energy carrier. By 2030, ammonia is anticipated to be the prevalent mode for maritime hydrogen export and import [2]. With its existing infrastructure, Europe can already import millions of tonnes of ammonia annually for chemical purposes. However, to allow for substantial low-emission hydrogen exports to Europe in the form of ammonia, there is a necessity for considerable additional capacity.

Future Projections for Natural Gas Prices

As discussed in the sensitivity analysis in Section 5.2.3, low natural gas prices are more favorable towards ammonia production than LNG. Figure 28 presents the natural gas import prices for various regions based on STEPS, APS, and NZE in 2030 and 2050. Both historically and in the future projections, Japan has high natural gas prices compared to other regions because of being entirely dependent on LNG. Total China and Europe natural gas consumption from LNG accounts for around 25% of and 19% [1]. Further, the United States is independent of imports, and the price for natural gas is considerably lower than for the other regions.

Illustrated in Figure 28, the United States thrives on relatively low natural gas prices compared to the other regions in all the scenarios. Consequently, the United States as a location for the ammonia plant would improve its competitiveness towards LNG. Additionally, regions in the Middle East, such as Saudi Arabia, have similar costs of natural gas as in the United States, thereby expanding competitive ammonia production across regions. However, it is important to point out that LNG plants would generally be built in carefully selected locations close to low-cost production wells where prices are below the market prices shown in Figure 28. LNG (or ammonia) produced by such strategically positioned plants can be highly profitable if market prices in importing regions such as the EU, China, and Japan remain high.

Electricity Prices

Since the ammonia plants consume much more electricity than the LNG plants, electricity supply is an important consideration. Electricity imports can be a promising alternative regardless of the plant scale low-cost and low-carbon electricity is available (e.g., Norwegian or Canadian hydropower). In such cases, long-term agreements securing low electricity costs for the ammonia plant will be an important risk-reduction mechanism. However, if the electricity supply is more expensive

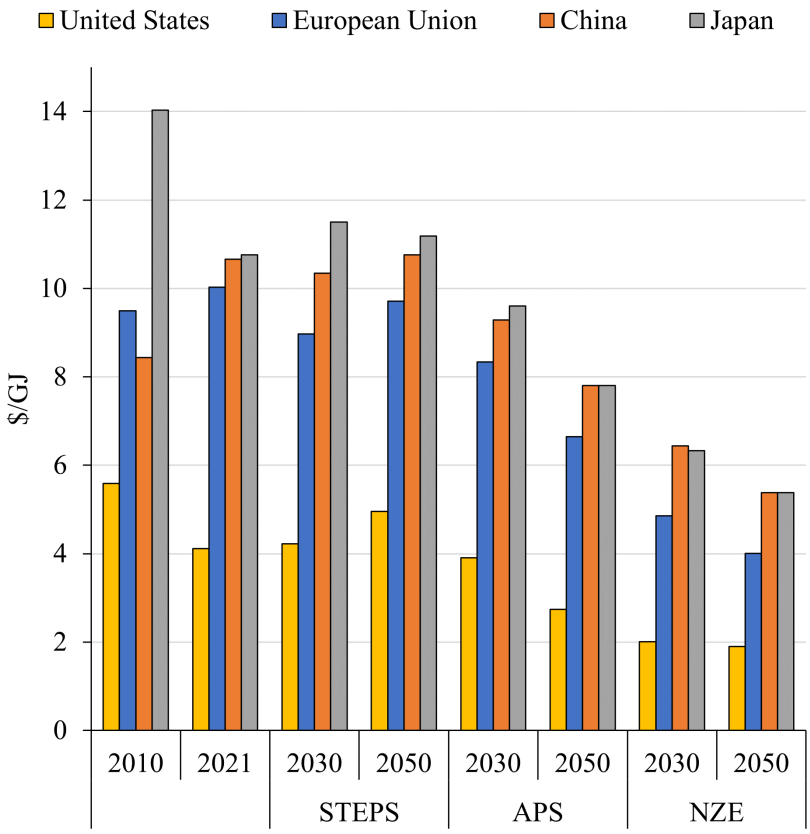

Figure 28: Import natural gas prices per scenario [2]. The prices of natural gas are represented as average values calculated on the basis of gross calorific value. In the United States, the cost of natural gas corresponds to the prevailing wholesale rate in the internal market. The prices in the European Union and China incorporate a mix of both pipeline and LNG imports. Japan's gas price, however, is exclusively determined by LNG imports. The LNG prices referred to are those recorded at the customs border before the process of regasification.

or relatively carbon-intensive, on-site carbon-free electricity production by combusting a portion of the produced hydrogen would be the preferred alternative. On-site electricity production will be more economical for large-scale plants such as the 10x train, where full-size combined cycle power plants can be utilized.

As the base case parameter for grid emission intensity was assumed to be carbon neutral, the ammonia value chain has zero emissions. To account for additional emissions in the 1x LNG and ammonia value chains, a sensitivity analysis was conducted to assess the impact of higher CO_2 emissions from the external power supply shown in Figure 29. Due to almost six times higher power requirements for the ammonia plant, the respective LCOP are affected more than LNG, illustrated as a steeper curve in Figure 29a. Further, the 1x ammonia value chain loses competitiveness against LNG where grid emissions are increased, shown in Figure 29b. For a typical natural gas-fired combined cycle power plant, 330 kg of CO_2 is emitted per MWh produced [118]. At a CO_2 price of \$100/tonne, this would increase the LCOP by 2.4% and 8.4% for the 1x LNG and ammonia value chains, respectively.

CO_2 Prices and EU Carbon Border Adjustment Mechanism

As studied in the sensitivity analysis in Section 5.2.3, CO_2 taxation is critical for the ammonia value chain to compete with LNG. The emission distribution in the LNG value chain is an important aspect to consider. Some countries have already implemented CO_2 tax rates regimes, while some

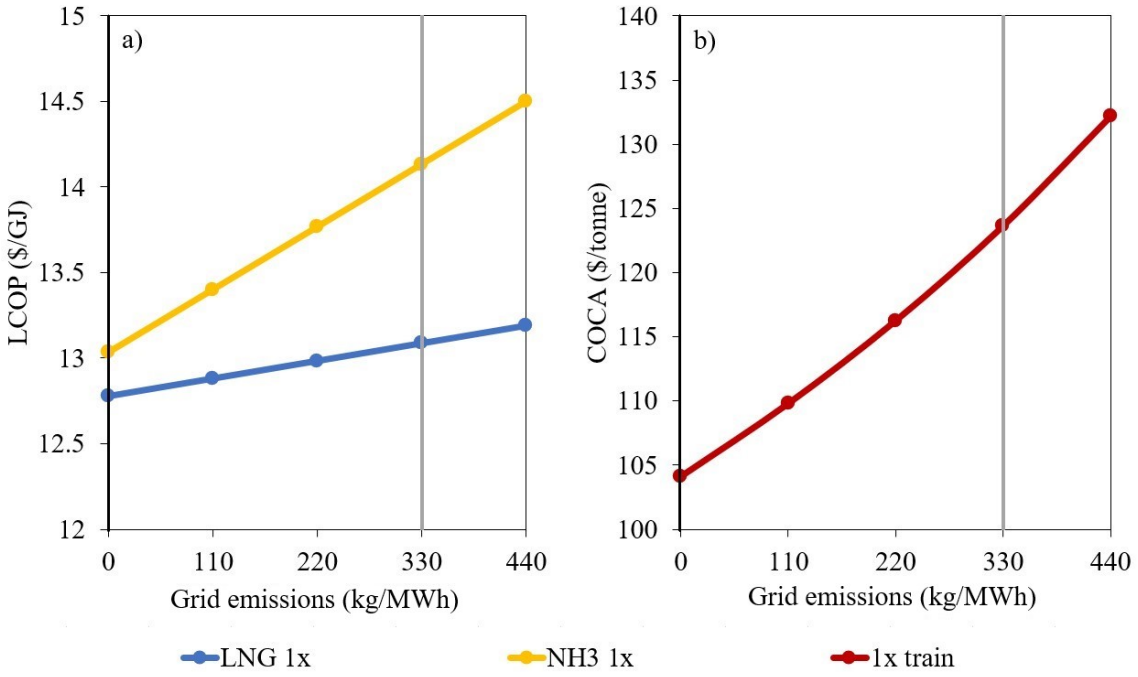

Figure 29: Sensitivity analysis of electricity grid emission intensities impact on LCOP and COCA. The black line is the base case, assuming carbon-free electricity. The grey line is a typical natural gas combined-cycle power plant at 330 kg/MWh [118].

countries have not yet defined a CO_2 pricing policy but intend to in the future [122]. Therefore, LNG trade between nations could possibly lead to different prices for CO_2 emissions.

In this work, LNG is produced in the United States and shipped to Germany to provide increased energy security in Europe. At the start of 2023, the price for CO_2 in the United States and Europe was \$0/tonne [123] and \$100/tonne, respectively [122]. From Section 5.1, around 90% of the total LNG value chain emissions is from downstream combustion of natural gas. Previous studies indicate that the upstream CO_2 emissions from extraction, processing, and transportation account for the same fraction as the LNG plant and shipping emissions in the LNG value chain [124]. Therefore, when the upstream emissions are accounted for, the downstream emissions are around 82% of the total LNG value chain emissions. Consequently, demand centers are more affected by CO_2 pricing than producers.

Figure 30 presents current pricing for CO_2 in the European Union and future projections for CO_2 prices in the APS and NZE scenarios. The European Union is the only region with stated policies for increased CO_2 prices towards 2050. However, advanced economies with net zero emission pledges need to substantially increase the CO_2 prices in the APS and NZE scenarios. Additionally, the CO_2 tax rates in emerging markets increase, but at a considerably slower rate than for the advanced economies. Lastly, CO_2 prices in other emerging markets and developing countries increase even slower, except for the 2050 NZE scenario.

To account for imported emissions where CO_2 prices are lower and reduce the risk of "carbon leakage," the EU has implemented the Carbon Border Adjustment Mechanism (CBAM) [125]. Carbon border adjustments represent a new wave of trade policy instruments developed to discourage the relocation of carbon-heavy economic operations from regions with more robust climate policies to those with less rigorous regulations. These adjustments could enhance the environmental impact of climate strategies by preventing changes in economic behavior that might increase greenhouse emissions. Additionally, these adjustments are viewed as a method to safeguard industrial competitiveness by diminishing the appeal for companies to transfer their manufacturing processes

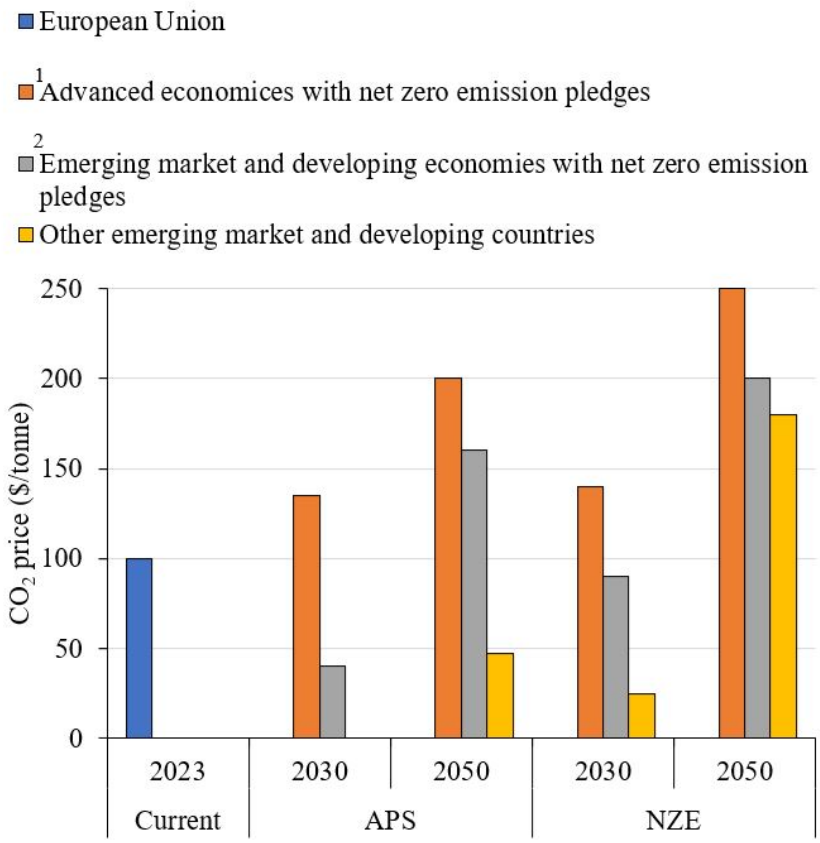

Figure 30: CO_2 prices for electricity, industry and energy production in selected regions by scenario [2].[1]Includes all OECD countries except Mexico. [2]Includes China, India, Indonesia, Brazil and South Africa.

overseas. For example, the CBAM would also account for production and upstream emissions from LNG production in the US, thus pricing full lifecycle emissions. This would further increase the incentive for natural gas exporters to decarbonize their production processes when exporting to the EU. Ammonia from the 10x train would already be economically viable in the EU, but this is not yet possible because ammonia production using currently available ammonia technologies would be significantly more expensive, and ammonia end-use possibilities are still very limited.

The Economic Value of CO_2 for EOGR applications

CO_2 transport and storage is a serious bottleneck to the deployment of CCS around the world because of a lack of pipeline infrastructure connecting CO_2 sources to storage sites [82]. However, the possibility to site ammonia production facilities close to oil and gas reservoirs that can also serve as CO_2 storage facilities can turn this drawback into a large benefit via enhanced oil and gas recovery (EOGR). EOGR combined with CO_2 capture, transport, and storage is a promising method for cost-effective CO_2 emission reduction, particularly given its existing implementation in the oil and gas industry and its ability to generate valuable products. As discussed in the sensitivity analysis in Section 5.2.3, integrating EOGR close to the ammonia production could potentially lower the levelized costs for ammonia significantly. Consequently, when constructing ammonia production facilities close to oil and gas reservoirs, a thorough analysis should be conducted to evaluate the opportunities of EOGR to maximize the competitiveness of the ammonia value chain. If implemented well, CO_2 from a well-sited ammonia production facility can significantly increase the value of local oil and gas reservoirs by reducing production costs and extending production lifetimes. This synergistic integration appears highly promising and should be encouraged by

policies in natural gas exporting regions.

MA-ATR Ammonia Plant Feasibility

An important factor to consider is that the MA-ATR ammonia technology for ammonia production used in this work is not a mature technology. Several years of research and development (R&D), technology improvements, and subsidies from various policymakers are required for future blue ammonia production plants before reaching a cost-effective and defined ammonia value chain. In addition to various subsidies for enabling low-carbon solutions, CO_2 prices need to increase in order for CO_2 intensive process to become more expensive and therefore improve the competitiveness of cleaner fuels.

The causality dilemma, also known as the chicken-and-egg problem, is used in situations where it is difficult to assess which of several events are causes and which are effects. This terminology can be used to facilitate how various components in the ammonia value chain are dependent upon each other. The ammonia production plant requires infrastructure to transport the product to demand centers. Further, transportation industries are dependent upon exporting and importing terminals where storage and regasification facilities are in place. Lastly, downstream users of ammonia are dependent upon utilization technologies such as ammonia-fired power plants, ammonia engines, or fertilizer production plants.

Already existing ammonia production plants based on reference technologies such as the KBR and LAC process discussed in Section 2.5.4 can work as a catalyst towards improving ammonia value chain components until the MA-ATR process reaches technological maturity. Briefly discussed in Section 5.2.1, the 1x MA-ATR provides 27.5% cost savings compared to the LAC plant using the assumptions for raw material costs and natural gas input flow rate as discussed by Arnaiz del Pozo et al. 2022 [11]. Further, this cost increase could be applied to the complete 1x MA-ATR value chain to find a price for the LAC premium, which reflects the additional levelized costs for implementing existing technologies for ammonia production. The LAC premium equals \$2.74/GJ for the 1x ammonia scenario. The respective COCA increases to \$148/tonne when accounting for the LAC premium, which reflects the price CO_2 price where already existing ammonia production technologies would emerge as competitive against LNG.

Policies must be implemented to encourage the use of ammonia as a substitute for natural gas and other carbon-intensive fuels. The most important policy lever must be subsidies for using ammonia in various end-use applications, possibly starting with ship engines. Once this demand is created by policy incentives, the free market will naturally invest in better production (e.g., the scale-up of GSR and MA-ATR), distribution (e.g., ammonia carriers and import/export terminals), and end-use technologies (e.g., better engines, turbines, and fuel cells running on ammonia) to maximize profitability. The ammonia end-use subsidy can be gradually ramped down as technologies and scale improve until CO_2 pricing alone is enough to allow ammonia to continue taking market share from natural gas and other carbon-intensive fuels.

To paint a full strategic picture of how the competitiveness of ammonia can be maximized based on this work, the following recommendations are given:

- The starting point must be policies that make even today's ammonia competitive in the most suitable markets (e.g., shipping fuel). This will require direct subsidies for the use of ammonia fuel in addition to rising CO_2 taxes.
- Once a sufficiently high demand for ammonia is created, suppliers must be strategic about meeting this demand in the most cost-effective manner.
- Production facilities must be built in regions with the cheapest natural gas and opportunities for creating extra value from the captured CO_2 via EOGR.

- Suppliers must invest in the scale-up of next-generation ammonia production technologies such as MA-ATR and GSR with an emphasis on minimizing the costs of key components such as membranes, oxygen carriers, and hydrogen compressors.
- If low-cost and low-carbon electricity is locally available (e.g., Norwegian or Canadian hydropower), the plants can be designed to maximize electricity consumption. Otherwise, the plants must be configured for on-site hydrogen-fired power production.
- Distribution networks must be established in the most suitable niches first. Shipping fuels are a good first target because the ammonia distribution network can be limited to ammonia carriers and import/export terminals. Later, the distribution network can be extended to other opportunities inland.

6 Conclusion

In light of the recent Russia-Ukraine crisis, global concerns over energy security have escalated, contributing to a rise in demand for energy carriers like LNG. However, this narrative shifts under the APS and NZE, wherein the demand for cleaner, low-carbon alternatives grows. In these changing dynamics, ammonia stands out as a promising contender. Projected to become the prevalent mode of maritime hydrogen export and import by 2030, ammonia could potentially replace LNG, mainly if additional capacity is constructed to support low-emission hydrogen exports to key regions, such as Europe. This possibility indicates a significant shift in the global energy landscape, positioning ammonia as a potent alternative to LNG in the face of growing energy security concerns.

This thesis comprehensively evaluates the prospects of blue ammonia as a low-carbon alternative to LNG, emphasizing its economic competitiveness, technological feasibility, and environmental implications. This research's significant contributions lie in the in-depth techno-economic analysis of the LNG and ammonia value chain from the production facility in the US to the importing terminal in Germany. By modeling all four scenarios in Aspen Plus and conducting independent economic assessments for the production plants, terminals, and shipping using the SEA Tool, a consistent methodology was employed to enable comparison between the energy carriers. Further, accounting for economies of scale and extracting natural gas from various reservoir sizes, a 1x and a 10x train approach was taken for both energy vectors.

The present work indicates that larger-scale plants improve the prospects of ammonia using a CO_2 price of \$100/tonne and natural and electricity prices of \$2.5/GJ and \$60/MWh, respectively. For the 1x train size, the LCOP is \$12.78/GJ for LNG and \$13.03/GJ for ammonia, with ammonia achieving competitiveness at a carbon tax rate of \$104.08/tonne. However, when scaled to a 10x train size, the LCOP decreases to \$11.35/GJ for LNG and \$10.04/GJ for ammonia. This scale-up substantially lowers the carbon tax rate required for competitiveness, reducing it to \$78.81/tonne for ammonia. Additionally, the larger-scale operations lead to a 12% cost reduction over a 25-year plant lifetime, emphasizing the potential benefits of larger-scale ammonia production. According to IEA's projected CO_2 prices required to limit global temperature rise to 2 degrees, the CO_2 prices required for ammonia to achieve cost-parity with LNG are well below that of policymakers. Where CO_2 prices exceed cost-parity, the ammonia value chains become more profitable than LNG, specifically expressed in large-scale operations.

The sensitivity analysis reveals that the price of natural gas significantly influences the LCOP and COCA, with the ammonia plants being more affected by variations in natural gas prices due to their lower thermal efficiency. The sensitivity of the ammonia plants, particularly the 10x train, is pronounced in regions with low natural gas prices, such as the US and the Middle East, suggesting a strategic advantage in constructing larger ammonia plants in such areas. Implications for CO_2 STU costs emerged as essential factors impacting the economics of the ammonia plants. The strategic location of ammonia manufacturing facilities near oil and gas sites could capitalize on enhanced oil and gas recovery opportunities and increase competitiveness. The study also demonstrates that electricity cost variations strongly impact the economics of ammonia plants due to their substantial electricity consumption. This suggests that plants could be designed with electricity imports in locations with access to low-cost and low-carbon electricity and low-cost natural gas (e.g., Norway or Canada).

The breakeven CO_2 price can be reduced drastically if the plant is located ideally in a region with cheaper natural gas and larger CO_2 revenues than our central assumptions. If the 10x ammonia fuel facility consumes natural gas costing \$1.5/GJ and gets \$20/tonne of revenues for the CO_2 it produces, a CO_2 price of \$25/tonne creates competitiveness against large-scale LNG operations. At CO_2, tax rates of \$200/tonne and \$250/tonne, which reflect IEA's projected prices for OECD countries in the APS and NZE in 2050, the 10x ammonia value chain present cost savings of 43%

and 51%, respectively. If the CO_2 price projections from the IEA actually occur, the 10x ammonia value chain provides a lucrative opportunity for early investors to transition from LNG to ammonia with rising CO_2 prices. The European Union's CBAM could further boost low-carbon solutions' competitiveness by accounting for emissions from imports where CO_2 prices are lower.

The analysis has further unveiled the substantial impact of cost and material choices related to the CWHE used in LNG plants, highlighting a potential challenge in scaling up due to the limited suppliers and the high costs of this critical component. The sensitivity to economies of scale and modular scaling is especially crucial for the economics of the ammonia plants, with the 10x train appearing more beneficial.

The costs associated with the MA-ATR process membranes and the choice of material for compressors in the ammonia value chain also notably influence LCOP and COCA. Achieving cost reductions in these areas could further enhance the competitiveness of ammonia against LNG. However, while these findings provide a comprehensive assessment of the economic viability of ammonia in comparison to LNG under the studied conditions, it is imperative to note that several factors, such as policy changes, technological advancements, and market dynamics, could further influence these outcomes. Specifically, policies will be required to create demand for initially more expensive ammonia fuel to start driving down costs via technological learning and scale. For example, blue ammonia production using currently available technologies at a scale applicable to current markets will require CO_2 prices twice as high as the 10x MA-ATR train to compete with LNG.

In order to accelerate ammonia's acceptance as a viable replacement for carbon-intensive fuels, strategic implementation of supportive policies, including subsidies for ammonia end-use applications, is imperative. The progressive ramp-down of such incentives can be pursued once the evolution and scaling up of technology bring down costs until a reasonable CO_2 tax is sufficient to support further growth. If policy action makes ammonia economically attractive, the free market can be relied upon to build production facilities in regions with affordable natural gas and potential value from captured CO_2 through EOGR, invest in the scale-up of next-gen production technologies, and strategically extend distribution networks to access an increasingly broad range of end-use applications. These steps will pave the way for ammonia's market expansion at the expense of natural gas and other carbon-intensive fuels, making a large contribution to the urgent global need for clean, secure, practical, and affordable energy.

Bibliography

[1] BP. 'Natural Gas'. In: *Statistical Review of World Energy* (2022). URL: https://www.bp.com/content/dam/bp/business-sites/en/global/corporate/pdfs/energy-economics/statistical-review/bp-stats-review-2022-full-report.pdf (visited on 14/03/2023).

[2] IEA. 'Outlook for gaseous fuels'. In: *World Energy Outlook 2022* (2022). URL: https://www.iea.org/reports/world-energy-outlook-2022.

[3] The World Bank. 'Global Poverty: The Biggest 1 Setback in Decades'. In: *Poverty and Shared Prosperity 2022* (2022). URL: https://www.worldbank.org/en/publication/poverty-and-shared-prosperity (visited on 02/06/2023).

[4] S. Mokhatab et al. 'Chapter 1 - LNG Fundamentals'. In: *Handbook of Liquefied Natural Gas* (2014), pp. 1–101.

[5] D.A Economides M.J. Wood. 'The state of natural gas'. In: *Journal of Natural Gas Science and Engineering* (2009), pp. 1–13. DOI: https://doi.org/10.1016/j.jngse.2009.03.005.. URL: https://www.sciencedirect.com/science/article/pii/S187551000900002X.

[6] W. Lim, K. Choi and I. Moon. 'Current status and perspectives of liquefied natural gas (LNG) plant design'. In: *Industrial & Engineering Chemistry Research* (2013), pp. 3065–3088.

[7] Schalk Cloete et al. 'Cost-effective clean ammonia production using membrane-assisted autothermal reforming'. In: *Chemical Engineering Journal* (2020). DOI: 10.1016/j.cej.2020.126550.

[8] Nazir H et al. 'Is the H2 economy realizable in the foreseeable future?' In: *Part II: H2 storage, transportation, and distribution. Int J Hydrogen Energy.* (2020). DOI: 10.1016/j.ijhydene.2020.03.092. URL: https://www.sciencedirect.com/science/article/pii/S0360319920320966.

[9] Bartels J. A. 'A feasibility study of implementing an Ammonia Economy'. In: (2008). URL: https://dr.lib.iastate.edu/server/api/core/bitstreams/c0443ee4-2e07-4213-9dbd-ee251dad41ec/content (visited on 29/04/2023).

[10] IEA. 'Hydrogen Production'. In: *Global Hydrogen Review 2022* (2022). URL: https://www.iea.org/reports/global-hydrogen-review-2022.

[11] Carlos Arnaiz del Pozo and Schalk Cloete. 'Techno-economic assessment of blue and green ammonia as energy carriers in a low-carbon future'. In: *Energy Conversion and Management* 255 (2022). DOI: 10.1016/j.enconman.2022.115312.

[12] Ratan Raj et al. 'A techno-economic assessment of the liquefied natural gas (LNG) production facilities in Western Canada'. In: *Sustainable Energy Technologies and Assessment (18)* (2016), pp. 140–152. DOI: https://doi.org/10.1016/j.seta.2016.10.005. URL: https://www.sciencedirect.com/science/article/pii/S2213138816301278?via%5C%3Dihub#b0180.

[13] C.T Sen. 'Trends and Developments in the LNG Industry'. In: *Report of the Potential Gas Committee* (2002), pp. 89–98.

[14] IPCC. 'Energy Carriers'. In: *Climate Change 2007: Working Group III: Mitigation of Climate Change* (2007). URL: https://archive.ipcc.ch/publications_and_data/ar4/wg3/en/ch4s4-3-4.html (visited on 18/04/2023).

[15] IEA. 'Final energy consumption by carrier in the Sustainable Development Scenario, 2018 and 2040'. In: (2018). URL: https://www.iea.org/data-and-statistics/charts/final-energy-consumption-by-carrier-in-the-sustainable-development-scenario-2018-and-2040.

[16] Agustin Valera-Medina and Rene Banares-Alcantara. 'Chapter 2: Energy Storage Technologies: Power-to-X'. In: *Techno-Economic Challenges of Green Ammonia as an Energy Vector* (2020).

[17] BP. 'Natural Gas'. In: *bp Energy Outlook 2022 edition* (2022). URL: https://www.bp.com/content/dam/bp/business-sites/en/global/corporate/pdfs/energy-economics/energy-outlook/bp-energy-outlook-2022.pdf.

[18] Gordonnat J and Hunt J. 'Subsea cable key challenges of an intercontinental power link: case study of Australia–Singapore interconnector.' In: *Energy Transit 4, 169–188* (2020). DOI: https://doi.org/10.1007/s41825-020-00032-z. URL: https://link.springer.com/article/10.1007/s41825-020-00032-z.

[19] BP. 'Natural Gas'. In: *Statistical Review of World Energy* (2021). URL: https://www.bp.com/content/dam/bp/business-sites/en/global/corporate/pdfs/energy-economics/statistical-review/bp-stats-review-2021-full-report.pdf (visited on 14/03/2023).

[20] engineeringtoolbox.com. 'Environmental emission of carbon dioxide CO2 when combustion fuels like coal, oil, natural gas, LPG and bio energy.' In: *Combustion of Fuels - Carbon Dioxide Emission* (2023). URL: https://www.engineeringtoolbox.com/co2-emission-fuels-d_1085.html (visited on 08/01/2023).

[21] IEA. 'Gas'. In: *Fuels and Technologies* (2022). URL: https://www.iea.org/fuels-and-technologies/gas (visited on 10/03/2023).

[22] IPCC. 'Energy Systems'. In: *Climate Change 2014: Mitigation of Climate Change. Contribution of Working Group III to the Fifth Assessment Report of the Intergovernmental Panel on Climate Change* (2014). URL: https://www.ipcc.ch/report/ar5/wg3/ (visited on 17/01/2023).

[23] Sam Nierop and Simon Humperdinck. 'International comparison of fossil power efficiency and CO2 intensity'. In: (2018). URL: https://guidehouse.com/-/media/www/site/downloads/energy/2018/intl-comparison-of-fossil-power-efficiency--co2-in.pdf (visited on 02/03/2023).

[24] P Forster et al. 'Changes in Atmospheric Constituents and in Radiative Forcing'. In: *Climate Change 2013: The Physical Science Basis* (2007). URL: https://archive.ipcc.ch/publications_and_data/ar4/wg1/en/ch2.html (visited on 15/03/2023).

[25] IEA. 'Methane and climate change'. In: *Global Methane Tracker 2022* (2022). URL: https://www.iea.org/reports/global-methane-tracker-2022/methane-and-climate-change (visited on 15/03/2023).

[26] EIA. 'Delivery and storage of natural gas'. In: *Natural gas explained* (2022). URL: https://www.eia.gov/energyexplained/natural-gas/delivery-and-storage.php (visited on 07/03/2023).

[27] NaturalGas.org. 'The Transportation of Natural Gas'. In: *From Wellhead to Burner Tip* (2013). URL: http://naturalgas.org/naturalgas/transport/ (visited on 21/01/2023).

[28] Energy Infrastructure. 'Underground Natural Gas Storage'. In: *Energy 101* (2016). URL: https://www.energyinfrastructure.org/energy-101/natural-gas-storage (visited on 17/02/2023).

[29] IEA. 'Chapter 2: Producing hydrogen and hydrogen-based products'. In: *The Future of Hydrogen* (2019). URL: https://www.iea.org/reports/the-future-of-hydrogen.

[30] Energy.gov. 'Fuel Cells'. In: *Hydrogen and Fuel Cell Technolgies Office* (). URL: https://www.energy.gov/eere/fuelcells/fuel-cells (visited on 27/03/2023).

[31] Energy.gov. 'Hydrogen: A Clean, Flexible Energy Carrier'. In: *Office of Energy Efficiency & Renewable Energy* (2017). URL: https://www.energy.gov/eere/articles/hydrogen-clean-flexible-energy-carrier (visited on 22/03/2023).

[32] IEA. 'Hydrogen Demand'. In: *Global Hydrogen Review 2022* (2022). URL: https://www.iea.org/reports/global-hydrogen-review-2022.

[33] Agustin Valera-Medina and Rene Banares-Alcantara. 'Chapter 1: Introduction'. In: *Techno-Economic Challenges of Green Ammonia as an Energy Vector* (2020).

[34] S&P Global. 'Exploring innovative technologies to achieve a low carbon future/support the decarbonization of the global economy'. In: *Clean Energy Technology Brochure* (2019). URL: https://www.spglobal.com/commodityinsights/en/ci/products/hydrogen-global-market.html (visited on 04/02/2023).

[35] Engineering ToolBox. 'Fuels - Higher and Lower Calorific Values'. In: (2003). URL: https://www.engineeringtoolbox.com/fuels-higher-calorific-values-d_169.html (visited on 20/02/2023).

[36] Barton Smith et al. 'New Materials for Hydrogen Pipelines'. In: *Hydrogen Pipeline Working Group Meeting* (2005). URL: https://www.energy.gov/eere/fuelcells/articles/new-materials-hydrogen-pipelines-0 (visited on 22/05/2023).

[37] European Commision. 'Assessment of Hydrogen Delivery Options'. In: *Science for Policy Briefs* (2021). URL: https://joint-research-centre.ec.europa.eu/system/files/2021-06/jrc124206_assessment_of_hydrogen_delivery_options.pdf (visited on 28/01/2023).

[38] K. Xu. 'Hydrogen embrittlement of carbon steels and their welds'. In: (2012), pp. 526–561. DOI: 10.1533/9780857093899.3.526.

[39] Hao Li et al. 'Safety of hydrogen storage and transportation: An overview on mechanisms, techniques, and challenges'. In: *Energy Reports* 8 (2022), pp. 6258–6269. DOI: 10.1016/j.egyr.2022.04.067.

[40] O. Elishav et al. 'Storage and Distribution of Ammonia'. In: *Techno-Economic Challenges of Green Ammonia as an Energy Vector* (2020).

[41] Michael J. Moran et al. 'Fundamentals of Engineering Thermodynamics, 9th Edition'. In: (2018).

[42] Neera Jain and A.G. Alleyne. 'Thermodynamics-based optimization and control of vapor-compression cycle operation: Optimization criteria'. In: *Proceedings of the American Control Conference* (2011). URL: https://ieeexplore.ieee.org/document/5991005.

[43] Ipieca. 'Pinch Analysis'. In: (2013). URL: https://www.ipieca.org/resources/energy-efficiency-solutions/efficient-use-of-heat/pinch-analysis/ (visited on 01/04/2023).

[44] Ipieca.org. 'Combined-cycle gas turbines'. In: *Energy efficient solutions* (2022). URL: https://www.ipieca.org/resources/energy-efficiency-solutions/combined-cycle-gas-turbines-2022 (visited on 22/10/2022).

[45] Carlos Arnaiz del Pozo et al. 'Efficiency evaluation of closed and open cycle pure refrigerant cascade natural gas liquefaction process through exergy analysis'. In: *Journal of Natural Gas Science and Engineering* 89 (2021). DOI: 10.1016/j.jngse.2021.103868.

[46] Carlos Arnaiz del Pozo, Schalk Cloete and Ángel Jiménez Álvaro. 'SEA Tool User Guide'. In: (2022). URL: https://github.com/SINTEF/Scale-Coupled-Open-Innovation-Network/blob/main/Economics/SEA%5C%20Tool%5C%20-%5C%20User%5C%20Guide.docx (visited on 05/06/2023).

[47] Will Kenton. 'Economies of Scale: What Are They and How Are They Used?' In: *Business Essentials* (2022). URL: https://www.investopedia.com/terms/e/economiesofscale.asp (visited on 02/05/2023).

[48] Jurie Steyn. 'Small-scale versus Large-scale LNG Plants'. In: (2021).

[49] Miguel Angel Gonzalez-Salazar. 'System analysis of waste heat applications with LNG regasification'. In: (). URL: https://www.researchgate.net/publication/283488427_System_analysis_of_waste_heat_applications_with_LNG_regasification.

[50] IGU. 'World LNG Report'. In: (2022). URL: https://www.igu.org/resources/world-lng-report-2022/.

[51] S. Mokhatab et al. 'Chapter 3 - Natural Gas Liquefaction'. In: *Handbook of Liquefied Natural Gas* (2014), pp. 147–183.

[52] McKinsey. 'Global gas outlook to 2050'. In: (2021). URL: https://www.mckinsey.com/~/media/mckinsey/industries/oil%5C%20and%5C%20gas/our%5C%20insights/global%5C%20gas%5C%20outlook%5C%20to%5C%202050/global%5C%20gas%5C%20outlook%5C%202050_final.pdf (visited on 18/05/2023).

[53] Statista. 'Largest natural gas liquefaction plants worldwide by capacity as of April 2022'. In: *Chemicals & Resources> Fossil Fuels* (2022). URL: https://www.statista.com/statistics/1251181/lng-global-liquefaction-capacity-by-plant/ (visited on 05/03/2023).

[54] D. Wood and S. Mokhtahab. 'Global LNG: Profitable Year So Far, But Cost and Demand Challenges Confront Suppliers'. In: *World Oil 228 (10)* (2007), pp. 129–132.

[55] Ratan Raj et al. 'A techno-economic study of shipping LNG to the Asia-Pacific from Western Canada by LNG carrier'. In: *Sustainable Energy Technologies and Assessment (34)* (2016), pp. 979–992. DOI: https://doi.org/10.1016/j.seta.2016.10.005. URL: https://www.sciencedirect.com/science/article/pii/S2213138816301278?via%5C%3Dihub#b0180.

[56] YoungMan Lee et al. 'Trends and Technologies in LNG Carriers and Offshore LNG Facilities Young Man Lee, Tai-Ik Cho, Jung Han Lee, Oh Yig Kwon, Daewoo Shipbuilding & Marine Engineering Co., Ltd'. In: (2008). DOI: 10.4043/19339-MS.

[57] Sphera. 'GHG Intensity of Natural Gas Transport'. In: *GIIGL, LNG Carbon Offsetting* (2017). URL: https://sphera.com/research/greenhouse-gas-intensity-study-of-natural-gas/ (visited on 17/05/2023).

[58] H. Rogers. 'LNG Plant Cost Escalation'. In: *The Oxford Institute for Energy Studies* (2014). DOI: https://doi.org/10.26889/9781907555947. URL: https://www.oxfordenergy.org/wpcms/wp-content/uploads/2014/02/NG-83.pdf.

[59] Claudio Steuer. 'Cost of Liquefaction Plant Projects'. In: *Outlook for Competitive LNG Supply, Oxford Institute for Energy Studies* (2019). URL: http://www.jstor.org/stable/resrep31040.11 (visited on 08/01/2023).

[60] Riviera Newsletters. 'Raising the bar on LNG tank size'. In: (2013). URL: https://www.rivieramm.com/news-content-hub/news-content-hub/raising-the-bar-on-lng-tank-size-39565 (visited on 16/04/2023).

[61] Sanja Pekic. 'CNOOC to build 6 LNG storage tanks at Binhai LNG'. In: (2021). URL: https://www.offshore-energy.biz/cnooc-to-build-6-lng-storage-tanks-at-binhai-lng/ (visited on 02/03/2023).

[62] H. Rogers. 'The LNG Shipping Forecast: costs rebounding, outlook uncertain'. In: *The Oxford Institute for Energy Studies* (2018). URL: https://www.oxfordenergy.org/wpcms/wp-content/uploads/2018/02/The-LNG-Shipping-Forecast-costs-rebounding-outlook-uncertain-Insight-27.pdf (visited on 04/02/2023).

[63] Fearnpulse. 'Gas: VLGC rates'. In: *Fearnleys Weekly Report* (2023). URL: https://fearnpulse.com/ (visited on 22/05/2023).

[64] Radius Logistics. 'Why are shipping rates so volatile?' In: (2023). URL: https://radiuslogistics.co.uk/guide/why-are-shipping-rates-so-volatile/.

[65] D. Andress and R. Watkins. 'Beauty of Simplicity: Phillips Optimized Cascade LNG Liquefaction Process'. In: *Advances in Cryogenic Engineering* 49 (2004). DOI: 10.1063/1.1774671.

[66] S Mokhatab and D Messersmith. 'Liquefaction technology selection for baseload LNG plants'. In: *BONUS REPORT: LNG TECHNOLOGY* (2018). URL: https://www.hydrocarbonprocessing.com/magazine/2018/july-2018/bonus-report-lng-technology/liquefaction-technology-selection-for-baseload-lng-plants (visited on 07/01/2023).

[67] IEA. 'The future of ammonia production'. In: *Ammonia Technology Roadmap* (2021). URL: https://www.iea.org/reports/ammonia-technology-roadmap/executive-summary.

[68] European Comission. *EU Delegated Acts on Renewable Hydrogen.* 2023. URL: https://ec.europa.eu/commission/presscorner/detail/en/qanda_23_595 (visited on 01/05/2023).

[69] Rafiqul Islam et al. 'Energy efficiency improvements in ammonia production - Perspectives and uncertainties'. In: *Energy* 30 (2005), pp. 2487–2504. DOI: 10.1016/j.energy.2004.12.004.

[70] IEA. 'Resource requirements and other uses of low-carbon fuels'. In: *The Role of Low-Carbon Fuels in the Clean Energy Transitions of the Power Sector* (2021). URL: https://www.iea.org/reports/the-role-of-low-carbon-fuels-in-the-clean-energy-transitions-of-the-power-sector.

[71] IRENA. 'Production processes, technology status and costs'. In: *Innovation Outlook Renewable Ammonia* (2022). URL: https://www.irena.org/-/media/Files/IRENA/Agency/Publication/2022/May/IRENA_Innovation_Outlook_Ammonia_2022.pdf.

[72] Agustin Valera-Medina and Rene Banares-Alcantara. 'Techno-Economic Aspects of Production, Storage and Distribution of Ammonia'. In: *Techno-Economic Challenges of Green Ammonia as an Energy Vector* (2020).

[73] IEA. 'Production and transport of low-carbon hydrogen and ammonia'. In: *The Role of Low-Carbon Fuels in the Clean Energy Transitions of the Power Sector* (2021). URL: https://www.iea.org/reports/the-role-of-low-carbon-fuels-in-the-clean-energy-transitions-of-the-power-sector.

[74] Haldor Topsøe. 'Ammonfuel: An industrial view of ammonia as a marine fuel'. In: (2020). URL: https://www.topsoe.com/hubfs/DOWNLOADS/DOWNLOADS%5C%20-%5C%20White%5C%20papers/Ammonfuel%5C%20Report%5C%20Version%5C%2009.9%5C%20August%5C%203_update.pdf.

[75] Hydrogen Council. 'Hydrogen Decarbonization Pathways: A Life-Cycle Assessment'. In: (2021). URL: https://hydrogencouncil.com/wp-content/uploads/2021/01/Hydrogen-Council-Report_Decarbonization-%20Pathways_Part-1-Lifecycle-Assessment.pdf (visited on 29/04/2023).

[76] Nils Lindstrand. 'Unlocking ammonia's potential for shipping'. In: *The case for two-stroke ammonia engines* (2021). URL: https://www.man-es.com/discover/two-stroke-ammonia-engine (visited on 29/05/2023).

[77] S. Patel. '"Mitsubishi Power developing 100% ammonia-capable gas turbine'. In: (2021). URL: www.powermag.com/mitsubishi-power-developing-100-ammonia-capable-gas-turbine (visited on 09/02/2023).

[78] Aliaksei Patonia and Rahmatallah Poudineh. 'Green ammonia and investors'. In: *Ammonia as a storage solution for future decarbonized energy systems* (2020). URL: https://www.jstor.org/stable/pdf/resrep30957.10.pdf.

[79] Statista. 'Household electricity prices worldwide in June 2022, by select country'. In: *Energy & Environment, Energy* (2023). URL: https://www.statista.com/statistics/263492/electricity-prices-in-selected-countries/ (visited on 07/03/2023).

[80] Dan Webb. 'Large Scale Ammonia Storage and Handling'. In: (). URL: https://irc.wisc.edu/export.php?ID=17 (visited on 08/01/2023).

[81] IEA. 'Assumptions'. In: *The Future of Hydrogen* (2019). URL: https://www.iea.org/reports/the-future-of-hydrogen.

[82] Simon Roussanaly and Alv-Arne Grimstad. 'The Economic Value of CO2 for EOR Applications'. In: *Energy Procedia* (2014), pp. 7836–7843. DOI: https://doi.org/10.1016/j.egypro.2014.11.818. URL: https://www.sciencedirect.com/science/article/pii/S1876610214026332.

[83] Agustin Valera-Medina and Rene Banares-Alcantara. 'Chapter 2: Ammonia Production Technologies'. In: *Techno-Economic Challenges of Green Ammonia as an Energy Vector* (2020).

[84] KBR. 'Purifier Ammonia Process'. In: (2022). URL: https://www.kbr.com/sites/default/files/2022-09/Purifier-Ammonia-Process-Handout.pdf (visited on 11/05/2023).

[85] Carlos Arnaiz del Pozo, Schalk Cloete and Ángel Jiménez Álvaro. 'Standardized Economic Assessement (SEA) Tool'. In: (2022). URL: https://github.com/SINTEF/Scale-Coupled-Open-Innovation-Network/blob/main/Economics/SEA%5C%20Tool%5C%20-%5C%20Template.xlsm (visited on 05/06/2023).

[86] Zhe Wang et al. 'Combined Analysis of Parameter Sensitivity and Exergy for Natural Gas Liquefaction in Cryogenic Fuel Production Process'. In: *Processes* 8 (2020), p. 561. DOI: 10.3390/pr8050561.

[87] Tatiana Morosuk. 'Advanced exergetic analysis of a refrigeration system for liquefaction of natural gas'. In: *International Journal of Energy and Environmental Engineering* 1 (2010).

[88] GE. 'LMS100 aeroderivative gas turbine'. In: (2022). URL: https://www.ge.com/gas-power/products/gas-turbines/lms100 (visited on 12/11/2022).

[89] Laura A. Pellegrini, Giorgia De Guido and Valentina Valentina. 'Energy and exergy analysis of acid gas removal processes in the LNG production chain'. In: *Journal of Natural Gas Science and Engineering* (2019). DOI: https://doi.org/10.1016/j.jngse.2018.11.016. URL: https://www.sciencedirect.com/science/article/abs/pii/S1875510018305092.

[90] Mark Pillarella et al. 'The C3MR liquefaction cycle: Versatility for a fast growing, ever changing LNG industry'. In: (2007). URL: http://www.ivt.ntnu.no/ept/fag/tep4215/innhold/LNG%5C%20Conferences/2007/fscommand/PS2_5_Pillarella_s.pdf (visited on 27/02/2023).

[91] GE. 'LM2500 aeroderivative gas turbine'. In: (2022). URL: https://www.ge.com/gas-power/products/gas-turbines/lm2500 (visited on 12/11/2022).

[92] Solomon A. Wassie et al. 'Techno-economic assessment of membrane-assisted gas switching reforming for pure H2 production with CO2 capture'. In: *International Journal of Greenhouse Gas Control* (2018), pp. 163–174. DOI: 10.1016/j.ijggc.2018.03.021.

[93] Schalk Cloete, Mohammed Khan and Shahriar Amini. 'Economic assessment of membrane-assisted autothermal reforming for cost effective hydrogen production with CO2 capture'. In: *International Journal of Hydrogen Energy* 44 (2019). DOI: 10.1016/j.ijhydene.2018.12.110.

[94] V. Spallina et al. 'Techno-economic assessment of membrane assisted fluidized bed reactors for pure H2 production with CO2 capture'. In: *Energy Conversion and Management* 120 (2016), pp. 257–273.

[95] shiptraffic.net. 'Port of Sabine Pass to Port of Wilhelmshaven: 6284 nautical miles'. In: *Sea route & distance* (2023). URL: http://www.shiptraffic.net/2001/05/sea-distances-calculator.html (visited on 07/02/2023).

[96] Turton R et al. 'Process Equipment Design and Performance'. In: *Analysis, synthesis, and design of chemical processes* (2008).

[97] IEAGHG R&D Programme. 'Effects of Plant Location on the Costs of CO2 Capture'. In: *IEAGHG Technical Report2018-04* (2018). URL: http://documents.ieaghg.org/index.php/s/nsoj00DazltwJNb (visited on 05/04/2023).

[98] La'o Hamutuk. 'Chapter 5. Employment and Infrastructure'. In: *Sunrise LNG in Timor-Leste: Dreams, Realities and Challenges* (2008). URL: https://www.laohamutuk.org/Oil/LNG/chap5.htm (visited on 09/01/2023).

[99] K.M. Guthrie. 'Data and Techniques for Prelimiary Capital Cost Estimating'. In: (1969). URL: https://openlibrary.org/books/OL14799127M/Data_and_techniques_for_preliminary_capital_cost_estimating..

[100] Maurice Stewart. 'Materials selection for pressure vessels'. In: *Surface Production Operations* (2021). DOI: https://doi.org/10.1016/B978-0-12-803722-5.00004-5. URL: https://www.sciencedirect.com/science/article/abs/pii/B9780128037225000045.

[101] Loto C.A. 'Corrosion Resistance of Heat Exchangers Made of Stainless Steel: A Review.' In: *International Journal of Electrochemical Science* (2012).

[102] Leyens C. and Peters M. 'Structure and Properties of Titanium and Titanium Alloys'. In: *Titanium and Titanium Alloys: Fundamentals and Applications* (2003).

[103] Shubkin R.L. 'Materials Performance'. In: *Selection of Nickel Alloys for Heat Exchangers* (1998).

[104] Carlos Arnaiz del Pozo et al. 'Exergoeconomic assessment of air separation units for pressurized O2 production incorporating two-phase expanders'. In: *Cryogenics 124* (2022). DOI: https://doi.org/10.1016/j.cryogenics.2022.103477. URL: https://www.sciencedirect.com/science/article/pii/S0011227522000595.

[105] Gazzani M, Macchi E and Manzolini G. 'CO2 capture in natural gas combined cycle with SEWGS'. In: *Part A: thermodynamic performances. Int J Greenh Gas Contr* (2011). DOI: https://doi.org/10.1016/j.ijggc.2012.06.010. URL: https://www.sciencedirect.com/science/article/abs/pii/S1750583612001454.

[106] IEA. 'Power generation technology costs and assumptions'. In: *World Energy Outlook 2022* (2022). URL: https://www.iea.org/data-and-statistics/data-product/world-energy-outlook-2022-free-dataset# (visited on 01/02/2023).

[107] Gas Turbine World. '2020 Simple Cycle Genset Price'. In: *2020 GTW Handbook* (2020). URL: https://gasturbineworld.com/shop/annual-handbook/2020-handbook-volume-35/ (visited on 18/01/2023).

[108] Martin P., Pigourier J. and Fisher B. 'LNG Process Selection, No Easy Task'. In: *Hydrocarbon Engineering 9* (2004), pp. 75–79. URL: https://www.researchgate.net/publication/292014779_LNG_process_selection_no_easy_task/citations.

[109] Jessica Aizarani. 'Average spot charter rate for a 160,000 cubic meter liquefied natural gas storage vessel worldwide from 2015 to 2021'. In: *Chemicals & Resources - Fossil Fuels* (2023). URL: https://www.statista.com/statistics/1112660/lng-tanker-average-spot-charter-rate/ (visited on 19/04/2023).

[110] SAGA LNG. 'LNT40 - WUHUMAX LNG Carrier'. In: *40k Wuhu max – Data sheet* (2019). URL: https://sagalng.com/wp-content/uploads/2017/05/40k-Wuhu-max-Data-sheet.pdf (visited on 04/04/2023).

[111] Insee. 'International prices of imported raw materials - Heavy fuel oil (North west Europe) 380 cst Cargo FOB - Prices in euros per ton - FOB – 3,5% of sulfur'. In: *Prices of oil and imported raw materials* (2023). URL: https://www.insee.fr/en/statistiques/serie/010751333#Documentation (visited on 10/01/2023).

[112] BW LPG. 'BW Gemini'. In: (2023). URL: https://www.bwlpg.com/vessel/bw-gemini/ (visited on 28/02/2023).

[113] BW LPG. 'Frequently Asked Questions'. In: *LPG Propulsion* (2023). URL: https://www.bwlpg.com/fleet/lpg-propulsion/frequently-asked-questions/ (visited on 12/04/2023).

[114] Riviera. 'Mozah launches Q-max era 1'. In: (2008). URL: https://www.rivieramm.com/news-content-hub/news-content-hub/mozah-launches-q-max-era-1-53908 (visited on 09/01/2023).

[115] Splash247. 'VLGC spot rates hit five-year high, closing in on $100,000 a day'. In: (2020). URL: https://splash247.com/vlgc-spot-rates-hit-five-year-high-closing-in-on-100000-a-day/ (visited on 06/05/2023).

[116] Acquaviva J. 'High-performance, durable, palladium alloy membrane for hydrogen separation and purification.' In: (2009). URL: chrome-extension://efaidnbmnnnibpcajpcglclefindmkaj/https://www.hydrogen.energy.gov/pdfs/review11/pd005_damle_2011_p.pdf (visited on 04/04/2023).

[117] Nazreen Begum Najibullah Khan et al. 'A case study: Application of energy and exergy analysis for enhancing the process efficiency of a three stage propane pre-cooling cycle of the cascade LNG process'. In: *Journal of Natural Gas Science and Engineering 29* (2016), pp. 125–133. DOI: https://doi.org/10.1016/j.jngse.2015.12.034.

[118] Energy Market Authority Singapore. 'Emissions Intensity of Power Plants'. In: *Technical Consultancy Study for Emissions Intensity of Power Plants* (2022). URL: https://www.ema.gov.sg/cmsmedia/Consultations/Electricity/2023/Annex-Technical-Consultancy-Study-for-Emissions-Intensity-of-Power-Plants_09Jan2023.pdf (visited on 06/05/2023).

[119] Flex LNG. 'FLEX LNG Fleet List'. In: (2023). URL: https://www.flexlng.com/fleet-list/.

[120] EIA. 'How much electricity does an American home use?' In: (2022). URL: https://www.eia.gov/tools/faqs/faq.php?id=97&t=3 (visited on 05/01/2023).

[121] Linde Engineering. 'Coil-wound heat exchangers'. In: (2019). URL: https://www.linde-engineering.com/en/images/Coil-wound-heat-exchanger-2019_tcm19-5793.pdf (visited on 01/03/2023).

[122] Ember. 'Carbon Price Tracker'. In: (2023). URL: https://ember-climate.org/data/data-tools/carbon-price-viewer/ (visited on 22/05/2023).

[123] The World Bank. 'Carbon Pricing Dashboard'. In: (2023). URL: https://carbonpricingdashboard.worldbank.org/map_data.

[124] Herbert Smith Freehills. 'Decarbonisation of the LNG Supply Chain: Challenges and the Way Forward'. In: (2021). URL: https://www.herbertsmithfreehills.com/latest-thinking/decarbonisation-of-the-lng-supply-chain-challenges-and-the-way-forward (visited on 29/03/2023).

[125] European Commision. 'Carbon Border Adjustment Mechanism'. In: (2023). URL: https://taxation-customs.ec.europa.eu/carbon-border-adjustment-mechanism%5C_en (visited on 27/05/2023).

A LNG

A.1 Aspen Plus: Full C3MR LNG Flowsheet

This page is intentionally blank due to leaving as much as possible space for Figure A.1.

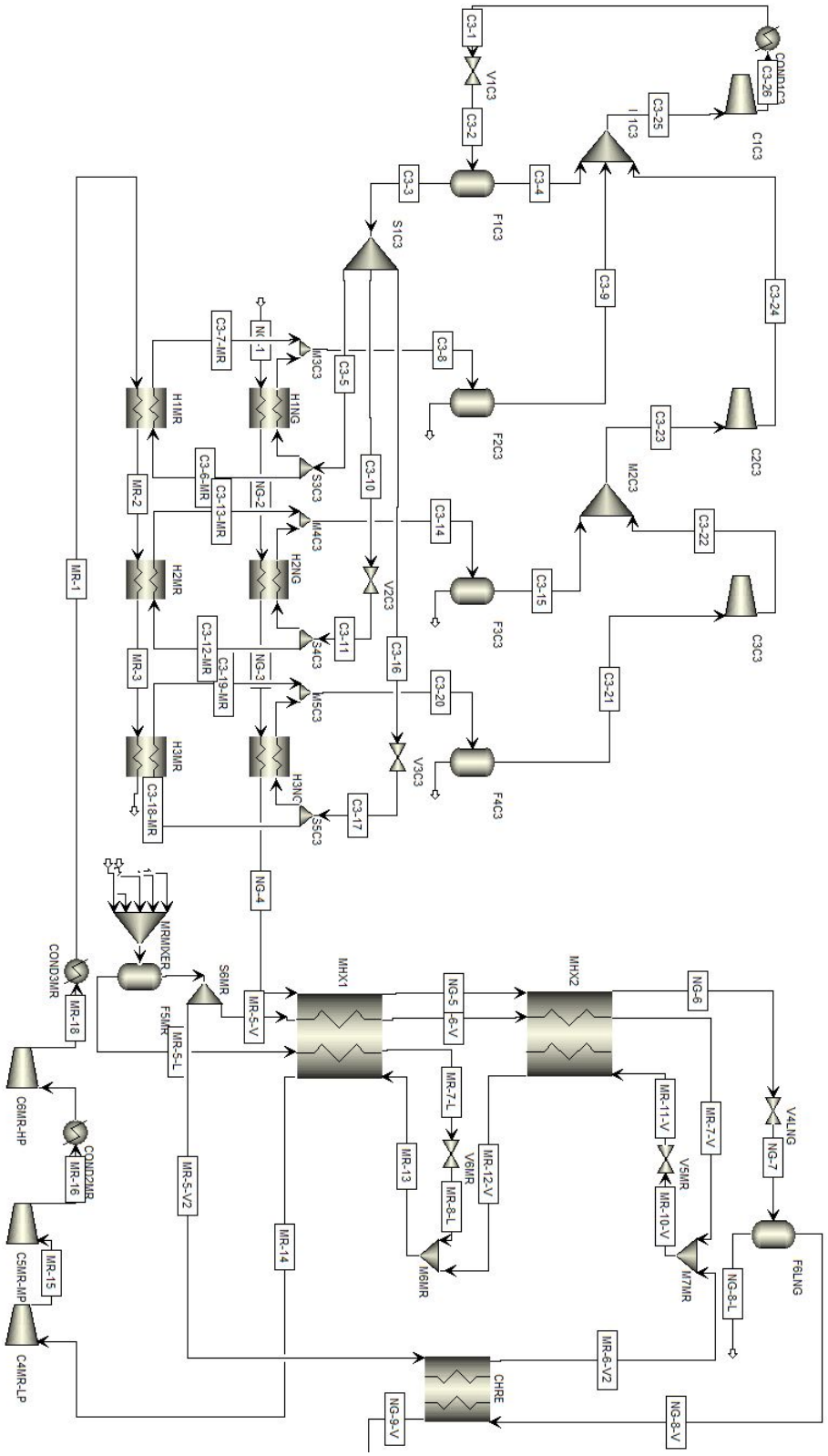

Figure A.1: The complete C3MR process flowsheet in Aspen Plus. NG-9-V enters either a flare in the 1x train or compressor stages before entering the gas turbines in the 10x train.

A.2 Aspen Plus: Main Cryogenic Heat Exchanger Profiles

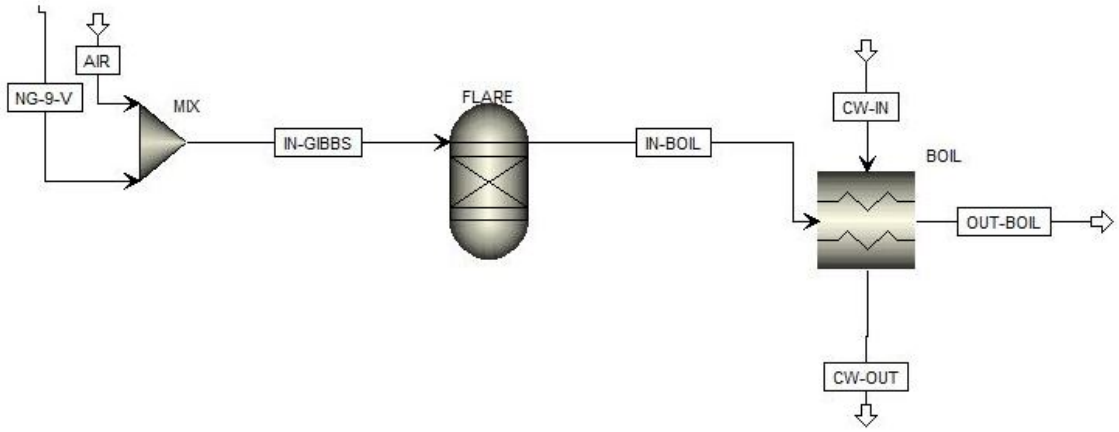

Figure A.2: C3MR LNG plant 1x train configurations with the flare and boiler for providing heat to the acid gas removal unit. Here, the plant consumes electricity from the grid.

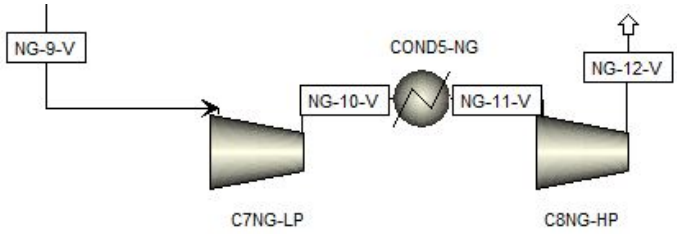

Figure A.3: C3MR LNG plant 10x train configurations with compressor stages before entering the two LMS100 gas turbines for the major power requirements and the LM2500 for other auxiliary components in the plant.

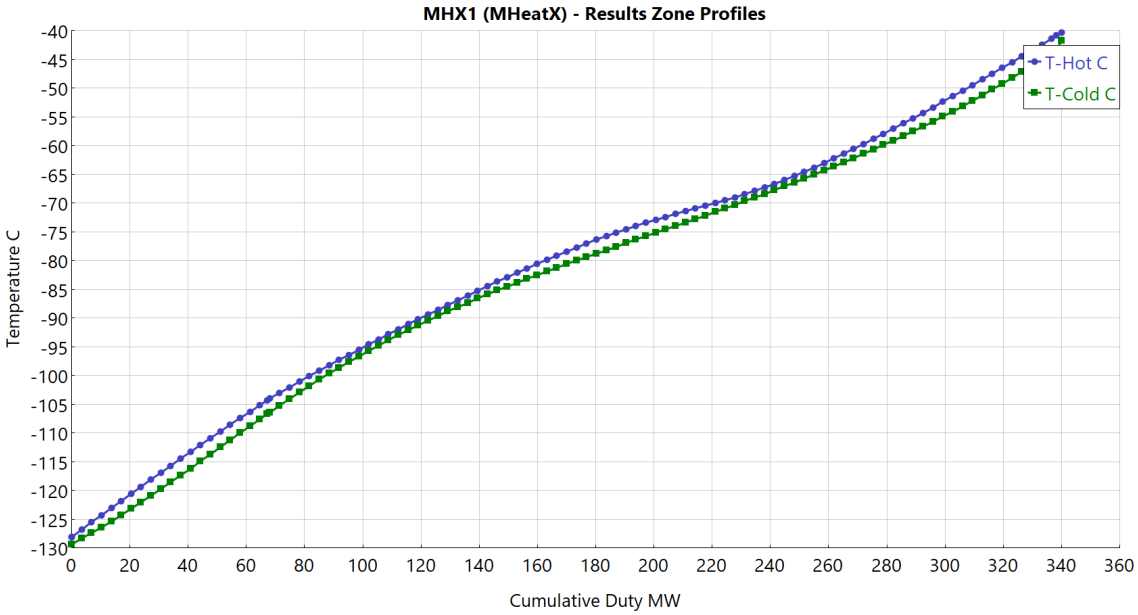

Figure A.4: Temperature profile of hot and cold composite curves for the bottom part of the MCHE.

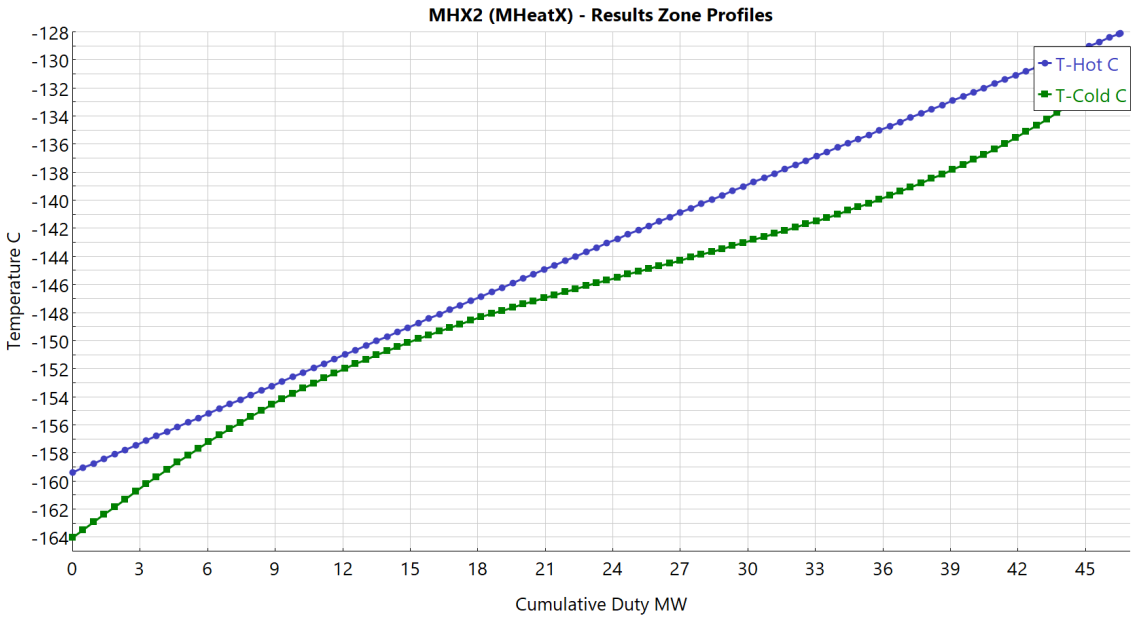

Figure A.5: Temperature profile of hot and cold composite curves for the upper part of the MCHE.

A.3 Aspen Plus: C3MR LNG Design Workbook

1x Train

	Units	AIR	C1	C2	C3	C3-1	C3-2
− MIXED Substream							
+ Mass Flows	kg/sec	41,1246	14,3723	25,0435	10,8567	81,7281	81,7281
Temperature	C	25	-40,3113	-40,3113	-40,3113	20	-4,39178
Pressure	bar	1,01	38,5	38,5	38,5	8,36818	4,1355
Molar Vapor Fraction		1	1	0	0	0	0,170316
− Mole Fractions							
N2		0	0	0	0	0	0
CH4		0	1	0	0	0	0
C2H6		0	0	1	0	0	0
C3H8		0	0	0	1	1	1
C4H10		0	0	0	0	0	0
CO2		0	0	0	0	0	0
H2O		0	0	0	0	0	0
O2		0	0	0	0	0	0
CO		0	0	0	0	0	0
AIR		1	0	0	0	0	0

	Units	C3-3	C3-4	C3-5	C3-6-MR	C3-6-NG	C3-7-MR
− MIXED Substream							
+ Mass Flows	kg/sec	67,8085	13,9196	23,2405	19,5004	3,74013	19,5004
Temperature	C	-4,39178	-4,39178	-4,39178	-4,39178	-4,39178	5,92832
Pressure	bar	4,1355	4,1355	4,1355	4,1355	4,1355	4,1355
Molar Vapor Fraction		0	1	0	0	0	1
− Mole Fractions							
N2		0	0	0	0	0	0
CH4		0	0	0	0	0	0
C2H6		0	0	0	0	0	0
C3H8		1	1	1	1	1	1

	Units	C3-7-NG	C3-8	C3-9	C3-9-L	C3-10	C3-11
− MIXED Substream							
+ Mass Flows	**kg/sec**	**3,74013**	**23,2405**	**23,2405**		**23,9127**	**23,9127**
Temperature	C	6,0723	5,95149	5,95149		-4,39178	-24,8996
Pressure	bar	4,1355	4,1355	4,1355	4,1355	4,1355	2,04374
Molar Vapor Fraction		1	1	1		0	0,128501
− Mole Fractions							
N2		0	0	0		0	0
CH4		0	0	0		0	0
C2H6		0	0	0		0	0
C3H8		1	1	1		1	1

	Units	C3-12-MR	C3-12-NG	C3-13-MR	C3-13-NG	C3-14	C3-15
− MIXED Substream							
+ Mass Flows	**kg/sec**	**18,6487**	**5,26399**	**18,6487**	**5,26399**	**23,9127**	**23,9127**
Temperature	C	-24,8996	-24,8996	-15,0551	-14,9083	-15,0228	-15,0228
Pressure	bar	2,04374	2,04374	2,04374	2,04374	2,04374	2,04374
Molar Vapor Fraction		0,128501	0,128501	1	1	1	1
− Mole Fractions							
N2		0	0	0	0	0	0
CH4		0	0	0	0	0	0
C2H6		0	0	0	0	0	0
C3H8		1	1	1	1	1	1

	Units	C3-15-L	C3-16	C3-17	C3-18-MR	C3-18-NG	C3-19-MR
− MIXED Substream							
+ Mass Flows	**kg/sec**		**20,6553**	**20,6553**	**14,7237**	**5,93167**	**14,7237**
Temperature	C		-4,39178	-42,3113	-42,3113	-42,3113	-32,3147
Pressure	bar	2,04374	4,1355	1,01	1,01	1,01	1,01
Molar Vapor Fraction			0	0,225059	0,225059	0,225059	1
− Mole Fractions							
N2			0	0	0	0	0
CH4			0	0	0	0	0
C2H6			0	0	0	0	0
C3H8			1	1	1	1	1

	Units	C3-19-NG	C3-20	C3-21	C3-21-L	C3-22	C3-23
− MIXED Substream							
+ Mass Flows	**kg/sec**	**5,93167**	**20,6553**	**20,6553**		**20,6553**	**44,568**
Temperature	C	-31,8809	-32,1901	-32,1901		-6,05301	-10,8678
Pressure	bar	1,01	1,01	1,01	1,01	2,04374	2,04374
Molar Vapor Fraction		1	1	1		1	1
− Mole Fractions							
N2		0	0	0		0	0
CH4		0	0	0		0	0
C2H6		0	0	0		0	0
C3H8		1	1	1		1	1

	Units	C3-24	C3-25	C3-26	C4	CO2	CW-IN
− MIXED Substream							
+ Mass Flows	**kg/sec**	**44,568**	**81,7281**	**81,7281**	**3,74225**	**30,63**	**1,82937**
Temperature	C	18,3593	10,9398	43,67	-40,3113	15	129
Pressure	bar	4,1355	4,1355	8,36818	38,5	70	2,515
Molar Vapor Fraction		1	1	1	0	1	0
− Mole Fractions							
N2		0	0	0	0	0,0089	0
CH4		0	0	0	0	0,89	0
C2H6		0	0	0	0	0,07	0
C3H8		1	1	1	0	0,01	0
C4H10		0	0	0	1	0,0011	0
CO2		0	0	0	0	0,02	0
H2O		0	0	0	0	0	1

	Units	CW-OUT	IN-BOIL	IN-GIBBS	MR-1	MR-2	MR-3
− MIXED Substream							
✚ Mass Flows	**kg/sec**	**1,82937**	**42,0568**	**42,0568**	**58,2434**	**58,2434**	**58,2434**
Temperature	C	131	800,091	22,2042	20	-2,39178	-22,8996
Pressure	bar	2,515	1,01	1,01	40	39,5	39
Molar Vapor Fraction		1	1	1	1	0,744931	0,507839
− Mole Fractions							
N2		0	0,494294	0,0048357	0,0689187	0,0689187	0,0689187
CH4		0	0	0,0309863	0,409026	0,409026	0,409026
C2H6		0	0	3,75479e-06	0,380251	0,380251	0,380251
C3H8		0	0	6,48915e-09	0,112408	0,112408	0,112408
C4H10		0	0	6,3716e-12	0,0293959	0,0293959	0,0293959
CO2		0	0,0309935	0	0	0	0
H2O		1	0,0619833	0	0	0	0
O2		0	0,0884645	0	0	0	0
CO		0	6,37831e-11	0	0	0	0
AIR		0	0,324265	0,964174	0	0	0
NH3		0	4,20515e-19	0	0	0	0

	Units	MR-4	MR-5	MR-5-L	MR-5-V	MR-5-V2	MR-6-V
− MIXED Substream							
✚ Mass Flows	**kg/sec**	**58,2434**	**58,2434**	**42,6329**	**15,2442**	**0,366269**	**15,2442**
Temperature	C	-40,3113	-40,0861	-40,0861	-40,0861	-40,0861	-130,086
Pressure	bar	38,5	38,5	38,5	38,5	38,5	36
Molar Vapor Fraction		0,339959	0,342033	0	1	1	0
− Mole Fractions							
N2		0,0689187	0,0689187	0,0212134	0,160689	0,160689	0,160689
CH4		0,409026	0,409026	0,283008	0,651447	0,651447	0,651447
C2H6		0,380251	0,380251	0,488459	0,172091	0,172091	0,172091
C3H8		0,112408	0,112408	0,163201	0,0146989	0,0146989	0,0146989
C4H10		0,0293959	0,0293959	0,0441186	0,00107392	0,00107392	0,00107392

	Units	MR-6-V2	MR-7-L	MR-7-V	MR-8-L	MR-10-V	MR-11-V
− MIXED Substream							
✚ Mass Flows	**kg/sec**	**0,366269**	**42,6329**	**15,2442**	**42,6329**	**15,6104**	**15,6104**
Temperature	C	-160,75	-130,086	-160,75	-132,124	-160,748	-165,745
Pressure	bar	36	36	33,5	3,25417	33,5	3,25417
Molar Vapor Fraction		0	0	0	0,0426098	0	0,0722098
− Mole Fractions							
N2		0,160689	0,0212134	0,160689	0,0212134	0,160689	0,160689
CH4		0,651447	0,283008	0,651447	0,283008	0,651447	0,651447
C2H6		0,172091	0,488459	0,172091	0,488459	0,172091	0,172091
C3H8		0,0146989	0,163201	0,0146989	0,163201	0,0146989	0,0146989
C4H10		0,00107392	0,0441186	0,00107392	0,0441186	0,00107392	0,00107392

	Units	MR-12-V	MR-13	MR-14	MR-15	MR-16	MR-17
− MIXED Substream							
✚ Mass Flows	**kg/sec**	**15,6104**	**58,2434**	**58,2434**	**58,2434**	**58,2434**	**58,2434**
Temperature	C	-132,117	-130,673	-40,7798	19,3471	88,0124	20
Pressure	bar	3,25417	3,25417	3,25417	8,59497	22,5657	22,1657
Molar Vapor Fraction		0,72646	0,26556	0,999501	1	1	1
− Mole Fractions							
N2		0,160689	0,0689187	0,0689187	0,0689187	0,0689187	0,0689187
CH4		0,651447	0,409026	0,409026	0,409026	0,409026	0,409026
C2H6		0,172091	0,380251	0,380251	0,380251	0,380251	0,380251
C3H8		0,0146989	0,112408	0,112408	0,112408	0,112408	0,112408
C4H10		0,00107392	0,0293959	0,0293959	0,0293959	0,0293959	0,0293959

	Units	MR-18	N2	NG-1	NG-2	NG-3	NG-4
− MIXED Substream							
+ Mass Flows	**kg/sec**	**58,2434**	**4,22863**	**30,63**	**30,63**	**30,63**	**30,63**
Temperature	C	65,1665	-40,3113	15	-2,39178	-22,8996	-40,3113
Pressure	bar	40,8	38,5	70	69,5	69	68,5
Molar Vapor Fraction		1	1	1	1	1	1
− Mole Fractions							
N2		0,0689187	1	0,00908163	0,00908163	0,00908163	0,00908163
CH4		0,409026	0	0,908163	0,908163	0,908163	0,908163
C2H6		0,380251	0	0,0714286	0,0714286	0,0714286	0,0714286
C3H8		0,112408	0	0,0102041	0,0102041	0,0102041	0,0102041
C4H10		0,0293959	0	0,00112245	0,00112245	0,00112245	0,00112245

	Units	NG-5	NG-6	NG-7	NG-8-L	NG-8-V	NG-9-V	OUT-BOIL
− MIXED Substream								
+ Mass Flows	**kg/sec**	**30,63**	**30,63**	**30,63**	**29,6979**	**0,932119**	**0,932119**	**42,0568**
Temperature	C	-126,157	-160,75	-162,388	-162,388	-162,388	-42,5437	718,261
Pressure	bar	66	63,5	1,01	1,01	1,01	1,01	1,01
Molar Vapor Fraction		0	0	0,0301336	0	1	1	1
− Mole Fractions								
N2		0,00908163	0,00908163	0,00908163	0,0051701	0,134978	0,134978	0,494294
CH4		0,908163	0,908163	0,908163	0,909507	0,864917	0,864917	0
C2H6		0,0714286	0,0714286	0,0714286	0,0736446	0,000104807	0,000104807	0
C3H8		0,0102041	0,0102041	0,0102041	0,0105211	1,81131e-07	1,81131e-07	0
C4H10		0,00112245	0,00112245	0,00112245	0,00115732	1,77849e-10	1,77849e-10	0
CO2		0	0	0	0	0	0	0,0309935
H2O		0	0	0	0	0	0	0,0619833
O2		0	0	0	0	0	0	0,0884645
CO		0	0	0	0	0	0	6,37831e-11
AIR		0	0	0	0	0	0	0,324265
NH3		0	0	0	0	0	0	4,20515e-19

Figure A.6: Material flows for the 1x C3MR LNG plant

10x Train

	Units	C1	C2	C3	C3-1	C3-2	C3-3
MIXED Substream							
Mass Flows	**kg/sec**	**13,6845**	**25**	**10,2815**	**80,8485**	**80,8485**	**67,0787**
Temperature	C	-40,3113	-40,3113	-40,3113	20	-4,39178	-4,39178
Pressure	bar	38,5	38,5	38,5	8,36818	4,1355	4,1355
Molar Vapor Fraction		1	0	0	0	0,170316	0
Mole Fractions							
N2		0	0	0	0	0	0
CH4		1	0	0	0	0	0
C2H6		0	1	0	0	0	0
C3H8		0	0	1	1	1	1

	Units	C3-4	C3-5	C3-6-MR	C3-6-NG	C3-7-MR	C3-7-NG
MIXED Substream							
Mass Flows	**kg/sec**	**13,7698**	**23,3232**	**19,5816**	**3,74158**	**19,5816**	**3,74158**
Temperature	C	-4,39178	-4,39178	-4,39178	-4,39178	5,83354	5,98364
Pressure	bar	4,1355	4,1355	4,1355	4,1355	4,1355	4,1355
Molar Vapor Fraction		1	0	0	0	1	1
Mole Fractions							
N2		0	0	0	0	0	0
CH4		0	0	0	0	0	0
C2H6		0	0	0	0	0	0
C3H8		1	1	1	1	1	1

	Units	C3-8	C3-9	C3-9-L	C3-10	C3-11	C3-12-MR
MIXED Substream							
Mass Flows	**kg/sec**	**23,3232**	**23,3232**		**23,5135**	**23,5135**	**18,2422**
Temperature	C	5,85762	5,85762		-4,39178	-24,8996	-24,8996
Pressure	bar	4,1355	4,1355	4,1355	4,1355	2,04374	2,04374
Molar Vapor Fraction		1	1		0	0,128501	0,128501
Mole Fractions							
N2		0	0		0	0	0
CH4		0	0		0	0	0
C2H6		0	0		0	0	0
C3H8		1	1		1	1	1

	Units	C3-12-NG	C3-13-MR	C3-13-NG	C3-14	C3-15	C3-15-L
MIXED Substream							
Mass Flows	**kg/sec**	**5,27135**	**18,2422**	**5,27135**	**23,5135**	**23,5135**	
Temperature	C	-24,8996	-14,8051	-15,2113	-14,8962	-14,8962	
Pressure	bar	2,04374	2,04374	2,04374	2,04374	2,04374	2,04374
Molar Vapor Fraction		0,128501	1	1	1	1	
Mole Fractions							
N2		0	0	0	0	0	
CH4		0	0	0	0	0	
C2H6		0	0	0	0	0	
C3H8		1	1	1	1	1	

	Units	C3-16	C3-17	C3-18-MR	C3-18-NG	C3-19-MR	C3-19-NG
− MIXED Substream							
+ Mass Flows	**kg/sec**	**20,242**	**20,242**	**14,3209**	**5,92111**	**14,3209**	**5,92111**
Temperature	C	-4,39178	-42,3113	-42,3113	-42,3113	-32,4947	-31,5166
Pressure	bar	4,1355	1,01	1,01	1,01	1,01	1,01
Molar Vapor Fraction		0	0,225059	0,225059	0,225059	1	1
− Mole Fractions							
N2		0	0	0	0	0	0
CH4		0	0	0	0	0	0
C2H6		0	0	0	0	0	0
C3H8		1	1	1	1	1	1

	Units	C3-20	C3-21	C3-21-L	C3-22	C3-23	C3-24
− MIXED Substream							
+ Mass Flows	**kg/sec**	**20,242**	**20,242**		**20,242**	**43,7556**	**43,7556**
Temperature	C	-32,2086	-32,2086		-6,07333	-10,8166	18,4153
Pressure	bar	1,01	1,01	1,01	2,04374	2,04374	4,1355
Molar Vapor Fraction		1	1		1	1	1
− Mole Fractions							
N2		0	0		0	0	0
CH4		0	0		0	0	0
C2H6		0	0		0	0	0
C3H8		1	1		1	1	1

	Units	C3-19-NG	C3-20	C3-21	C3-21-L	C3-22	C3-23
− MIXED Substream							
+ Mass Flows	**kg/sec**	**5,93167**	**20,6553**	**20,6553**		**20,6553**	**44,568**
Temperature	C	-31,8809	-32,1901	-32,1901		-6,05301	-10,8678
Pressure	bar	1,01	1,01	1,01	1,01	2,04374	2,04374
Molar Vapor Fraction		1	1	1		1	1
− Mole Fractions							
N2		0	0	0		0	0
CH4		0	0	0		0	0
C2H6		0	0	0		0	0
C3H8		1	1	1		1	1

	Units	C3-25	C3-26	C4	CO2	MR-1	MR-2
− MIXED Substream							
+ Mass Flows	**kg/sec**	**80,8485**	**80,8485**	**3,63301**	**31,1**	**55,7025**	**55,7025**
Temperature	C	10,8918	43,6208	-40,3113	15	20	-2,39178
Pressure	bar	4,1355	8,36818	38,5	70	40	39,5
Molar Vapor Fraction		1	1	0	1	0,998443	0,719012
− Mole Fractions							
N2		0	0	0	0,0089	0,0529858	0,0529858
CH4		0	0	0	0,89	0,407968	0,407968
C2H6		0	0	0	0,07	0,397638	0,397638
C3H8		1	1	0	0,01	0,111514	0,111514
C4H10		0	0	1	0,0011	0,0298946	0,0298946
CO2		0	0	0	0,02	0	0

	Units	MR-3	MR-4	MR-5	MR-5-L	MR-5-V	MR-5-V2
− MIXED Substream							
+ Mass Flows	**kg/sec**	**55,7025**	**55,7025**	**55,7025**	**42,4112**	**12,7995**	**0,491876**
Temperature	C	-22,8996	-40,3113	-38,8267	-38,8267	-38,8267	-38,8267
Pressure	bar	39	38,5	38,5	38,5	38,5	38,5
Molar Vapor Fraction		0,469225	0,293637	0,308255	0	1	1
− Mole Fractions							
N2		0,0529858	0,0529858	0,0529858	0,0177593	0,132037	0,132037
CH4		0,407968	0,407968	0,407968	0,29065	0,671237	0,671237
C2H6		0,397638	0,397638	0,397638	0,494271	0,180788	0,180788
C3H8		0,111514	0,111514	0,111514	0,154608	0,0148077	0,0148077
C4H10		0,0298946	0,0298946	0,0298946	0,0427122	0,00113083	0,00113083

	Units	MR-6-V	MR-6-V2	MR-7-L	MR-7-V	MR-8-L	MR-10-V
− MIXED Substream							
+ Mass Flows	**kg/sec**	**12,7995**	**0,491876**	**42,4112**	**12,7995**	**42,4112**	**13,2913**
Temperature	C	-128,827	-158,25	-128,827	-158,25	-131,02	-158,246
Pressure	bar	36	36	36	33,5	3,224	33,5
Molar Vapor Fraction		0	0	0	0	0,0425526	0
− Mole Fractions							
N2		0,132037	0,132037	0,0177593	0,132037	0,0177593	0,132037
CH4		0,671237	0,671237	0,29065	0,671237	0,29065	0,671237
C2H6		0,180788	0,180788	0,494271	0,180788	0,494271	0,180788
C3H8		0,0148077	0,0148077	0,154608	0,0148077	0,154608	0,0148077
C4H10		0,00113083	0,00113083	0,0427122	0,00113083	0,0427122	0,00113083

	Units	MR-11-V	MR-12-V	MR-13	MR-14	MR-15	MR-16
− MIXED Substream							
+ Mass Flows	**kg/sec**	**13,2913**	**13,2913**	**55,7025**	**55,7025**	**55,7025**	**55,7025**
Temperature	C	-162,871	-131,015	-129,804	-40,569	19,7034	81,304
Pressure	bar	3,224	3,224	3,224	3,224	8,54645	20,5585
Molar Vapor Fraction		0,0665803	0,716908	0,2412	1	1	1
− Mole Fractions							
N2		0,132037	0,132037	0,0529858	0,0529858	0,0529858	0,0529858
CH4		0,671237	0,671237	0,407968	0,407968	0,407968	0,407968
C2H6		0,180788	0,180788	0,397638	0,397638	0,397638	0,397638
C3H8		0,0148077	0,0148077	0,111514	0,111514	0,111514	0,111514
C4H10		0,00113083	0,00113083	0,0298946	0,0298946	0,0298946	0,0298946

	Units	MR-17	MR-18	N2	NG-1	NG-2	NG-3
− MIXED Substream							
+ Mass Flows	**kg/sec**	**55,7025**	**55,7025**	**3,10349**	**30,63**	**30,63**	**30,63**
Temperature	C	20	72,0008	-40,3113	15	-2,39178	-22,8996
Pressure	bar	20,1585	40,8	38,5	70	69,5	69
Molar Vapor Fraction		1	1	1	1	1	1
− Mole Fractions							
N2		0,0529858	0,0529858	1	0,00908163	0,00908163	0,00908163
CH4		0,407968	0,407968	0	0,908163	0,908163	0,908163
C2H6		0,397638	0,397638	0	0,0714286	0,0714286	0,0714286
C3H8		0,111514	0,111514	0	0,0102041	0,0102041	0,0102041
C4H10		0,0298946	0,0298946	0	0,00112245	0,00112245	0,00112245

	Units	NG-4	NG-5	NG-6	NG-7	NG-8-L
− MIXED Substream						
+ Mass Flows	**kg/sec**	**30,63**	**30,63**	**30,63**	**30,63**	**29,2548**
Temperature	C	-40,3113	-128,187	-158,25	-162,06	-162,06
Pressure	bar	68,5	66	63,5	1,01	1,01
Molar Vapor Fraction		1	0	0	0,0451621	0
− Mole Fractions						
N2		0,00908163	0,00908163	0,00908163	0,00908163	0,00421663
CH4		0,908163	0,908163	0,908163	0,908163	0,909119
C2H6		0,0714286	0,0714286	0,0714286	0,0714286	0,0748017
C3H8		0,0102041	0,0102041	0,0102041	0,0102041	0,0106867
C4H10		0,00112245	0,00112245	0,00112245	0,00112245	0,00117554

	Units	NG-8-V	NG-9-V	NG-10-V	NG-11-V	NG-12-V
− **MIXED Substream**						
+ **Mass Flows**	**kg/hr**	**4950,73**	**4950,73**	**4950,73**	**4950,73**	**4950,73**
Temperature	C	-162,06	-53,2257	133,697	20	208,423
Pressure	bar	1,01	1,01	8	8	48
Molar Vapor Fraction		1	1	1	1	1
− **Mole Fractions**						
N2		0,11194	0,11194	0,11194	0,11194	0,11194
CH4		0,887948	0,887948	0,887948	0,887948	0,887948
C2H6		0,000112027	0,000112027	0,000112027	0,000112027	0,000112027
C3H8		1,96602e-07	1,96602e-07	1,96602e-07	1,96602e-07	1,96602e-07
C4H10		1,96591e-10	1,96591e-10	1,96591e-10	1,96591e-10	1,96591e-10

Figure A.7: Material flows for the 10x C3MR LNG plant

B Ammonia

B.1 Aspen Plus: Full MA-ATR Ammonia Flowsheet

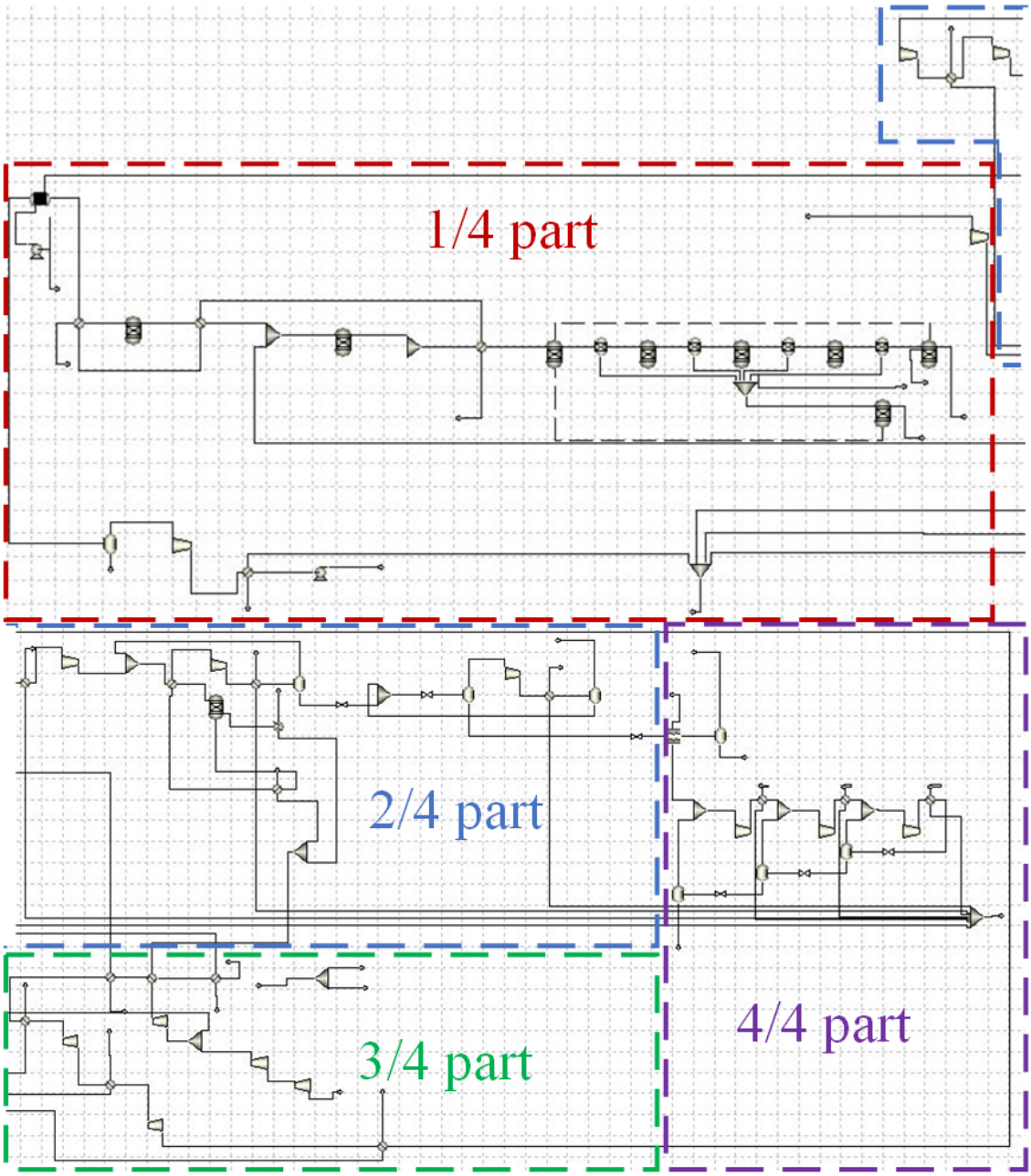

Figure B.1: The complete MA-ATR process flowsheet in Aspen Plus. The figure is split in two for visual purposes, where the upper right connects to the lower left. The figure is further divided into sub-figures with material stream information in Figures B.2-B.5

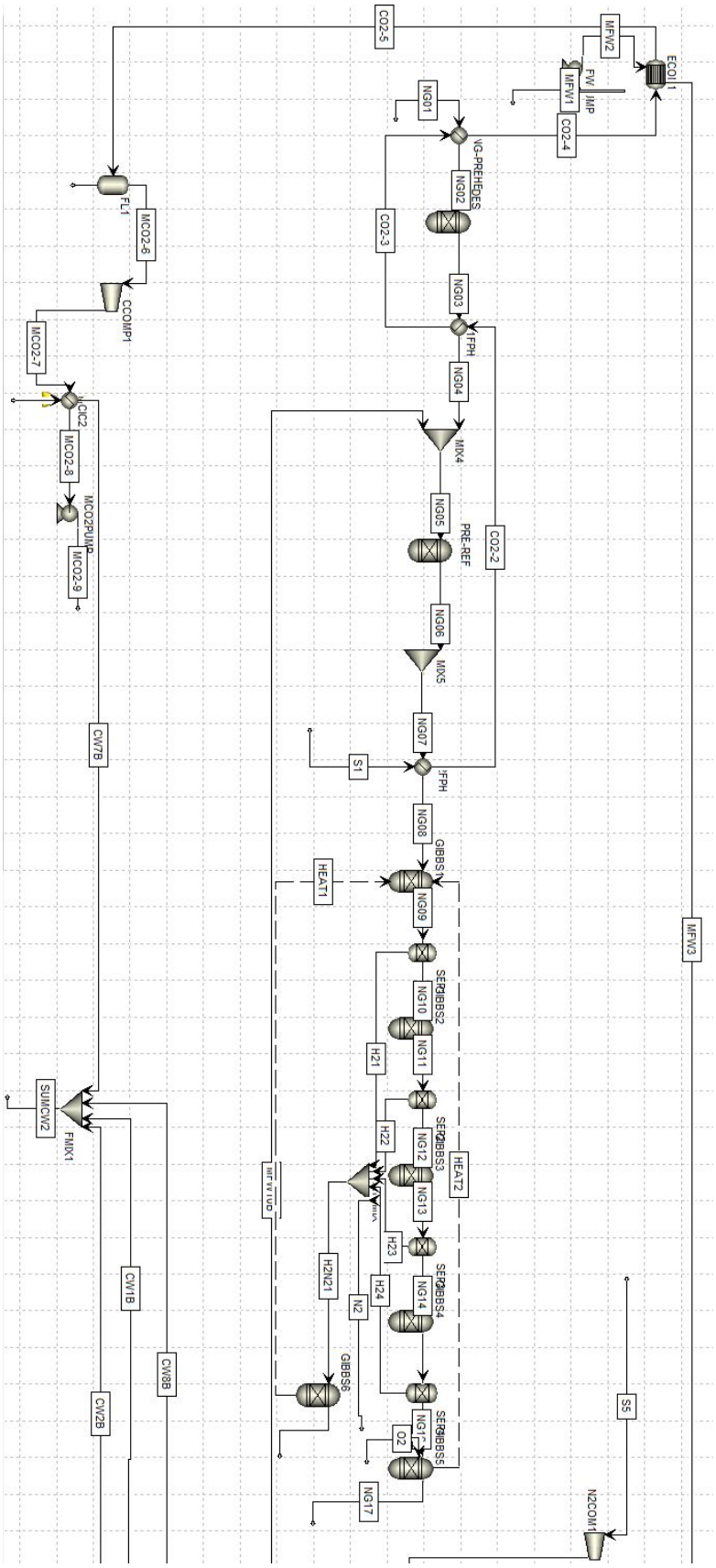

Figure B.2: 1/4 part of the MA-ATR process flowsheet in Aspen Plus

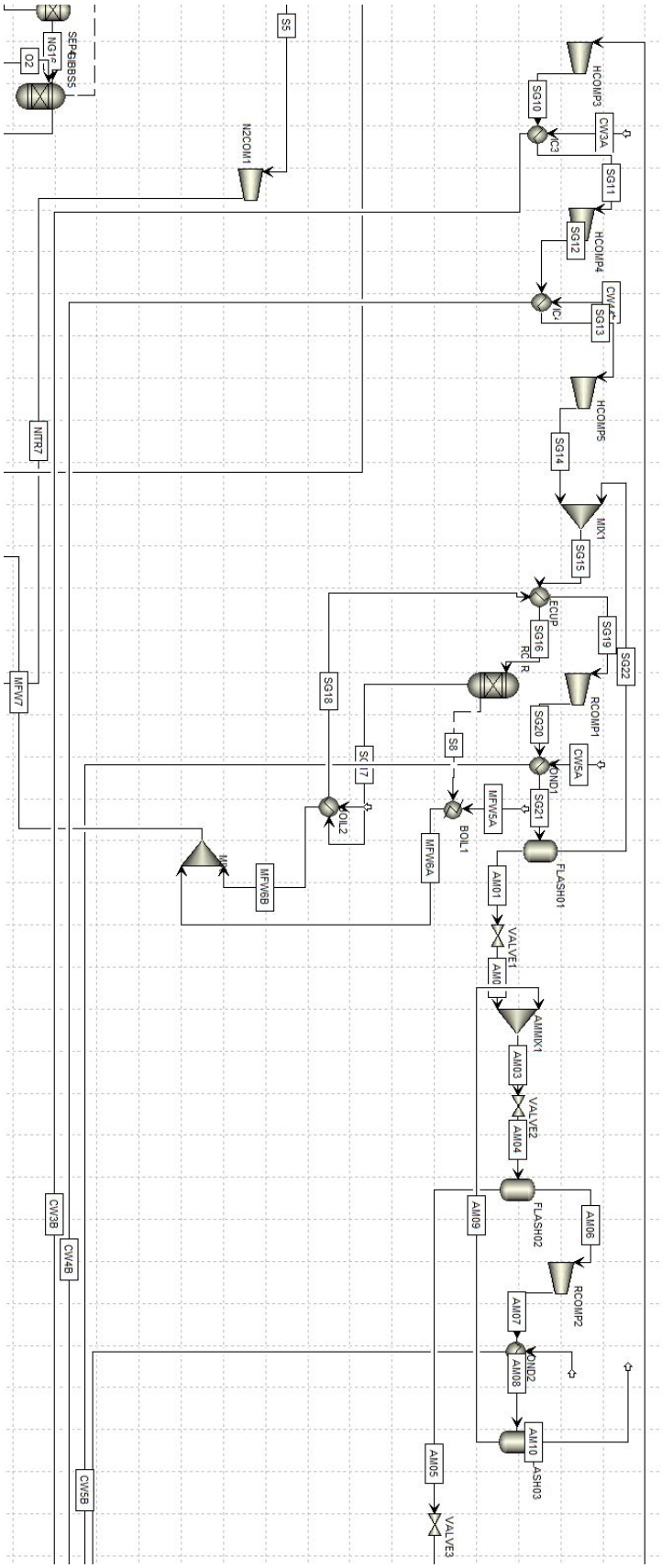

Figure B.3: 2/4 part of the MA-ATR process flowsheet in Aspen Plus

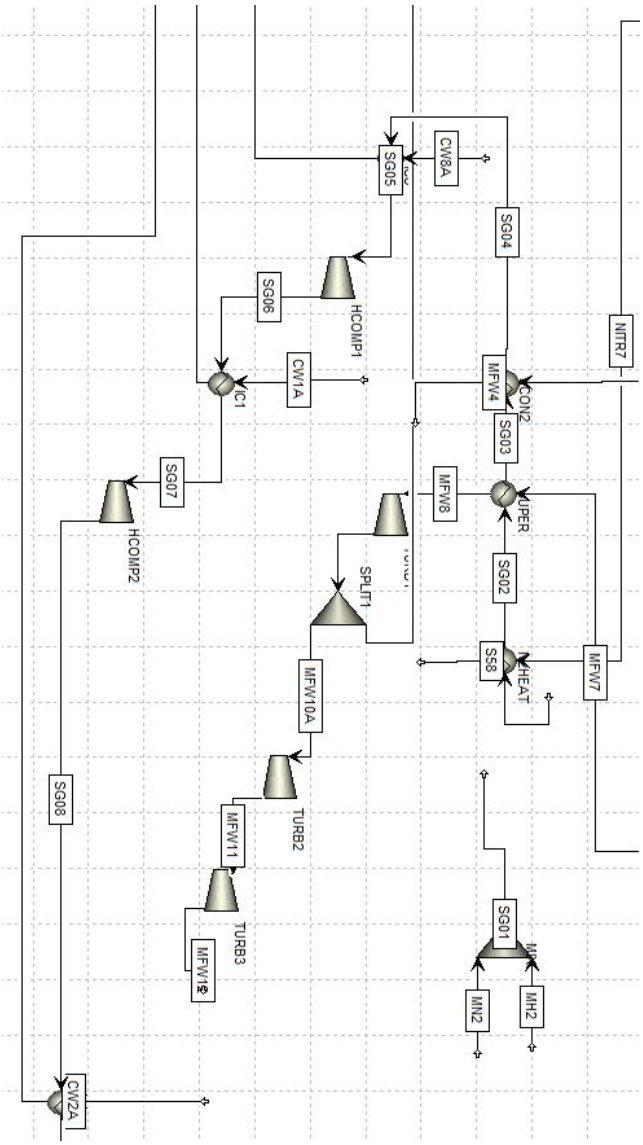

Figure B.4: 3/4 part of the MA-ATR process flowsheet in Aspen Plus

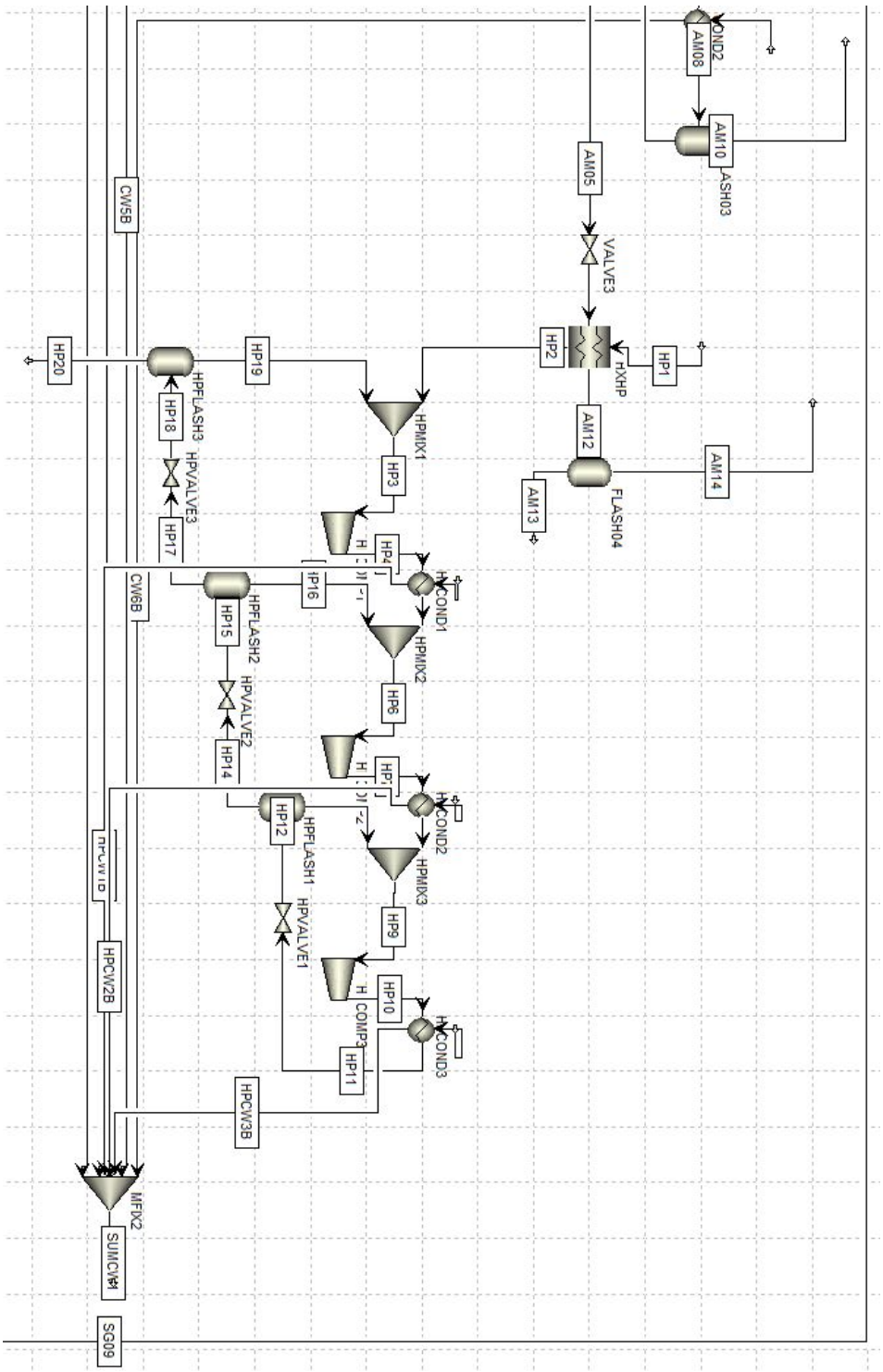

Figure B.5: 4/4 part of the MA-ATR process flowsheet in Aspen Plus. In the 10x train, AM10 and AM14 is recycled instead of flared and used in the hydrogen gas turbine.

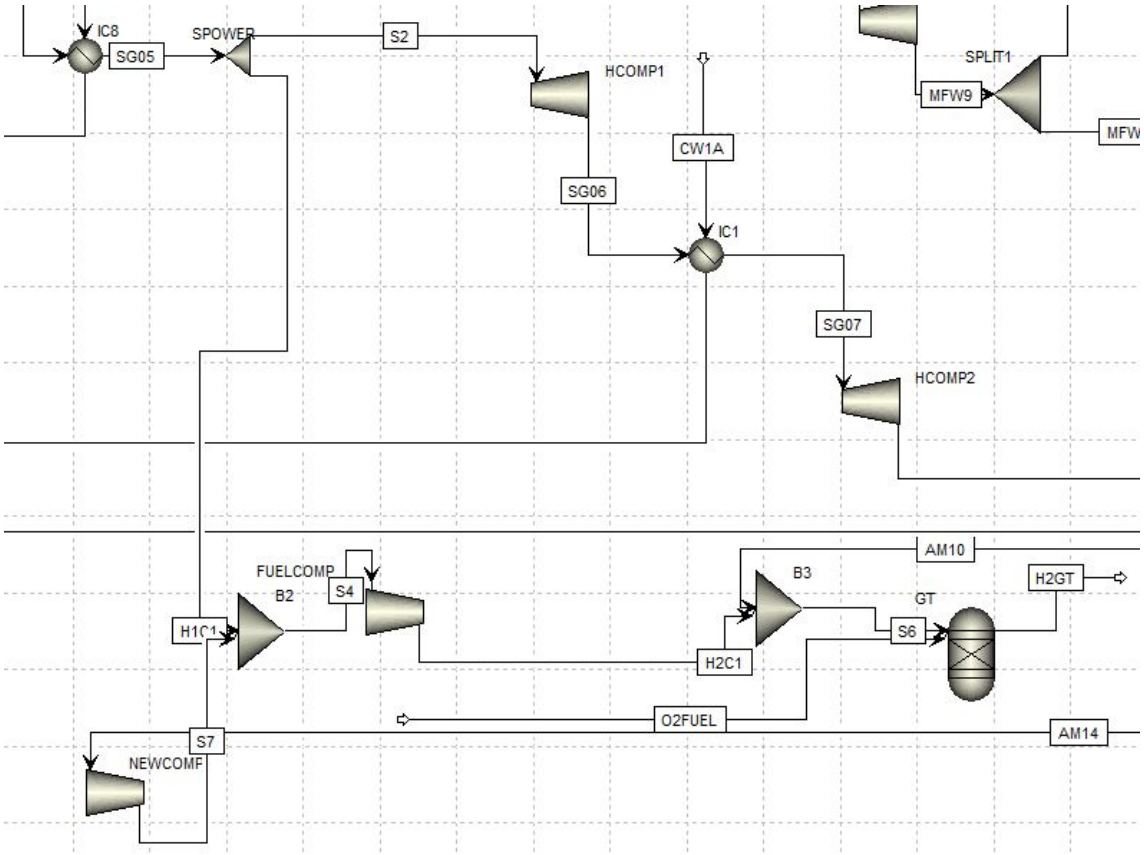

Figure B.6: MA-ATR plant 10x train configurations with the ammonia streams AM10 and AM14 recycled for used as fuel in the hydrogen power plant. Further, a splitter, SPOWER provides the right permeate stream required for the hydrogen power plant. Here, the streams are compressed before entering the power plant, which is modeled as "GT"

B.2 Aspen Plus: MA-ATR Ammonia Design Workbook

1x Train

	Units	AM01	AM02	AM03	AM04	AM05	AM06
− MIXED Substream							
+ Mass Flows	kg/sec	62,8062	62,8062	63,3878	63,3878	62,1937	1,19413
Temperature	C	20	22,9839	22,9572	21,5217	21,5217	21,5217
Pressure	bar	206,253	56	56	20	20	20
Molar Vapor Fraction		0	0,012475	0,0123593	0,0249444	0	1
− Mole Fractions							
NH3		0,985832	0,985832	0,985921	0,985921	0,998817	0,481828
N2		0,00344097	0,00344097	0,00341863	0,00341863	0,000248493	0,127336
H2		0,0103357	0,0103357	0,0102667	0,0102667	0,000677914	0,385083
H2O		9,61866e-05	9,61866e-05	9,53098e-05	9,53098e-05	9,77472e-05	3,19595e-08
AR		0,000294981	0,000294981	0,000298002	0,000298002	0,000158474	0,00575203

	Units	AM07	AM08	AM09	AM10	AM11	AM12
− MIXED Substream							
+ Mass Flows	kg/sec	1,19413	1,19413	0,581581	0,612549	62,1937	62,1937
Temperature	C	147,17	20	20	20	-31,0979	-34,0983
Pressure	bar	60	56,142	56,142	56,142	1,1	1,078
Molar Vapor Fraction		1	0,634199	0	1	0,185092	0,00824891
− Mole Fractions							
NH3		0,481828	0,481828	0,995613	0,185481	0,998817	0,998817
N2		0,127336	0,127336	0,000992422	0,200211	0,000248493	0,000248493
H2		0,385083	0,385083	0,00276835	0,6056	0,000677914	0,000677914
H2O		3,19595e-08	3,19595e-08	8,73497e-08	1,05966e-11	9,77472e-05	9,77472e-05
AR		0,00575203	0,00575203	0,000626037	0,00870866	0,000158474	0,000158474

	Units	AM13	AM14	CO2-2	CO2-3	CO2-4	CO2-5
− MIXED Substream							
+ Mass Flows	kg/sec	61,6969	0,496808	102,581	102,581	102,581	102,581
Temperature	C	-34,0983	-34,0983	440,494	382,487	206,123	18,6773
Pressure	bar	1,078	1,078	48,51	47,5398	46,5891	45,6574
Molar Vapor Fraction		0	1	1	1	1	0,637967
− Mole Fractions							
NH3		0,999869	0,872388	1,57409e-18	1,57409e-18	1,57409e-18	1,57409e-18
N2		8,99827e-07	0,0300162	0,00824227	0,00824227	0,00824227	0,00824227
H2		1,95929e-06	0,0819467	6,15965e-11	6,15965e-11	6,15965e-11	6,15965e-11
H2O		9,85602e-05	1,2863e-09	0,362258	0,362258	0,362258	0,362258
AR		2,96281e-05	0,0156494	0,0101632	0,0101632	0,0101632	0,0101632
O2		0	0	0,000975787	0,000975787	0,000975787	0,000975787
CO2		0	0	0,61836	0,61836	0,61836	0,61836
CH4		0	0	8,47588e-39	8,47588e-39	8,47588e-39	8,47588e-39
CO		0	0	6,5587e-11	6,5587e-11	6,5587e-11	6,5587e-11

	Units	AM14	CO2-2	CO2-3	CO2-4	CO2-5
− MIXED Substream						
✚ Mass Flows	**kg/sec**	**0,496808**	**102,581**	**102,581**	**102,581**	**102,581**
Temperature	C	-34,0983	440,494	382,487	206,123	18,6773
Pressure	bar	1,078	48,51	47,5398	46,5891	45,6574
Molar Vapor Fraction		1	1	1	1	0,637967
− Mole Fractions						
NH3		0,872388	1,57409e-18	1,57409e-18	1,57409e-18	1,57409e-18
N2		0,0300162	0,00824227	0,00824227	0,00824227	0,00824227
H2		0,0819467	6,15965e-11	6,15965e-11	6,15965e-11	6,15965e-11
H2O		1,2863e-09	0,362258	0,362258	0,362258	0,362258
AR		0,0156494	0,0101632	0,0101632	0,0101632	0,0101632
O2		0	0,000975787	0,000975787	0,000975787	0,000975787
CO2		0	0,61836	0,61836	0,61836	0,61836
CH4		0	8,47588e-39	8,47588e-39	8,47588e-39	8,47588e-39
CO		0	6,5587e-11	6,5587e-11	6,5587e-11	6,5587e-11

	Units	CW1A	CW1B	CW2A	CW2B	CW3A	CW3B
− MIXED Substream							
✚ Mass Flows	**kg/sec**	**355,694**	**355,694**	**375,774**	**375,774**	**112,002**	**112,002**
Temperature	C	15	27,0047	15	27	15	46,9999
Pressure	bar	2	1,96	2	1,96	2	1,96
Molar Vapor Fraction		0	0	0	0	0	0
− Mole Fractions							
NH3		0	0	0	0	0	0
N2		0	0	0	0	0	0
H2		0	0	0	0	0	0
H2O		1	1	1	1	1	1

	Units	CW4A	CW4B	CW5A	CW5B	CW6A	CW6B
− MIXED Substream							
✚ Mass Flows	**kg/sec**	**141,096**	**141,096**	**3343,53**	**3343,53**	**32,3283**	**32,3283**
Temperature	C	15	47,0009	15	22,0002	15	22,0028
Pressure	bar	2	1,96	2	1,97	2	1,96
Molar Vapor Fraction		0	0	0	0	0	0
− Mole Fractions							
NH3		0	0	0	0	0	0
N2		0	0	0	0	0	0
H2		0	0	0	0	0	0
H2O		1	1	1	1	1	1

	Units	CW4A	CW4B	CW5A	CW5B	CW6A	CW6B
− MIXED Substream							
✚ Mass Flows	**kg/sec**	**141,096**	**141,096**	**3343,53**	**3343,53**	**32,3283**	**32,3283**
Temperature	C	15	47,0009	15	22,0002	15	22,0028
Pressure	bar	2	1,96	2	1,97	2	1,96
Molar Vapor Fraction		0	0	0	0	0	0
− Mole Fractions							
NH3		0	0	0	0	0	0
N2		0	0	0	0	0	0
H2		0	0	0	0	0	0
H2O		1	1	1	1	1	1

	Units	CW7A	CW7B	CW8A	CW8B	CWIN	CWOUT
− MIXED Substream							
+ **Mass Flows**	**kg/sec**	**317,382**	**317,382**	**777,854**	**777,854**	**6013,57**	**6013,57**
Temperature	C	15	26,9996	15	27,0094	15	15,0119
Pressure	bar	2	1,96	2	1,96	1,01	2
Molar Vapor Fraction		0	0	0	0	0	0
− **Mole Fractions**							
NH3		0	0	0	0	0	0
N2		0	0	0	0	0	0
H2		0	0	0	0	0	0
H2O		1	1	1	1	1	1

	Units	CWPRES	CWTR1	FMW5B	H2+N2	H2N21	H2N22
− MIXED Substream							
+ **Mass Flows**	**kg/sec**	**1**	**19,4619**	**33,8543**	**63,3528**	**63,3528**	**63,3528**
Temperature	C	15	18,6773	282	700	839,247	700
Pressure	bar	2	45,6574	114,5	5	5	5
Molar Vapor Fraction		0	0	0	1	1	1
− **Mole Fractions**							
NH3		0	0	0	0,00113763	0	0,00113763
N2		0	2,0353e-08	0	0,249636	0,249914	0,249636
H2		0	3,08675e-16	0	0,748872	0,749756	0,748872
H2O		1	0,999375	1	4,81027e-05	0	4,81027e-05
AR		0	7,58687e-07	0	0,000306655	0,000306299	0,000306655
O2		0	7,96678e-08	0	1,22798e-30	2,40234e-05	1,22798e-30
CO2		0	0,000623779	0	0	0	0

	Units		H21	H22	H23	H24	HP1	HP2
− MIXED Substream								
+ **Mass Flows**	**kg/sec**	**8**	**7,84142**	**1,90055**	**0,929143**	**0,560344**	**11,5069**	**11,5069**
Temperature	C	0	939,037	818,118	760,157	721,484	-35,0146	-34,0146
Pressure	bar	5	51,0645	51,0645	51,0645	51,0645	0,895	0,8771
Molar Vapor Fraction		1	1	1	1	1	0	1
− **Mole Fractions**								
NH3		3	0	0	0	0	1	1
N2		6	0	0	0	0	0	0
H2		2	1	1	1	1	0	0

	Units		HP3	HP4	HP5	HP6	HP7	HP8
− MIXED Substream								
+ **Mass Flows**	**kg/sec**	**5069**	**12,5893**	**12,5893**	**12,5893**	**13,3606**	**13,3606**	**13,3606**
Temperature	C	0146	-34,1041	71,6139	20	18,3176	76,7167	20
Pressure	bar	8771	0,8771	3	2,94	2,94	5,5	5,39
Molar Vapor Fraction		1	1	1	1	1	1	1
− **Mole Fractions**								
NH3		1	1	1	1	1	1	1

	Units	HP9	HP10	HP11	HP12	HP13	HP14
− MIXED Substream							
+ **Mass Flows**	**kg/sec**	**14,1171**	**14,1171**	**14,1171**	**14,1171**	**0,756568**	**13,3606**
Temperature	C	19,2734	75,6238	20	6,42005	6,42004	6,42004
Pressure	bar	5,39	9,8	9,604	5,39	5,39	5,39
Molar Vapor Fraction		1	1	0	0,0535922	1	0
− **Mole Fractions**							
NH3		1	1	1	1	1	1

	Units	HP15	HP16	HP17	HP18	HP19	HP20
MIXED Substream							
Mass Flows	**kg/sec**	**13,3606**	**0,771268**	**12,5893**	**12,5893**	**1,08237**	**11,5069**
Temperature	C	-9,3318	-9,3318	-9,3318	-35,0146	-35,0146	-35,0146
Pressure	bar	2,94	2,94	2,94	0,895	0,895	0,895
Molar Vapor Fraction		0,0577273	1	0	0,0859757	1	0
Mole Fractions							
NH3		1	1	1	1	1	1

	Units	HPCW1A	HPCW1B	HPCW2A	HPCW2B	HPCW3A	HPCW3B
MIXED Substream							
Mass Flows	**kg/sec**	**41,6951**	**41,6951**	**49,6138**	**49,6138**	**569,859**	**569,859**
Temperature	C	15	22,0074	15	22,0031	15	22,0035
Pressure	bar	2	1,6	2	1,6	2	1,6
Molar Vapor Fraction		0	0	0	0	0	0
Mole Fractions							
NH3		0	0	0	0	0	0
N2		0	0	0	0	0	0
H2		0	0	0	0	0	0
H2O		1	1	1	1	1	1

	Units	MCO2-6	MCO2-7	MCO2-8	MCO2-9	MFW1	MFW2
MIXED Substream							
Mass Flows	**kg/sec**	**83,1189**	**83,1189**	**83,1189**	**83,1189**	**88,6111**	**88,6111**
Temperature	C	18,6773	81,8458	20	24,5698	15	16,0138
Pressure	bar	45,6574	88	86,241	110	1,01	85
Molar Vapor Fraction		1	1	0	0	0	0
Mole Fractions							
NH3		0	0	0	0	0	0
N2		0,0129196	0,0129196	0,0129196	0,0129196	0	0
H2		9,6551e-11	9,6551e-11	9,6551e-11	9,6551e-11	0	0
H2O		0,000707162	0,000707162	0,000707162	0,000707162	1	1
AR		0,0159302	0,0159302	0,0159302	0,0159302	0	0
O2		0,00152948	0,00152948	0,00152948	0,00152948	0	0
CO2		0,968914	0,968914	0,968914	0,968914	0	0
CH4		0	0	0	0	0	0
CO		1,02806e-10	1,02806e-10	1,02806e-10	1,02806e-10	0	0

	Units	MFW3	MFW4	MFW5A	MFW6A	MFW6B	MFW7
MIXED Substream							
Mass Flows	**kg/sec**	**88,6111**	**88,6111**	**54,9263**	**54,9263**	**33,8543**	**88,7806**
Temperature	C	185	282	282	430	430	430
Pressure	bar	84,6	84,2	112,2	112,2	112,2	112,2
Molar Vapor Fraction		0	0	0	1	1	1
Mole Fractions							
NH3		0	0	0	0	0	0
N2		0	0	0	0	0	0
H2		0	0	0	0	0	0
H2O		1	1	1	1	1	1

	Units	MFW8	MFW9	MFW10A	MFW10B	MFW11	MFW12
MIXED Substream							
Mass Flows	**kg/sec**	**88,7806**	**88,7806**	**31,2924**	**57,4882**	**31,2924**	**31,2924**
Temperature	C	550	442,564	442,564	442,564	185,169	28,8937
Pressure	bar	110	52,6	52,6	52,6	3	0,03
Molar Vapor Fraction		1	1	1	1	1	0,953439
Mole Fractions							
NH3		0	0	0	0	0	0
N2		0	0	0	0	0	0
H2		0	0	0	0	0	0
H2O		1	1	1	1	1	1

	Units	MH2	MN2	N2	NG01	NG02	NG03
− MIXED Substream							
✚ Mass Flows	**kg/sec**	**11,5585**	**52,4493**	**52,1213**	**30,63**	**30,63**	**30,63**
Temperature	C	700	700	680	15	300	304,312
Pressure	bar	5	5	5	70	68,6	67,914
Molar Vapor Fraction		1	1	1	1	1	1
− Mole Fractions							
NH3		0	0	0	0	0	0
N2		0	0,998288	0,99868	0,0089	0,0089	0,0089
H2		0,997629	0	0	0	0	7,3635e-06
H2O		0,00237056	0	0	0	0	3,28523e-07
AR		0	0,00171168	0,001224	0	0	0
O2		0	0	9,59999e-05	0	0	0
CO2		0	0	0	0,02	0,02	0,0199998
CH4		0	0	0	0,89	0,89	0,908308
CO		0	0	0	0	0	0
C2H6		0	0	0	0,07	0,07	0,0393458
C3H8		0	0	0	0,01	0,01	0,0163551
C4H10		0	0	0	0,0011	0,0011	0,00708406

	Units	NG04	NG05	NG06	NG17	NITR7	O2
− MIXED Substream							
✚ Mass Flows	**kg/sec**	**30,63**	**88,1182**	**88,1182**	**102,581**	**52,1213**	**25,6941**
Temperature	C	385	413,759	395,58	700	213,751	368
Pressure	bar	66,862	52,6	52,0845	49,5	5,1	50
Molar Vapor Fraction		1	1	1	1	1	1
− Mole Fractions							
NH3		0	0	0	1,57409e-18	0	0
N2		0,0089	0,00309342	0,00299732	0,00824227	0,99868	0,011853
H2		7,3635e-06	2,55937e-06	0,0307105	6,15965e-11	0	0
H2O		3,28523e-07	0,652425	0,601091	0,362258	0	0
AR		0	0	0	0,0101632	0,001224	0,038035
O2		0	0	0	0,000975787	9,59999e-05	0,950112
CO2		0,0199998	0,00695145	0,0222685	0,61836	0	0
CH4		0,908308	0,315705	0,342933	8,47588e-39	0	0
CO		0	0	0	6,5587e-11	0	0
C2H6		0,0393458	0,0136756	0	0	0	0
C3H8		0,0163551	0,00568461	0	0	0	0
C4H10		0,00708406	0,00246224	0	0	0	0

	Units	S1	S5	S58	SG01	SG02	SG03
− MIXED Substream							
✚ Mass Flows	**kg/sec**	**102,581**	**52,1213**	**52,1213**	**64,0078**	**63,3528**	**63,3528**
Temperature	C	700	8,98664	680	699,999	581,56	457,487
Pressure	bar	49,5	1,1	5	5	4,9	4,802
Molar Vapor Fraction		1	1	1	1	1	1
− Mole Fractions							
NH3		1,57409e-18	0	0	0	0,00113763	0,00113763
N2		0,00824227	0,99868	0,99868	0,249071	0,249636	0,249636
H2		6,15965e-11	0	0	0,748723	0,748872	0,748872
H2O		0,362258	0	0	0,00177911	4,81027e-05	4,81027e-05
AR		0,0101632	0,001224	0,001224	0,000427062	0,000306655	0,000306655
O2		0,000975787	9,59999e-05	9,59999e-05	0	1,22798e-30	1,22798e-30
CO2		0,61836	0	0	0	0	0

	Units	SG04	SG05	SG06	SG07	SG08	SG09
− MIXED Substream							
✚ Mass Flows	**kg/sec**	**63,3528**	**63,3528**	**63,3528**	**63,3528**	**63,3528**	**63,3528**
Temperature	C	232,549	25	120,1	25	125,009	25
Pressure	bar	4,706	4,61377	10	9,8	22	21,56
Molar Vapor Fraction		1	1	1	1	1	1
− Mole Fractions							
NH3		0,00113763	0,00113763	0,00113763	0,00113763	0,00113763	0,00113763
N2		0,249636	0,249636	0,249636	0,249636	0,249636	0,249636
H2		0,748872	0,748872	0,748872	0,748872	0,748872	0,748872
H2O		4,81027e-05	4,81027e-05	4,81027e-05	4,81027e-05	4,81027e-05	4,81027e-05
AR		0,000306655	0,000306655	0,000306655	0,000306655	0,000306655	0,000306655

	Units	SG10	SG11	SG12	SG13	SG14	SG15
− MIXED Substream							
✚ Mass Flows	**kg/sec**	**63,3528**	**63,3528**	**63,3528**	**63,3528**	**63,3528**	**214,346**
Temperature	C	123,741	45	142,947	45	140,095	55,5793
Pressure	bar	48	47,04	100	98	205	205
Molar Vapor Fraction		1	1	1	1	1	1
− Mole Fractions							
NH3		0,00113763	0,00113763	0,00113763	0,00113763	0,00113763	0,0511193
N2		0,249636	0,249636	0,249636	0,249636	0,249636	0,237001
H2		0,748872	0,748872	0,748872	0,748872	0,748872	0,710814
H2O		4,81027e-05	4,81027e-05	4,81027e-05	4,81027e-05	4,81027e-05	1,49702e-05
AR		0,000306655	0,000306655	0,000306655	0,000306655	0,000306655	0,00105172

	Units	SG16	SG17	SG18	SG19	SG20	SG21
− MIXED Substream							
✚ Mass Flows	**kg/sec**	**214,346**	**214,346**	**214,346**	**213,8**	**213,8**	**213,8**
Temperature	C	321,306	450	360,001	80	91,2893	20
Pressure	bar	200,938	198,948	194,948	191,007	210	206,253
Molar Vapor Fraction		1	1	1	1	1	0,815744
− Mole Fractions							
NH3		0,0511193	0,24174	0,24174	0,241762	0,241762	0,241762
N2		0,237001	0,189305	0,189305	0,18931	0,18931	0,18931
H2		0,710814	0,567694	0,567694	0,567723	0,567723	0,567723
H2O		1,49702e-05	1,7685e-05	1,7685e-05	1,77274e-05	1,77274e-05	1,77274e-05
AR		0,00105172	0,00124245	0,00124245	0,0011868	0,0011868	0,0011868

	Units	SG22	SUMCW1	SUMCW2	NG07	NG08	NG09
− MIXED Substream							
✚ Mass Flows	**kg/sec**	**150,994**	**4290,12**	**1826,7**	**88,1182**	**88,1182**	**88,1182**
Temperature	C	20	23,4805	27,0048	395,58	550	939,037
Pressure	bar	206,253	1,6	1,96	52,0845	51,0645	51,0645
Molar Vapor Fraction		1	0	0	1	1	1
− Mole Fractions							
NH3		0,073695	0	0	0	0	0,000158415
N2		0,231294	0	0	0,00299732	0,00299732	0,0019622
H2		0,693623	0	0	0,0307105	0,0307105	0,524824
H2O		5,37971e-09	1	1	0,601091	0,601091	0,224333
AR		0,00138824	0	0	0	0	0
O2		0	0	0	0	0	9,45987e-19
CO2		0	0	0	0,0222685	0,0222685	0,0406835
CH4		0	0	0	0,342933	0,342933	0,0740064
CO		0	0	0	0	0	0,134023

	Units	NG10	NG11	NG12	NG13	NG14	NG15	NG16
− **MIXED Substream**								
✚ **Mass Flows**	**kg/hr**	**288996**	**288996**	**282154**	**282154**	**278810**	**278810**	**276792**
Temperature	C	939,037	818,118	818,118	760,157	760,157	721,484	721,484
Pressure	bar	51,0645	51,0645	51,0645	51,0645	51,0645	51,0645	51,0645
Molar Vapor Fraction		1	1	1	1	1	1	1
− **Mole Fractions**								
NH3		0,000333383	0,000132039	0,000175021	0,000101847	0,000120039	7,97741e-05	8,90505e-05
N2		0,00412943	0,00387518	0,00513666	0,00492405	0,0058036	0,00563032	0,00628503
H2		0	0,245583	0	0,151552	0	0,10417	0
H2O		0,472106	0,270219	0,358182	0,237275	0,279658	0,199265	0,222436
AR		0	0	0	0	0	0	0
O2		0	2,60838e-20	0	2,43752e-21	0	3,8413e-22	0
CO2		0,0856179	0,20021	0,265384	0,332729	0,392162	0,43392	0,484378
CH4		0,155745	0,101662	0,134756	0,104516	0,123184	0,102651	0,114588
CO		0,282049	0,178302	0,236344	0,168885	0,199052	0,154266	0,172205
C2H6		1,88538e-05	1,59702e-05	2,11689e-05	1,73331e-05	2,04292e-05	1,74432e-05	1,94716e-05
C3H8		7,43139e-09	9,03807e-09	1,19802e-08	1,09751e-08	1,29356e-08	1,18144e-08	1,31882e-08
C4H10		1,23281e-12	2,34344e-12	3,1063e-12	3,34272e-12	3,93981e-12	3,99029e-12	4,45429e-12

Figure B.7: Material flows for the 1x MA-ATR ammonia plant

10x Train

	Units	AM01	AM02	AM03	AM04	AM05	AM06
MIXED Substream							
Mass Flows	**kg/sec**	**54,7984**	**54,7984**	**55,3059**	**55,3059**	**54,264**	**1,04188**
Temperature	C	20	22,9839	22,9572	21,5217	21,5217	21,5217
Pressure	bar	206,253	56	56	20	20	20
Molar Vapor Fraction		0	0,012475	0,0123593	0,0249444	0	1
Mole Fractions							
NH3		0,985832	0,985832	0,985921	0,985921	0,998817	0,481828
N2		0,00344097	0,00344097	0,00341863	0,00341863	0,000248493	0,127336
H2		0,0103357	0,0103357	0,0102667	0,0102667	0,000677914	0,385083
H2O		9,61866e-05	9,61866e-05	9,53098e-05	9,53098e-05	9,77472e-05	3,19595e-08
AR		0,000294981	0,000294981	0,000298002	0,000298002	0,000158474	0,00575203

	Units	AM07	AM08	AM09	AM10	AM11	AM12
MIXED Substream							
Mass Flows	**kg/sec**	**1,04188**	**1,04188**	**0,50743**	**0,534449**	**54,264**	**54,264**
Temperature	C	147,17	20	20	20	-31,0979	-34,098
Pressure	bar	60	56,142	56,142	56,142	1,1	1,078
Molar Vapor Fraction		1	0,634199	0	1	0,185092	0,00824972
Mole Fractions							
NH3		0,481828	0,481828	0,995613	0,185481	0,998817	0,998817
N2		0,127336	0,127336	0,000992422	0,200211	0,000248493	0,000248493
H2		0,385083	0,385083	0,00276835	0,6056	0,000677914	0,000677914
H2O		3,19595e-08	3,19595e-08	8,73497e-08	1,05966e-11	9,77472e-05	9,77472e-05
AR		0,00575203	0,00575203	0,000626037	0,00870866	0,000158474	0,000158474

	Units	AM13	AM14	CO2-1	CO2-2	CO2-3	CO2-4
MIXED Substream							
Mass Flows	**kg/sec**	**53,8305**	**0,43351**	**102,755**	**102,581**	**102,581**	**102,581**
Temperature	C	-34,098	-34,098	700	440,494	382,487	206,123
Pressure	bar	1,078	1,078	49,5	48,51	47,5398	46,5891
Molar Vapor Fraction		0	1	1	1	1	1
Mole Fractions							
NH3		0,999869	0,8724	0	1,57409e-18	1,57409e-18	1,57409e-18
N2		8,99745e-07	0,0300132	0,0138448	0,00824227	0,00824227	0,00824227
H2		1,95911e-06	0,0819386	0	6,15965e-11	6,15965e-11	6,15965e-11
H2O		9,85603e-05	1,28635e-09	0,360396	0,362258	0,362258	0,362258
AR		2,96257e-05	0,0156482	0,0102112	0,0101632	0,0101632	0,0101632
CO2		0	0	0,615548	0,61836	0,61836	0,61836
O2		0	0	0	0,000975787	0,000975787	0,000975787
CH4		0	0	0	8,47588e-39	8,47588e-39	8,47588e-39
CO		0	0	0	6,5587e-11	6,5587e-11	6,5587e-11

	Units	CO2-5	CW1A	CW1B	CW2A	CW2B	CW3A
MIXED Substream							
Mass Flows	**kg/sec**	**102,581**	**310,676**	**310,676**	**327,864**	**327,864**	**97,7483**
Temperature	C	30,0968	15	26,9918	15	26,9999	15
Pressure	bar	45,6574	2	1,96	2	1,96	2
Molar Vapor Fraction		0,638319	0	0	0	0	0
Mole Fractions							
NH3		1,57409e-18	0	0	0	0	0
N2		0,00824227	0	0	0	0	0
H2		6,15965e-11	0	0	0	0	0
H2O		0,362258	1	1	1	1	1
AR		0,0101632	0	0	0	0	0
CO2		0,61836	0	0	0	0	0
O2		0,000975787	0	0	0	0	0

	Units	CW3B	CW4A	CW4B	CW5A	CW5B	CW6A
− MIXED Substream							
+ Mass Flows	**kg/sec**	**97,7483**	**123,116**	**123,116**	**2917,23**	**2917,23**	**28,1997**
Temperature	C	46,9912	15	46,9983	15	22,0002	15
Pressure	bar	1,96	2	1,96	2	1,97	2
Molar Vapor Fraction		0	0	0	0	0	0
− Mole Fractions							
NH3		0	0	0	0	0	0
N2		0	0	0	0	0	0
H2		0	0	0	0	0	0
H2O		1	1	1	1	1	1

	Units	CW6B	CW7A	CW7B	CW8A	CW8B	CWIN
− MIXED Substream							
+ Mass Flows	**kg/sec**	**28,1997**	**345,991**	**345,991**	**624,257**	**624,257**	**5289,01**
Temperature	C	22,0045	15	26,9979	15	26,9999	15
Pressure	bar	1,96	2	1,96	2	1,96	1,01
Molar Vapor Fraction		0	0	0	0	0	0
− Mole Fractions							
NH3		0	0	0	0	0	0
N2		0	0	0	0	0	0
H2		0	0	0	0	0	0
H2O		1	1	1	1	1	1

	Units	CW6B	CW7A	CW7B	CW8A	CW8B	CWIN
− MIXED Substream							
+ Mass Flows	**kg/sec**	**28,1997**	**345,991**	**345,991**	**624,257**	**624,257**	**5289,01**
Temperature	C	22,0045	15	26,9979	15	26,9999	15
Pressure	bar	1,96	2	1,96	2	1,96	1,01
Molar Vapor Fraction		0	0	0	0	0	0
− Mole Fractions							
NH3		0	0	0	0	0	0
N2		0	0	0	0	0	0
H2		0	0	0	0	0	0
H2O		1	1	1	1	1	1

	Units	CWOUT	CWPRES	CWTR1	FMW5B	H1C1	H2+N2
− MIXED Substream							
+ Mass Flows	**kg/sec**	**5289,01**	**1**	**19,4466**	**32,6465**	**8,07748**	**63,3528**
Temperature	C	15,0119	15	30,0968	274	25	700
Pressure	bar	2	2	45,6574	114,5	4,61377	5
Molar Vapor Fraction		0	0	0	0	1	1
− Mole Fractions							
NH3		0	0	0	0	0,00113763	0,00113763
N2		0	0	3,25512e-08	0	0,249636	0,249636
H2		0	0	4,92088e-16	0	0,748872	0,748872
H2O		1	1	0,999245	1	4,81027e-05	4,81027e-05
AR		0	0	1,01306e-06	0	0,000306655	0,000306655
CO2		0	0	0,000754013	0	0	0

	Units	H2+N2	H2C1	H2GT	H2N21	H2N22	H21
− MIXED Substream							
+ Mass Flows	kg/sec	63,3528	8,51099	24,0454	63,3528	63,3528	7,84142
Temperature	C	700	341,741	25	839,247	700	939,037
Pressure	bar	5	35	35	5	5	51,0645
Molar Vapor Fraction		1	1	1	1	1	1
− Mole Fractions							
NH3		0,00113763	0,0246885	0	0	0,00113763	0
N2		0,249636	0,243699	0,233704	0,249914	0,249636	0
H2		0,748872	0,730844	0	0,749756	0,748872	1
H2O		4,81027e-05	4,68025e-05	0,701162	0	4,81027e-05	0
AR		0,000306655	0,000721347	0,001019	0,000306299	0,000306655	0
CO2		0	0	0	0	0	0
O2		1,22798e-30	1,19479e-30	0,0641149	2,40234e-05	1,22798e-30	0

	Units	H22	H23	H24	HP1	HP2	HP3
− MIXED Substream							
+ Mass Flows	kg/sec	1,90055	0,929143	0,560344	10,0397	10,0397	10,984
Temperature	C	818,118	760,157	721,484	-35,0146	-34,0146	-34,1041
Pressure	bar	51,0645	51,0645	51,0645	0,895	0,8771	0,8771
Molar Vapor Fraction		1	1	1	0	1	1
− Mole Fractions							
NH3		0	0	0	1	1	1
N2		0	0	0	0	0	0
H2		1	1	1	0	0	0

	Units	HP4	HP5	HP6	HP7	HP8	HP9
− MIXED Substream							
+ Mass Flows	kg/sec	10,984	10,984	11,657	11,657	11,657	12,3171
Temperature	C	71,6139	20	18,3176	76,7167	20	19,2734
Pressure	bar	3	2,94	2,94	5,5	5,39	5,39
Molar Vapor Fraction		1	1	1	1	1	1
− Mole Fractions							
NH3		1	1	1	1	1	1

	Units	HP10	HP11	HP12	HP13	HP14	HP15
− MIXED Substream							
+ Mass Flows	kg/sec	12,3171	12,3171	12,3171	0,660099	11,657	11,657
Temperature	C	75,6238	20	6,42005	6,42004	6,42004	-9,3318
Pressure	bar	9,8	9,604	5,39	5,39	5,39	2,94
Molar Vapor Fraction		1	0	0,0535922	1	0	0,0577273
− Mole Fractions							
NH3		1	1	1	1	1	1

	Units	HP16	HP17	HP18	HP19	HP20	HPCW1A
− MIXED Substream							
+ Mass Flows	kg/sec	0,672925	10,984	10,984	0,944361	10,0397	36,3796
Temperature	C	-9,3318	-9,3318	-35,0146	-35,0146	-35,0146	15
Pressure	bar	2,94	2,94	0,895	0,895	0,895	2
Molar Vapor Fraction		1	0	0,0859757	1	0	0
− Mole Fractions							
NH3		1	1	1	1	1	0

	Units	HPCW1B	HPCW2A	HPCW2B	HPCW3A	HPCW3B	MCO2-6
− MIXED Substream							
+ Mass Flows	**kg/sec**	**36,3796**	**43,3055**	**43,3055**	**497,229**	**497,229**	**83,1342**
Temperature	C	22,0072	15	22,0002	15	22,0031	30,0968
Pressure	bar	1,6	2	1,6	2	1,6	45,6574
Molar Vapor Fraction		0	0	0	0	0	1
− Mole Fractions							
NH3		0	0	0	0	0	0
N2		0	0	0	0	0	0,0129124
H2		0	0	0	0	0	9,64976e-11
H2O		1	1	1	1	1	0,00133246
AR		0	0	0	0	0	0,0159212
CO2		0	0	0	0	0	0,968305
O2		0	0	0	0	0	0,00152862

	Units	CO2-7	MCO2-8	MCO2-9	MFW1	MFW2	MFW3
− MIXED Substream							
+ Mass Flows	**kg/sec**	**83,1342**	**83,1342**	**83,1342**	**83,3333**	**83,3333**	**83,3333**
Temperature	C	95,1903	20	24,5484	15	16,3348	190
Pressure	bar	88	86,241	110	1,01	111,6	111,2
Molar Vapor Fraction		1	0	0	0	0	0
− Mole Fractions							
NH3		0	0	0	0	0	0
N2		0,0129124	0,0129124	0,0129124	0	0	0
H2		9,64976e-11	9,64976e-11	9,64976e-11	0	0	0
H2O		0,00133246	0,00133246	0,00133246	1	1	1
AR		0,0159212	0,0159212	0,0159212	0	0	0
CO2		0,968305	0,968305	0,968305	0	0	0
O2		0,00152862	0,00152862	0,00152862	0	0	0

	Units	MFW4	MFW5A	MFW6A	MFW6B	MFW7	MFW8
− MIXED Substream							
+ Mass Flows	**kg/sec**	**83,3333**	**52,965**	**52,965**	**32,6465**	**85,6116**	**85,6116**
Temperature	C	274	274	350	350	350	550
Pressure	bar	110,8	112,2	112,2	112,2	112,2	110
Molar Vapor Fraction		0	0	1	1	1	1
− Mole Fractions							
NH3		0	0	0	0	0	0
N2		0	0	0	0	0	0
H2		0	0	0	0	0	0
H2O		1	1	1	1	1	1

	Units	MFW9	MFW10A	MFW10B	MFW11	MFW12	MH2
− MIXED Substream							
+ Mass Flows	**kg/sec**	**85,6116**	**28,1233**	**57,4882**	**28,1233**	**28,1233**	**11,5585**
Temperature	C	442,564	442,564	442,564	185,169	28,8937	700
Pressure	bar	52,6	52,6	52,6	3	0,03	5
Molar Vapor Fraction		1	1	1	1	0,953439	1
− Mole Fractions							
NH3		0	0	0	0	0	0
N2		0	0	0	0	0	0
H2		0	0	0	0	0	0,997629
H2O		1	1	1	1	1	0,00237056

	Units		MN2	N2	NG01	S6	S7	S58
− MIXED Substream								
✚ Mass Flows	**kg/sec**	**685**	**52,4493**	**52,1213**	**30,63**	**9,04544**	**0,43351**	**52,1213**
Temperature	C	700	700	680	15	324,402	107,559	680
Pressure	bar	5	5	5	70	35	5	5
Molar Vapor Fraction		1	1	1	1	1	1	1
− Mole Fractions								
NH3		0	0	0	0	0,0328048	0,8724	0
N2		0	0,998288	0,99868	0,0089	0,241504	0,0300132	0,99868
H2		529	0	0	0	0,724522	0,0819386	0
H2O		056	0	0	0	4,444e-05	1,28635e-09	0
AR		0	0,00171168	0,001224	0	0,00112452	0,0156482	0,001224
CO2		0	0	0	0,02	0	0	0
O2		0	0	9,59999e-05	0	1,13448e-30	0	9,59999e-05
CH4		0	0	0	0,89	0	0	0
CO		0	0	0	0	0	0	0
C2H6		0	0	0	0,07	0	0	0
C3H8		0	0	0	0,01	0	0	0
C4H10		0	0	0	0,0011	0	0	0

	Units	SG01	SG02	SG03	SG04	SG05	SG06
− MIXED Substream							
✚ Mass Flows	**kg/sec**	**64,0078**	**63,3528**	**63,3528**	**63,3528**	**63,3528**	**55,2753**
Temperature	C	699,999	581,56	372,334	191,651	25	120,1
Pressure	bar	5	4,9	4,802	4,706	4,61377	10
Molar Vapor Fraction		1	1	1	1	1	1
− Mole Fractions							
NH3		0	0,00113763	0,00113763	0,00113763	0,00113763	0,00113763
N2		0,249071	0,249636	0,249636	0,249636	0,249636	0,249636
H2		0,748723	0,748872	0,748872	0,748872	0,748872	0,748872
H2O		0,00177911	4,81027e-05	4,81027e-05	4,81027e-05	4,81027e-05	4,81027e-05
AR		0,000427062	0,000306655	0,000306655	0,000306655	0,000306655	0,000306655

	Units	SG07	SG08	SG09	SG10	SG11	SG12
− MIXED Substream							
✚ Mass Flows	**kg/sec**	**55,2753**	**55,2753**	**55,2753**	**55,2753**	**55,2753**	**55,2753**
Temperature	C	25	125,009	25	123,741	45	142,947
Pressure	bar	9,8	22	21,56	48	47,04	100
Molar Vapor Fraction		1	1	1	1	1	1
− Mole Fractions							
NH3		0,00113763	0,00113763	0,00113763	0,00113763	0,00113763	0,00113763
N2		0,249636	0,249636	0,249636	0,249636	0,249636	0,249636
H2		0,748872	0,748872	0,748872	0,748872	0,748872	0,748872
H2O		4,81027e-05	4,81027e-05	4,81027e-05	4,81027e-05	4,81027e-05	4,81027e-05
AR		0,000306655	0,000306655	0,000306655	0,000306655	0,000306655	0,000306655

	Units	SG13	SG14	SG15	SG16	SG17	SG18
− MIXED Substream							
✚ Mass Flows	**kg/sec**	**55,2753**	**55,2753**	**187,017**	**187,017**	**187,017**	**187,017**
Temperature	C	45	140,095	55,5793	321,306	450	360,001
Pressure	bar	98	205	205	200,938	198,948	194,948
Molar Vapor Fraction		1	1	1	1	1	1
− Mole Fractions							
NH3		0,00113763	0,00113763	0,0511193	0,0511193	0,24174	0,24174
N2		0,249636	0,249636	0,237001	0,237001	0,189305	0,189305
H2		0,748872	0,748872	0,710814	0,710814	0,567694	0,567694
H2O		4,81027e-05	4,81027e-05	1,49702e-05	1,49702e-05	1,7685e-05	1,7685e-05
AR		0,000306655	0,000306655	0,00105172	0,00105172	0,00124245	0,00124245

	Units	SG19	SG20	SG21	SG22	SUMCW1	SUMCW2
MIXED Substream							
Mass Flows	**kg/sec**	**186,541**	**186,541**	**186,541**	**131,742**	**3743,2**	**1608,79**
Temperature	C	80	91,2893	20	20	23,4804	26,9979
Pressure	bar	191,007	210	206,253	206,253	1,6	1,96
Molar Vapor Fraction		1	1	0,815744	1	0	0
Mole Fractions							
NH3		0,241762	0,241762	0,241762	0,073695	0	0
N2		0,18931	0,18931	0,18931	0,231294	0	0
H2		0,567723	0,567723	0,567723	0,693623	0	0
H2O		1,77274e-05	1,77274e-05	1,77274e-05	5,37971e-09	1	1
AR		0,0011868	0,0011868	0,0011868	0,00138824	0	0

	Units		NG02	NG03	NG04	NG05	NG06	NG07
MIXED Substream								
Mass Flows	**kg/sec**	**9**	**30,63**	**30,63**	**30,63**	**88,1182**	**88,1182**	**88,1182**
Temperature	C	9	300	304,312	385	413,759	395,58	395,58
Pressure	bar	6	68,6	67,914	66,862	52,6	52,0845	52,0845
Molar Vapor Fraction		0	1	1	1	1	1	1
Mole Fractions								
NH3		0	0	0	0	0	0	0
N2		0	0,0089	0,0089	0,0089	0,00309342	0,00299732	0,00299732
H2		0	0	7,3635e-06	7,3635e-06	2,55937e-06	0,0307105	0,0307105
H2O		1	0	3,28523e-07	3,28523e-07	0,652425	0,601091	0,601091
AR		0	0	0	0	0	0	0
CO2		0	0,02	0,0199998	0,0199998	0,00695145	0,0222685	0,0222685
O2		0	0	0	0	0	0	0
CH4		0	0,89	0,908308	0,908308	0,315705	0,342933	0,342933
CO		0	0	0	0	0	0	0
C2H6		0	0,07	0,0393458	0,0393458	0,0136756	0	0
C3H8		0	0,01	0,0163551	0,0163551	0,00568461	0	0
C4H10		0	0,0011	0,00708406	0,00708406	0,00246224	0	0

	Units	NG08	NG09	NG10	NG11	NG12	NG13
MIXED Substream							
Mass Flows	**kg/sec**	**88,1182**	**88,1182**	**80,2768**	**80,2768**	**78,3762**	**78,3762**
Temperature	C	550	939,037	939,037	818,118	818,118	760,157
Pressure	bar	51,0645	51,0645	51,0645	51,0645	51,0645	51,0645
Molar Vapor Fraction		1	1	1	1	1	1
Mole Fractions							
NH3		0	0,000158415	0,000333383	0,000132039	0,000175021	0,000101847
N2		0,00299732	0,0019622	0,00412943	0,00387518	0,00513666	0,00492405
H2		0,0307105	0,524824	0	0,245583	0	0,151552
H2O		0,601091	0,224333	0,472106	0,270219	0,358182	0,237275
AR		0	0	0	0	0	0
CO2		0,0222685	0,0406835	0,0856179	0,20021	0,265384	0,332729
O2		0	9,45987e-19	0	2,60838e-20	0	2,43752e-21
CH4		0,342933	0,0740064	0,155745	0,101662	0,134756	0,104516
CO		0	0,134023	0,282049	0,178302	0,236344	0,168885

	Units	NG14	NG15	NG16	NG17	NITR7	O2
− MIXED Substream							
+ Mass Flows	kg/hr	278810	278810	276792	369291	187637	92498,7
Temperature	C	760,157	721,484	721,484	700	213,751	368
Pressure	bar	51,0645	51,0645	51,0645	49,5	5,1	50
Molar Vapor Fraction		1	1	1	1	1	1
− Mole Fractions							
NH3		0,000120039	7,97741e-05	8,90505e-05	1,57409e-18	0	0
N2		0,0058036	0,00563032	0,00628503	0,00824227	0,99868	0,011853
H2		0	0,10417	0	6,15965e-11	0	0
H2O		0,279658	0,199265	0,222436	0,362258	0	0
AR		0	0	0	0,0101632	0,001224	0,038035
CO2		0,392162	0,43392	0,484378	0,61836	0	0
O2		0	3,8413e-22	0	0,000975787	9,59999e-05	0,950112
CH4		0,123184	0,102651	0,114588	8,47588e-39	0	0
CO		0,199052	0,154266	0,172205	6,5587e-11	0	0

	Units	O2FUEL	S1	S2	S4	S5	S6	S7
− MIXED Substream								
+ Mass Flows	kg/sec	15	102,581	55,2753	8,51099	52,1213	9,04544	0,43351
Temperature	C	25	700	25	27,6584	8,98664	324,402	107,559
Pressure	bar	35	49,5	4,61377	4,61377	1,1	35	5
Molar Vapor Fraction		1	1	1	1	1	1	1
− Mole Fractions								
NH3		0	1,57409e-18	0,00113763	0,0246885	0	0,0328048	0,8724
N2		0	0,00824227	0,249636	0,243699	0,99868	0,241504	0,0300132
H2		0	6,15965e-11	0,748872	0,730844	0	0,724522	0,0819386
H2O		0	0,362258	4,81027e-05	4,68025e-05	0	4,444e-05	1,28635e-09
AR		0	0,0101632	0,000306655	0,000721347	0,001224	0,00112452	0,0156482
CO2		0	0,61836	0	0	0	0	0
O2		1	0,000975787	1,22798e-30	1,19479e-30	9,59999e-05	1,13448e-30	0

Figure B.8: Material flows for the 10x MA-ATR ammonia plant

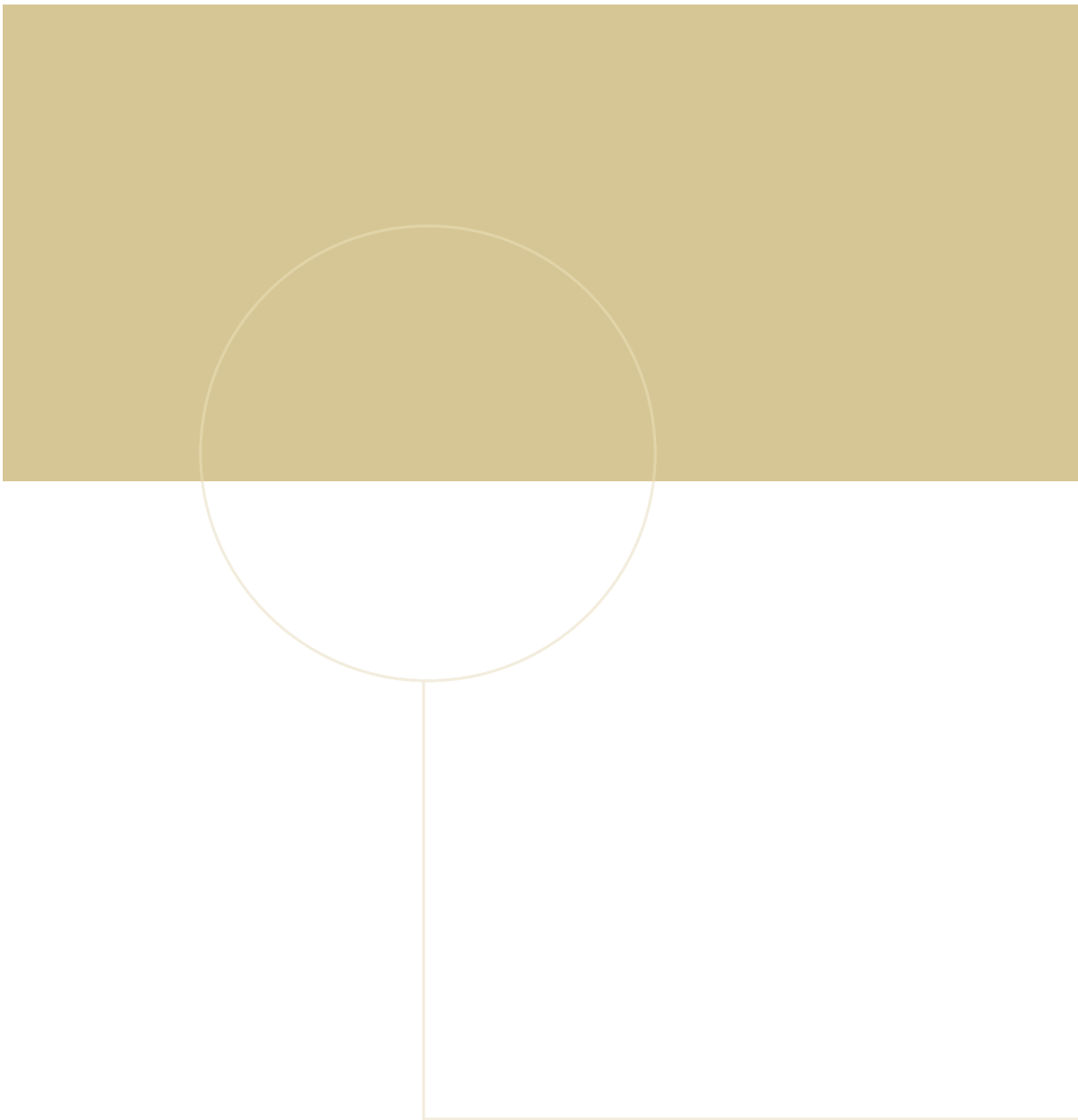

NTNU

Norwegian University of
Science and Technology